2-2014

Studies in Asymmetric Synthesis: Supramolecular Catalysis, C-H Activation, and D-Cycloserine Synthesis

Nathan C. Thacker
University of Nebraska-Lincoln, nathan.thacker@huskers.unl.edu

STUDIES IN ASYMMETRIC SYNTHESIS: SUPRAMOLECULAR CATALYSIS, C-H ACTIVATION, AND D-CYCLOSERINE SYNTHESIS

By

Nathan C. Thacker

A DISSERTATION

Presented to the Faculty of

The Graduate College at the University of Nebraska

In Partial Fulfillment of Requirements

For the Degree of Doctor of Philosophy

Major: Chemistry

Under the Supervision of Professor James M. Takacs

Lincoln, Nebraska

February 2014

STUDIES IN ASYMMETRIC SYNTHESIS: SUPRAMOLECULAR CATALYSIS, C-H ACTIVATION, AND D-CYCLOSERINE SYNTHESIS

Nathan C. Thacker, Ph.D.

University of Nebraska, 2014

Advisor: James M. Takacs

Rh-catalyzed asymmetric hydrogenation has emerged as a powerful tool for the manufacturing of chiral pharmaceuticals. While the mechanism is well understood, catalyst design *a priori* is not yet possible. Supramolecular catalysis, the use of non-covalent forces to affect a catalytic process, can afford the catalyst diversity required to uncover efficient catalysts and further our understanding. Using a modular design and self-assembly, a large scale supramolecular catalyst screening in a catalyst scaffold optimization study of rhodium-catalyzed asymmetric hydrogenation was carried out. Analyzing the data yields some new insights into the roles of each module making up the supramolecular catalyst. Perhaps most surprisingly, the presence of a chiral recognition element positioned remote to the site of catalysis can significantly impact the catalytic activity and enantioselectivity.

1,1-Disubstituted alkenes are a challenging class of substrates for the asymmetric hydroboration reaction. Differentiation of the prochiral faces has been met with few successes from either stoichiometric or catalytic approaches. Takacs *et al.* revealed amide and ester groups direct the γ-selective Rh-catalyzed hydroboration of 1,1-

disubstituted-β,γ-unsaturated alkenes. In the work described herein, analogous oxime-directing groups were used in an attempt to diversify the substrate scope. Unlike the amide- or ester-directed examples, we find oxime-directed hydroboration proceeds through an unusual C-H activation/metallation that proves crucial to turnover of borylated products. Whereas it was previously presumed that certain reduced byproducts were derived from adventitious H_2 reduction, deuterium-labeling experiments suggest competing pathways from a common intermediate leading to both borylated and reduced products.

In 1993, the World Health Organization (WHO) declared tuberculosis (TB) a global public emergency. Current drug treatments have reduced the mortality rate 40% since 1990, but increasing numbers of drug-resistant tuberculosis strains have been reported. D-Cyloserine (DCS) is a second line drug for the treatment of TB. In a collaborative effort with Professors Robert Powers (UNL-Chemistry) and Raul Barletta (UNL Veterinary and Biomedical Sciences), experiments with an isotopically-labeled DCS were proposed to elucidate the mechanism. Previously reported routes were not amenable to the milligram quantities available for isotopically labeled serine starting material. The synthetic route that will be described was used to produce both labeled and unlabeled DCS.

ACKNOWLEDGEMENTS

I would like to start by thanking my advisor Professor James M. Takacs. His support and guidance throughout my graduate studies has been invaluable to me in my research and development as a scientist. I will miss our everyday conversations on chemistry and Nebraska football.

I thank my committee members for their helpful comments and discussions: Professor Berkowitz, Professor DiMagno, Professor Li, and Professor Ducharme. In addition, I'd like to thank Professor DiMagno and Professor Dussault for writing letters of recommendation on my behalf.

I have been blessed to work alongside terrific colleagues in the JMT lab. I thank Professor Shin Moteki for teaching me skills in the laboratory as well as fishing skills on the lake. I thank Dr. Sean Smith for the good times shared in the lab and our infamous bowling competition. The next generation of JMT lab looks to be a good group. In particular, I thank current group members Gia Hoang and Veronika Shoba for their strong work ethic, and I wish them the best of luck in their future endeavors.

Last but not least, I thank my parents for their unwavering support throughout my graduate career. Their support has meant the world to me.

PREFACE

The introductory chapter of this dissertation serves as a review of supramolecular catalysts in which a metal structurally assembles the catalyst. In contrast to previously published reviews, a direct analysis from the contribution of the supramolecular interactions on the catalytic reaction will be highlighted. This chapter represents a subset of our investigation on supramolecular catalysts for a review in preparation. The subsequent chapters cover research related to asymmetric synthesis, specifically, asymmetric catalysis and isotopically labeled-compound synthesis for a collaborative project. The second chapter is a summary of our findings from the catalyst scaffold optimization of a supramolecular asymmetric hydrogenation catalyst; its focus is on catalyst structure-activity relationships. The third chapter is an ongoing mechanistic investigation into an unusual C-H activation found during the oxime-directed rhodium-catalyzed hydroboration. The fourth chapter describes an asymmetric synthesis of an isotopically-labeled tuberculosis drug D-cycloserine to support a collaborative project with Professors Robert Powers (UNL-Chemistry) and Raul Barletta (UNL Veterinary and Biomedical Sciences.

TABLE OF CONTENTS

TABLE OF FIGURES

Chapter 1

Chapter 2

Chapter 3

Chapter 4

TABLE OF TABLES

Chapter 2

Chapter 3

TABLE OF SCHEMES

Chapter 3

Chapter 4

LIST OF ABBREVIATIONS

acac	Acetylacetone
aq	Aqueous
Ar	Aryl
B	Borane
BArF	$B(3,5\text{-}(CF_3)_2C_6H_3]_4]^-$
BF4	Tetrafluoroborate
BINAP	2,2'-Bis(diphenylphosphino)-1,1'-binaphthyl
BINOL	1,1'-Bi-2,2'-naphthol
Bn	Benzylic
box	Bisoxazoline
CAH	Catalyzed asymmetric hydrogenation
CAHB	Catalyzed asymmetric hydroboration
CAMP	Methylcyclohexyl-*o*-anisylphosphine
catBH	Catecholborane
CCl_4	Carbon tetrachloride
CD	Circular dichrooism
CDI	1,1-carbonyldiiimidazole
cod	Cyclooctadiene
DCE	Dichloroethane

DCM	Dichloromethane
DCS	D-cycloserine
de	Diastereomeric excess
DFT	Density functional theory
DIAD	Diisopropyl azodicarboxylate
DIOP	*O*-Isopropylidene-2,3-dihydroxy-1,4-bis(diphenylphosphino)butane
DIPAMP	Ethane-1,2-diylbis[(2-methoxyphenyl)phenylphosphane
DMB	2,5-dimethylborolane
DMF	N,N-dimethylformamide
DNA	Deoxyribonucleic acid
DOSY	Diffusion-ordered NMR spectroscopy
DPEN	Diphenylethylenediamine
dppe	Diphenylphosphinoethane
DuPhos	Class of phospholanes developed by DuPont
EDR	Extensively-drug resistant
ee	Enantiomeric excess
Equiv	Equivalent
Et	Ethyl
EtOAc	Ethyl acetate

EtOH	Ethanol
FAB	Fast-atom bombardment
FTIR	Fourier-Transform Infrared
GC	Gas chromatography
GPC	Gel-permeation chromatography
h	Hour
HB	Hydroboration
HCl	Hydrochloric Acid
HIV	Human immunodefiency virus
HPLC	High-performance liquid chromatography
HRMS	High-resolution mass spectrometry
Hz	Hertz
Ipc_2BH	Diisopinocampheylborane
$IPcBH_2$	Monoisopinocapheylborane
IR	Infrared
J	Coupling Constant
JOSIPHOS	Class of ferrocenyl ligands developed by Josi Puleo
L	Ligand
LCS	L-cyloserine
L-DOPA	L-3,4-dihydroxyphenylalanine

M	Molarity
m-	Meta
MALDI	Matrix-assisted laser desorption/ionization
MDR	Multi-drug resistant
Me	Methyl
MeOH	Methanol
min	Minutes
MOF	Metal-Organic Framework
Mp	Melting point
MS	Mass spectrometry
MTPA	Methoxy-α-(trifluoromethyl)phenylacetyl acid
N2	Nitrogen
NaH	Sodium hydride
NaOAc	Sodium acetate
nbd	Norbornadiene
NHC	N-heterocyclic carbene
NMR	Nuclear magnetic resonance
[O]	Oxidation
o-	Ortho

ONIOM	Own n-layered integrated molecualr orgbital and molecualr mechanics
OTf	Triflate
p-	Para
PAMP	2-Methoxyphenyl(phenyl)phosphane
Pd/C	Palladium on carbon
Ph	Phenyl
pinBH	Pinacolborane
Psi	Pounds per square inch
QMM	Quantum mechanics guided molecular mechanics method
rac	Racemic
rt	Room temperature
SAL	Self-assembling ligand
SAXS	Small-angle X-ray scattering
$SOCl_2$	Thionyl chloride
TADDOL	α,α,α',α'-Tetraaryl-1,3-dioxolan-4,5-dimethanol
TB	Tuberculosis
TBAF	Tetra-butyl ammonium fluoride
TBDPS	Tert-butyl diphenylsilyl
t-butyl	Tetra-butyl

THF	Tetrahydrofuran
TLC	Thin-layer chromatography
tmdBH	4,5,6-trimethyl-1,3,2-dioxaborinane
UNL	University of Nebraska-Lincoln
UV-Vis	Ultraviolet-visible spectroscopy
WHO	World health organization
XRD	X-ray diffraction
(X)-Taddol	[$(3,5\text{-Me})_2C_6H_3$]-aryl substituted TADDOL
ΔES	Difference in enantioselectivity
$\Delta\Delta G^{\ddagger}$	Difference in activation energy

CHAPTER ONE: SUPRAMOLECULAR CATALYSIS

1.1 Introduction

The macromolecular frameworks which direct the three-dimensional assembly of enzymes commonly incorporate structural motifs such as hydrogen-bonding and metal complexation. The active site of these enzymes must be somewhat rigid to selectively accommodate a complex substrate yet flexible enough to distort it as needed to accommodate the transition-state structure.[1] The study of the interactions which govern the assembly of these macromolecules has been broadly named supramolecular chemistry. Synthetic methodologies for supramolecular chemistry generally focus on the construction of macromolecules via non-covalent interactions including metal-ligand coordination, hydrogen-bonding, and dipole-dipole or ionic interactions, although van der Waals attractions and the avoidance of hydrophobic interactions likely also play important but less well-defined roles. When these reversible intermolecular forces are used to optimize a catalyst in effecting its reaction, this field is known as supramolecular catalysis.

A supramolecular approach to catalyst design has some potential advantages over traditional methods. While monodentate ligands have been used very effectively in applications requiring the use of two or more equivalents of ligand, fine-tuning the catalyst from steric and electronic substituents effects alone by combinatorial strategies is often a challenge. Bidentate ligands offer more control to precisely define the chiral space, but building large ligand libraries for screening by one ligand at a time synthesis can be very tedious. Supramolecular approaches hope to offer the opportunity to control

the chiral space and provide the opportunity to construct large ligand libraries through self-assembly. The three common approaches to self-assembled supramolecular catalysts via non-covalent interactions: metal-ligand coordination, hydrogen-bonding, and dipole-dipole or ionic interaction, are illustrated in (Figure 1A). Metal-directed self-assembly forms the basis for the work described in Chapter 2 of this thesis, and therefore this introductory chapter will focus on similar approaches.

Typical architectural assemblies of a metal-directed self-assembled supramolecular catalyst are shown below (Figure 1B). Bifunctional ligands with two binding sites can be used in an orthogonal binding approach. A metal ion, participating in a structural role, binds preferentially to the primary binding site assembling the bidentate ligand. The secondary binding site would then be available for chelation to a catalytically active metal ion. Alternatively, addition of chelating bridging ligands to coordinating metal ions form discrete or networked metal-organic frameworks (MOFs). These catalysts could participate in host-guest chemistry wherein a substrate's conformation inside the cavity can lead to a chemo-, regio-, or stereoselective chemical transformation. A catalytic active site(s) introduced to the inside of the cavity might successfully exploit the cavity to effect a size- or shape- selective reaction. Lastly, self-assembling polymers may be formed with two orthogonally-binding ligands in an appropriately designed monomeric unit. Addition of a structural metal and catalytically active metal self-assembles the heterogeneous polymeric catalyst.

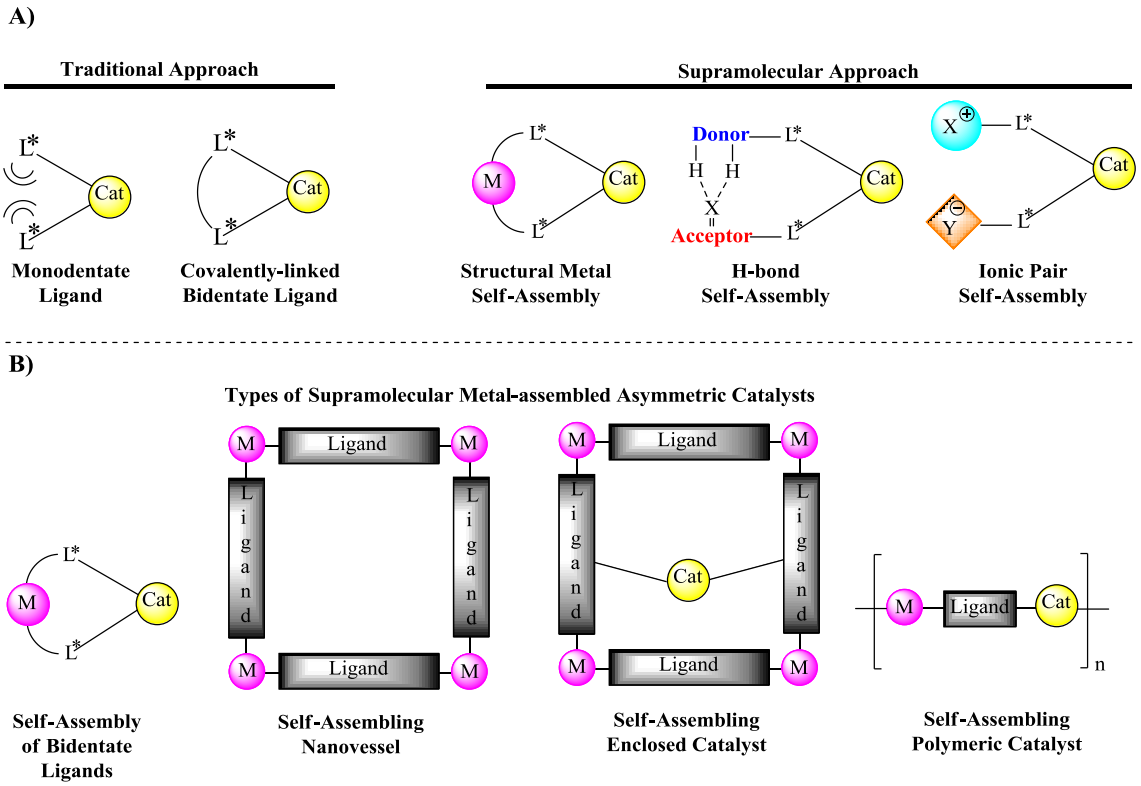

Figure 1 Design of a supramolecular catalyst. A) Traditional approaches versus supramolecular approaches. B) Architectures common in metal-organized supramolecular catalyst systems.

This chapter will review progress in the design of asymmetric supramolecular catalysis via metal-directed self-assembly. Its organization features a different type of analysis from traditional reviews of the young, but rapidly developing, field.[2-14] The focus of this brief review is to summarize the influence of the supramolecular catalyst scaffold/framework with, where possible, the direct comparison to the corresponding combination of monomeric ligands. Included in this discussion is a brief review over the development of some metal-organic frameworks that have been used for asymmetric catalysis. MOFs are often excluded from reviews on asymmetric supramolecular

catalysis; we argue that their synthesis via self-assembly and potential secondary interactions with substrates warrants their inclusion. While organocatalysts are outside the scope of this review and not incorporated in this discussion, remarkable enhancements from supramolecular interactions have been observed in asymmetric organocatalytic MOF catalysis.[15-23]

1.2 Homogeneous Organometallic catalysis – Neutral and anionic ligand-metal coordination to form supramolecular chelating ligands

Van Leeuwen and Reek, two of the major players in this field, jointly published one of the earliest examples using a Lewis acid-Lewis base interaction to assemble a chiral bidentate ligand (Figure 2).[24] Zinc-porphyrins were used as templates to coordinate with a series of pyridyl-substituted BINOL-phosphite ligands. Following the titration of the pyridyl-substituted ligands with bis-porphyrin template **B** by UV-Vis confirmed the expected ratio of 2 ligands to 1 template **B**. The coordination behavior of the rhodium-chelated ligands was further studied with high-pressure NMR spectroscopy under syn gas (20 bars 1:1 H_2/CO, toluene-d_8). Upon addition of template **B**, the rhodium-hydride shifted from δ = -9.5 to -11.1 ppm; this is believed to be a shielding effect of the porphyrin to rhodium. Monodentate ligand **L1** and the **L1**-(mono-porphyrin)template A, gave similar very low enantioselectivity (6-7% ee) in the rhodium-catalyzed asymmetric hydroformylation reaction. Use of the bis-zinc porphyrin (template **B**) with two equivalents of pyridyl phosphite gave a modest increase in enantioselectivity up to 33% ee. Since the combination of template **A** + **L1** and **L1** gave similar results, the increase in

enantioselectivity when using the combination of template **B** + **L1** is construed to arise from supramolecular organization.

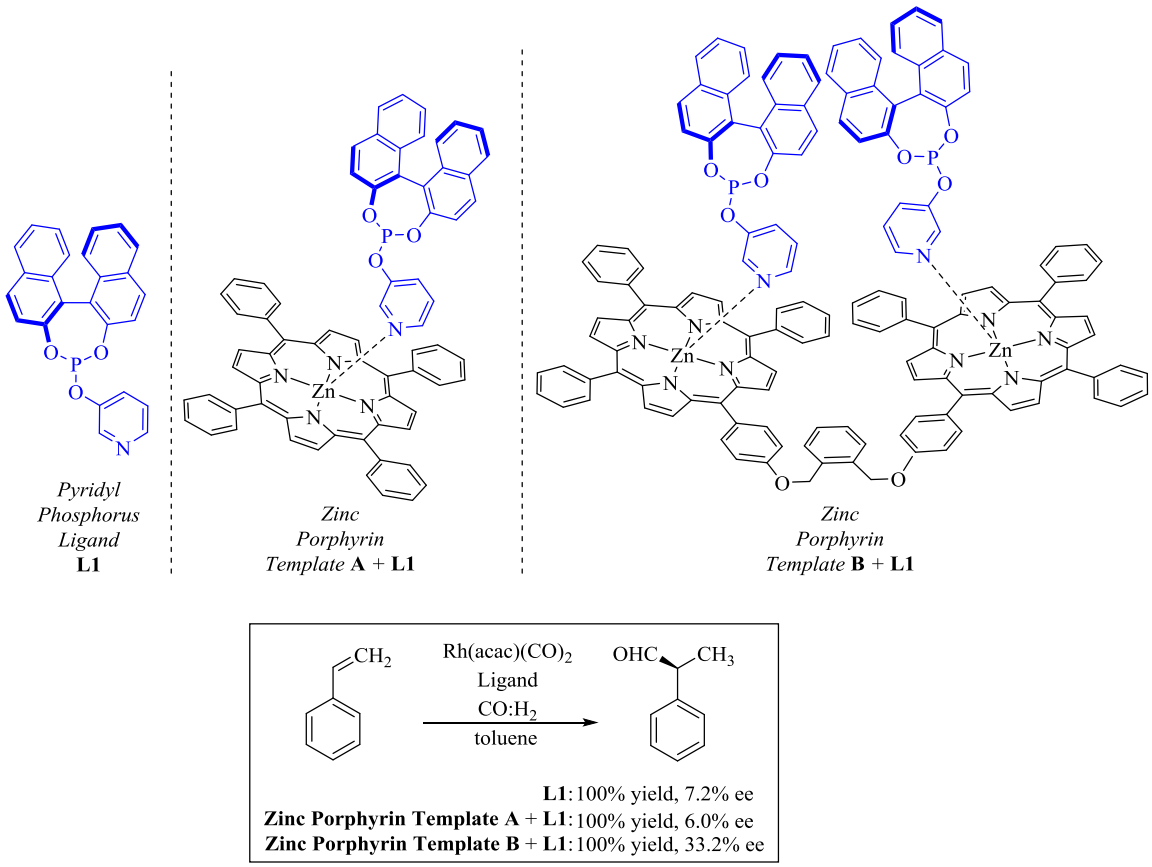

Figure 2 Metal-porphyrin templates organize pyridyl phosphorus ligating groups. Adapted from Ref 24 with permission from The Royal Society of Chemistry

Van Leeuwen and Reek designed a new template by covalently linking one phosphite ligating group to the zinc-porphyrin. Addition of a series of phosphine substituted pyridines generates a series of supramolecular catalyst scaffolds *in situ*. These catalysts, named SUPRAPhos, have been successfully used for asymmetric hydroformylation,[25,26] asymmetric hydrogenation,[27] and palladium catalyzed alkylation.[28,29] Van Leeuwen and Reek demonstrated the asymmetric hydrogenation of a tri-substituted cyclic enamide in

one of the more remarkable examples of the influence of the supramolecular scaffold (Figure 3).[27] This particular alkene substrate had proven notoriously difficult to reduce with high enantioselectivity via rhodium catalyzed asymmetric hydrogenation (Rh-CAH).[30] The monodentate control ligand, (BINOL)PO-Ph, was reactive but gave no asymmetric induction. The chiral (BINOL)P-functionalized porphyrin **C** in combination with PPh_3 also failed to afford high enantioselectivity. However, the chiral (BINOL)P-functionalized zinc porphyrin **C** in combination with *ortho*, *meta*- and *para*-diphenylphosphine-substituted pyridines gave interesting results. While the *ortho*- and *para*-substituted pyridylphosphines (**L2** and **L4**, respectively) furnished low conversion and low enantioselectivity (44-62% yields, 27-47% ee), the *meta*-pyridyldiphenylphosphine ligand (**L3**) afforded quantitative yield and high enantioselectivity (94% ee). The ^{31}P NMR of a 1:1 mixture of BINOL-zinc porphyrin **C** and **L3** with $Rh(cod)_2BF_4$ confirmed formation of the desired 1:1 bidentate ligand to rhodium chelate. Coupling constants were $J_{P\text{-}P} = 41$ Hz, $J_{Rh\text{-}P} = 263$ Hz for the BINOL phosphite and $J_{P\text{-}P} = 41$ Hz, $J_{Rh\text{-}P} = 146$ Hz for the phosphine.

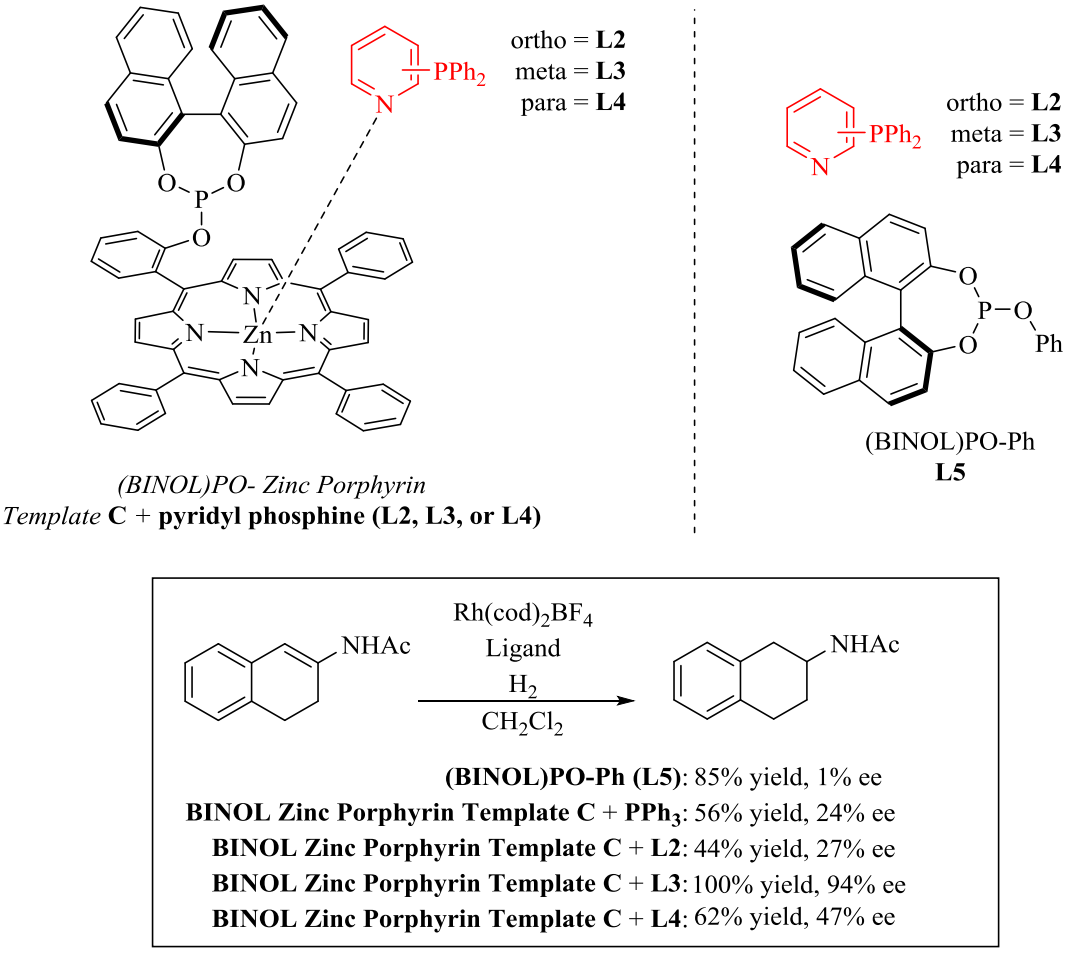

(BINOL)PO- Zinc Porphyrin Template **C** + **pyridyl phosphine (L2, L3, or L4)**

Figure 3 SUPRAPhos library finds an effective asymmetric hydrogenation catalyst. Adapted from Ref 27 with permission from John Wiley and Sons.

In trying to assess the role of the supramolecular scaffold in his supramolecular catalysts, Reek reported a supramolecular hydroformylation catalyst in which the Lewis acid-Lewis base interaction changed the preferred coordination geometry at rhodium (Figure 4).[31] UV-Vis spectra confirmed the expected binding of the two porphyrin moieties to the 4-pyridyl substituted phosphoramidite. Using high pressure NMR, the authors determined the rhodium hydride was *cis* to the bulky monodentate ligand. After coordination of the two zinc porphyrins, the H-coupling is consistent with a trans-

coordination of hydride with respect to the phosphorus ligand. This example illustrates how supramolecular organization may influence the preferred confirmation of rhodium species. Asymmetric hydroformylation of 2-octene with monodentate phosphoramidite ligand **L6** gave low conversion and low selectivity. Use of phosphoramidite ligand **L6** coordinated to two equivalents of zinc porphyrin **A**, afforded the 2- and 3-branched isomers in 29% and 27% yields. The selectivity was increased modestly as well.

.

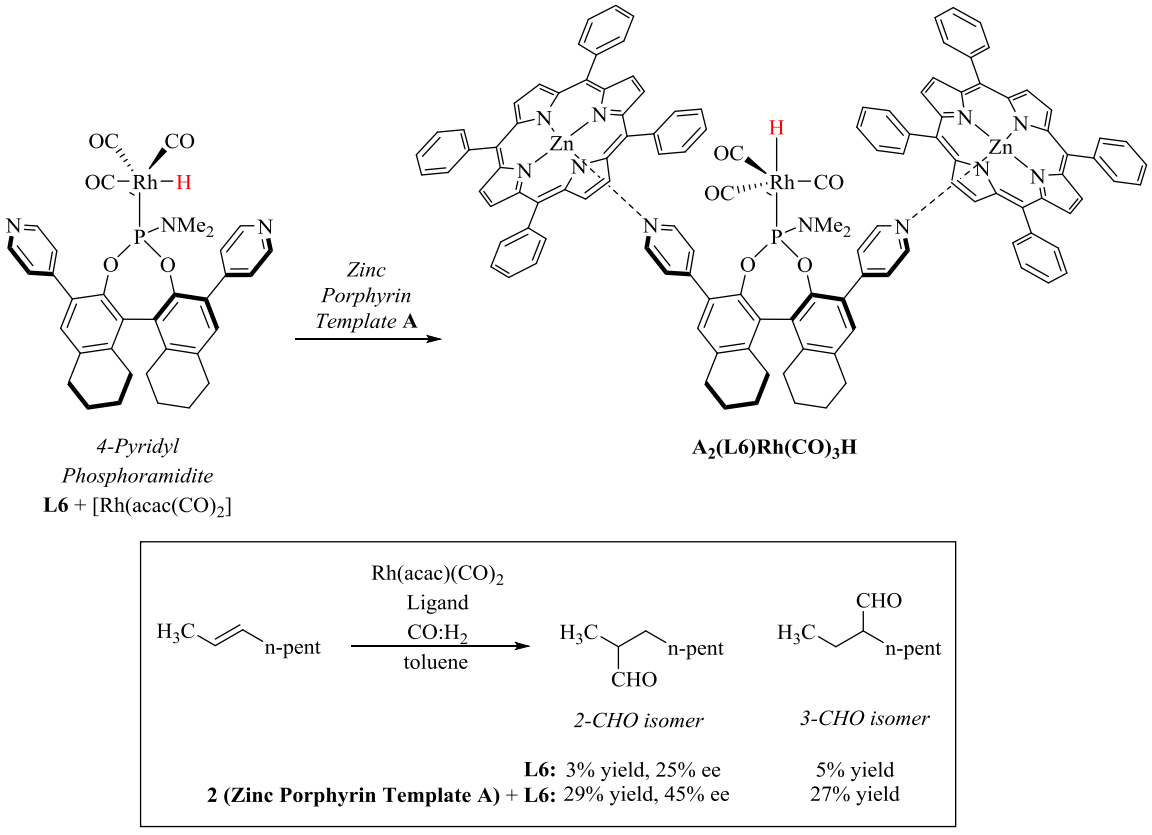

Figure 4 Zinc template influences geometry of hydride and its implications in asymmetric hydroformylation of styrene. Adapted from Ref 31with permission from John Wiley and Sons.

Takacs and coworkers were next publishing in this field and with a new approach of using a structural metal to bring two ligating groups together.[33-35] Bisoxazolines of complementary chirality combine with Zn(II) to form the thermodynamically favored heteroleptic complex nearly exclusively as judged by NMR (Figure 5A). [32] When bisoxazolines with substituted tethers and ligating groups are used, the resulting heteroleptic complex constitutes a chiral bidentate catalyst that has been generated by *in situ* metal-directed self-assembly. These catalysts have been used effectively in palladium-catalyzed asymmetric allylic amination,[33] rhodium-catalyzed asymmetric hydroboration,[34,35] and rhodium-catalyzed asymmetric hydrogenation.[36,37] Selected examples are shown in Figure 5.

For the Pd-catalyzed asymmetric allylic amination (Figure 5B), carrying out the corresponding reaction using the reference monodentate phosphite, (TADDOL)POPh afforded the substituted product with moderate enantioselectivity, 48% ee. Screening the reaction with a series of identically (TADDOL)P-functionalized scaffolds of incrementally varied structure afforded a range of selectivity from racemic to 82% ee.[33] The variation in selectivity noted for a large group of ligands with the same ligating groups gave rise to the idea of ligand (or catalyst) scaffold optimization. In analyzing the data, we find that scaffolds bearing two $ArCH_2O$- tethers generally afforded higher selectivity than tethers in which the (TADDOL)P-ligating groups were appended via ArO-linkages. In contrast, asymmetric hydroborations of styrene derivatives found ArO-linked tethers generally gave the higher enantioselectivity.[34,35] Again, as perhaps inferred by the term "ligand/catalyst scaffold optimization", we found that a different catalyst scaffold was required for optimum results with each *ortho*-substituted styrene suggesting

each substrate requires a slightly different catalyst pocket (or perhaps in analogy to biocatalysts, active site) for optimum results. Consider the following selected examples for the hydroborations of *ortho*-methoxystyrene and *ortho*-fluorostyrene: catalyst **L8** gives 99% ee for *ortho*-methoxystyrene but only 76% ee for *ortho*-fluorostyrene; catalyst **L9** gives 66% ee for *ortho*-methoxystyrene and 91% ee for *ortho*-fluorostyrene. The results indicate that very subtle changes to the substrate can significantly alter requirements for an effective catalyst structure.

The results obtained in the asymmetric hydrogenation studies (the subject of the studies reported in Chapter 2 of this thesis) revealed that like the Pd-catalyzed allylic aminations, use of $ArCH_2O$-linked tethers increases the efficiency and selectivity of a catalyst.[36,37] However, this study also uncovered that use of these tethers comes with a cost; the catalyst becomes too flexible and fail to respond to incremental catalyst scaffold optimizations (i.e., are difficult to optimize) when two $ArCH_2O$-linked phosphites are combined in the same scaffold. In those studies we find that catalyst scaffolds bearing one ArO- and one $ArCH_2O$-linked chiral phosphite provided a better balance between rigidity and flexibility (vide infra).

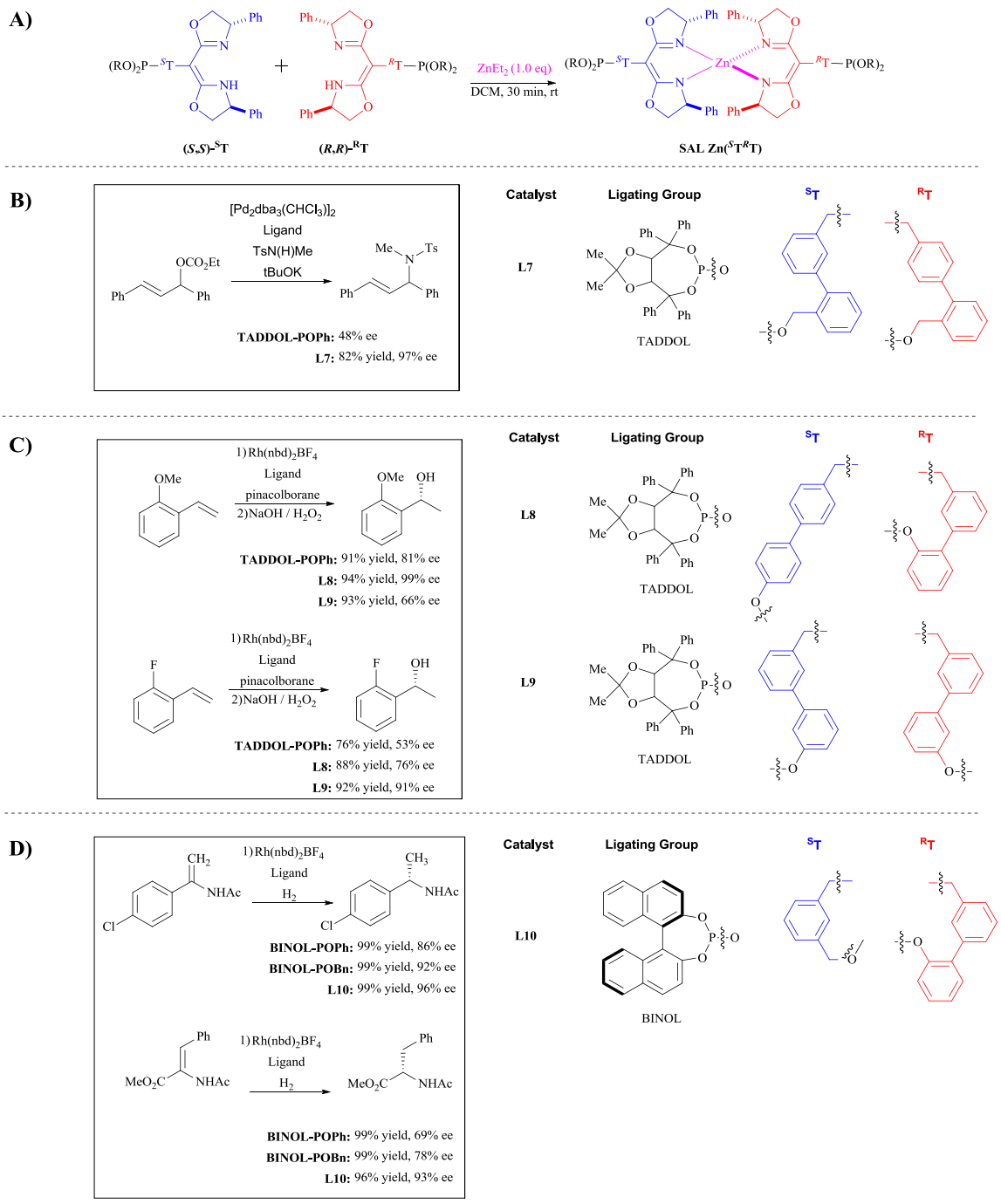

Figure 5 Selected examples of catalysis using Takacs supramolecular catalysts. A) Self-assembly of heteroleptic bisoxazoline-zinc complex affords heteroleptic complex.; B) Pd-catalyzed allylic alkylation affords product in increased selectivity.; C) Substrate tailored Rh-catalyzed asymmetric hydroboration of ortho-substituted styrenes.; D) Rh-catalzyed asymmetric hydrogenation of two substrates with a mixed ArO- and $ArCH_2O$- linked scaffold gives highest selectivity.

While the Takacs group has thus far been unable to obtain a crystal structure of their supramolecular catalyst, several studies to obtain some structural information of these supramolecular catalysts were conducted.[35] Circular dichroism (CD), an experiment which detects the differential absorption of left and right circularly polarized light was used to determine if any noticeable structural changes occurred with the addition of rhodium. The CD spectrum for a zinc-chelated self-assembled ligand shows a large bisignate curve with a zero-crossing around 316 nm (Figure 6A). Upon addition of rhodium, this bisignate curve is lost, suggesting a significant conformational change upon binding. High resolution fast atom bombardment (FAB) mass spectrometry found a peak consistent with the expected hetero-bimetallic complex. ^{31}P NMR data confirmed the data with expected $J_{Rh\text{-}P}$ couplings of 249 and 254 Hz and $J_{P\text{-}P}$ coupling of 38.8 Hz. DFT calculations using mixed basis sets (B3LYP/6-31G for non-metal atoms and B3LYP/LanL2DZ for metal atoms) were carried out to study the preliminary topography around rhodium. The models suggest that a chiral pocket may be formed around the catalytic center (Figure 6B).

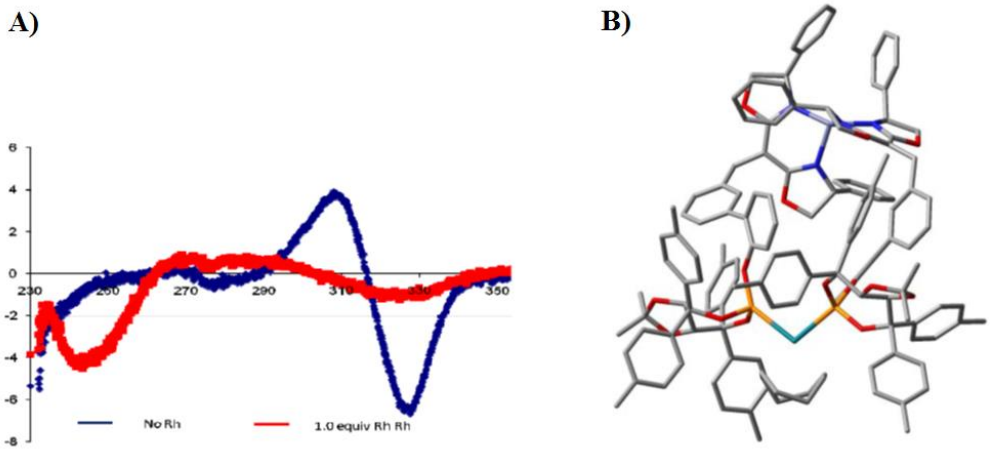

Figure 6 Structural characterization of Takacs' supramolecular catalyst. A) CD spectra indicates a structural change occurs from addition of rhodium to zinc-chelated self-assembled ligand. B) DFT model (B3LYP/6-31G for non-metal atoms and B3LYP/LanL2DZ for metal atoms) of supramolecular catalyst suggests a chiral pocket may form around catalytic site. Reproduced from Ref. 35 with permission from the Royal Society of Chemistry.

Van Leeuwen developed a new strategy using supramolecular interactions to relay chirality through an organizational metal to two achiral ditopic ligands. (Figure 7).[38] Combinations of phosphine-substituted Schiff bases and chiral diols self-assemble around titanium forming chiral bidentate ligands. The chiral TADDOL diol combined with achiral phosphine **L11** alone gave poor selectivity in the rhodium-catalyzed asymmetric hydrogenation reaction. In contrast, the titanium-assembled **L12** and **L13** afforded 81-87% ee. ^{1}H NMR characterization of the heterobimetallic complex [Rh(**L12**)(nbd)]BF_4 complex found distinct chemical shifts in equal intensities for the two imine and methoxy hydrogens; this suggests [Rh(**L12**)(nbd)]BF_4 exists as a single diastereomer (Figure 8). ^{31}P NMR data confirmed this conclusion with expected $J_{Rh\text{-}P}$ couplings of 159 and 151 Hz and $J_{P\text{-}P}$ coupling of 30.8 Hz. Furthermore, matrix-assisted laser desorption/ionization

(MALDI) mass spectrometry identified a peak corresponding to the expected mass of the [Rh(**L12**)(nbd)]BF_4.

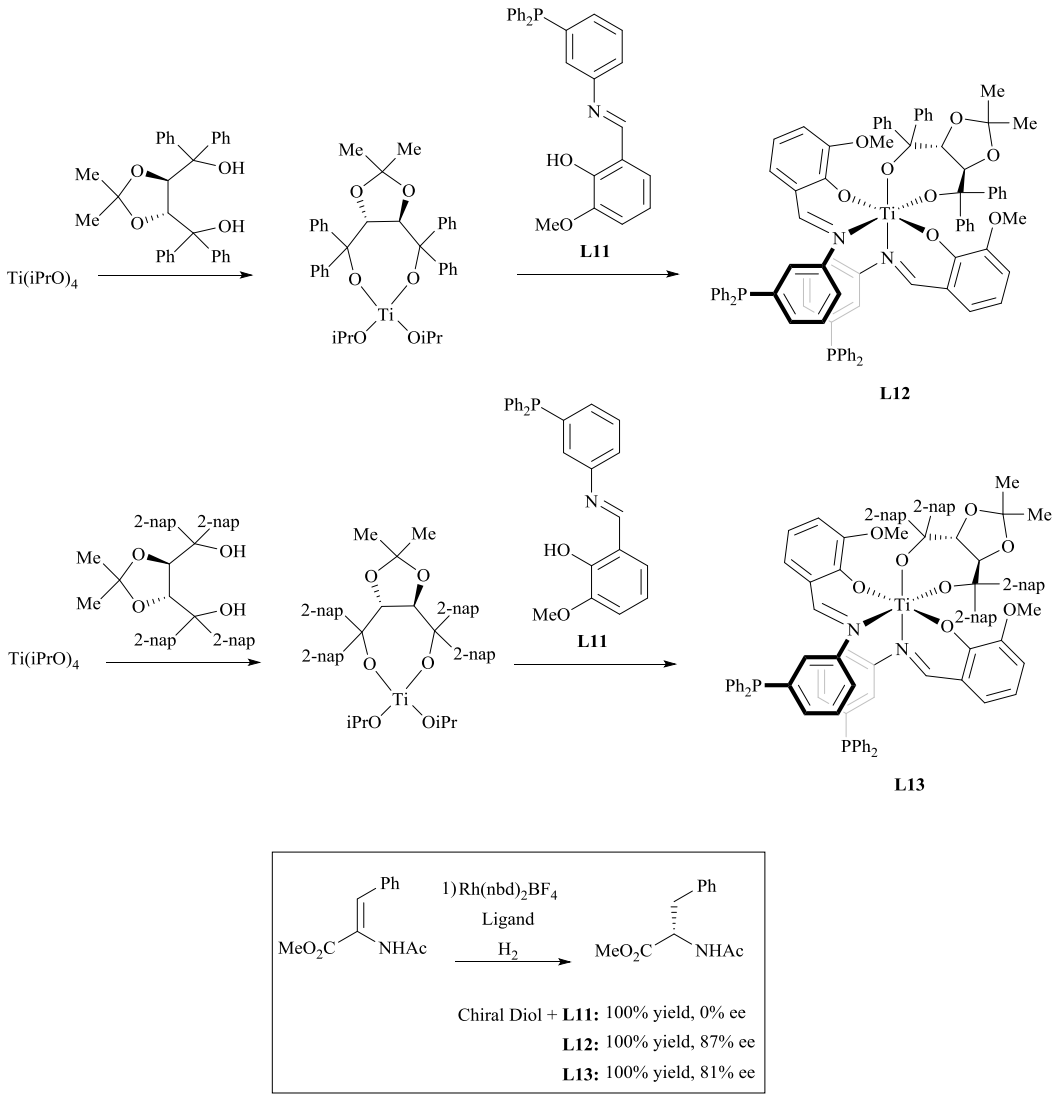

Figure 7 Rh-catalyzed asymmetric hydrogenation with a catalyst relying on transfer of chirality from a remote diol. Adapted with permission from *J. Am. Chem. Soc*. **2011**, *133*, 18562-18565. Copyright 2014 American Chemical Society

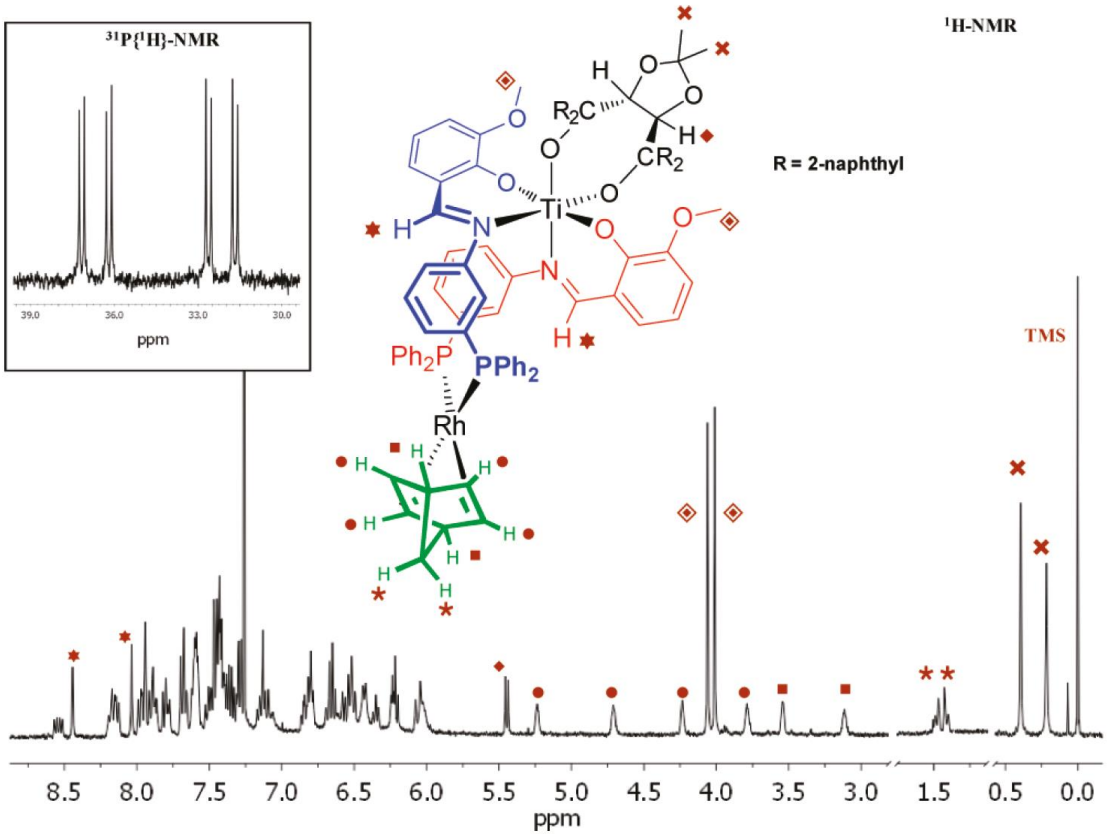

Figure 8 Supramolecular catalyst **L13** selectively forms one diastereomer upon chelation to rhodium as evidenced by H NMR and ^{31}P NMR. Reprinted with permission from *J. Am. Chem. Soc.* **2011**, *133*, 18562-18565. Copyright 2014 American Chemical Society

1.3 Homogeneous Organometallic catalysis – Supramolecular capsules and boxes with enclosed catalytically active site

Hupp and Nguyen designed a supramolecular "box" with an encapusultated or enclosed site for catalysis inside the box (Figure 9).[39] Zinc porphyrin templates (**T** or **T'**) bearing tin porphyrin bridging ligands (**A** or **C**) were used to form the outer walls that enclose a catalytically-active manganese porphyrin (**M**). Tin porphyrins were ligated by chiral N-acetyl protected phenylalanine to create a chiral environment around the

manganese active site. Conditions were reported under which the encapsulated catalyst could be assembled via a one-pot synthesis. Fluorescence spectroscopy was used to confirm the location of the manganese porphyrin as inside the assembly. The addition of manganese porphyrin to a solution of **AAT_4** results in fluorescence quenching from the surrounding zinc porphyrin; nearly complete quenching was observed at a 1:1 stoichiometry of **AAT_4** : **M**. While chiral assemblies **$CMCT_4$** and **$CMCT'_4$** gave only 12-14% ee for the asymmetric sulfur oxidation of methyl p-tolyl sulfide, the control reaction of manganese porphyrin **M** with N-acetyl-D-phenylalanine afforded completely racemic product. This supramolecular system is reportedly the first example of remote asymmetric induction from the surrounding environment of an achiral abiotic homogeneous catalyst.

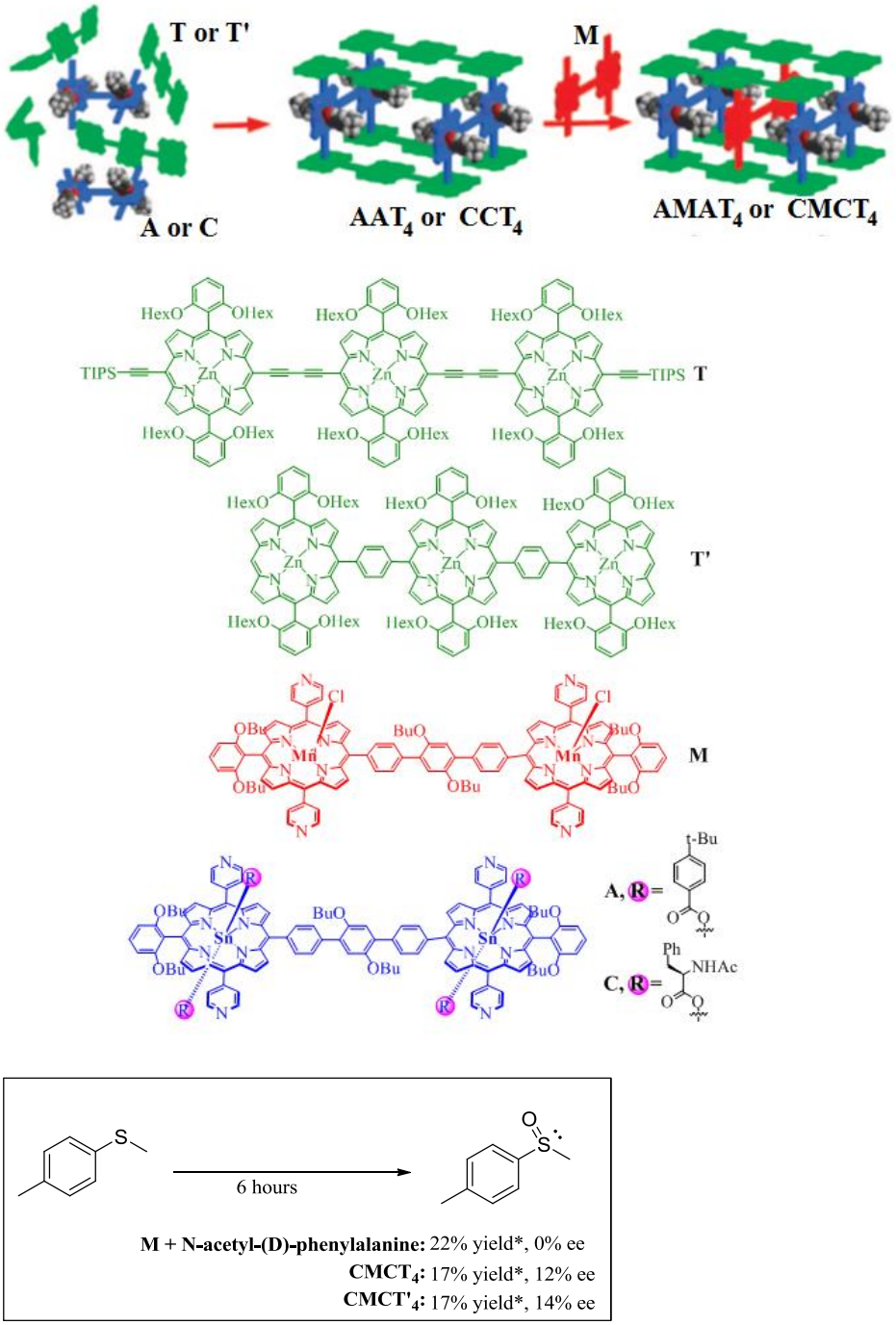

Figure 9 Enantioselective sulfoxidation reactions catalyzed by supramolecular porphyrin boxes. *Reactions were stopped <25% yields to compare reaction rates of oxidizing subunit M alone compared to when it is enclosed in supramolecular box. Reprinted with permission from *J. Am. Chem. Soc.* **2008**, *130*, 16828-16829. Copyright 2014 American Chemical Society

Reek devised a system to encapsulate a chiral bidentate phosphoramidite ligand inside a molecular "box" (Figure 10).[40] The zinc-salphen D was used as a template to coordinate with bispyridyl-substituted phosphoramidite ligand **L14**. Reek had previously reported a similar approach using an achiral catalyst to affect the regioselective hydroformylation of unfunctionalized alkenes. [41] Circular dichroism (CD) was used to monitor complexation of **L14** as titrated with zinc salphen **D**. A single inflection point in the series of CD spectra was observed after a 1:1 stoichiometry was reached; this suggests the formation of a discrete assembly that does not undergo any significant structural changes after the molecular box assembles. Diffusion-ordered NMR (DOSY),[42] an NMR technique used to approximate the hydrodynamic radius of a molecule in solution, was used to estimate a hydrodynamic radius of 1 nm; the result closely matches the dimension expected from the computational model for **L15**-Rh(acac) as determined using Spartan© PM3. The addition of rhodium acac affords the **L15**-Rh(acac) complex. Its ^{31}P NMR spectrum shows the expected doublet ($J_{P\text{-}Rh}$ = 290 Hz), and electrospray ionization mass spectrometry found a peak corresponding to the **L15**-Rh(acac) species.

L15-Rh(acac) catalyzed the asymmetric hydroformylation reaction of 2-octene demonstrating that the unusual catalyst systems could be used for the asymmetric hydroformylation reaction of an non-functionalized (i.e., lacking a strong directing groups) internal alkene. Due to alkene isomerization, obtaining high yields is challenging for these troublesome hydroformylation substrates.[41] Interactions with the supramolecular catalyst scaffold had little or no effect on the regioselectivity for *trans* 2-

octene, although an increase in enantioselectivity was observed for the reaction with the supramolecular catalyst compared to that with the chiral phosphoramidite **L15** alone (i.e., 72% to 22% ee). *Cis* 2-octene afforded more dramatic effects. The encapsulated catalyst **L15**-Rh(acac) favored formation of the 3-substituted carboxaldehyde isomer with a concurrent substantial increase in enantiomeric excess from 4% to 86% ee; however, the yields were low for the reasons stated above. When the reaction times were extended in an attempt to obtain more practical yields, a slight drop in regioselectivity and enantioselectivity was accompanied by the increase in yield. Starting from cis-2-octene, (S)-2-ethylheptanal was formed in 57% yield and 76% ee.

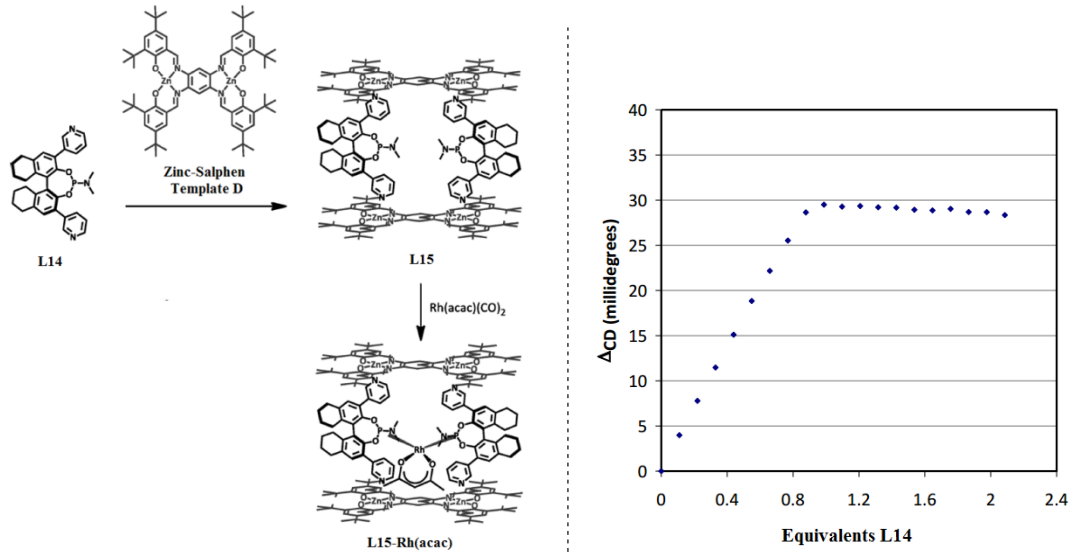

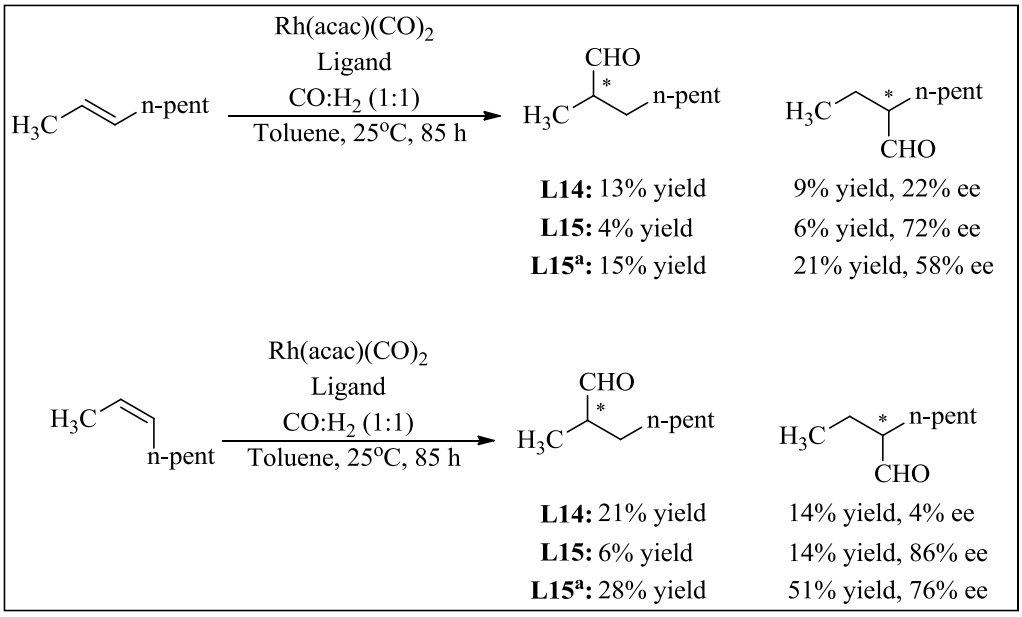

Figure 10 Self-assembly of a confined chiral rhodium catalyst for the asymmetric hydroformylation of unfunctionalized alkenes. [a]At 40°C for 5 days. Adapted with permission from *J. Am. Chem. Soc.* **2012**, *134*, 2860-2863. Copyright 2014 American Chemical Society

1.4 Homogeneous Organometallic catalysis – Self-assembly of supramolecular nanovessels for asymmetric catalysis

A number of research groups have pursued the idea that supramolecular assemblies could also function as a "nanovessel" or "molecular flask." Encapsulated guests might be forced to adopt a preferred reactive confirmation once confined inside the vessel. If the nanovessel is chiral, it might promote enantioselective catalysis inside the vessel; Bergman and Raymond have reported the only two examples of using host-assemblies to catalyze an enantioselective transformation (Figure 11).[43,44] [44] It should be noted that Fujita also reported a [2+2] cycloaddition promoted by a chiral supramolecular assembly, but a stoichiometric equivalent of catalyst was required.[45] Bergman and Raymond's supramolecular assemblies possess a well-defined cavity for guest recognition and encapsulation and function well in aqueous environments.[46-53] The clusters are assembled via coordination of six bis(catecholate)-functionalized ligands with four gallium metals; three catecholate groups coordinate to each gallium ion in an octahedral arrangement possessing either a right(Δ)- or left(Λ)-handed helicity at the metal center (Figure 11A).[54] Racemic **L16** was resolved with (S)-*N*-methylnicotinium iodide. Ion exchange chromatography with tetramethyl ammonium and potassium iodide salts affords the "empty" resolved host rendering it capable of exchange with a cationic substrate.[55] CD spectra of the resolved hosts show the expected two mirrored images. ΔΔΔΔ-**L16** was shown to promote a simple, but quite remarkable, aza-cope rearrangement in up to 64% ee and up to 74% yield (Figure 11A). This was an especially

significant conceptual advance since the cavity bears no specific identifiable coordinating groups to influence the selectivity; yet the reaction shows some selectivity.

Bergman, Toste, and Raymond recently reported a more robust nanovessel for asymmetric catalytic rearrangements with neutral substrates (Figure 11B).[44] Modifying the vertices of the bis(catecholate) ligand with chiral amide directing groups accomplishes two purposes: 1) The hydrogen-bonding interaction between the amide N-H and the catecholate oxygen gives the structure more strength; and 2) The chiral amide is capable of promoting chiral self-assembly eliminating the need for classical resolution. Using the tether derived from *(R)*-(-)-3,3-dimethyl-2-butyl amine affords the ΔΔΔΔ-**L17** host, while its antipode gives the ΛΛΛΛ -**L17** host. The CD-spectrum of ΔΔΔΔ-**L17** and ΛΛΛΛ -**L17** were mirror images of one another. The absolute configuration of ΔΔΔΔ-**L17** was determined by X-ray crystallography which clearly indicated the presence of hydrogen-bonding between the amide NH and catecholate at the vertices. The pure enantiomers incorporate 12 potassium ions capable of rapidly exchanging with guest molecules. Stereochemical analysis by ^{1}HNMR after the addition of a chiral ammonium guest molecule further confirmed the enantiomeric purity of the capsules. Inclusion of an enantiopure guest molecule to each enantiomer of **L17** afforded two different complexes as judged from their distinctly different ^{1}HNMR spectra due to diastereomeric interactions.

The catalyzed carbonyl-ene cyclization of a simple monoterpenoid substrate was examined with chiral hosts **L16** and **L17**. Chiral host **L16**, which had been designed for a cationic guest molecule, did not catalyze the carbonyl-ene cyclization of the monoterpenoid substrate. This suggests no reaction occurs outside or on the surface of the

nanovessels; the latter point can be problematic and difficult to assess. The two enantiomers of **L17,** ΔΔΔΔ-**L17** and ΛΛΛΛ -**L17,** afforded products in similarly high yield (92-94%) and matching diastereoselectivity and enantiopurity, but opposite configuration.

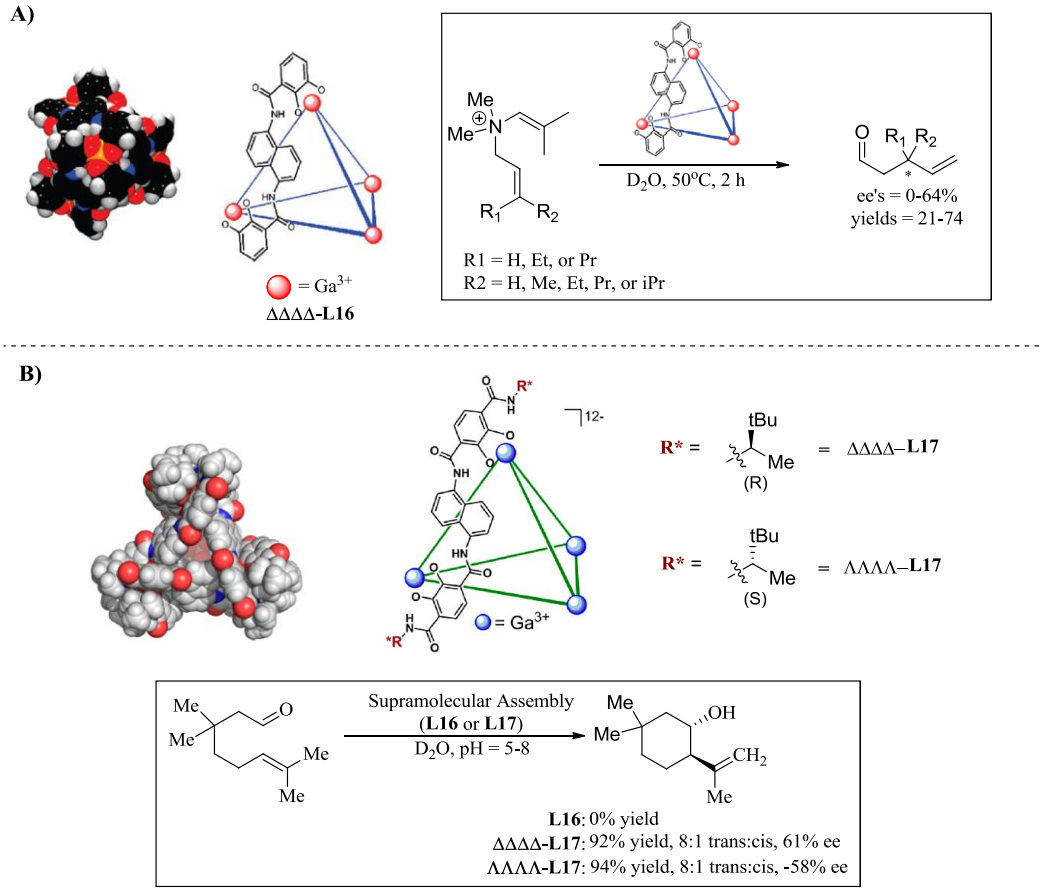

Figure 11 Chiral supramolecular host chemistry and its application to enantioselective catalysis of charged and neutral substrates. A) Space filling model of **L17** and the first reported example of a chiral host used in catalytic amounts catalyzing an asymmetric reaction (the Aza-Cope rearrangement) Adapted with permission from *J. Am. Chem. Soc.* **2009**, *131*, 17530-17531. Copyright 2014 American Chemical Society; B) Crystal structure of **L18** and application in enantioselective monoterpene-like cyclization of neutral substrates. Adapted with permission from *J. Am. Chem. Soc.* **2013**, *135*, 18802-18805. Copyright 2014 American Chemical Society

1.5 Heterogeneous Organometallic catalysis – metal-organic frameworks (MOFs)

Metal-organic frameworks (MOFs) are porous three-dimensional coordination polymers composed of organic bridging ligands and inorganic connecting points; while MOF catalysts are often considered separately from supramolecular catalyst systems, it seems more fitting to include them in this summary of recent advances in supramolecular asymmetric catalysts. Incorporating chirality and a catalytically active site in the bridging ligands transforms the MOF into a (supramolecular) heterogeneous asymmetric catalyst. These pores inside the MOF are capable of enzyme-like shape- and size- selectivity altered by modifying the bridging ligands, often done in a combinatorial fashion. A pore too large often fails induce chirality to the catalytic reaction, while a pore too narrow or small limits substrate access. Some benefits to using MOFs for asymmetric catalysis over traditional homogenous catalysts are their reusability, often lower tendency toward catalyst deactivation, and in ideal cases enzyme-like substrate size selectivity. Although the first report of MOFs use as asymmetric catalysts was less than 20 years ago, the burgeoning field has advanced significantly for both organocatalyzed and metal-catalyzed reactions.[56-58]

The first generation of asymmetric MOF catalysts tried to exploit induction from an inorganic coordination sphere to a remote achiral catalytic site (Figure 12A). Independently, Kim [59] and Lin[60] reported similar strategies in 2000-2001. In Kim's report, the chiral MOF **D-POST-1** was synthesized from tartaric acid-derived ligands with zinc at the connecting points (Figure 12B). X-ray crystallography revealed the void volume of the channels makes up 47% of the total volume, and 47 water molecules were found in each unit cell. The use of **D-POST-1** to catalyze the esterification of racemic 1-

phenyl-2-propanol afforded the esterified product in 8% ee. Although the enantiomeric excess was low, this publication demonstrated for the first time the use of a chiral MOF in an asymmetric transformation.

Eight years after Kim's first report, Tanaka reported modest selectivity could be obtained with a chiral MOF catalyst using the strategy of chiral relay.[61] Slow diffusion of the chiral bridging ligand 2,2'-dihydroxyl-1,1'-binaphthalene-1,1'-dicarboxylic acid (**L18**) with $Cu(NO_3)_2$ formed the chiral MOF $[Cu_2(\mathbf{L18})_2(H_2O)_2] \bullet MeOH \bullet 2H_2O$ (Figure 12C). Single crystal X-ray diffraction found that the four carboxylate oxygen atoms are each coordinated to the Cu(II) ion. Thermogravimetric analysis (TGA) found 19% of its mass was lost upon heating from 25-to-120 °C; this is attributed to loss of entrapped solvent molecules. Removal of the guest solvent molecules *in vacuo* converted the crystalline MOF into an amorphous solid as shown by X-Ray powder diffraction; however, crystallinity could be regained upon exposure to solvent vapor. The MOF was used in the asymmetric epoxide ring-opening of cyclohexene and cyclopentene oxides with aromatic amines. In a neat solution of amine and epoxide, MOF $[Cu_2(\mathbf{L18})_2(H_2O)_2]$ catalyzed the reaction giving the product in 51% yield and 51% ee. Hydrogen-bond donors such as BINOL have been shown to participate in organocatalyzed epoxide openings.[62] As a control experiment, the authors found that, while addition of *(S)*-BINOL to a mixture of amine and epoxide afforded ring-opened product, the 3% yield of product obtained was nearly racemic. The poor selectivity from the BINOL control reaction was interpreted as indicating that chirality form the BINOL subunits was relayed to the copper paddlewheels which were the sites responsible for catalyzing the

enantioselective epoxide opening. An alternative explanation is cooperative participation from the BINOL chiral hydrogen-bond donor and the Lewis acidic Cu center. To distinguish whether the catalysis was occurring inside the pores or on the surface, bulky arylamine nucleophiles, reactants that presumably cannot access the MOF pore interiors, were examined; aromatic amines with an *ortho*-methyl or *para*-methyl gave nearly racemic products and in much lower yield (i.e., 3-13%).

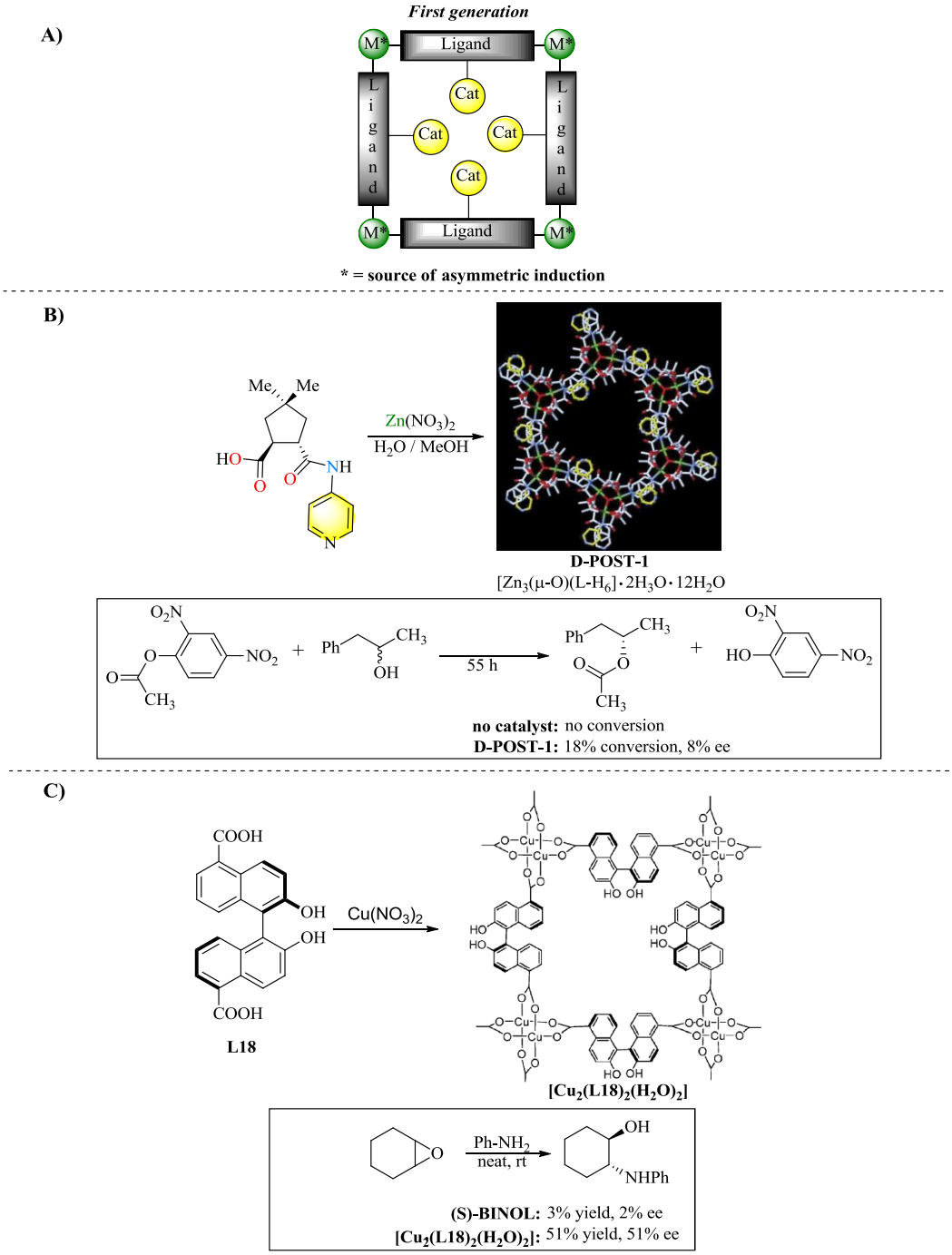

Figure 12 First generation of metal-organic frameworks use as asymmetric catalyst. A) General strategy using chiral relay to remote catalytically active site. B) Kim's tartrate-derived MOF and its use in the resolution of racemic alcohols. Reproduced from Ref 59 with permission from Nature Publishing Group C) Tanaka's BINOL derived bridging ligand forms MOFs and its use in the asymmetric ring-opening of meso-epoxides. Reproduced from Ref 61 with permission from Royal Society of Chemistry

In the second generation of MOF catalysts, the bridging ligand was used to immobilize a successful homogenous catalyst asking the question, how does incorporation inside a MOF influence catalyst reactivity (Figure 13A). Lin and co-workers immobilized ruthenium BINAP-derived catalysts on a porous zirconium amorphous surface with great success (Figure 13B).[63] X-ray powder diffraction confirmed **L19**-Ru-Zr was amorphous. IR spectra exhibit O-H stretching vibrations consistent the presence of MeOH solvates, and thermogravimetric analysis (TGA) confirmed the presence of solvates resulting in a ca. 20% loss of mass from when heated from 20-to-200 °C. Ru-BINAP-DPEN, the homogeneous analogue of **L19**-Ru-Zr, gives 80% ee in the hydrogenation of acetophenone.[64,65] Under similar conditions, **L19**-Ru-Zr affords the product in 96% ee; a series of ketones were studied and all afforded >90% ee (see reference 63). To examine the durability of this heterogeneous catalyst, **L19**-Ru-Zr was recycled; the catalyst was reused eight times with no decrease in selectivity, although after the sixth recycle, the reaction did not go to completion. Similar strategies in homogeneous catalyst immobilization were reported by Hupp for immobilizing a manganese epoxidation catalyst.[66]

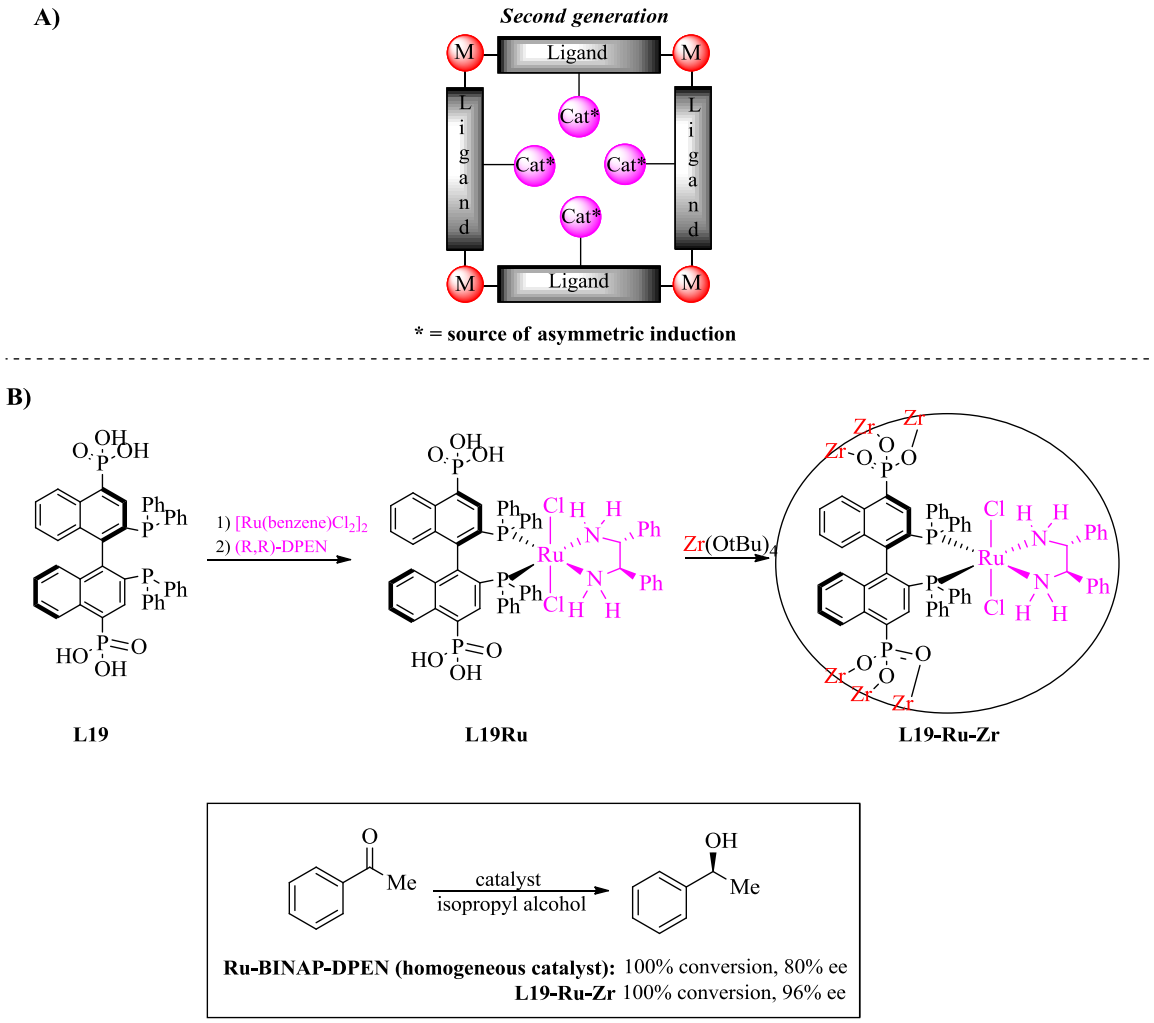

Figure 13 Second generation of metal-organic frameworks use as asymmetric catalyst. A) General strategy immobilizing chiral ligating groups into scaffold of MOFs. B) Lin's immobilization of Ru-BINAP-DPEN in a porous zirconium solid affords higher selectivity than homogeneous analogue. Reproduced from Ref 63 with permission from John Wiley and Sons.

Post-synthetic modification of a chiral MOF is a powerful new strategy that relies on incorporating orthogonally bifunctional groups bridging ligands (Figure 14A). Lin demonstrated this idea in a MOF assembled from pyridine-substituted BINOL derivative **L20** and Cd(II) ions (Figure 14B).[67] Single crystal x-ray crystallography found three

Cd(II) ions, six chloride ions, and three **L20** ligands in the unit cell. The diameter of the channels inside the MOF were large (1.6 x 1.8 nm across); PLATON calculations found 54% void space accessible to guests. Two-thirds of the BINOL ligands were found H-bonding with neighboring unit cells limiting their availability for post-synthetic modification. Nonetheless, added $Ti(OiPr)_4$ was found to react with the one-third of available chiral diols. This strategy was studied further with a series of MOFs composed of tetra-substituted BINOL derivatives.[68] The BINOL derivatives were functionalized with carboxylate-terminated tethers of varying lengths. Carboxylate-bridged copper paddlewheels were formed upon addition of copper(II) leaving the diols available for sequential $Ti(OiPr)_4$ addition. Crystal structures of a series of model MOFs (that is, methyl ether derivatives of diols) found the approximate void space to vary 69-90% dependent on tether length. To evaluate effectiveness of these functionalized MOFs in catalysis, the Lewis acid catalyzed addition of alkyl zincs to aldehydes was explored. The homogeneous catalyst derived from BINOL afforded the product in 88% ee. MOFs derived from **L20** and **L22-24** afforded 82-84% ee with similar conversions to the homogenous catalyst. Only the MOF derived from **L21** gave poor selectivity; this was attributed to the pore size being too small resulting only in non-selective surface catalysis. Similar results were found when substrates larger than acetophenone were used; they gave low selectivity and low yields.

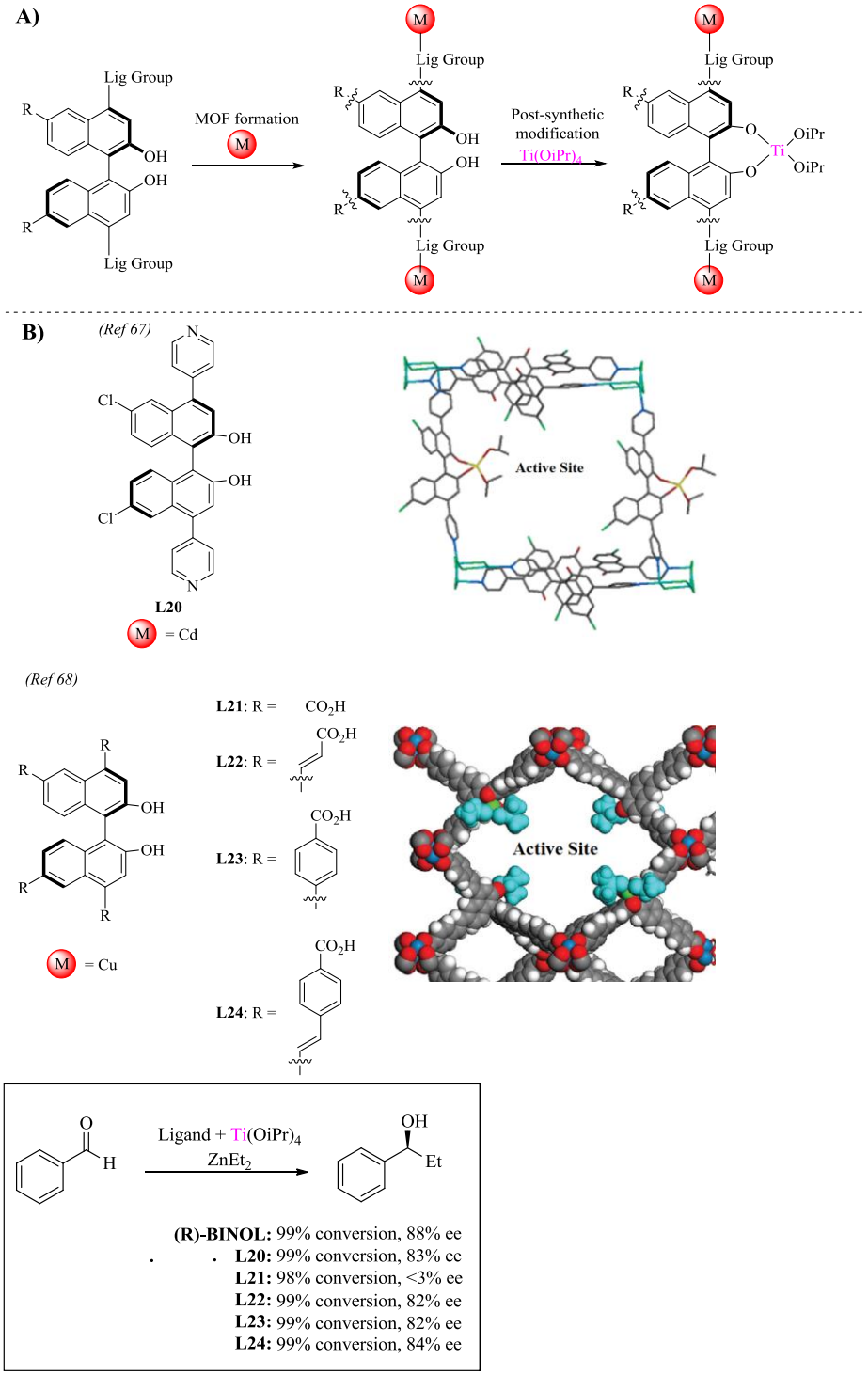

Figure 14 Tunable MOFs for asymmetric catalysis. Adapted with permission from *J. Am. Chem. Soc.* **2005**, *127*, 8940-8041. Copyright 2014 American Chemical Society. Reproduced from Ref 68 with permission from Nature Publishing Group.

Due to the crystalline nature of many MOFs, some details of their active sites are more accessible by crystallography than typically is obtained for homogeneous catalysts. In the course of their structure-activity studies, Lin and co-workers analyzed a MOF catalyst that gave low selectivity (ca 30% ee) in the titanium-catalyzed addition of alkyl zinc to aldehydes (Figure 15).[69] X-ray diffraction studies revealed substantial intermolecular BINOL-chelation that seems to account for the poorly selective catalyst.

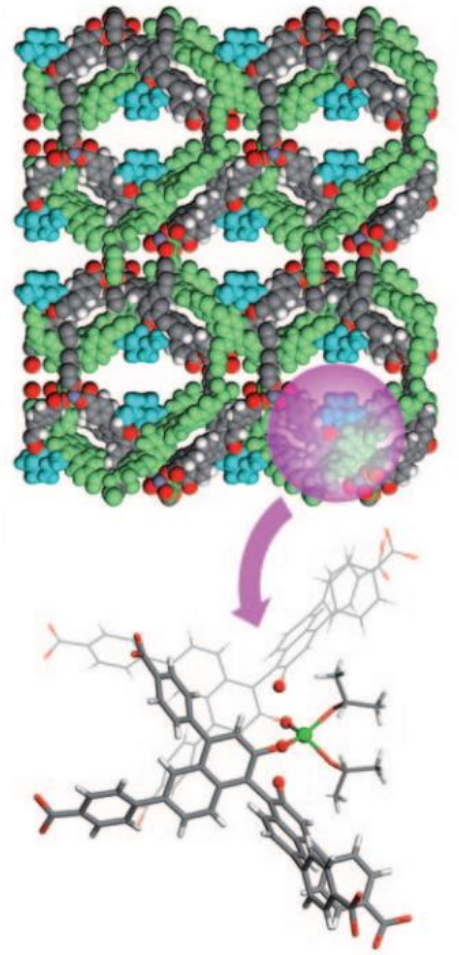

Figure 15 Interpenetrated networks form non-selective catalysts. Reproduced from Ref 69 with permission from John Wiley and Sons.

1.6 Heterogeneous Organometallic catalysis – Heterobimetallic polymers

Supramolecular polymers are chains of monomeric units held together by non-bonding forces.[71] When catalytically active functional groups are built into the monomeric subunits, the supramolecular polymer affords a heterogeneous catalyst. Ding and co-workers recently reported a series of heterobimetallic polymeric catalysts that show promise for rhodium-catalyzed asymmetric hydrogenation (Figure 16A).[75] MonoPhos (i.e., (BINOL)$PNMe_2$) and a 2,2':6',2"-terpyridine unit were connected by an alkyne linker. Upon the addition of Fe^{2+} salts, the Fe-bridged bis(MonoPhos) ligand structures were formed. Their structures were characterized by UV/Vis, IR, elemental analysis, and high resolution mass spectrometry. When cationic rhodium(I) was added to a solution of iron complex in dichloromethane, a solid precipitated from solution. Its analysis by powder x-ray diffraction showed the particles to be amorphous and by scanning electron microscope to be micron-sized. A series of heterogeneous catalysts with varying counterions were similarly prepared and isolated. As a model reaction these heterobimetallic oligomer or polymer catalysts were screened in heterogeneous asymmetric hydrogenation (Figure 16B). For the substrates examined, **L25** was found to be both remarkably reactive and selective, proving superior to even the homogeneous rhodium catalyst prepared with the chiral monodentate MonoPhos ligand. Furthermore, **L25** could be recycled more than ten times with no loss in catalytic activity or selectivity.

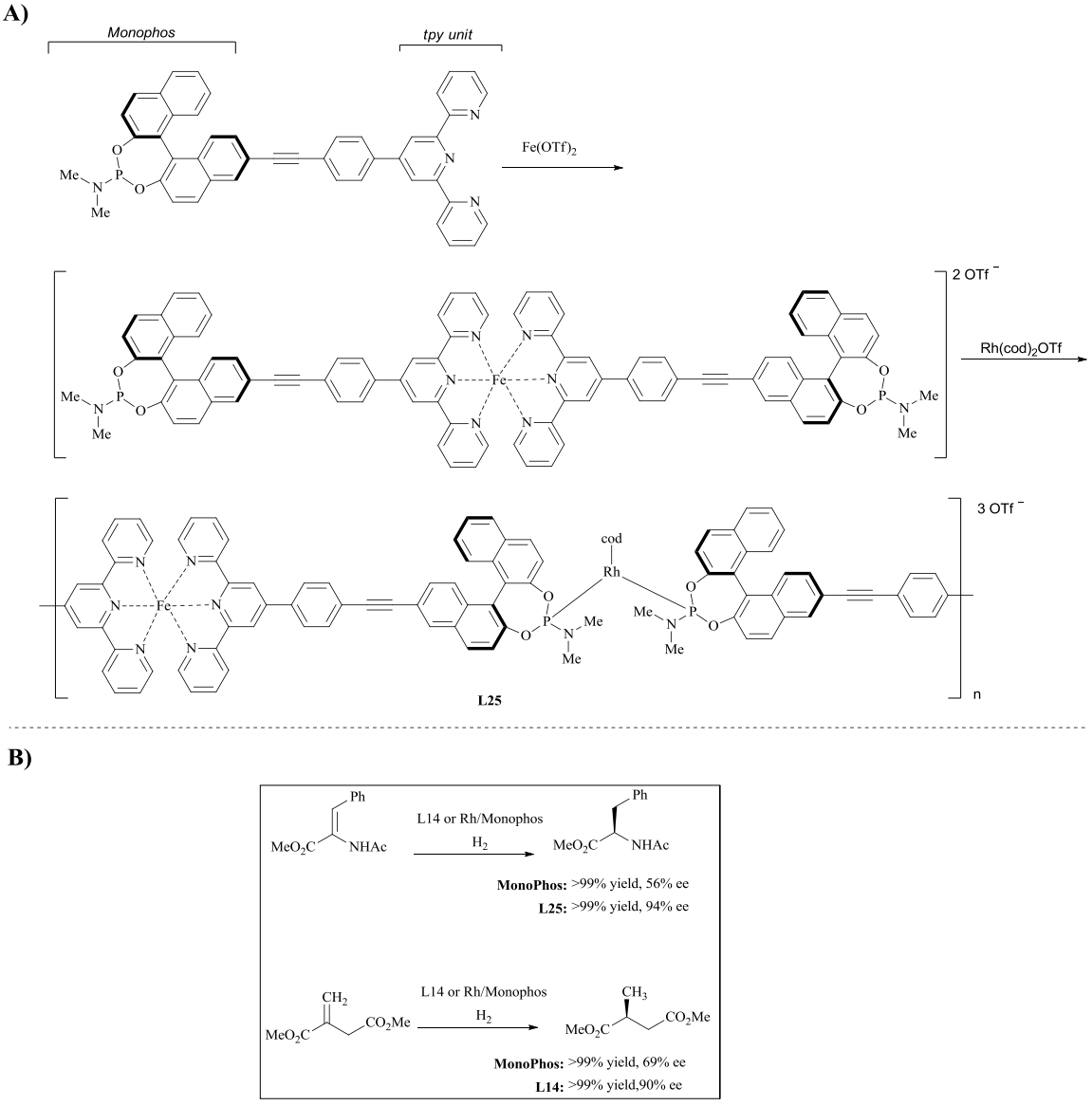

Figure 16 Formation of a heterobimetallic heterogeneous catalyst. A) Preparation via sequential addition; B) Asymmetric hydrogenation using heterogeneous catalyst gives excellent selectivity compared to monodentate ligand. Adapted from Ref 75 with permission from John Wiley and Sons.

1.7 Conclusions and future outlook

Computational modeling has yet to reach the point where it is feasible to design *a priori* an efficient tailor-made asymmetric catalyst. Thus catalyst development still requires novel discovery strategies and some luck to find successful hits. Supramolecular approaches to catalyst discovery is still a young field, but the results reported to date demonstrate some benefits through combinatorial synthesis and control of the active site topography that remains difficult using the traditional approaches involving monodentate or covalently-linked ligands.

Where does the field of supramolecular asymmetric catalysis go next? Cragg, Grothaus, and Newman analyzed the sources of new drugs (for human consumption) for the treatment of diseases from 1998-2008, a total of 1024 compounds.[76] Remarkably, while 57% of the drugs were either synthetically modified or inspired from the structures of natural products, only 6% were the actual isolated natural product itself. The ability to modify a polyfunctional natural product, that is, the post-synthetic modification of a natural product, is one direction for developing chemical transformations by supramolecular catalysis. The challenge lies in building enzyme-like site-specific selectivity at a targeted site in a polyfunctional molecule.[77] Scott Miller and co-workers have reported a series of small peptide catalysts for site-selective transformations on challenging natural product substrates.[78-82] Exploiting the control of active site topography and/or binding pocket accessibility to successfully target site-selective reactions on a complex natural product would add significant value to supramolecular catalysis.

A second area, identifying new reaction pathways, could be productively addressed with the right supramolecular catalyst. For example, David MacMillan recently discovered conditions for a new α-amino C-H arylation reaction from "reaction discovery screening."[83] Using the reaction discovery approach in a controlled supramolecular combinatorial screen for new reactions seems a likely and exciting future direction for the field.

1.8 References

1. Ringe, D.; Petsko, G. A. How enzymes work. *Science (Washington, DC, U. S.)* **2008**, *320*, 1428-1429.

2. Breit, B. Supramolecular approaches to generate libraries of chelating bidentate ligands for homogeneous catalysis. *Angew. Chem. , Int. Ed.* **2005**, *44*, 6816-6825.

3. Karakhanov, E. A.; Maksimov, A. L.; Runova, E. A. Design of supramolecular metal complex catalytic systems for organic and petrochemical synthesis. *Russ. Chem. Rev.* **2005**, *74*, 97-111.

4. Gasparini, G.; Dal Molin, M.; Prins, L. J. Dynamic Approaches towards Catalyst Discovery. *Eur. J. Org. Chem.* **2010**, 2429-2440.

5. Meeuwissen, J.; Reek, J. N. H. Supramolecular catalysis beyond enzyme mimics. *Nat. Chem.* **2010**, *2*, 615-621.

6. Chakrabarty, R.; Mukherjee, P. S.; Stang, P. J. Supramolecular Coordination: Self-Assembly of Finite Two- and Three-Dimensional Ensembles. *Chem. Rev. (Washington, DC, U. S.)* **2011**, *111*, 6810-6918.

7. Carboni, S.; Gennari, C.; Pignataro, L.; Piarulli, U. Supramolecular ligand-ligand and ligand-substrate interactions for highly selective transition metal catalysis. *Dalton Trans.* **2011**, *40*, 4355-4373.

8. Deuss, P. J.; den Heeten, R.; Laan, W.; Kamer, P. C. J. Bioinspired catalyst design and artificial metalloenzymes. *Chem. - Eur. J.* **2011**, *17*, 4680-4698.

9. Wiester, M. J.; Ulmann, P. A.; Mirkin, C. A. Enzyme Mimics Based Upon Supramolecular Coordination Chemistry. *Angew. Chem. , Int. Ed.* **2011**, *50*, 114-137.

10. Dong, Z.; Luo, Q.; Liu, J. Artificial enzymes based on supramolecular scaffolds. *Chem. Soc. Rev.* **2012**, *41*, 7890-7908.

11. Bellini, R.; van der Vlugt, J. I.; Reek, J. N. H. Supramolecular self-assembled ligands in asymmetric transition metal catalysis. *Isr. J. Chem.* **2012**, *52*, 613-629.

12. Briere, J.; Oudeyer, S.; Dalla, V.; Levacher, V. Recent advances in cooperative ion pairing in asymmetric organocatalysis. *Chem. Soc. Rev.* **2012**, *41*, 1696-1707.

13. Kumagai, N.; Shibasaki, M. Catalytic chemical transformations with conformationally dynamic catalytic systems. *Catal. Sci. Technol.* **2013**, *3*, 41-57.

14. Ballester, P.; Vidal-Ferran, A.; van Leeuwen, P. W. N. M. Modern strategies in supramolecular catalysis. *Adv. Catal.* **2011**, *54*, 63-126,, 6 plates.

15. Seo, J. S.; Whang, D.; Lee, H.; Jun, S. I.; Oh, J.; Jeon, Y. J.; Kim, K. A homochiral metal-organic porous material for enantioselective separation and catalysis. *Nature (London)* **2000**, *404*, 982-986.

16. Ingleson, M. J.; Barrio, J. P.; Bacsa, J.; Dickinson, C.; Park, H.; Rosseinsky, M. J. Generation of a solid Bronsted acid site in a chiral framework. *Chem. Commun. (Cambridge, U. K.)* **2008**, 1287-1289.

17. Vaidhyanathan, R.; Bradshaw, D.; Rebilly, J.; Barrio, J. P.; Gould, J. A.; Berry, N. G.; Rosseinsky, M. J. A family of nanoporous materials based on an amino acid backbone. *Angew. Chem. , Int. Ed.* **2006**, *45*, 6495-6499.

18. Banerjee, M.; Das, S.; Yoon, M.; Choi, H. J.; Hyun, M. H.; Park, S. M.; Seo, G.; Kim, K. Postsynthetic Modification Switches an Achiral Framework to Catalytically Active Homochiral Metal-Organic Porous Materials. *J. Am. Chem. Soc.* **2009**, *131*, 7524-7525.

19. Ferey, G.; Mellot-Draznieks, C.; Serre, C.; Millange, F. Crystallized Frameworks with Giant Pores: Are There Limits to the Possible?. *Acc. Chem. Res.* **2005**, *38*, 217-225.

20. Falck, J. R.; Kodela, R.; Manne, R.; Atcha, K. R.; Puli, N.; Dubasi, N.; Manthati, V. L.; Capdevila, J. H.; Yi, X.; Goldman, D. H.; Morisseau, C.; Hammock, B. D.; Campbell, W. B. 14,15-Epoxyeicosa-5,8,11-trienoic Acid (14,15-EET) Surrogates

Containing Epoxide Bioisosteres: Influence upon Vascular Relaxation and Soluble Epoxide Hydrolase Inhibition. *J. Med. Chem.* **2009**, *52*, 5069-5075.

21. Wang, M.; Xie, M.; Wu, C.; Wang, Y. From one to three: a serine derivate manipulated homochiral metal-organic framework. *Chem. Commun. (Cambridge, U. K.)* **2009**, 2396-2398.

22. Dang, D.; Wu, P.; He, C.; Xie, Z.; Duan, C. Homochiral Metal-Organic Frameworks for Heterogeneous Asymmetric Catalysis. *J. Am. Chem. Soc.* **2010**, *132*, 14321-14323.

23. Lun, D. J.; Waterhouse, G. I. N.; Telfer, S. G. A General Thermolabile Protecting Group Strategy for Organocatalytic Metal-Organic Frameworks. *J. Am. Chem. Soc.* **2011**, *133*, 5806-5809.

24. Slagt, V. F.; van Leeuwen, P. W. N. M.; Reek, J. N. H. Bidentate ligands formed by self-assembly. *Chem. Commun. (Cambridge, U. K.)* **2003**, 2474-2475.

25. Goudriaan, P. E.; Jang, X.; Kuil, M.; Lemmens, R.; Van Leeuwen, P. W. N. M.; Reek, J. N. H. Synthesis of building blocks for the development of the SUPRAPhos ligand library and examples of their application in catalysis. *Eur. J. Org. Chem.* **2008**, 6079-6092.

26. Goudriaan, P. E.; Kuil, M.; Jiang, X.; van Leeuwen, P. W. N. M.; Reek, J. N. H. SUPRAPhos ligands for the regioselective rhodium catalyzed hydroformylation of styrene forming the linear aldehyde. *Dalton Trans.* **2009**, 1801-1805.

27. Jiang, X.; Lefort, L.; Goudriaan, P. E.; de Vries, A. H. M.; van Leeuwen, P. W. N. M.; de Vries, J. G.; Reek, J. N. H. Screening of a supramolecular catalyst library in the search for selective catalysts for the asymmetric hydrogenation of a difficult enamide substrate. *Angew. Chem. , Int. Ed.* **2006**, *45*, 1223-1227.

28. Slagt, V. F.; Roeder, M.; Kamer, P. C. J.; Van Leeuwen, P. W. N. M.; Reek, J. N. H. Supraphos: A Supramolecular Strategy To Prepare Bidentate Ligands. *J. Am. Chem. Soc.* **2004**, *126*, 4056-4057.

29. Reek, J. N. H.; Roeder, M.; Goudriaan, P. E.; Kamer, P. C. J.; Van Leeuwen, P. W. N. M.; Slagt, V. F. Supraphos: A supramolecular strategy to prepare bidentate ligands. *J. Organomet. Chem.* **2005**, *690*, 4505-4516.

30. Bernsmann, H.; van den Berg, M.; Hoen, R.; Minnaard, A. J.; Mehler, G.; Reetz, M. T.; de Vries, J. G.; Feringa, B. L. PipPhos and MorfPhos: Privileged Monodentate Phosphoramidite Ligands for Rhodium-Catalyzed Asymmetric Hydrogenation. *J. Org. Chem.* **2005**, *70*, 943-951.

31. Bellini, R.; Chikkali, S. H.; Berthon-Gelloz, G.; Reek, J. N. H. Supramolecular Control of Ligand Coordination and Implications in Hydroformylation Reactions. *Angew. Chem. , Int. Ed.* **2011**, *50*, 7342-7345, S7342/1-S7342/51.

32. Takacs, J. M.; Hrvatin, P. M.; Atkins, J. M.; Reddy, D. S.; Clark, J. L. The selective formation of neutral, heteroleptic zinc(II) complexes via self-discrimination of chiral bisoxazoline racemates and pseudoracemates. *New J. Chem.* **2005**, *29*, 263-265.

33. Takacs, J. M.; Reddy, D. S.; Moteki, S. A.; Wu, D.; Palencia, H. Asymmetric Catalysis Using Self-Assembled Chiral Bidentate P,P-Ligands. *J. Am. Chem. Soc.* **2004**, *126*, 4494-4495.

34. Moteki, S. A.; Takacs, J. M. Exploiting self-assembly for ligand-scaffold optimization: substrate-tailored ligands for efficient catalytic asymmetric hydroboration. *Angew. Chem. , Int. Ed.* **2008**, *47*, 894-897.

35. Moteki, S. A.; Toyama, K.; Liu, Z.; Ma, J.; Holmes, A. E.; Takacs, J. M. Two-stage optimization of a supramolecular catalyst for catalytic asymmetric hydroboration. *Chem. Commun. (Cambridge, U. K.)* **2012**, *48*, 263-265.

36. Takacs, J. M.; Chaiseeda, K.; Moteki, S. A.; Reddy, D. S.; Wu, D.; Chandra, K. Rhodium-catalyzed asymmetric hydrogenation using self-assembled chiral bidentate ligands. *Pure Appl. Chem.* **2006**, *78*, 501-509.

37. Thacker, N. C.; Moteki, S. A.; Takacs, J. M. Ligand Scaffold Optimization of a Supramolecular Hydrogenation Catalyst: Analyzing the Influence of Key Structural Subunits on Reactivity and Selectivity. *ACS Catal.* **2012**, *2*, 2743-2752.

38. van Leeuwen, P. W. N. M.; Rivillo, D.; Raynal, M.; Freixa, Z. Enantioselective Supramolecular Catalysis Induced by Remote Chiral Diols. *J. Am. Chem. Soc.* **2011**, *133*, 18562-18565.

39. Lee, S. J.; Cho, S.; Mulfort, K. L.; Tiede, D. M.; Hupp, J. T.; Nguyen, S. T. Cavity-Tailored, Self-Sorting Supramolecular Catalytic Boxes for Selective Oxidation. *J. Am. Chem. Soc.* **2008**, *130*, 16828-16829.

40. Gadzikwa, T.; Bellini, R.; Dekker, H. L.; Reek, J. N. H. Self-Assembly of a Confined Rhodium Catalyst for Asymmetric Hydroformylation of Unfunctionalized Internal Alkenes. *J. Am. Chem. Soc.* **2012**, *134*, 2860-2863.

41. Kuil, M.; Soltner, T.; Van Leeuwen, P. W. N. M.; Reek, J. N. H. High-Precision Catalysts: Regioselective Hydroformylation of Internal Alkenes by Encapsulated Rhodium Complexes. *J. Am. Chem. Soc.* **2006**, *128*, 11344-11345.

42. Kharlamov, S. V.; Latypov, S. K. Modern diffusion-ordered NMR spectroscopy in chemistry of supramolecular systems: the scope and limitations. *Russ. Chem. Rev.* **2010**, *79*, 635-653.

43. Brown, C. J.; Bergman, R. G.; Raymond, K. N. Enantioselective Catalysis of the Aza-Cope Rearrangement by a Chiral Supramolecular Assembly. *J. Am. Chem. Soc.* **2009**, *131*, 17530-17531.

44. Zhao, C.; Sun, Q.; Hart-Cooper, W. M.; Di Pasquale, A. G.; Toste, F. D.; Bergman, R. G.; Raymond, K. N. Chiral Amide Directed Assembly of a Diastereo- and Enantiopure Supramolecular Host and its Application to Enantioselective Catalysis of Neutral Substrates. *J. Am. Chem. Soc.* **2013**, *135*, 18802-18805.

45. Nishioka, Y.; Yamaguchi, T.; Kawano, M.; Fujita, M. Asymmetric [2 + 2] Olefin Cross Photoaddition in a Self-Assembled Host with Remote Chiral Auxiliaries. *J. Am. Chem. Soc.* **2008**, *130*, 8160-8161.

46. Fiedler, D.; Leung, D. H.; Bergman, R. G.; Raymond, K. N. Selective Molecular Recognition, C-H Bond Activation, and Catalysis in Nanoscale Reaction Vessels. *Acc. Chem. Res.* **2005**, *38*, 349-358.

47. Fiedler, D.; van Halbeek, H.; Bergman, R. G.; Raymond, K. N. Supramolecular Catalysis of Unimolecular Rearrangements: Substrate Scope and Mechanistic Insights. *J. Am. Chem. Soc.* **2006**, *128*, 10240-10252.

48. Pluth, M. D.; Bergman, R. G.; Raymond, K. N. Supramolecular Catalysis of Orthoformate Hydrolysis in Basic Solution: An Enzyme-Like Mechanism. *J. Am. Chem. Soc.* **2008**, *130*, 11423-11429.

49. Hastings, C. J.; Fiedler, D.; Bergman, R. G.; Raymond, K. N. Aza Cope Rearrangement of Propargyl Enammonium Cations Catalyzed By a Self-Assembled "Nanozyme". *J. Am. Chem. Soc.* **2008**, *130*, 10977-10983.

50. Mugridge, J. S.; Szigethy, G.; Bergman, R. G.; Raymond, K. N. Encapsulated Guest-Host Dynamics: Guest Rotational Barriers and Tumbling as a Probe of Host Interior Cavity Space. *J. Am. Chem. Soc.* **2010**, *132*, 16256-16264.

51. Hastings, C. J.; Backlund, M. P.; Bergman, R. G.; Raymond, K. N. Enzyme-like Control of Carbocation Deprotonation Regioselectivity in Supramolecular Catalysis of the Nazarov Cyclization. *Angew. Chem. , Int. Ed.* **2011**, *50*, 10570-10573, S10570/1-S10570/9.

52. Wang, Z. J.; Brown, C. J.; Bergman, R. G.; Raymond, K. N.; Toste, F. D. Hydroalkoxylation Catalyzed by a Gold(I) Complex Encapsulated in a Supramolecular Host. *J. Am. Chem. Soc.* **2011**, *133*, 7358-7360.

53. Wang, Z. J.; Clary, K. N.; Bergman, R. G.; Raymond, K. N.; Toste, F. D. A supramolecular approach to combining enzymatic and transition metal catalysis. *Nat. Chem.* **2013**, *5*, 100-103.

54. Caulder, D. L.; Raymond, K. N. The rational design of high symmetry coordination clusters. *J. Chem. Soc. , Dalton Trans.* **1999**, 1185-1200.

55. Davis, A. V.; Fiedler, D.; Ziegler, M.; Terpin, A.; Raymond, K. N. Resolution of Chiral, Tetrahedral M4L6 Metal-Ligand Hosts. *J. Am. Chem. Soc.* **2007**, *129*, 15354-15363.

56. Ma, L.; Abney, C.; Lin, W. Enantioselective catalysis with homochiral metal-organic frameworks. *Chem. Soc. Rev.* **2009**, *38*, 1248-1256.

57. Yoon, M.; Srirambalaji, R.; Kim, K. Homochiral Metal-Organic Frameworks for Asymmetric Heterogeneous Catalysis. *Chem. Rev. (Washington, DC, U. S.)* **2012**, *112*, 1196-1231.

58. Falkowski, J. M.; Liu, S.; Lin, W. Metal-Organic Frameworks as Single-Site Solid Catalysts for Asymmetric Reactions. *Isr. J. Chem.* **2012**, *52*, 591-603.

59. Seo, J. S.; Whang, D.; Lee, H.; Jun, S. I.; Oh, J.; Jeon, Y. J.; Kim, K. A homochiral metal-organic porous material for enantioselective separation and catalysis. *Nature (London)* **2000**, *404*, 982-986.

60. Evans, O. R.; Ngo, H. L.; Lin, W. Chiral porous solids based on lamellar lanthanide phosphonates. *J. Am. Chem. Soc.* **2001**, *123*, 10395-10396.

61. Tanaka, K.; Oda, S.; Shiro, M. A novel chiral porous metal-organic framework: asymmetric ring opening reaction of epoxide with amine in the chiral open space. *Chem. Commun. (Cambridge, U. K.)* **2008**, 820-822.

62. Chawla, R.; Singh, A. K.; Yadav, L. D. S. Organocatalysis in synthesis and reactions of epoxides and aziridines. *RSC Adv.* **2013**, *3*, 11385-11403.

63. Hu, A.; Ngo, H. L.; Lin, W. Chiral, porous, hybrid solids for highly enantioselective heterogeneous asymmetric hydrogenation of Î²-keto esters. *Angew. Chem. , Int. Ed.* **2003**, *42*, 6000-6003.

64. Ohkuma, T.; Ooka, H.; Ikariya, T.; Noyori, R. Preferential hydrogenation of aldehydes and ketones. *J. Am. Chem. Soc.* **1995**, *117*, 10417-10418.

65. Doucet, H.; Ohkuma, T.; Murata, K.; Yokozawa, T.; Kozawa, M.; Katayama, E.; England, A. F.; Ikariya, T.; Noyori, R. Trans-[RuCl2(phosphine)2(1,2-diamine)] and chiral trans-[RuCl2(diphosphine)(1,2-diamine)]: shelf-stable precatalysts for the rapid, productive, and stereoselective hydrogenation of ketones. *Angew. Chem. , Int. Ed.* **1998**, *37*, 1703-1707.

66. Cho, S.; Ma, B.; Nguyen, S. T.; Hupp, J. T.; Albrecht-Schmitt, T. E. A metal-organic framework material that functions as an enantioselective catalyst for olefin epoxidation. *Chem. Commun. (Cambridge, U. K.)* **2006**, 2563-2565.

67. Wu, C.; Hu, A.; Zhang, L.; Lin, W. A Homochiral Porous Metal-Organic Framework for Highly Enantioselective Heterogeneous Asymmetric Catalysis. *J. Am. Chem. Soc.* **2005**, *127*, 8940-8941.

68. Ma, L.; Falkowski, J. M.; Abney, C.; Lin, W. A series of isoreticular chiral metal-organic frameworks as a tunable platform for asymmetric catalysis. *Nat. Chem.* **2010**, *2*, 838-846.

69. Ma, L.; Wu, C.; Wanderley, M. M.; Lin, W. Single-Crystal to Single-Crystal Cross-Linking of an Interpenetrating Chiral Metal-Organic Framework and Implications in Asymmetric Catalysis. *Angew. Chem. , Int. Ed.* **2010**, *49*, 8244-8248, S8244/1-S8244/16.

70. Song, F.; Wang, C.; Lin, W. A chiral metal-organic framework for sequential asymmetric catalysis. *Chem. Commun. (Cambridge, U. K.)* **2011**, *47*, 8256-8258.

71. Li, S.; Xiao, T.; Lin, C.; Wang, L. Advanced supramolecular polymers constructed by orthogonal self-assembly. *Chem. Soc. Rev.* **2012**, *41*, 5950-5968.

72. Roelfes, G.; Feringa, B. L. DNA-based asymmetric catalysis. *Angew. Chem. , Int. Ed.* **2005**, *44*, 3230-3232.

73. Boersma, A. J.; Megens, R. P.; Feringa, B. L.; Roelfes, G. DNA-based asymmetric catalysis. *Chem. Soc. Rev.* **2010**, *39*, 2083-2092.

74. Shi, L.; Wang, X.; Sandoval, C. A.; Li, M.; Qi, Q.; Li, Z.; Ding, K. Engineering a polymeric chiral catalyst by using hydrogen bonding and coordination interactions. *Angew. Chem. , Int. Ed.* **2006**, *45*, 4108-4112.

75. Yu, L.; Wang, Z.; Wu, J.; Tu, S.; Ding, K. Directed Orthogonal Self-Assembly of Homochiral Coordination Polymers for Heterogeneous Enantioselective Hydrogenation. *Angew. Chem. , Int. Ed.* **2010**, *49*, 3627-3630, S3627/1-S3627/34.

76. Cragg, G. M.; Grothaus, P. G.; Newman, D. J. Impact of Natural Products on Developing New Anti-Cancer Agents. *Chem. Rev. (Washington, DC, U. S.)* **2009**, *109*, 3012-3043.

77. Gonzalez-Sabin, J.; Moran-Ramallal, R.; Rebolledo, F. Regioselective enzymatic acylation of complex natural products: expanding molecular diversity. *Chem Soc Rev* **2011**, *40*, 5321-5335.

78. Lewis, C. A.; Miller, S. J. Site-selective derivatization and remodeling of erythromycin A by using simple peptide-based chiral catalysts. *Angew. Chem. , Int. Ed.* **2006**, *45*, 5616-5619.

79. Lewis, C. A.; Longcore, K. E.; Miller, S. J.; Wender, P. A. An Approach to the Site-Selective Diversification of Apoptolidin A with Peptide-Based Catalysts. *J. Nat. Prod.* **2009**, *72*, 1864-1869.

80. Fowler, B. S.; Laemmerhold, K. M.; Miller, S. J. Catalytic Site-Selective Thiocarbonylation and Deoxygenation of Vancomycin Reveal Hydroxyl-Dependent Conformational Effects. *J. Am. Chem. Soc.* **2012**, *134*, 9755-9761.

81. Pathak, T. P.; Miller, S. J. Site-Selective Bromination of Vancomycin. *J. Am. Chem. Soc.* **2012**, *134*, 6120-6123.

82. Han, S.; Miller, S. J. Asymmetric Catalysis at a Distance: Catalytic, Site-Selective Phosphorylation of Teicoplanin. *J. Am. Chem. Soc.* **2013**, *135*, 12414-12421.

83. McNally, A.; Prier, C. K.; MacMillan, D. W. C. Discovery of an Î±-Amino C-H Arylation Reaction Using the Strategy of Accelerated Serendipity. *Science (Washington, DC, U. S.)* **2011**, *334*, 1114-1117.

CHAPTER TWO: OPTIMIZATION OF A SUPRAMOLECULAR HYDROGENATION CATALYST

2.1 Rhodium-catalyzed asymmetric hydrogenation

Rhodium-catalyzed asymmetric hydrogenation (Rh-CAH) is one of the most useful reactions in asymmetric catalysis. The addition of H_2 to a prochiral alkene is atom economical and generates a minimal amount of waste. The substrate scope is diverse, and there has been a substantial amount of research into the mechanism of the reaction over the last 30 years. Historically, these traits have made the asymmetric hydrogenation one of the most studied reactions of asymmetric catalysis. The origin of asymmetric hydrogenation date back to early studies by 2001 Nobel laureate William Knowles, who sought an efficient route to synthesize the rare amino acid L-DOPA for the treatment of Parkinson's disease (Figure 1).[1] The then practiced route utilized a Pd/C promoted hydrogenation followed by a chiral resolution. While this route was effective in preparation of the desired L-isomer, it also generated a large amount of waste from the undesired D-isomer. Wilkinson hypothesized it might be possible to bypass this resolution by producing only the L-isomer through an asymmetric hydrogenation.

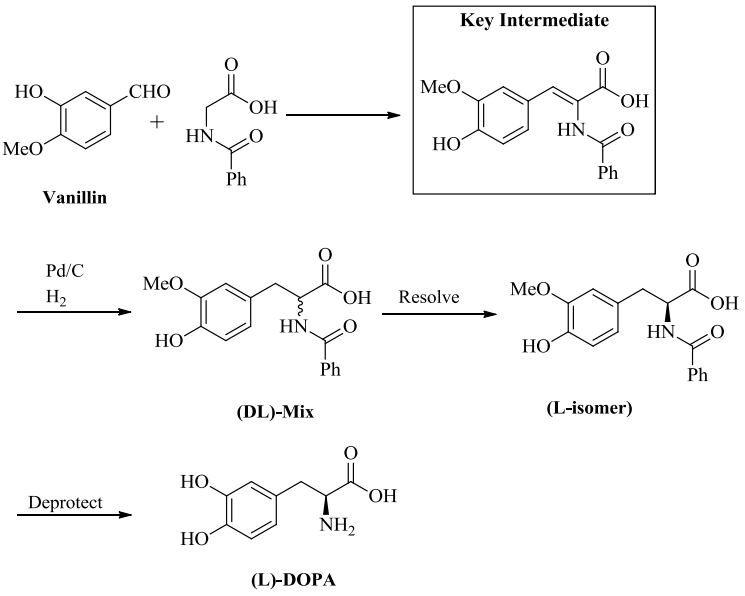

Figure 1 Preparation of the Parkinson's drug (L)-DOPA with a chiral resolution step

In the mid 1960's, Wilkinson developed the homogeneous catalyst, $Rh(PPh_3)_3Cl$, that proved quite reactive toward the hydrogenation of unhindered olefins.[2] A short time later, Horner and Mislow developed a chiral resolution for the preparation of chiral phosphines.[2] The chiral phosphines were found to be stable to racemization under mild conditions and could be used to prepare a chiral variant of $Rh(PPh_3)_3Cl$. As a model substrate for the (L)-DOPA precursor, the asymmetric hydrogenation of an *N*-acetyl protected dehydrophenylalanine derivative was explored (Figure 2). Horner and Mislow's chiral phosphines gave the reduced product in 28% ee. The first generation substituted a propyl group for a cyclohexyl which increased the enantioselectivity only slightly. Further modification resulted in the development of PAMP and CAMP which gave the products in 58% ee and 88% ee.

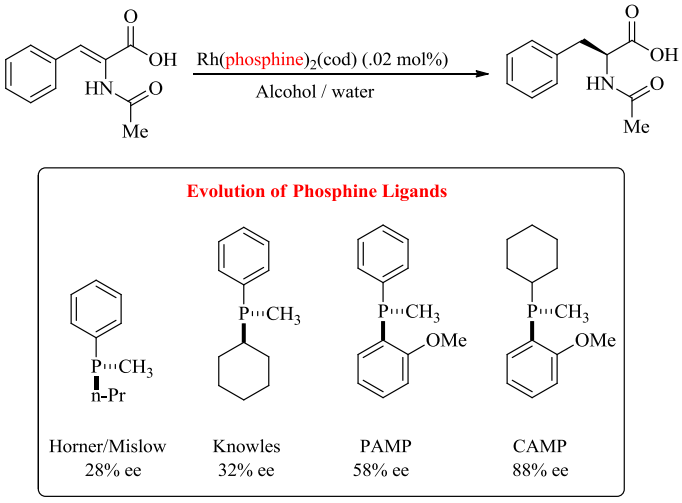

Figure 2 Evolution of monodentate phosphine ligands for the Rh-CAH

Bidentate phosphine catalysts started being explored in the early 1970's. It was believed the bidentate phosphine ligands would give a more rigid organized chiral space than the monodentate phosphines could achieve. Kagan developed the chiral bidentate ligand DIOP derived from chiral sugars.[3] DIOP was remarkable because the chirality was not on the phosphine itself, but on the backbone of the ligand. Using DIOP the product was obtained in 83% ee (Figure 3). Knowles connected two PAMP phosphine ligands with an ethylene bridge and named this ligand DIPAMP. DIPAMP gave the highest levels of enantioselectivity achieved up to that point in time, 95% ee.

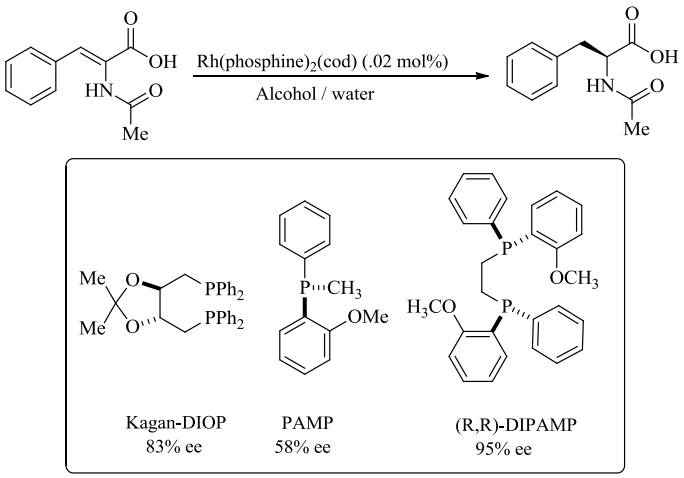

Figure 3 Evolution of chiral bidentate ligands for Rh-CAH

After being largely ignored in preference to chiral bidentate ligands, it was reported by Feringa and deVries in 2002 that certain monodentate BINOL phosphoramidites were very effective for the Rh-CAH of dehydroamino acid derivatives (Figure 4).[4] Despite not having the added rigidity from a linker, these ligands can be equally effective as bidentate ligands. Enantioselectivities of 92-99% ee were reported for both (E)- and (Z)-dehydroamino acid derivatives. A big advantage of these monodentate phosphoramidite ligands was their simple preparation from chiral diols enabling access to large libraries of chiral ligands for combinatorial screenings. Since the initial report, phosphite and phosphoramidite monodentate ligands have been shown to be very effective for the Rh-CAH of a wide variety of substrates.[5-12]

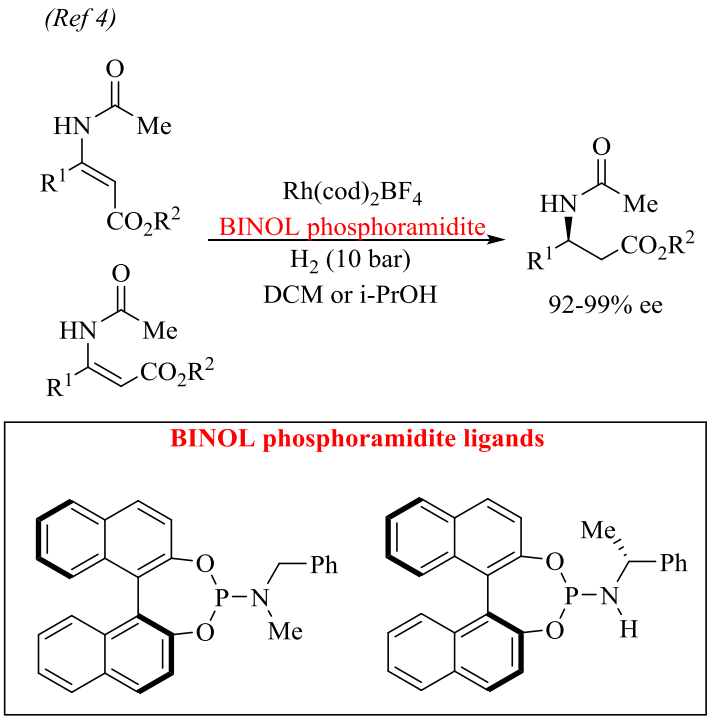

Figure 4 First report of effective BINOL phosphoramidite ligands in the Rh CAH

The mechanism of the rhodium-catalyzed asymmetric hydrogenation has been extensively studied over the last 30 years.[13-19] Experimental evidence suggests two distinct pathways leading to the hydrogenated product (Figure 5). If substrate coordination to rhodium occurs before oxidation addition of H_2, the mechanism is known as the Halpern-Brown unsaturated pathway.[14,17,19] If the order of addition is reversed and oxidative addition of H_2 precedes substrate coordination, this is known as the dihydride pathway.[20-23] While both have a common octahedral dihydride intermediate, the difference lies in whether stereoselection occurs from a square planar rhodium(I) or octahedral rhodium(III) complex. Thus far, evidence for the dihydride pathway has only been observed when electron rich phosphine ligands were used.

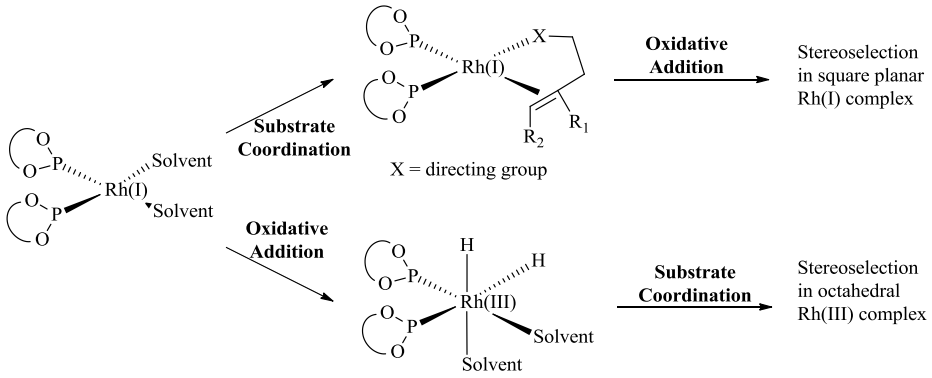

Figure 5 Stereoselection in the rhodium-catalyzed hydrogenation can occur through one of two pathways

In the Halpern-Brown unsaturated mechanism, the stereoselection is first determined from the addition of H_2 to the substrate-bound rhodium. The mechanism is summarized below (Figure 6). A doubly-solvated chiral rhodium(I) complex coordinates to the prochiral substrate affording two diastereomeric complexes differing in energy (Figure 6, A and A'). Oxidative addition of H_2 gives the octahedral Rh(III) complex through an "anti-lock and key" mechanism (Figure 6, C and C'). That is, the minor diastereomer reacts more quickly than the major diastereomer.[14,17,19] Landis and co-workers evaluated the different approaches of H_2 to rhodium using DFT and ONIOM calculations finding significant energy differences between the different transition states.[24-26] Labeling studies suggest the oxidative addition is irreversible when isotopic scrambling was not observed in presence of a D_2 atmosphere.[16,17] Migratory insertion of the alkene affords an alkyl metal hydride species (Figure 6, D and D'). Reductive elimination gives the chiral reduced product while regenerating the Rh(I) catalyst (Figure 6, E and E'). The mechanism is very well understood; the enantioselectivity can even be predicted using a quantum mechanics-guided molecular mechanics method (Q2MM). For example,

building upon their previous mechanistic studies,[27] Wiest and co-workers were able to corroborate experimental data for a series of widely used chiral bidentate phosphine ligands with predicted enantioselectivities.[28] The overall agreement between experimental and predicted selectivity for all examples had an average unsigned error of 0.8 kcal/mol.

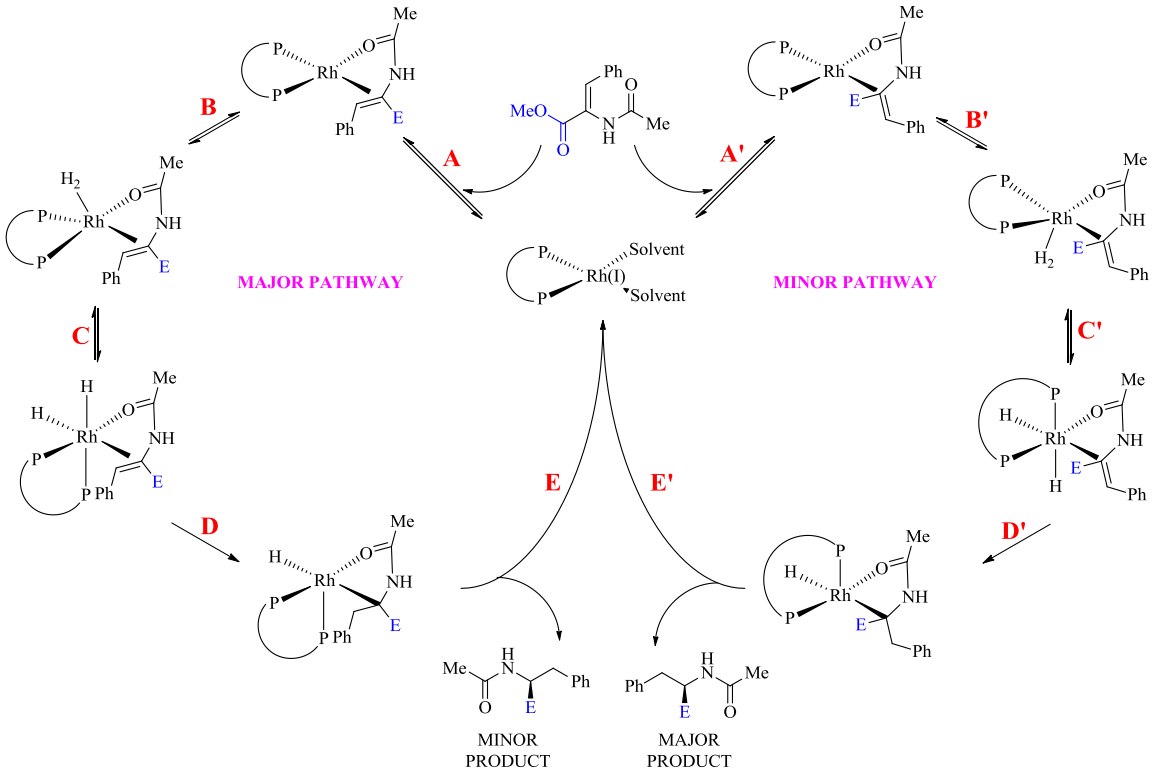

Figure 6 Halpern-Brown unsaturated mechanism for Rh-CAH

Conversely, the Rh(III) dihydride mechanism suggests oxidative addition to rhodium(I) occurs first, and the prochiral substrate's coordination is the stereoselective step.[20-23] Key evidence is observation of dihydride intermediates by H NMR at low temperatures. Thus far, dihydride intermediates have only been observed when electron-

rich P*-stereogenic phosphine ligands were used. The dihydride intermediates have never been observed with substrate pre-coordinated, because the migratory insertion occurs too quickly. This mechanism also provides stereochemical models where the predicted enantiomer from substrate precomplexation is not formed.[29]

Asymmetric hydrogenation is widely used in pharmaceutical applications today.[30] Because of this, many research groups are still pursuing this reaction for catalysts that are selective towards an ever growing library of compounds. Their ultimate goal is to find a "privileged" catalyst generally reactive and selective for many substrates. A supramolecular catalyst has the advantage of more chemical space to tailor the chiral pocket for the substrate.

Supramolecular chemistry has a long history, but as described in Chapter 1, the use of supramolecular catalysts for asymmetric catalysis is still at an early stage. The Takacs group has reported effective self-assembled supramolecular catalysts for reactions such as asymmetric allylic amination,[31] hydrogenation,[32] and hydroboration.[33,34] The studies described in this chapter are those carried out for Rh-CAH; herein we describe the first in-depth investigation into the significance of each component of a self-assembled supramolecular hydrogenation catalyst.[35]

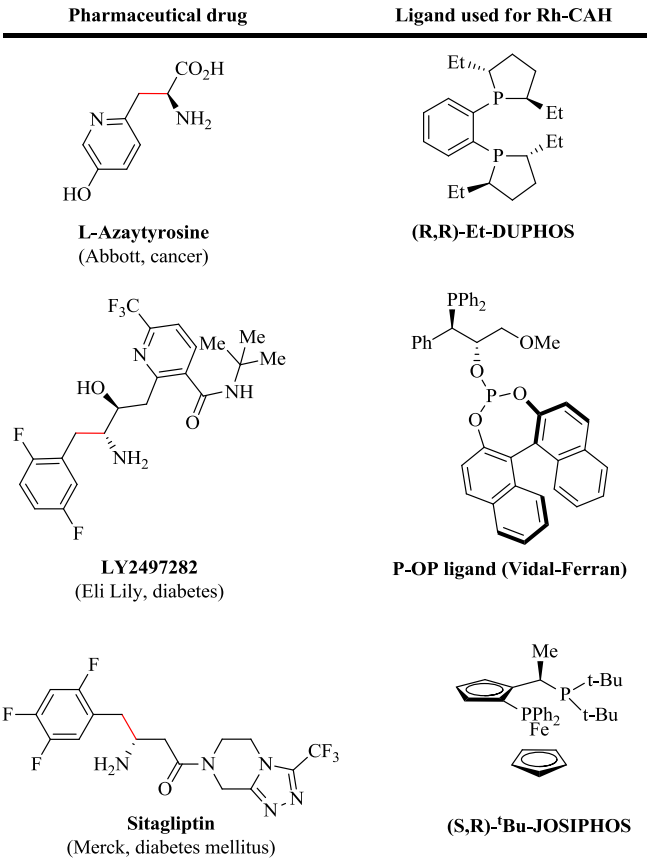

Figure 7 Pharmaceutical drugs synthesized with Rh-CAH as a key step. Asymmetric reduction marked by red bond.

2.2 Key components of a supramolecular catalyst

The Takacs supramolecular heterobimetallic catalyst can be divided into four customizable modules (Figure 8).[35] The active site can be modified with different catalytically active metals such as Pd, Rh, or Ir (Figure 8, I). The ligating group can be substituted with electronically different phosphorus ligands or nitrogen-based ligands (Figure 8, II). The scaffold building tether can vary the connectivity pattern of either mono- or bi-aryl tethers while controlling the connectivity to the ligating group through either a benzylic or phenolic linkage (Figure 8, III). Chirality-directed self-assembly

serves as the recognition elements which bring the complimentary bidentate ligand (Figure 8, IV).

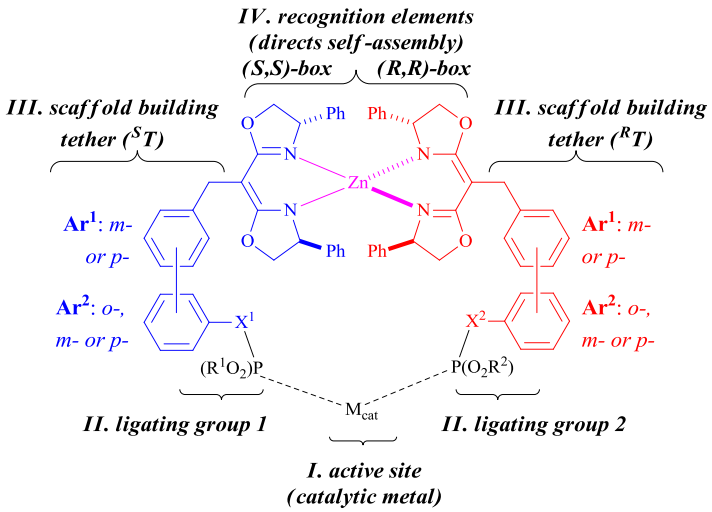

Figure 8 Strategy for optimization of a supramolecular catalyst. Reprinted with permission from *ACS Catal*. **2012**, *2*, 2743-2752. ©2014 American Chemical Society

Combination of equimolar equivalents of a remote phosphorus bearing *(S,S)*-bisoxazoline with a phosphorus bearing *(R,R)*-bisoxazoline in the presence of Zn(II) affords near exclusively the neutral heteroleptic complex SAL Zn(^{S}T^{R}T). The heteroleptic complex binds with nearly perfect tetrahedral geometry around zinc while the homoleptic complex is distorted to avoid unfavorable steric interactions between the phenyl substituents.[36,37] The difference in stability between the heteroleptic and homoleptic complexes, such as those whose crystals structures are shown (Figure 9, below) is estimated to be 4 kcal/mol or greater based on thermodynamic equilibria. In the example illustrated below, if ^{S}T = ^{R}T and both P(OR)$_2$ substituents are either (i) enantiomeric or (ii) achiral and otherwise identical on both subunits the zinc complex is meso by inversion symmetry. However, if ^{S}T ≠ ^{R}T, the zinc complex lacks inversion

symmetry and is chiral. In section 2.9, the impact of this will be described with respect to the asymmetric hydrogenation reaction.

.

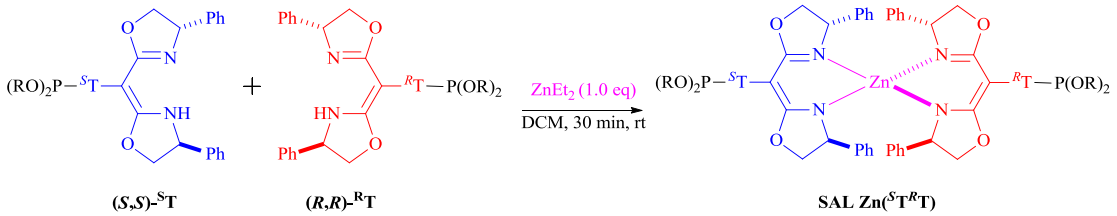

Figure 9 Chirality directed self-assembly affords heteroleptic bimetallic complex

Scaffold optimization involves varying the substitution patterns of the tethers attached to the bisoxazoline. The tethers were varied within a series of aryl and biaryl subunits of *ortho*-, *meta*-, or *para*-substitution (Figure 10). Typically, it has been found that the optimal catalyst bears a scaffold that varies from substrate to substrate, and similarly for different reactions. While some may see this as a disadvantage, we note the nature exploits the substrate selectivity as a hallmark of many biocatalysts (i.e., enzymes). The power of scaffold optimization lies in the rather unique ability to tailor the catalytic pocket for each substrate. In the course of the studies described below, one key feature will be that the flexibility of the catalyst can be tuned (or at least subtly varied) by changing the scaffold building tether subunit with either a benzylic or phenolic linkage to the ligating group. While this difference results in only 1 or 2 additional or fewer of degrees of conformational freedom in a structurally large (ca 2 kD) supramolecular catalyst, the impact on a catalyst's performance can be great. This will be described in further detail in section 2.7.

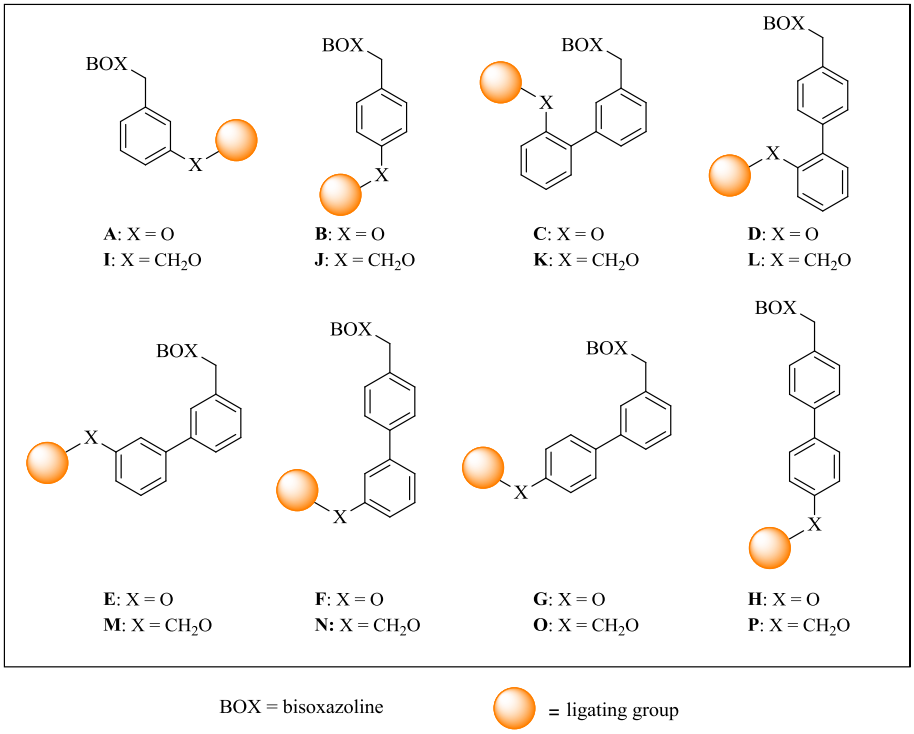

Figure 10 Library of tethers used in SAL synthesis

2.3 Ligating group and catalytic metal selection for catalyst scaffold optimization studies

The first step was selection of the ligating group. A series of chiral monodentate ligands were used to screen for candidates. Chiral phosphite ligands have been reported to be effective for the Rh-CAH.[5,6,10,12] The chiral diols BINOL, BIPHEP, and TADDOL were selected based upon their prior utility in asymmetric catalysis. To ascertain a sense of a chiral ligating group's effectiveness, two monodentate phosphite ligands modeling ultimate the tether backbone were synthesized with phenol (OPh) or benzylic (OBn) linkages.

.

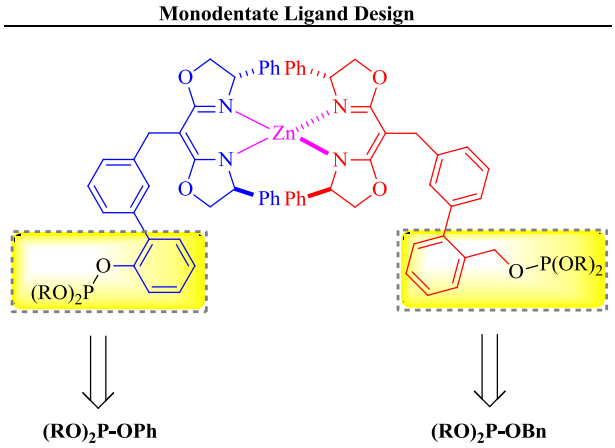

Figure 11 Strategy for selecting monodentate ligands for hydrogenation catalyst screening of substrates

Two prototypical enamides substrates were selected for this study, the dehydro phenylalanine derivative **S1** and 1,1-disubstituted eneacetamide **S2**. The substrates were screened with the TADDOL, BIPHEP, and BINOL derived phosphites with cationic $Rh(nbd)_2BF_4$ at 1 mol percent catalyst loading (Table 1). After the reaction, yields were determined with N-benzyl acetamide as internal standard on GC. Catalysts with TADDOL ligands **L1** and **L2** were active but non-selective in the hydrogenation of **S1** and **S2**. Biaryl backbones BIPHEP (**L3**, **L4**) and BINOL (**L5**, **L6**) gave higher selectivities than TADDOL. BINOL was chosen as the ligating group for this study, because the selectivity was good yet had some room for improvement by catalyst scaffold optimization, especially considering the energetics of enantioselective reactions. This was of course a risky proposal given that the previous hydrogenation study of BIPHEP-SALs showed only incrementally increases over the monodentate ligands. As a

benchmark for the scaffold optimization study, that is, a model system for the effect of mixed ArO- and $ArCH_2O$- phosphite linkages, the combination of (BINOL)POPh with (BINOL)POBn was also run. The effective use of mixtures of chiral monodentate ligands was first reported by Reetz[38] and since that report has been exploited for its versatility in identifying new catalysts.[39] In our hands, the **L5**/**L6** combination of chiral monodentate ligands were no more effective than **L5** or **L6** alone. This could suggest the an increase in selectivity from mixed scaffolds (something that we ultimately find, vide infra) results from supramolecular catalyst scaffold optimization rather than simply a mixed ligand effect.

Table 1 Ligating group selecting based on monodentate ligand screening[a]

Monodentate Ligands

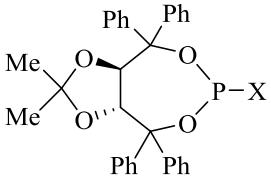

(R)-TADDOL
L1 (X = OPh)
L2 (X = OBn)

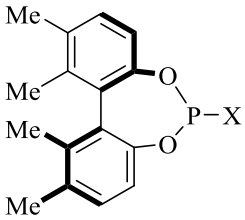

(R)-BIPHEP
L3 (X = OPh)
L4 (X = OBn)

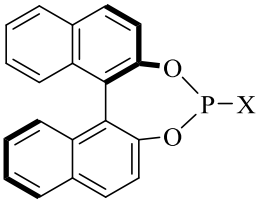

(R)-BINOL
L5 (X = OPh)
L6 (X = OBn)

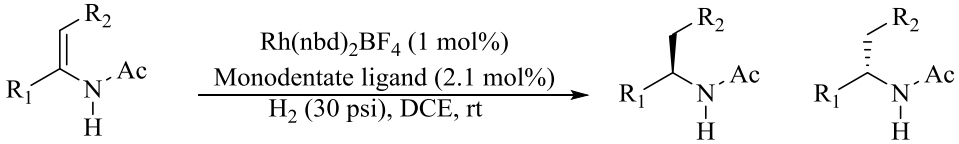

S1 (R^1 = CO_2Me, R^2 = Ph)
S2 (R^1 = 4-ClC_6H_4, R^2 = H)

(R)-1
(R)-2

(S)-1
(S)-2

		S1		**S2**	
Entry	Monodentate ligand	ee (%)[b]	yield (%)	ee (%)[b]	yield (%)
1	(R)-(TADDOL)POPh **L1**	4	97	10	99
2	(R)-(TADDOL)POBn **L2**	30	99	15	99
3	(R)-(BIPHEP)POPh **L3**	67	99	67	99
4	(R)-(BIPHEP)POBn **L4**	53	65	53	99
5	(R)-(BINOL)POPh **L5**	69	99	86	99
6	(R)-(BINOL)POBn **L6**	78	99	92	99
7	**L5** + **L6**[c]	78	99	92	99

[a]Reaction conditons: 1 mol% $Rh(nbd)_2BF_4$, 2.1 mol% monophosphite, DCE, rt, 16 h. Yields and enantioselectivity determined by chiral GC using N-benzyl acetamide as an internal standard. [b]Unless otherwise noted, the (S)-enantiomer predominates the reaction. [c]Equimolar amounts of each ligand.

The selection of metal precursor to be used in the catalyst scaffold optimization study was determined next. Alternate diene precursors, counterions, and metals to $Rh(nbd)_2BF_4$ were examined under a standard set of hydrogenation conditions (i.e,

substrate **S1** or **S2**, 1 mol% catalyst loading, BINOL phosphite **L6**, 30 psi H_2, DCE, 16 h). $Rh(cod)_2BF_4$ gave comparable results as $Rh(nbd)_2BF_4$, which indicates that the diene precursor has little or no effect on the reaction. (We had assumed at the onset, as others do, that diene would simple be reduced under the reaction conditions.) A "neutral" rhodium catalyst, $[Rh(nbd)Cl]_2$ did not show any catalytic activity as one would expect for rhodium with a covalently bound counterion and the need for two-point binding of the substrate with the catalyst. Substituting the $[BF_4]^-$ counterion with $[TfO]^-$ or $[B(C_6F_5)_4]^-$ (i.e., BArF) in the $Rh(nbd)_2X$ catalyst precursor gives catalysts that exhibit comparable reactivity and selectivity. Consider the results summarized above and given its favorable solubility properties and commercial availability, $Rh(nbd)_2BF_4$ was used in the scaffold optimization studies.

Iridium-catalyzed hydrogenation has been effective for the enantioselective hydrogenation of substrates lacking strong directing groups, and we also briefly considered catalysts based on iridium as an alternative to rhodium for the catalyst scaffold optimization studies.[40,41] However, $Ir(cod)_2BF_4$ is ineffective as a catalyst precursor under our stand reaction conditions with the selected chiral monophosphite ligands. This is perhaps not surprising. Effective iridium-catalysts typically employ *P,N*-ligands. Catalyst deactivation is believed to result from formation of bridged iridium-hydride complexes. Use of a non-coordinating counterion is important as strong coordination of the counterion inhibits olefin coordination and subsequent migratory insertion of an iridium di-hydride species.[42] High concentrations of iridium-dihydride lead to the catalyst deactivation.

2.4 SAL screening of dehydrophenylalanine derivative S1

BINOL-derived monodentate phosphites proved to be both reaction and reasonably enantioselectivity for the Rh-CAH of prototypical substrates **S1** and **S2** under our prescribed reaction conditions. The BINOL phosphite ligating group was appended to a series of SAL tethers. Among the set of possible tethers shown in Figure 10, all of the monoaryl and biaryl tethers bearing a benzylic linkage to the ligating group were synthesized and included in the study. Their inclusion reflects the preliminary evidence from the BIPHEP SALs and monodentate screening suggesting that $ArCH_2O$-linked phosphites were generally more successful than the corresponding the ArO-linked series. For the ArO-linked series, the monoaryl tethers were excluded based on unpublished gel permeation chromatography (GPC) results suggesting that the ArO-linked tethers do not quantitatively form the desired bidentate chelate due to distance between restricted P-P distance between ligating groups.

BINOL-bisphosphite SALs were prepared by adding an equivalent of $Zn(Et_2)$ to combinations of appropriately *(S,S)* or *(R,R)*-bisoxazoline coupled tethers. $Rh(nbd)_2BF_4$ was then added to the resulting Zn complex providing a series of *in situ* generated supramolecular catalysts. Initial screening of the pseudo-C_2-symmetric SALs, scaffolds comprised of *(R,R)* and *(S,S)*-bisoxazline coupled to identical tethers, were used to determine whether all of the catalyst combinations should be examined. Hydrogenation of **S1** revealed a range of enantioselectivity from racemic to 93% ee with yields ranging from no reaction to quantitative (Figure 12). While the large spread in the data looks promising in terms of scaffold optimization, only a couple catalysts give low enantioselectivity while the bulk of them give results within a relatively narrow range,

that is, 68–93% ee. This is not what one would hope to see in a large scale scaffold optimization study.

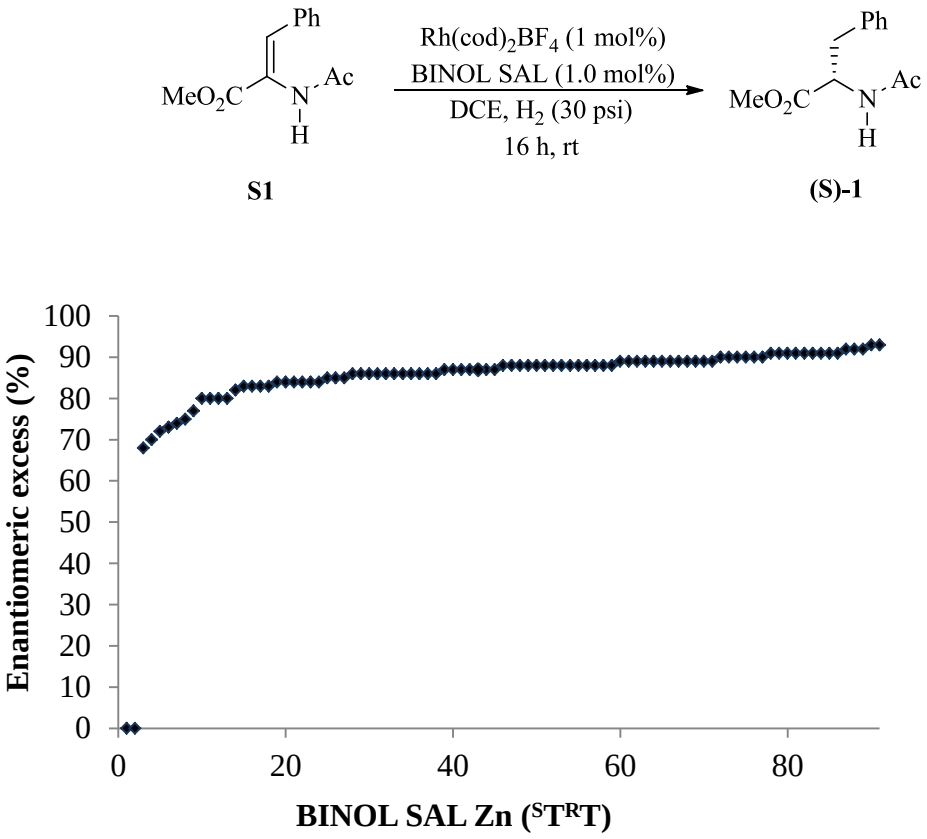

Figure 12 Hydrogenation of dehydrophenylalanine derivative **S1** with BINOL SALs

Figure 13 summarizes the full data set from screening the BINOL-SAL derived catalysts with **S1**. Tethers labeled **C-G** are ArO-linked phosphites, while those labeled **I-P** are $ArOCH_2$-linked phosphites. Catalysts bearing two ArO-linked tethers on the bidentate ligand are generally not reactive; see Figure 14 upper left quadrant. Interestingly, while these ArO,ArO-linked scaffolds are not reactive, they are still more selective than the corresponding monodentate ligands which gave only 69% ee for (BINOL)POPh **L5**. In

contrast, the $ArCH_2O$,$ArCH_2O$-linked scaffolds, that is, prepared from tethers I-P on both sides, are generally very reactive. The mixed ArO,$ArCH_2O$-linked scaffolds, with one tether selected from among tethers **C-G** and the other from among **I-P**, gave yields that had a exhibited wide variance from very low to quantitative. Based upon these initial results, it was decided not to screen the remaining untested pseudoC_2-symmetric ligands (i.e., the diastereomers of the ligands already screened) under the assumption that the box complex, the element that would differ in the diastereomer, was too far from the site of reaction and rather highly symmetric; the implication being that it the diastereomeric series of catalysts simply would behave similarly.

.

(R,R)-Bisoxazoline linked tethers

(S,S)-Bisoxazoline linked tethers		C	D	E	F	G	I	J	K	L	M	N	O	P
C	ee (%)	73	68	80	84	72			89	86	88	83	80	77
	yield (%)	2	6	8	11	2			100	21	24	7	5	4
D	ee (%)		74	86	75	0				82	88	86	86	87
	yield (%)		9	36	5	0				48	17	3	2	3
E	ee (%)			89	84	92					92	85	90	89
	yield (%)			38	5	96					73	95	100	100
F	ee (%)				85	85						86	84	88
	yield (%)				13	4						11	7	6
G	ee (%)					0							93	80
	yield (%)					0							18	30
I	ee (%)	93	86	89	88	88	87	89	90	87	89	87	89	88
	yield (%)	96	100	100	100	100	100	100	100	100	80	100	100	93
J	ee (%)	91	87	91	88	89		90	91	88	91	89	91	89
	yield (%)	100	85	100	70	100		100	100	100	100	100	100	100
K	ee (%)		90	88	83	91			91	87	80	87	88	86
	yield (%)		95	100	7	100			100	90	16	100	100	100
L	ee (%)			89	88	90				89	88	88	91	86
	yield (%)			92	54	100				100	27	100	100	100
M	ee (%)				70	91					86	86	88	84
	yield (%)				5	100					100	89	100	20
N	ee (%)					90						84	86	84
	yield (%)					7						16	7	30
O	ee (%)												92	83
	yield (%)												10	36
P	ee (%)													83
	yield (%)													50

LEGEND

0-29
30-69
70-89
90-94
95-100

Figure 13 Full data set from BINOL SAL hydrogenation screening of dehydropheylalanine derivative S1

2.5 Comparing supramolecular scaffolds with similar ligating groups (BINOL-SALs vs BIPHEP-SALs)

The chiral backbones of BINOL and BIPHEP are similar, but the question remains, how does a supramolecular catalyst with a particular scaffold and BINOL ligating groups compare to that with BIPHEP ligating groups on that same scaffold?[32] More specifically, if a non-selective catalyst with a BIPHEP ligating group is compared to a SAL with BINOL ligating groups, will their results correlate? Out of the 93 BINOL scaffolds screened with substrate **S1**, 39 could be directly compared under the same reaction conditions to the BIPHEP ligands screened in the previous study. When the data was sorted according to the ascending enantioselectivity from the BIPHEP SALs, it was very surprising to find only modest correlation between the two series of catalysts given the similarity of the ligating groups appended to the identical scaffold (Figure 14).

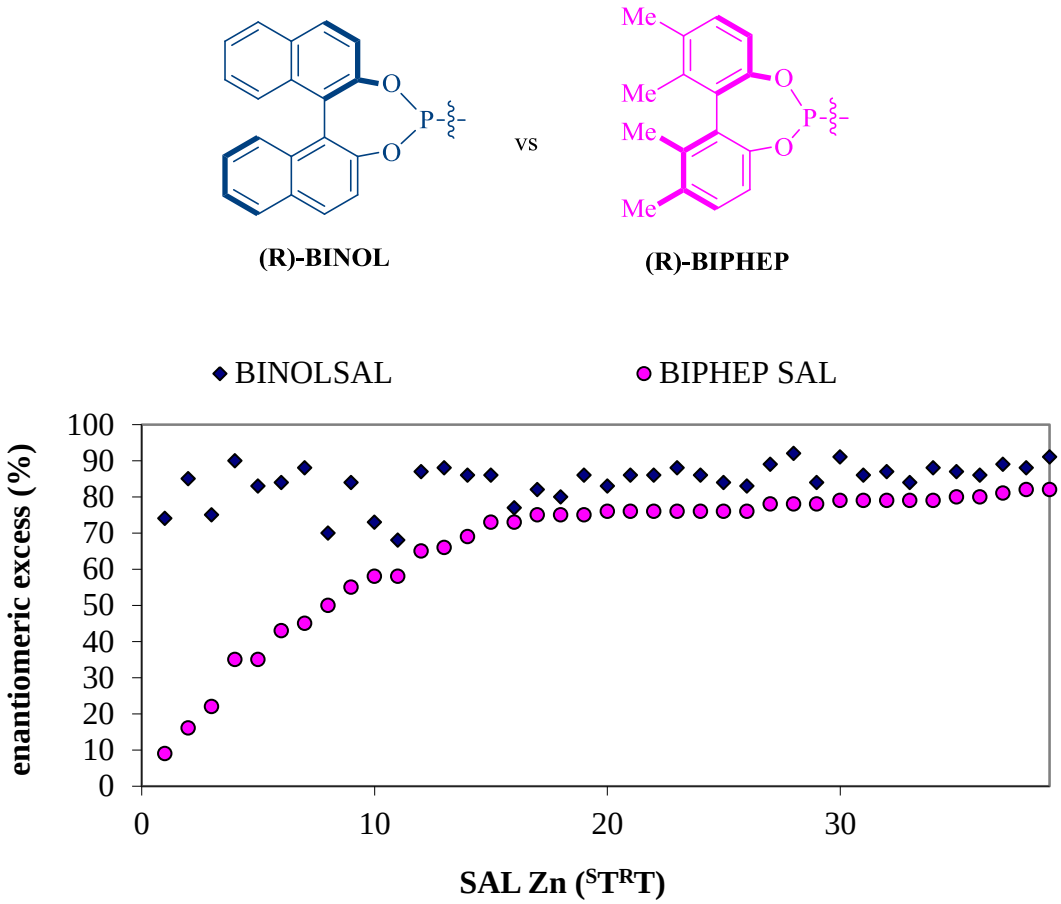

Figure 14 Comparison of BIPHEP SALs vs BINOL SALs in the hydrogenation of S1 (sorted by BIPHEP SALs)

Sorting by tether connectivity to the ligating group, a trend was discovered amongst the data (Figure 15). The ArO,ArO-linked scaffolds (i.e., $^{C\text{-}G}$T, $^{C\text{-}G}$T) exhibited markedly lower enantioselectivity for BIPHEP-SALs (9-58% ee) than the BINOL-SALs (68-84% ee). The $ArCH_2O$,ArO scaffolds ($^{I\text{-}P}$T,$^{C\text{-}G}$T) occupied the mid-range of selectivity within each series: BIPHEP-SALs (35-79% ee); BINOL-SALs (70-90% ee). $ArCH_2O$,$ArCH_2O$-linked SALs ($^{I\text{-}P}$T, $^{I\text{-}P}$T) were on average the most selective within each series: BIPHEP-SALs (76-82% ee); BINOL-SALs (83-92% ee).

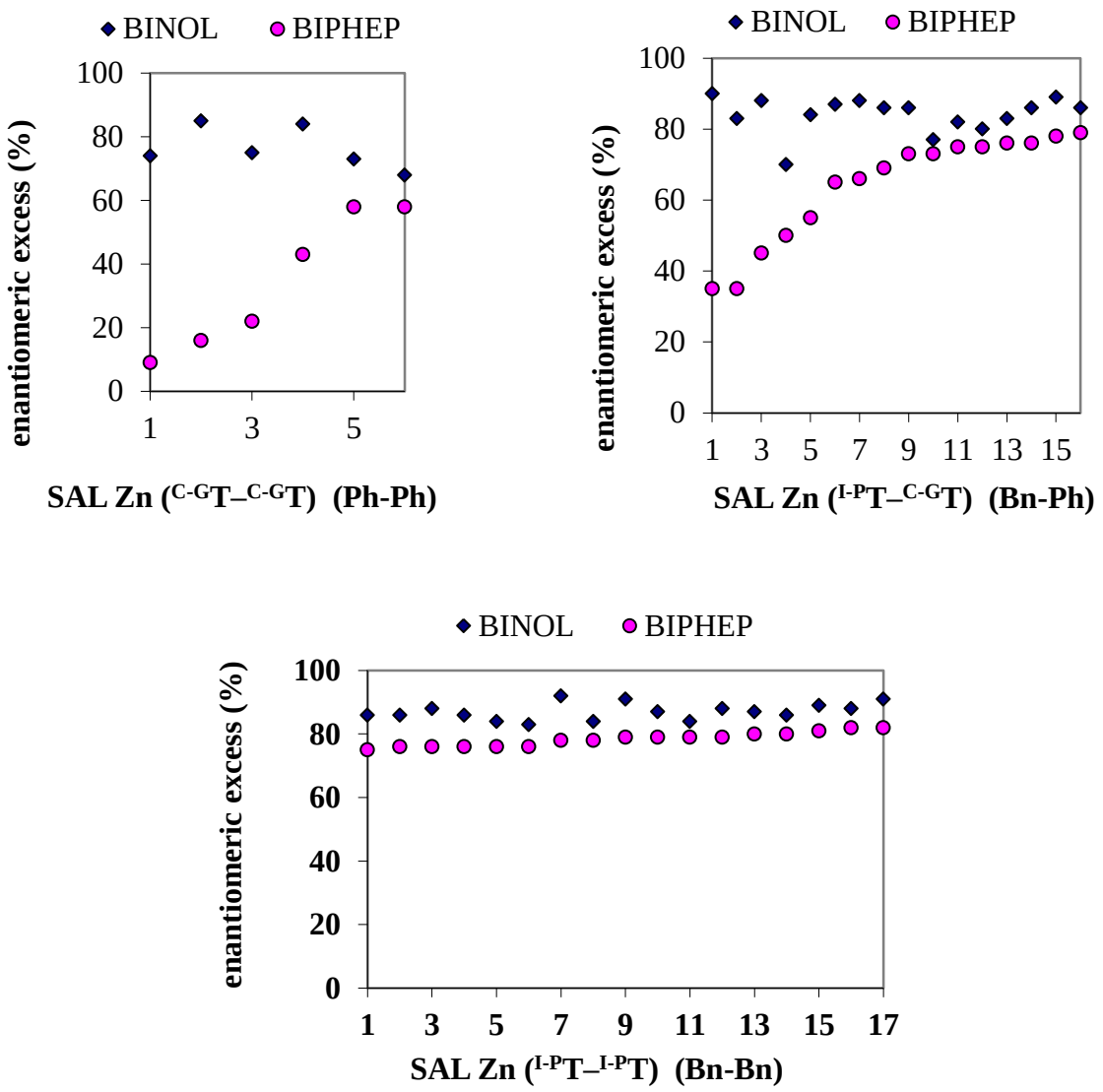

Figure 15 Comparison of BIPHEP vs BINOL SALs with respect to benzyl vs phenyl connectivity to ligating group in the hydrogenation of **S1** (sorted by BIPHEP)

The data might be consistent with a measure of catalyst scaffold flexibility. With each $ArCH_2O$-linked tethers ($^{I\text{-}P}T$), the scaffold has an additional degree of rotational freedom relative to the corresponding ArO,ArO-linked scaffolds ($^{C\text{-}G}T$, $^{C\text{-}G}T$). The ArO,ArO-linked scaffolds are perhaps too rigid which results in less effective catalysts. As the

degree of flexibility is increased to the other extreme in this study, that is, $ArCH_2O$,$ArCH_2O$-linked scaffolds, the extent to which catalyst scaffold optimization impacts the level of enantioselectivity is generally minimal. These data suggest that the delicate balance between flexibility and rigidity required for an effective catalyst. Why this effect is observed more clearly with the BIPHEP-SALs than the BINOL-SALs is not understood at this point.

2.6 Catalyst scaffold optimization study for enacetamide S2

When a similar screening of catalysts was carried out for the *para*-chloro eneacetamide **S2**, the results spanned a wide range of enantioselectivity, racemic to 96% ee (Figure 16). The data are arranged from lowest to highest enantioselectivity and color-coded by tether type ($ArCH_2O$- and/or ArO-linked) in Figure 17. Catalysts comprised of only ArO-linked tethers ($^{C\text{-}G}T$) afforded a range of selectivity from racemic to 90% ee. The mixed $ArCH_2O$,ArO-linked tethers ($^{I\text{-}P}T$, $^{C\text{-}G}T$) gave the widest range of anantioselectivity, ranging from racemic to 96% ee. The $ArCH_2O$,$ArCH_2O$-linked tethers ($^{I\text{-}P}T$, $^{I\text{-}P}T$) afforded the highest average level of enantiomeric excess and relatively narrow range of enantioselectivity, 74% to 94% ee.

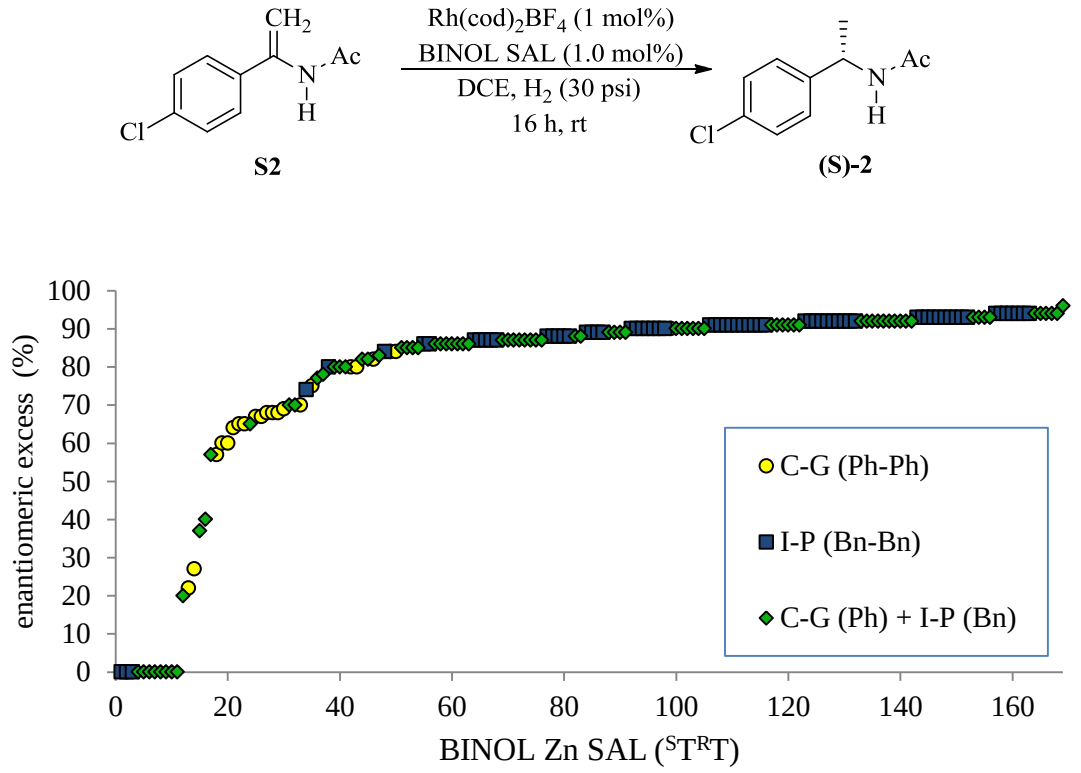

Figure 16 Hydrogenation of S2 with BINOL SAL Zn ($^{S}T^{R}T$) series

The full data on yields and enantioselectivity are summarized in Figure 17. The yield data also show wide variations among the catalysts. In spite of the close similarities among the catalysts screened, yields range from no reaction to quantitative. Since all reactions were run under a standard set of reaction conditions for a standard reaction time, low yields (i.e., low catalyst turnover numbers) may reflect catalyst decomposition and/or a slow catalyst (i.e., low catalyst turnover frequency). In either case the result is of significance from the standpoint of catalyst scaffold optimization.

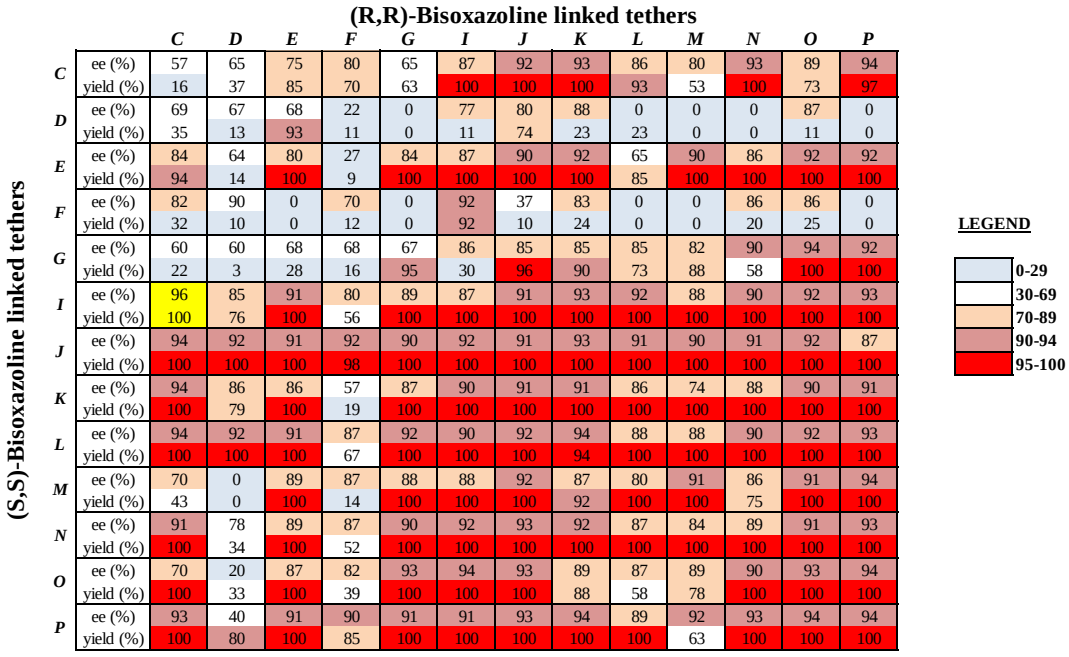

		C	D	E	F	G	I	J	K	L	M	N	O	P
C	ee (%)	57	65	75	80	65	87	92	93	86	80	93	89	94
	yield (%)	16	37	85	70	63	100	100	100	93	53	100	73	97
D	ee (%)	69	67	68	22	0	77	80	88	0	0	0	87	0
	yield (%)	35	13	93	11	0	11	74	23	23	0	0	11	0
E	ee (%)	84	64	80	27	84	87	90	92	65	90	86	92	92
	yield (%)	94	14	100	9	100	100	100	100	85	100	100	100	100
F	ee (%)	82	90	0	70	0	92	37	83	0	0	86	86	0
	yield (%)	32	10	0	12	0	92	10	24	0	0	20	25	0
G	ee (%)	60	60	68	68	67	86	85	85	85	82	90	94	92
	yield (%)	22	3	28	16	95	30	96	90	73	88	58	100	100
I	ee (%)	96	85	91	80	89	87	91	93	92	88	90	92	93
	yield (%)	100	76	100	56	100	100	100	100	100	100	100	100	100
J	ee (%)	94	92	91	92	90	92	91	93	91	90	91	92	87
	yield (%)	100	100	100	98	100	100	100	100	100	100	100	100	100
K	ee (%)	94	86	86	57	87	90	91	91	86	74	88	90	91
	yield (%)	100	79	100	19	100	100	100	100	100	100	100	100	100
L	ee (%)	94	92	91	87	92	90	92	94	88	88	90	92	93
	yield (%)	100	100	100	67	100	100	100	94	100	100	100	100	100
M	ee (%)	70	0	89	87	88	88	92	87	80	91	86	91	94
	yield (%)	43	0	100	14	100	100	100	92	100	100	75	100	100
N	ee (%)	91	78	89	87	90	92	93	92	87	84	89	91	93
	yield (%)	100	34	100	52	100	100	100	100	100	100	100	100	100
O	ee (%)	70	20	87	82	93	94	93	89	87	89	90	93	94
	yield (%)	100	33	100	39	100	100	100	88	58	78	100	100	100
P	ee (%)	93	40	91	90	91	91	93	94	89	92	93	94	94
	yield (%)	100	80	100	85	100	100	100	100	100	63	100	100	100

Figure 17 Full data set from BINOL SAL hydrogenation screening of **S2**

(BINOL)SAL Zn(IC) was identified as the best scaffold among the supramolecular catalysts screened giving 96% ee and quantitative conversion for substrate **S2**. As a side note, (BINOL)SAL Zn(IC) also gave the highest selectivity for substrate **S1** as well. In order to further assess catalyst efficiency, the screening results were analyzed with respect by comparing to percent yield against the percent enantiomeric excess. Figure 18 shows the percent yield plotted on the x-axis, and the percent enantiomeric excess on the y-axis; the values closest to the origin are not reactive and not selective. The ArO,ArO-linked scaffolds are predominantly found in this region. The upper-quadrant represents catalysts which are both highly reactive and highly enantioselective. This region is occupied mostly by scaffolds possessing at least one $ArCH_2O$-linked tether.

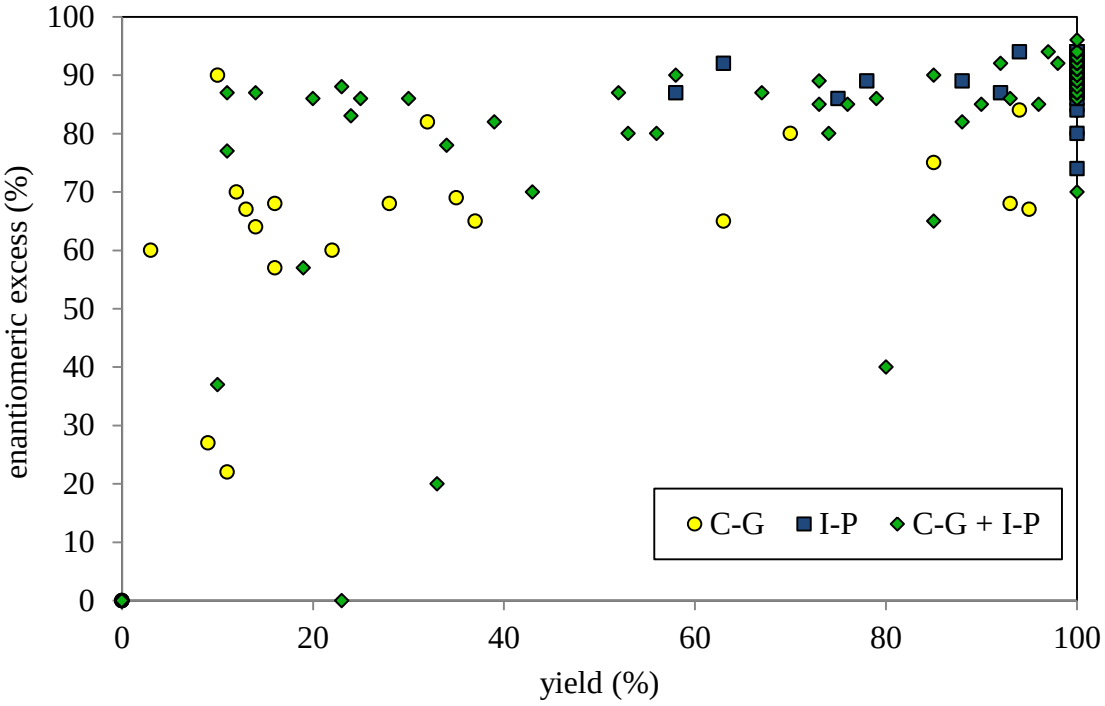

Figure 18 Plot of catalyst performance (% ee vs % yield) in the catalyzed asymmetric hydrogenation of **S2** coded by tether combination

Note that some data points in Figure 18 overlap. Surface plots examining the heavily occupied high yield-high enantioselectivity quadrant of Figure 19 better displays the number of redundant catalyst results. In a system where catalyst scaffold optimization is effective, small modifications to the tether structures are expected to affect catalyst performance. At the time this study was carried out, little thought had been given to how best to make use of catalyst scaffold optimization. That is, although usage of the term catalyst scaffold optimization was introduced into the literature by Takacs, others whose research fit into its description had given little strategic thought as how to productively apply the concept or even systematically evaluate its application beyond making a series

of random changes to the scaffold. Based on the study described here, we suggest that if changing the tethers has little effect on catalyst effectiveness, then the catalyst may be too flexible and unlikely to be optimized by such a study. In this context, Graph A highlights the hydrogenation results from scaffolds with $ArCH_2O$,$ArCH_2O$-linkages, while graph B corresponds to results from mixed scaffolds (i.e., $ArCH_2O$,ArO-linkages) (Figure 19). These plots reveal that, in general, the extra methylene linkage makes catalysts (in this case) more effective but less amenable to favorable scaffold optimization; in short, scaffolds that are too flexible, in this case, behave similarly to having no connected catalyst scaffold (i.e., similar to catalysts using two monophosphite ligands). Mixed $ArCH_2O$,ArO-linked scaffolds, which may be intermediate in terms of scaffold flexibility, give catalysts which exhibit a very broad range of selectivity and reactivity.

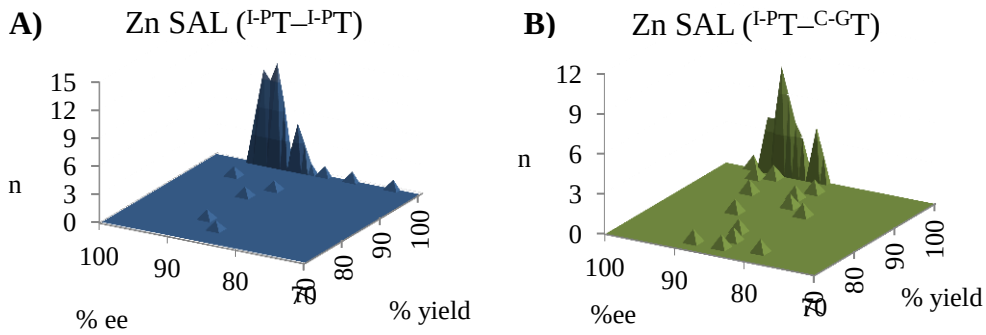

Figure 19 Surface plots highlighting relative abundance of hydrogenation catalysts with closely-related scaffolds that are selective and efficient. A) Scaffolds with two $ArCH_2O$ tethers. B) Scaffolds with mixed ArO linkage and $ArCH_2O$ linkage.

2.7 Examining the effect of small changes to the most efficient catalyst

(BINOL)SAL Zn(IC) was found to be the best catalyst scaffold in this study, giving the highest selectivity for both substrates with near quantitative conversion. The catalyst scaffold contains both an ArO-linked and an $ArCH_2O$-linked tether suggesting the need for a balance between flexibility and rigidity as discussed in previous sections. In this section, we drill down through the data to analyze how small changes to this optimal scaffold affect reactivity and selectivity. Is this a sharply unique optimum where any subtle change seriously erodes performance, or is this the best among a broad array of similar structures that differ incrementally in their performance?

The results obtained for several small systematic changes in the structure are summarized in Figure 20. Overall, the structural changes mostly led to noticeable but only incremental, changes in performance. For example, when the results obtained for catalysts wherein the phosphite ligating group on the ArO-linked tether varies from the *ortho*- to *meta*- to *para*-position, that is, (BINOL)SAL Zn(IE) and (BINOL)SAL Zn(IG) respectively, the enantioselectivity decreases from 93% to 89% to 88% ee for **S1** and from 96% to 91% to 88% ee for **S2**; all reactions proceed in high yield under the standard reaction conditions. Modifying to the biaryl in the (*R*)-bisoxazoline subunit, that is, from the *meta*- to *para*-linked biaryls as in (BINOL)SAL Zn(ID), affords a catalyst giving lower enantioselectivity for **S1** (86% ee) and both lower enantioselectivity (85% ee) and yield (76%) for substrate **S2**. Replacing the ArO-linked phosphite by an $ArCH_2O$-linked phosphite (i.e., (BINOL)SAL Zn (IK)) or moving the monoaryl $ArCH_2O$-linkage from meta to para (i.e., (BINOL)SAL Zn(JC)) had surprisingly little impact on the catalyst efficiency, 90-94% ee and quantitative yield for both substrates.

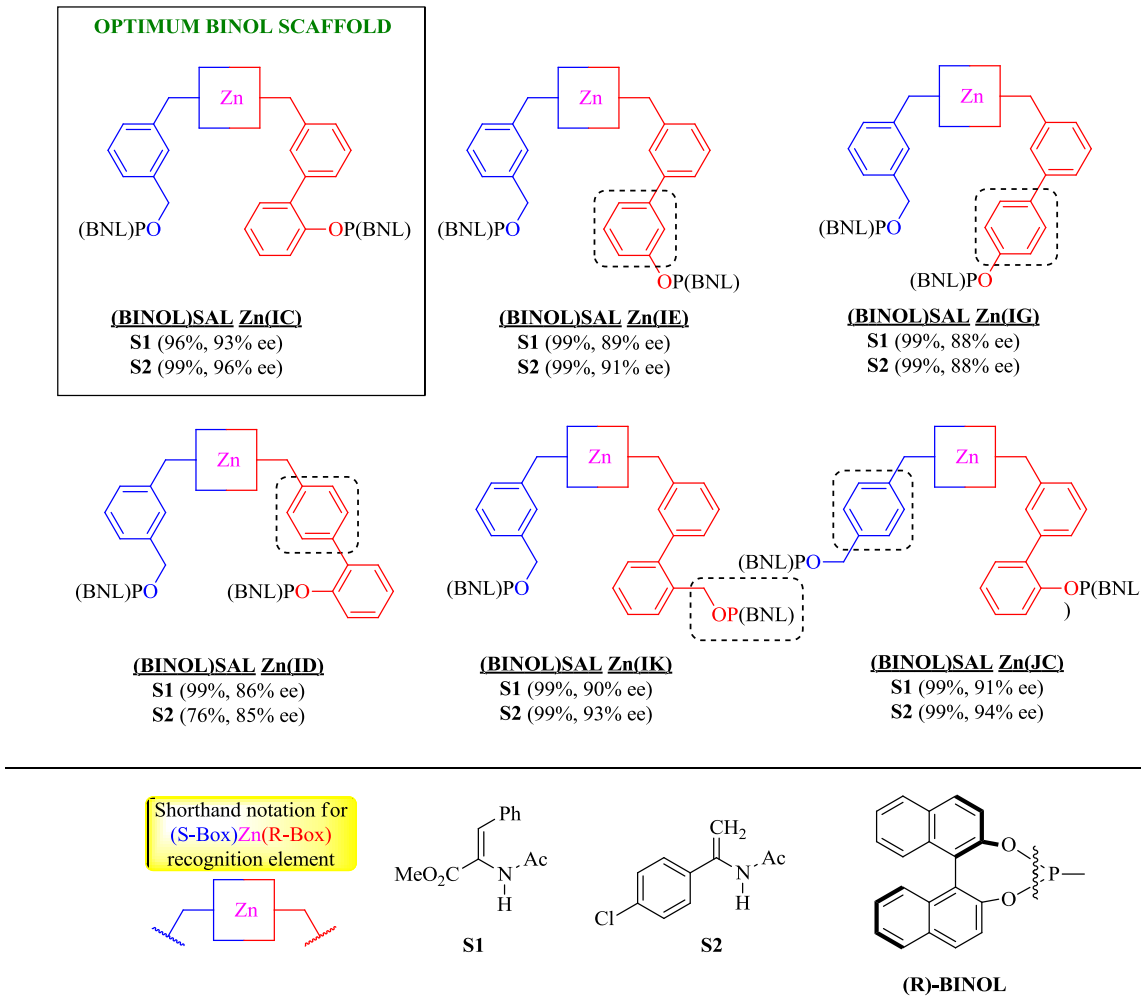

Figure 20 Incremental effect of varying the structure of an empirically determined optimal catalyst scaffold

An interesting question arose at this point during this study. Is the optimum scaffold identified in this study also optimal for other ligating groups? The corresponding (BIPHEP)SAL Zn(IC) and (TADDOL)SAL Zn(IC) catalysts were prepared and evaluated in comparison to (BINOL)SAL Zn(IC) and the corresponding monophosphites (Figure 21). Remarkably, the structurally similar (BIPHEP)SAL Zn(IC) was a poor

catalyst giving low reactivity and enantioselectivity. Furthermore, (TADDOL)SAL Zn(IC) was ineffective as well. Unlike (BINOL)SAL Zn(IC), both analogues were less efficient than their corresponding monophosphites. With the exception of (BIPHEP)POPh, BINOL, BIPHEP, and TADDOL monophosphites all gave near quantitative conversion. This is not to say that another catalyst scaffold could be found for BIPHEP and TADDOL, we might argue that would indeed be the case. The scaffold and ligating group are not independent contributors to catalyst efficient; they are intimately coupled.

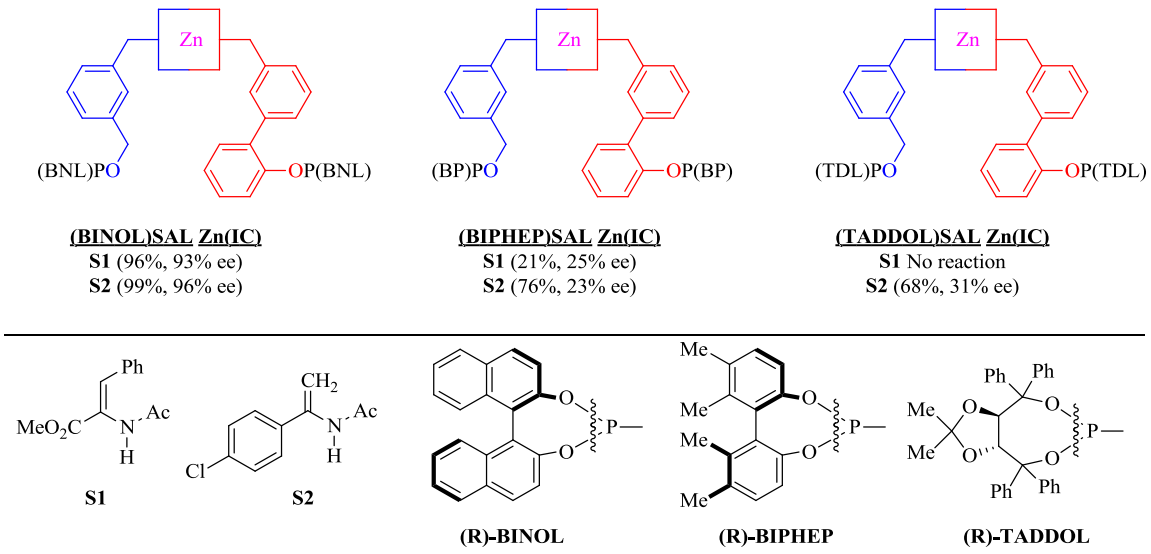

Figure 21 Influence of the ligating group on the performance of SAL Scaffold Zn(IC)

2.8 Influence of the chiral recognition element (BINOL) SAL Zn

If identical achiral substituents are appended to (*R*)-box and (*S*)-box, the heterochiral Zn complex is meso (achiral) as a consequence of inversion symmetry. However, when the two substituents attached to (*R*)-box and (*S*)-box differ and are not enantiomers, the heterochiral zinc complex lacks a center of inversion and is chiral. For example, a large optical rotation was observed for the mixed cyano/benzyl complexes.[36]

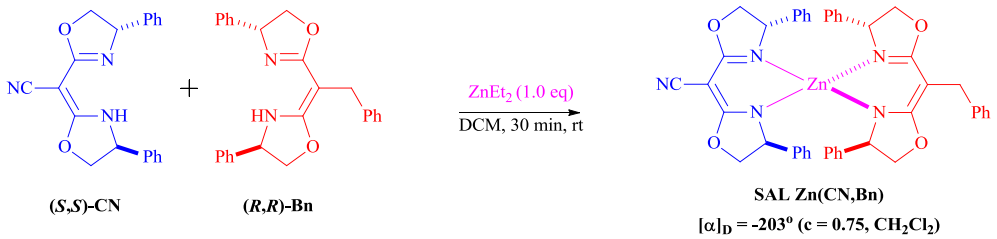

Figure 22 Complexation of a chiral pseudo-racemic Zn complex. Reproduced from Ref 36 with permission from the Centre de la Recherche Scientifique (CNRS) and the Royal Society of Chemistry

A subtle stereochemical feature of the catalysts examined raised the question of how the chiral recognition subunit impacts catalyst performance, if at all. Of the 169 supramolecular catalysts studied with **S2**, all with the same (BINOL)PO-ligating group, 13 have two identical tethers ; the remaining 156 are comprised of non-identical tethers. Consider the two complexes (BINOL)SAL Zn (IC) and (BINOL)SAL Zn(CI) (Figure 23). These scaffolds differ only by the interchange of the two tether subunits appended to the zinc core. Since the two different tethers have chiral ligating groups of matching handedness but differ in the configuration of the chiral recognition subunit, the two ligands (and the derived supramolecular catalyst) are diastereomers. Diastereomeric catalysts are not required to have similar reactivity and selectivity, but since the

recognition subunit is located quite far from the site of catalysis, it was not expected that a large difference in catalyst performance would be observed. Nonetheless, the two diastereomeric catalysts exhibit a marked difference in enantioselectivity from 96% ee to 87% ee for **S2**.

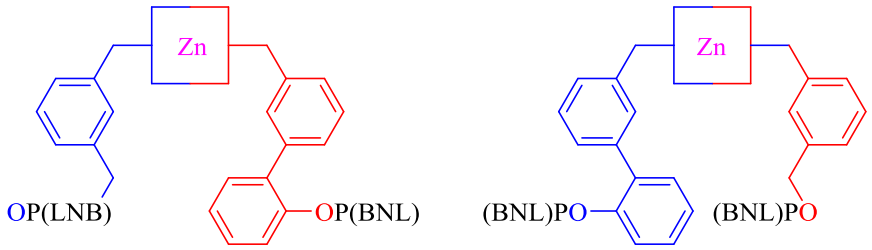

(BINOL)SAL Zn(IC)
S2 (99%, 96% ee)

(BINOL)SAL Zn(CI)
S2 (99%, 87% ee)

Figure 23 Diastereomeric catalysts have different performances

When comparing enantioselectivity achieved via selective diastereomeric reaction pathways, it is important to consider the logarithmic relationship between enantiomeric excess and the differences in activation energies leading to *(S)*- and *(R)*-products. For example, comparing the $\Delta\Delta G^{\ddagger}$ (*R/S*) values of 96% ee and 87% ee translates to a difference in enantioselectivity (Δes) of 0. 73 kcal/mol for the diastereomeric (BINOL)SAL Zn(IC) and (BINOL)SAL Zn(CI) catalysts. It seems quite remarkable that the bisoxazoline Zn complex, positioned far from the catalytically active site, has such a significant influence. Since it is believed that H_2 association and oxidative addition are the enantiodetermining steps, it seems reasonable to presume that the catalyst scaffold folds in such a way that the box complex impedes the approach of H_2 for one of the diastereomers creating a matched/mismatched is relationship between the chiral elements

(i.e., recognition subunit and ligating groups) within the catalyst.

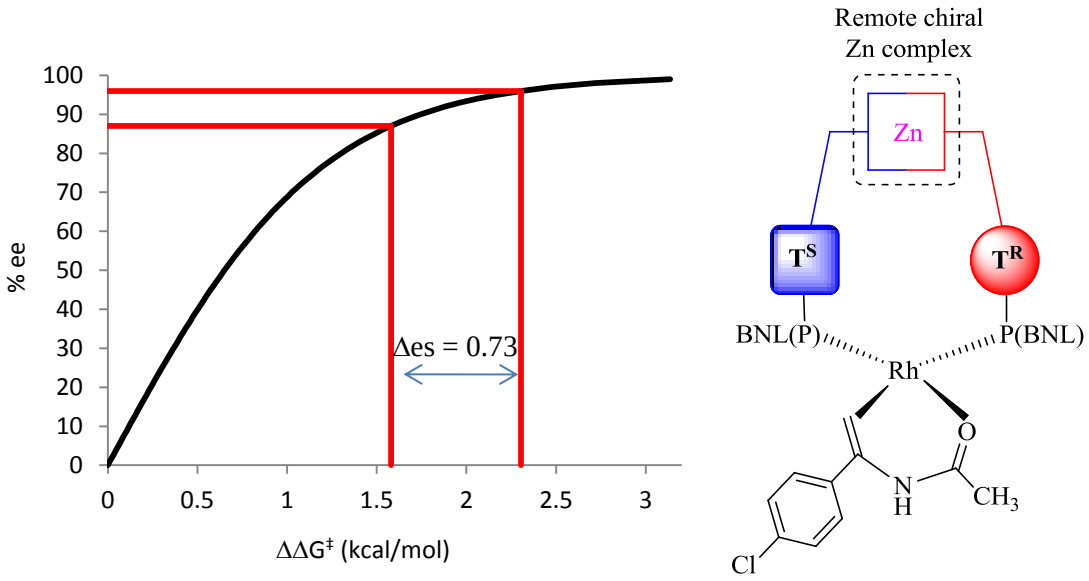

Figure 24 Theoretical relationship between enantioselectivity and $\Delta\Delta G^{\ddagger}$

Is difference in performance between the diastereomeric (BINOL)SAL Zn(IC) and (BINOL)SAL Zn(CI) catalysts typical or an exception? In total, 78 pairs of diastereomeric catalysts were identified in the screening set and compared for catalytic efficiency. The tethers were sorted by their composition of ArO-linked and $ArCH_2O$-linked tethers. To simplify the data, the Δes values were plotted unsigned (i.e., their absolute values) against the observed difference in reactivity (as judged by the yield obtained under the standard reaction conditions) (Figure 25). As expected, most catalysts were not strongly influenced from the presence of the chiral box moiety and exhibited minimal changes in reactivity and/or Δes; see the data points clustered about the origin in Figure 25. Generally, catalyst pairs that exhibited a substantial difference in

enantioselectivity also exhibited a large difference in reactivity as well; see the upper and lower right regions of the plot.

The data in Figure 25 are color-coded by type of linkage to the two ligating groups. Scaffolds composed of two $ArCH_2O$-linkages, the most flexible catalysts, were impacted the least from the chiral recognition element. The most rigid scaffolds, that is, those with only ArO-linkages had a significant number of catalysts that exhibited large differences in yield under standard reaction conditions. The differences might be attributed to differing turnover frequency (i.e., reaction rates) and/or turnover numbers and catalyst deactivation; the data collected cannot distinguish between the two possibilities. The scaffolds with mixed linkages of one ArO-linked and one $ArCH_2O$-linked phosphite exhibited the largest influence from the chiral recognition element. This is perhaps not unexpected as these catalysts were the most receptive to the scaffold optimization.

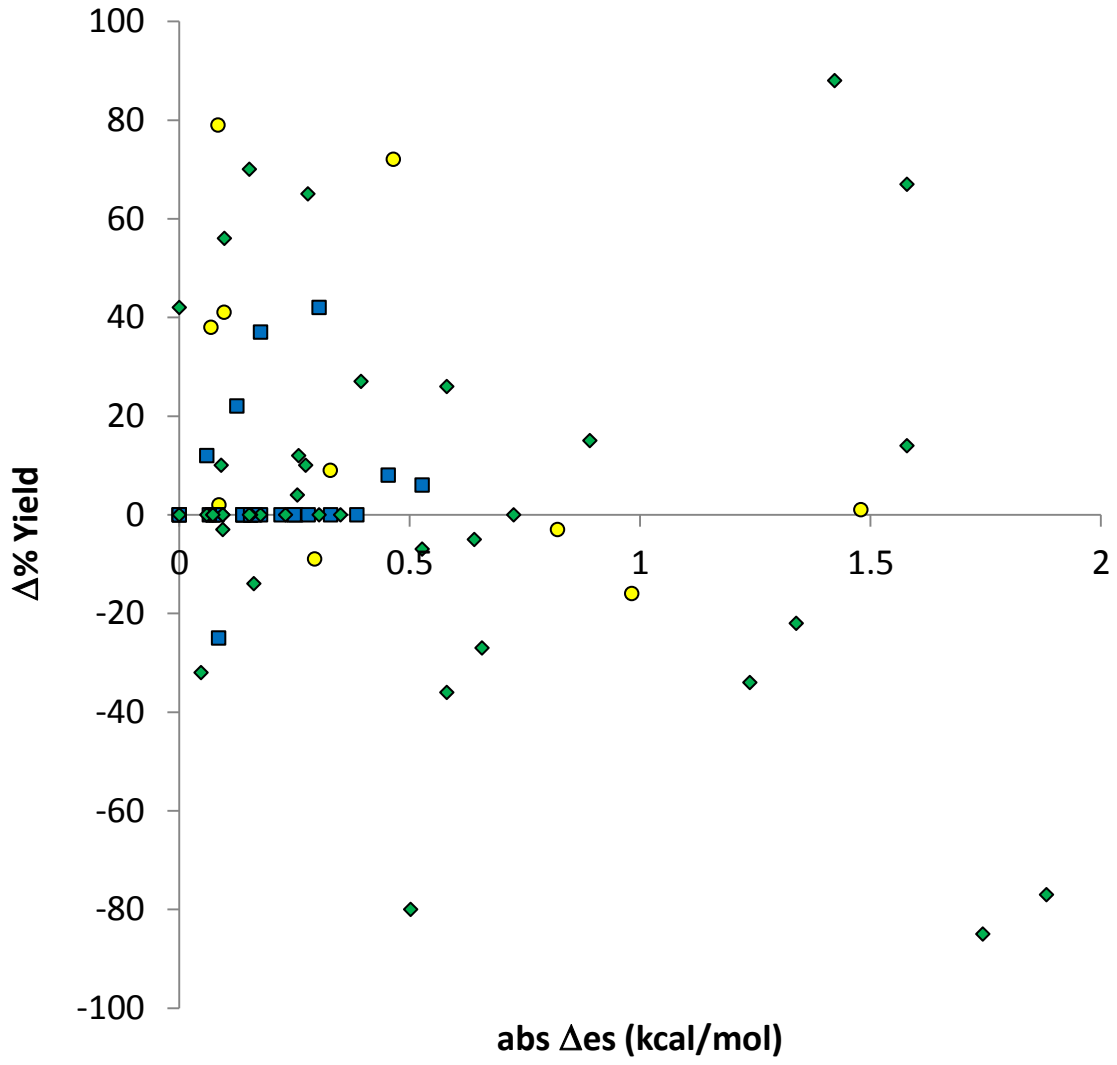

Figure 25 Differences in yield and enantioselectivity between 78 pairs of diastereomeric catalysts in the CAH of S2 with (BINOL)SAL Zn($^{S}T^{R}T$). Yellow circle points represent scaffolds with only tethers C-G, the blue squares only I-P, and the green diamonds are for mixed combinations of C-G and I-P

A few specific examples of matched/mismatched catalytic performances are highlighted in Table 2 to illustrate the wide range of effects found. Examples were found

for the scaffolds with mixed tethers **C-G** and **I-P**(entries 1-7) and those comprised of only $ArCH_2O$ tethers **I-P** (entries 8-9) and ArO tethers **C-G** (10-11). As a representative of catalysts which had little difference between reactivity or selectivity with the diastereomeric catalysts, (BINOL)SAL Zn(OG) (entry 1) and its complimentary diastereomer were both quite effective in the Rh-CAH of **S2**. (BINOL)SAL Zn(LC) (entry 3) and (BINOL)SAL Zn(CL) gave similar reactivity but a significant difference in selectivity. Not all diastereomeric catalysts efficiency comparisons result in changes in both selectivity and reactivity. (BINOL)SAL Zn(NG) (entry 4) and its diastereomeric scaffold (BINOL)SAL Zn(GN) both gave high selectivity, yet one diastereomer was less reactive. There were some striking examples where one diastereomer was quite effective while the other was unreactive and non-selective (entries 5-7). While most of the flexible doubly $ArCH_2O$-linked scaffolds showed no influence by the chiral recognition subunit, several examples were identified where significant differences in selectivity and/or reactivity were observed (entries 8-9). The more rigid scaffolds containing only ArO-linkages were less selective and reactive as a whole, several examples that were moderately selective were identified where their diastereomeric partners gave less effective catalytic performances (entries 10-11).

Table 2 Selected examples where diastereomeric catalysts exhibit matched/mismatched reactivity and/or selectivity in the CAH of S2.[a]

Entry	Zn ($^{S}T^{R}T$)	% yield (% ee)	Zn ($^{S}T^{R}T$)	yield (% ee)	Δes (kcal/mol)
1	OG	99 (94)	GO	99 (93)	0.09
2	IC	99 (96)	CI	99 (87)	0.73

3	LC	99 (94)	CL	93 (86)	0.53
4	NG	99 (90)	GN	58 (90)	0
5	LD	96 (92)	DL	23 (0)	1.88
6	FP	85 (90)	PF	nr	
7	JF	98 (92)	FJ	10 (37)	1.42
8	KL	94 (94)	LK	99 (86)	0.58
9	KM	87 (92)	MK	99 (74)	0.55
10	EG	99 (84)	GE	28 (68)	0.46
11	EC	94 (84)	CE	85 (75)	0.29

[a]All examples gave predominantly the (S) enantiomer

To further illustrate the importance of the chiral recognition element, the bisoxazoline zinc complex was eliminated and replaced with a relatively unstructured straight chain alkyl linker. This approach was effective for Reetz and co-workers when used for the screening of simple to prepare bidentate ligands for the Rh-CAH of a series of prochiral substrates.[43] In their report, reactivity and selectivity was affected varying the chain length between the two ligating groups. In our case, the bidentate ligands were prepared from 1,n-diols (Table 3). While reactivity for the ligands was generally high, selectivity varied wildly for **S1** and **S2**. The 1,4-butane diol derived bisphosphite was slightly more selective in the CAH than the monodentate ligands **L5** or **L6** for **S1**, but nowhere near as selective as (BINOL)SAL Zn(IC); the tether structure is important.

Table 3 Alkyl chain linked phosphites in the Rh-CAH of S1 and S2

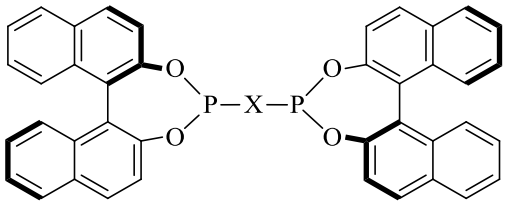

L7 ($X = O(CH_2)_3O$)
L8 ($X = O(CH_2)_4O$)
L9 ($X = O(CH_2)_5O$)
L10 ($X = O(CH_2)_6O$)

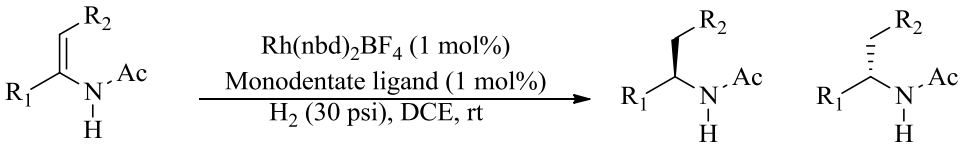

S1 ($R^1 = CO_2Me$, $R^2 = Ph$)
S2 ($R^1 = 4\text{-}ClC6H4$, $R^2 = H$)

(R)-2
(R)-3

(S)-2
(S)-3

		S1		**S2**	
Entry	Bidentate ligand	ee (%)	yield (%)	ee (%)	yield (%)
1	L7	20	99	26	93
2	L8	87	99	68	90
3	L9	71	99	64	87
4	L10	13	90	53	99

2.9 Characterization of Rh[BINOL(SAL) Zn(IC)](nbd)]BF_4

A question that often arises is whether these supramolecular catalysts are (in all cases) monomeric or perhaps di- or oligomeric in these reactions (Figure 26). The "in all cases" variant is of course not possible to answer definitively. The first approach we tried, attempts to grow a crystal of Rh[(BINOL)SAL Zn(IC)(nbd)]BF_4 suitable for X-ray analysis, were unsuccessful.

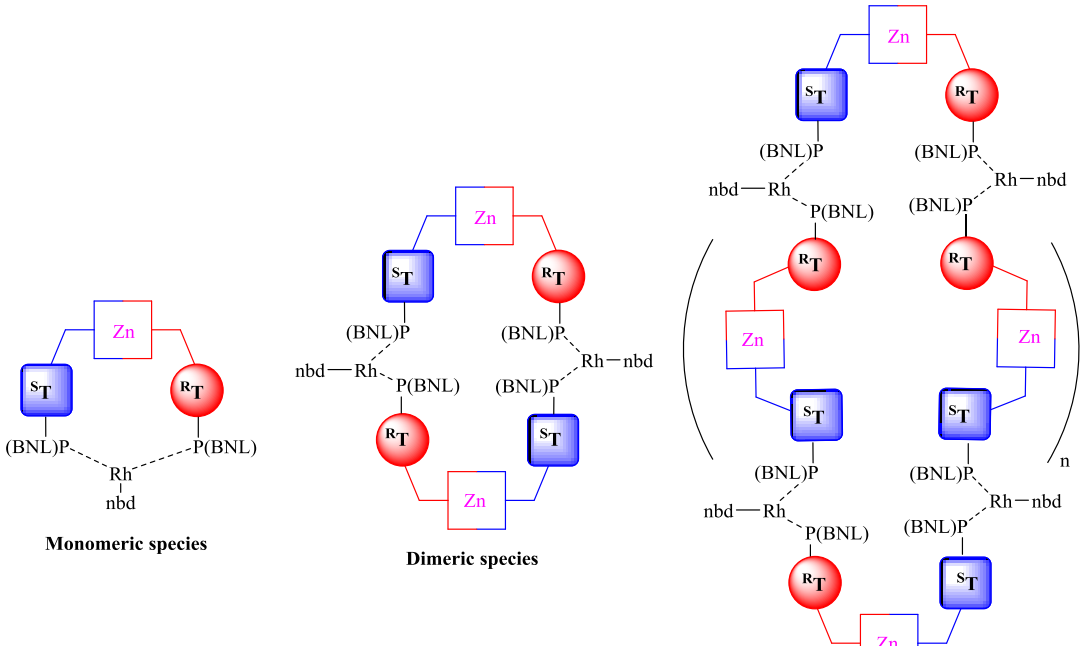

Figure 26 Catalytic species possible in solution for (BINOL)SAL Zn($^{S}T^{R}T$)

Another common technique used to characterize bidentate ligands is NMR. By comparing literature values for P-Rh-P coupling constants, the catalyst structure can be inferred. The flexible nature of these supramolecular catalysts increases the difficulty in obtaining reliable structural information via NMR. Dr. Shin Moteki was able to characterize a related (TADDOL)SAL bound to rhodium(I) with a triflate counterion.[44] The data was consistent for cis-chelation of the bidentate ligant to rhodium. Rhodium complexes with biaryl-type phosphorus based ligands often have more complicated spectra from a reversible dimerization process wherein η-arene coordinated dirhodium complexes may be formed. These interactions have been well characterized in Rh-

BINOL phosphinite[45] and Rh-BINAP complexes.[46] η^6-Arene coordinated rhodium complexes to the related diphenylphosphine ligands have also been observed in Rh-dppe complexes.[47] When 2 equivalents of (BINOL)POBn or (BINOL)POPh were added to 1 equivalent of $Rh(nbd)_2BF_4$ in $CDCl_3$, 2 sets of doublets corresponding to the bidentate rhodium complex and the η-arene coordinated dirhodium complex (Figure 27). The upfield doublet corresponds to the η-arene complex; addition of MeOH disrupts the pi-complexation and results in only the downfield doublet remaining.

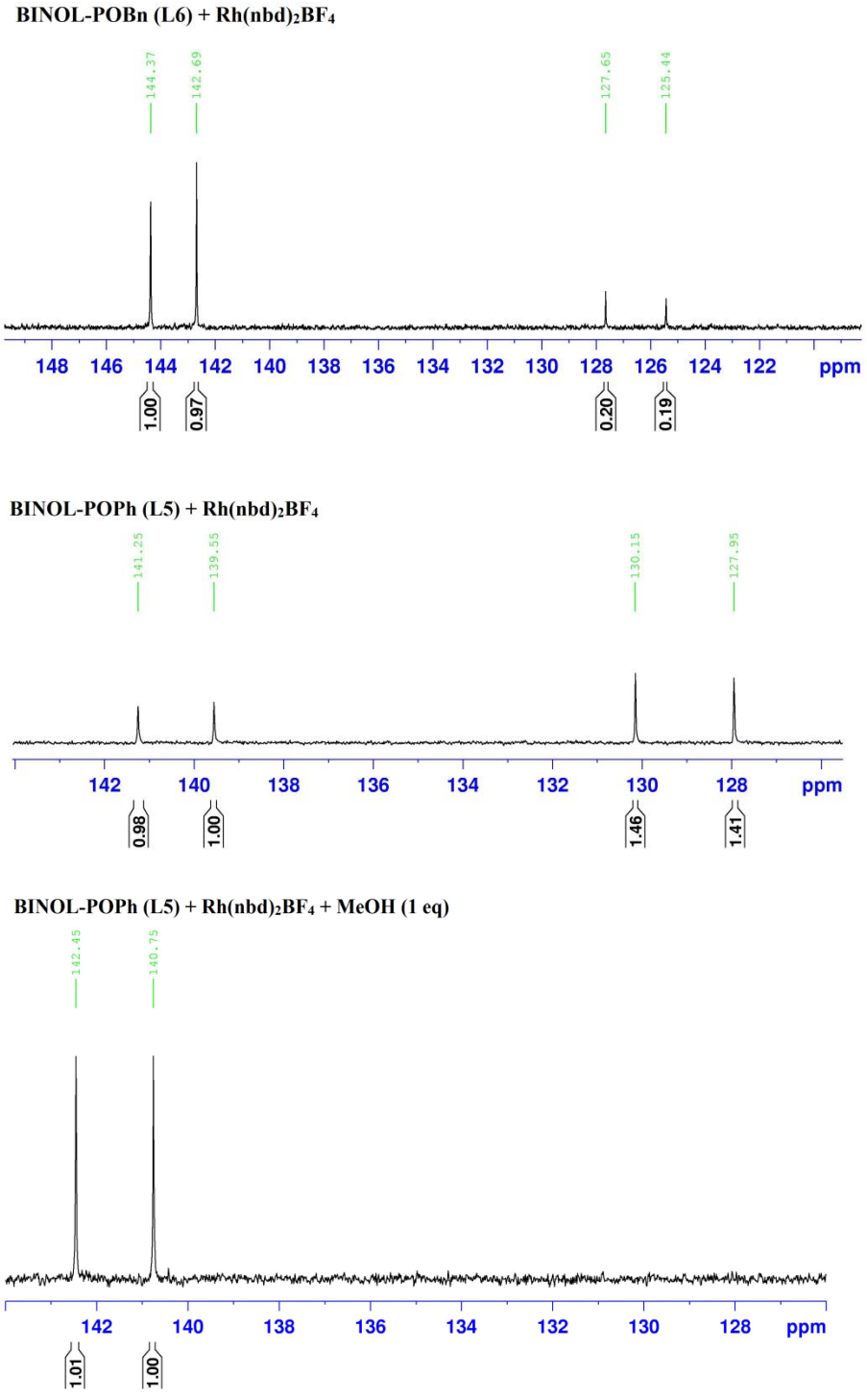

Figure 27 ^{31}P NMR study showing dynamic behavior of BINOL phosphite-Rh complexes.

(BINOL)SAL Zn(IC) gives two singlets in the ^{31}P for two chemically distinct phosphite ligands (Figure 28). However, upon addition of $Rh(nbd)_2BF_4$, a broad peak was formed. Lowering the temperature to slow dynamic behavior in the catalyst did not resolve the broad peak. The addition of MeOH or substrates **S1** or **S2** did not help either.

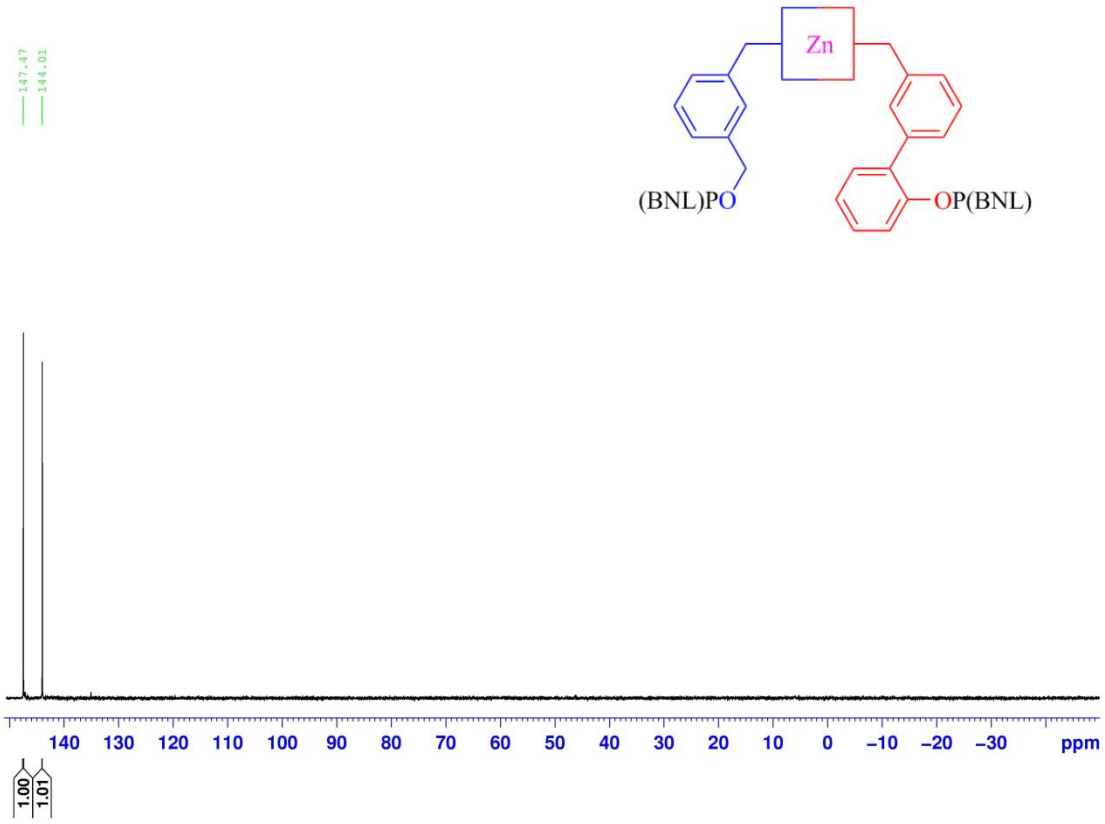

Figure 28 ^{31}P NMR of (BINOL)SAL Zn(IC)

High-resolution mass spectrometry is another common technique for obtaining structural information. However, methods such as fast atom bombardment (FAB) or the more mild matrix-assisted laser desorption/ionization (MALDI) technique were unsuccessful in characterizing the (BINOL)SAL scaffold; a parent ion was not found. It

is not uncommon to have difficulty in characterization of an effective catalyst. Catalysts may owe their efficiency due to their relative instability of their chemical intermediates. Joost Reek and co-workers recently reported the stability of a catalytic intermediate in the Pd-catalyzed allylic alkylation reaction had an inverse relationship to reactivity of the catalyst.[48] That is, ineffective catalysts were more easily characterized from their added stability, while effective catalysts were difficult to detect.

Yet another technique of structural characterization typically used for polymers is gel-permeation chromatography (GPC). This technique uses a size-exclusion matrix to differentiate different sizes (i.e., the hydrodynamic radius of the structure) of molecules in solution (Figure 29). The differentiation occurs as smaller molecules penetrate the stationary porous phase which slows their elution time from the column. Larger molecules not able to pass into and then through the stationary phase will elute more quickly since they have fewer interactions inside the column. This technique is commonly applied to polymers where polystyrene standards of large molecular weights can be used to determine the relative size of a synthesized polymer.

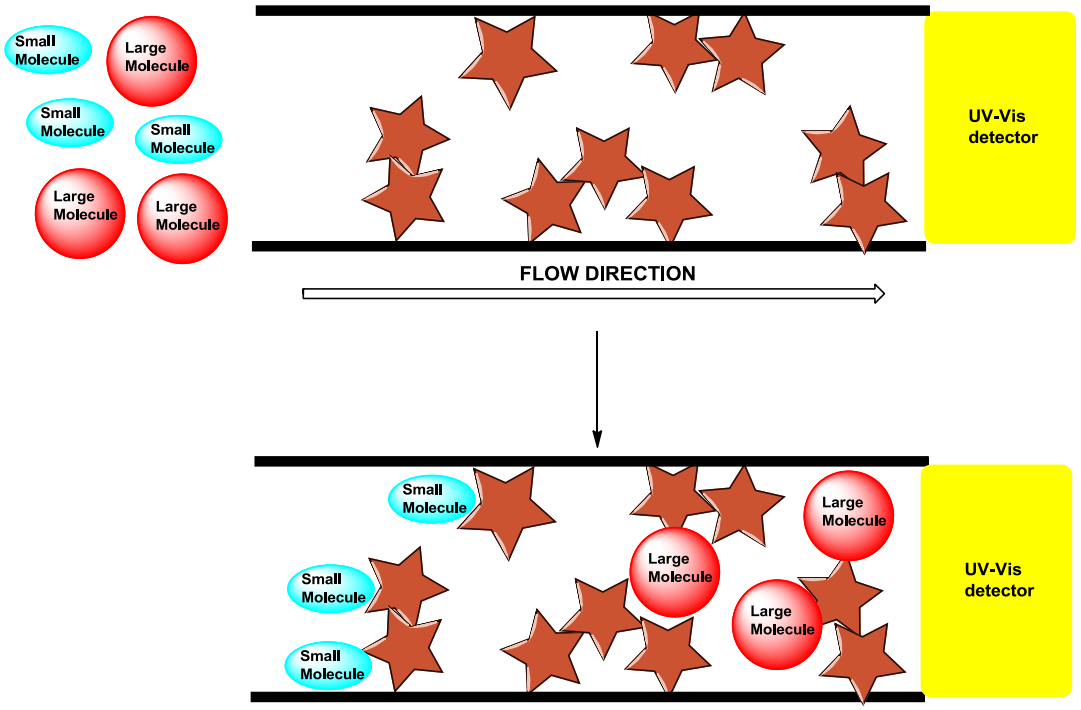

Figure 29 In size exclusion chromatography, smaller molecules spend more time interacting with the porous column, while larger molecules are able to pass through more quickly.

It should be possible to get some structural information if the retention times vary as a function of structural changes in going subunit to SAL to supramolecular catalyst. Ligands before and after zinc and rhodium addition were injected on a GPC column (4.6 mm Jordi Gel DVB (cross-lined divinylbenzene stationary phase) column, Pore size 100 Å, $CHCl_3$ as the eluent). No significant change was observed upon addition of zinc to the tethers (Table 4, entries 1-3). The lack of a change in retention time is likely a result of the structural change not being significant enough to have the retention time effected. However, upon addition of rhodium, the complex exhibited a longer retention time (Table

4, entry 4). We interpret this change in the following way; as rhodium chelates to the bidentate ligand, the structure is made more compact explaining the longer retention time.

Table 4 GPC studies on BINOL catalysts

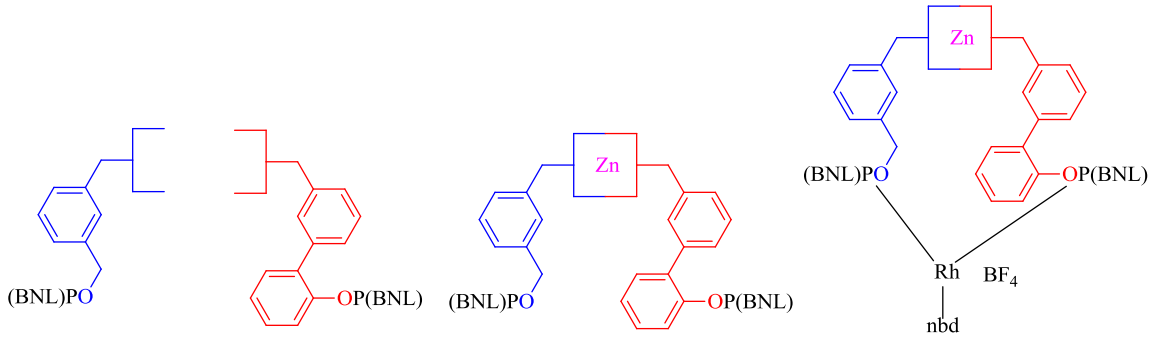

BINOL tether I **BINOL tether C** **(BINOL)SAL Zn(IC)** **[(BINOL)SAL Zn(IC) Rh(nbd)]BF_4**

Entry	ligand	Retention Time (min)
1	BINOL tether I	7.5
2	BINOL tether C	7.4
3	(BINOL)SAL Zn(IC)	7.4
4	[(BINOL)SAL Zn(IC)Rh(nbd)]BF4	8.1

Conditions: 4.6 mm Jordi Gel DVB column, Pore size 100 Å, flow rate = 0.7 mL/min, mobile phase ($CHCl_3$)

Scaffolds which bear only one ligating group are monodentate ligands and must form a dimer upon addition of rhodium. Thus, these catalysts serve as excellent controls for effectively doubling the size of (BINOL)SAL Zn(IC) catalyst. Because the truncated ligands only have one large BINOL phosphite, they are smaller than the bidentate scaffold and thus have longer retention times than the free (BINOL)SAL Zn(IC) scaffold (Table 5, entries 1 and 3). Upon addition of rhodium, both of the catalysts eluted with shorter retention times suggesting an increase in the size of the catalyst (Table 5, entries 2 and 4). Since the rhodium-chelated truncated ligands had shorter retention times than

[(BINOL)SAL Zn(IC)]Rh(nbd)BF_4, this result gives some evidence the desired 1:1 catalyst rhodium complex is forming

Table 5 GPC data on truncated BINOL catalysts

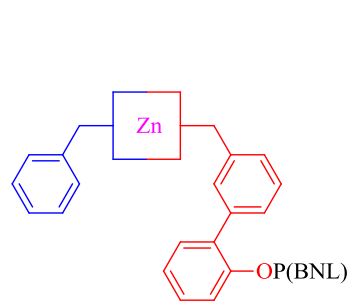

(BINOL)SAL Zn(I-truncated)

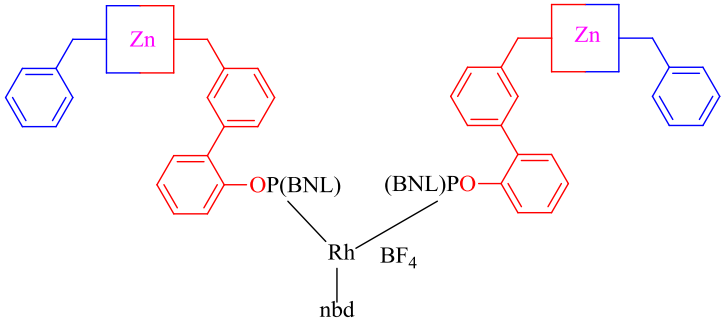

[(BINOL)SAL-Zn(I-truncated)]$_2$Rh(nbd)BF_4

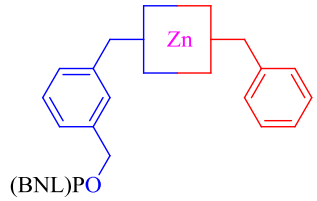

(BINOL)SAL Zn(C-truncated)

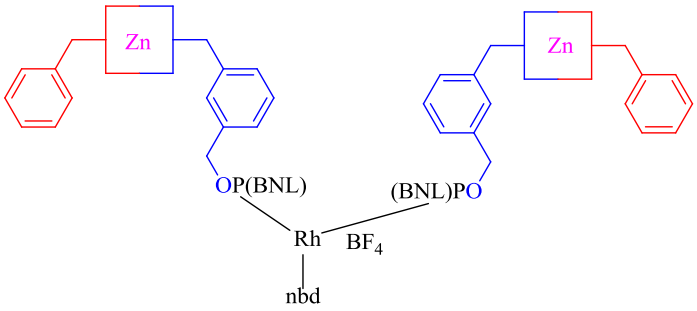

[(BINOL)SAL-Zn(C-truncated)]$_2$Rh(nbd)BF_4

Entry	ligand	Retention Time (min)
1	(BINOL)SAL-Zn(I-truncated)	8.4
2	[(BINOL)SAL-Zn(I-truncated)]$_2$Rh(nbd)BF_4	7.6
3	(BINOL)SAL-Zn(C-truncated)	8.2
4	[(BINOL)SAL-Zn(C-truncated)]$_2$Rh(nbd)BF_4	6.5

Conditions: 4.6 mm Jordi Gel DVB column, Pore size 100 Å, flow rate = 0.7 mL/min, mobile phase ($CHCl_3$)

These truncated ligands can also be used as hydrogenation catalysts to compare their reactivity. The (BINOL)SAL Zn(I-truncated) and (BINOL)POPh are both phenol linked

phosphites (Table 6, entries 1-2). Their reactivity however is significantly different under identical reaction conditions which may be a result of the truncated ligand being too bulky for effective catalysis. The phenol ligating group keeps the bulky substituent nearby. (BINOL)SAL Zn(C-truncated) and (BINOL)POBn are $ArCH_2O$-linked phosphites (Table 6, entries 3-4). These two catalysts gave comparable performance to one another. The bulkiness of the truncated ligand may not be a factor from the increased degree of freedom in the benzylic linkage to the phosphite. Since neither of the truncated ligands outperformed the bidentate (BINOL)SAL Zn(IC), this further supports the catalytically active species to be the bidentate catalyst.

Table 6 Truncated monophosphite ligands do not out perform s(BINOL)SAL Zn(IC)

		S1		**S2**	
Entry	ligand	ee (%)	yield (%)	ee (%)	yield (%)
1	BINOL-POPh	69	99	86	99
2	(BINOL)SAL-Zn(I-truncated)	30	2	65	13
3	BINOL-POBn	82	99	92	99
4	(BINOL)SAL-Zn(C-truncated)	85	99	92	99
5[c]	(BINOL)SAL Zn(IC)	93	96	96	99

Reaction conditons: 1 mol% $Rh(nbd)_2BF_4$, 2.1 mol% monophosphite, DCE, rt, 16 h. Yields and enantioselectivity determined by chiral GC using N-benzyl acetamide as an internal standard. [b]Unless otherwise noted, the (S)-enantiomer predominates the reaction. [c]1 mol% of bisphosphite was used.

2.10 Conclusions and future directions

Structure-activity studies are commonly undertaken to determine which structural elements are important factors in the success of a catalyst system. Small molecule catalysts, while often effective, omit some of the key structural features of enzymes due to their limited chiral space. Supramolecular catalyst systems are being pursued with the hope to organize the topography around a catalytic pocket and thus more closely mimic enzyme-like structures. However, much less is known about strategies for optimizing the performance of supramolecular catalyst systems. Understanding which factors are important in a supramolecular catalyst will be crucial to design effective enzyme-like catalysts. Among the more surprising aspects of this study is that the remotely positioned chiral recognition element can have a significant influence the effectiveness of the catalyst system in a matched/mismatched relationship with the chiral ligating groups.

Thus far, these supramolecular systems have only explored the hydroboration of styrenes, hydrogenation of prochiral enamides (present study), and asymmetric allylic amination. In unpublished work, some striking success has been realized in finding catalysts that can distinguish between closely related sites for reaction, that is, site selective catalysts. It is expected that future studies will be directed along these lines focusing on complex transformations involving substrates with multiple potential sites of reaction. The post-synthetic modification of natural products is a vastly underdeveloped aspect of organic synthesis. Enzyme-like supramolecular catalysts hold promise for such transformations and should complement other approaches. For example, Scott Miller has reported some small peptide catalysts capable of post-synthetic modifications via a variety of transformations on polyfunctionized natural products.[49-55] However, while the

use of synthetic peptide catalysts requires their *de novo* synthesis and are limited to solvents that promote hydrogen-bonding to preserve catalyst structural integrity, the bisoxazoline-zinc chiral recognition element exploits combinatorial diversification. Their utility may in part reflect the fact that their facile self-assembly by chiral discrimination is reminiscent of a "click" reaction, one that occurs rapidly and in near-quantitative yields.[56]

As supramolecular catalysis is developed, it is intriguing to think of the possibilities of substituting zinc for a metal which may participate in redox chemistry. Ruthenium catalysts have been exploited by McMillan and co-workers for their redox properties and their compatibility with organocatalysts.[57] Not only would substitution of zinc for ruthenium add another catalytic metal, it would also change the geometry around the metal from tetrahedral to octahedral. Bonnet, Collin, and Sauvage reported the stepwise synthesis of an octahedral ruthenium complex with three different substituents.[58] Conditions may be found that allow for three complimentary groups, each with a role in the catalysis, to organize around the ruthenium center giving way to a diverse new family of self-assembled supramolecular catalysts.

2.11 Experimental

Reactions were carried out in a dry atmosphere (N_2). Dichloromethane (DCM), tetrahydrofuran (THF), and methanol (MeOH) were freshly distilled under the following conditions: DCM from calcium hydride, THF from sodium metal and benzophenone, and MeOH from Mg. All synthesized compounds were purified with flash chromatography with the indicated solvents using EMD Silica Gel 60 Geduran ®. Thin

layer chromatography analyses were performed on Analtech Silica Gel HLF (0.25 m) precoated analytical plates and visualized with use of handheld short wavelength UV light, vanillin stain (ethanol, H_2SO_4, and vanillin), and Ninhydrin stain (ethanol, acetic acid, and ninhydrin). All reactions were performed in a chemical fume hood or in a glovebox with a nitrogen environment. NMR spectra were recorded on either a 400 MHz or a 300 MHz Bruker Advance NMR spectrometer using $CHCl_3$ (δ 7.27 ppm), $CDCl_3$ (δ 77.0 ppm), or CH_2Cl_2 (δ 5.30 ppm) for reference. Gas chromatography analysis was performed with a CP-Chirasil-Dex CB column (I.D. = 0.25 mm) using a temperature program of 140-200 ^oC at 1 ^oC/min). Peaks are expressed as m (unresolved multiplet), q (quartet), t (triplet), d (doublet), s (singlet), bs (broad singlet). IR spectra were recorded using an Avatar 360 FT-IR. Optical rotations were measured in solutions, 1.0 g/100 mL CH_3Cl unless indicated otherwise, and recorded using an Autopol III automatic polarimeter. HRMS analyses were performed by the Nebraska Center for Mass Spectrometry. All phenolic tethers were prepared using procedures described in the literature.

Screening protocols and compilation of screening data for SAL hydrogenation studies

Screening protocol procedures for SAL hydrogenation screening

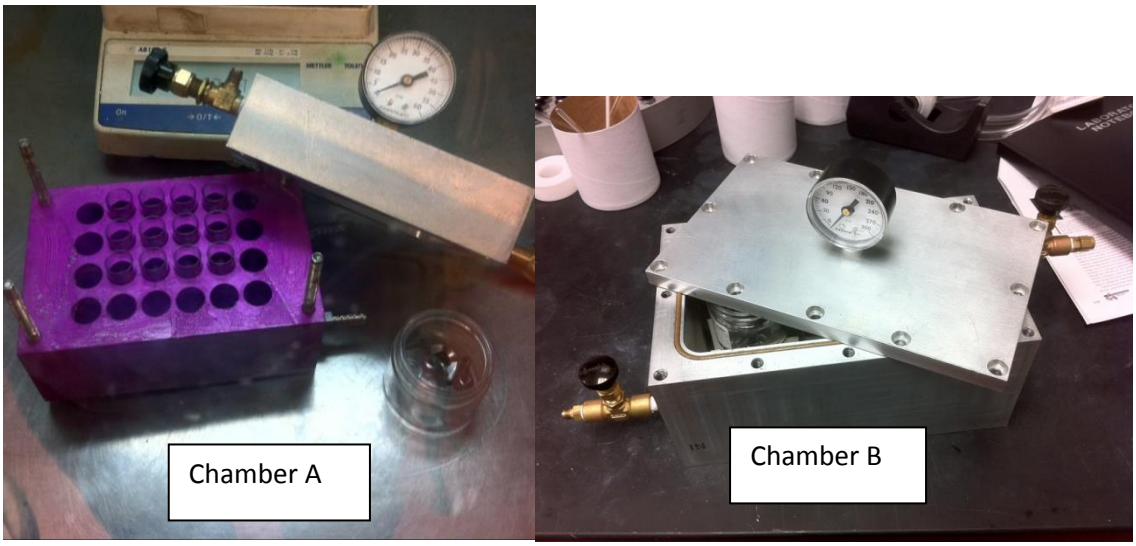

Supporting Information Figure 1: Hydrogenation chambers used for the hydrogenation screenings; Chamber A is used for up to 24 small scale screenings, and Chamber B can be used for up to 72 small scale screenings or can accommodate sixteen 20 mL vials for large scale vials for screening.

Stock solutions BINOL tether ((S,S)-I) (3.0 mg, 4.0 μmol) in 2.3 mL CH_2Cl_2 and BINOL tether ((R,R)-C) (3.4 mg, 4.2 μmol) in 2.2 mL CH_2Cl_2 were prepared. An aliquot of each of the tether stock solutions (0.10 mL, .18 mmol SAL) was transferred to a vial containing three glass beads (added to aid with stirring). A stock solution of $ZnEt_2$ (2.0 μmol/mL in CH_2Cl_2) was prepared from $ZnEt_2$ (1.0 M in hexanes). Approximately 0.10 mL (.20 μmol $ZnEt_2$) of the freshly prepared $ZnEt_2$ stock solution was added to the hydrogenation vials and the vials were stirred on an orbital shaker (ca 125

revolutions/min) over a 30 minute period. The CH_2Cl_2 was removed under reduced pressure (ca 30 min) and the catalysts were redissolved in dichloroethane (0.20 mL). A stock solution of $Rh(nbd)_2BF_4$ (3.0 mg, 8.0 μmol) in dichloroethane (4.4 mL) was prepared and an aliquot of the $Rh(nbd)_2BF_4$ stock solution (0.10 mL, .18 μmol Rh) was added to each vial. The resulting metal-ligand complex was stirred on an orbital shaker shaker (ca 30 min at 125 revolutions/min.) A stock solution of N-(1-(4-chlorophenyl)vinyl)acetamide (3.6×10^1 mg, 0.18 mmol) in dichloroethane (1.0 mL) was prepared and an aliquot (0.10 mL, 1.8×10^{-2} mmol) was added to each reaction vial. The vials were loaded into the hydrogenation chamber. The chamber was purged with H_2 (5 X 30 psi). The chamber was charged with H_2 (30 psi) and lightly shaken (ca 125 revolutions/min) at ambient temperature for 16 h, at which point the hydrogen pressure was released. A stock solution of an internal standard, N-benzyl acetamide, was prepared (82 mg in 3.0 mL ethyl acetate). An aliquot (0.10 mL, 1.8×10^{-2} mmol) was added to each of the reaction vials. The organics were filtered through a small plug of silica gel. Ethyl acetate (1 mL) was used to rinse the vial and silica plug. An additional wash (ethyl acetate, 0.5 mL) was used to rinse the silica plug. Combined organics were then analyzed via gas chromatography CP-Chirasil-Dex CB column (I.D. = 0.25 mm) using a temperature program of 140-200^{o}C at 1 ^{o}C/min). The (S)-enantiomer eluted at 22.2 min (97.9%) and the (R)-enantiomer at 23.2 min (2.1%); $[\alpha]_D$ = -154 (c = 0.5, EtOH); ^{1}H NMR (400 MHz, $CDCl_3$) δ 7.33-7.25 (4H, m), 5.76 (1H, bs), 5.11 (1H, m), 2.00 (3H, s), 1.48 (3H, d, *J* = 6.9 Hz); ^{13}C NMR (100 MHz) δ 169.11, 141.79, 133.06, 128.77, 127.58, 48.20, 23.41, 21.69

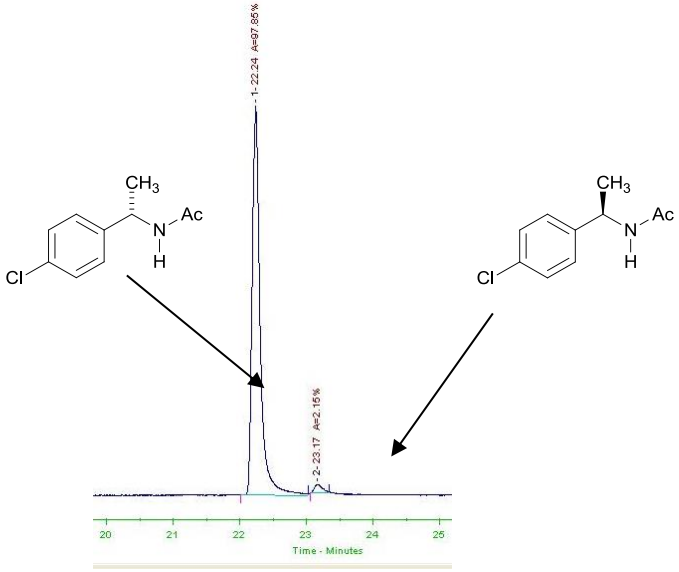

Compilation of p-Cl screening with self-assembling ligands (SALs) with p-Cl eneacetamide

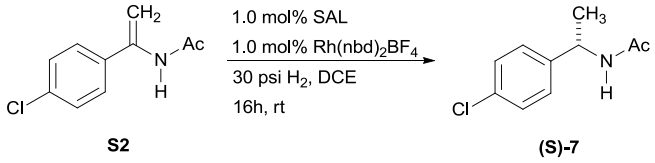

S2 **(S)-7**

(R,R)-Bisoxazoline linked tethers

(S,S)-Bisoxazoline linked tethers		C	D	E	F	G	I	J	K	L	M	N	O	P
C	ee (%)	57	65	75	80	65	87	92	93	86	80	93	89	94
	yield (%)	16	37	85	70	63	100	100	100	93	53	100	73	97
D	ee (%)	69	67	68	22	0	77	80	88	0	0	0	87	0
	yield (%)	35	13	93	11	0	11	74	23	23	0	0	11	0
E	ee (%)	84	64	80	27	84	87	90	92	65	90	86	92	92
	yield (%)	94	14	100	9	100	100	100	100	85	100	100	100	100
F	ee (%)	82	90	0	70	0	92	37	83	0	0	86	86	0
	yield (%)	32	10	0	12	0	92	10	24	0	0	20	25	0
G	ee (%)	60	60	68	68	67	86	85	85	85	82	90	94	92
	yield (%)	22	3	28	16	95	30	96	90	73	88	58	100	100
I	ee (%)	96	85	91	80	89	87	91	93	92	88	90	92	93
	yield (%)	100	76	100	56	100	100	100	100	100	100	100	100	100
J	ee (%)	94	92	91	92	90	92	91	93	91	90	91	92	87
	yield (%)	100	100	100	98	100	100	100	100	100	100	100	100	100
K	ee (%)	94	86	86	57	87	90	91	91	86	74	88	90	91
	yield (%)	100	79	100	19	100	100	100	100	100	100	100	100	100
L	ee (%)	94	92	91	87	92	90	92	94	88	88	90	92	93
	yield (%)	100	100	100	67	100	100	100	94	100	100	100	100	100
M	ee (%)	70	0	89	87	88	88	92	87	80	91	86	91	94
	yield (%)	43	0	100	14	100	100	100	92	100	100	75	100	100
N	ee (%)	91	78	89	87	90	92	93	92	87	84	89	91	93
	yield (%)	100	34	100	52	100	100	100	100	100	100	100	100	100
O	ee (%)	70	20	87	82	93	94	93	89	87	89	90	93	94
	yield (%)	100	33	100	39	100	100	100	88	58	78	100	100	100
P	ee (%)	93	40	91	90	91	91	93	94	89	92	93	94	94
	yield (%)	100	80	100	85	100	100	100	100	100	63	100	100	100

LEGEND

- 0-29
- 30-69
- 70-89
- 90-94
- 95-100

Phenol-linked tethers are C-G.

Benzyl-linked tethers are I-P.

Compilation of Diastereomeric data

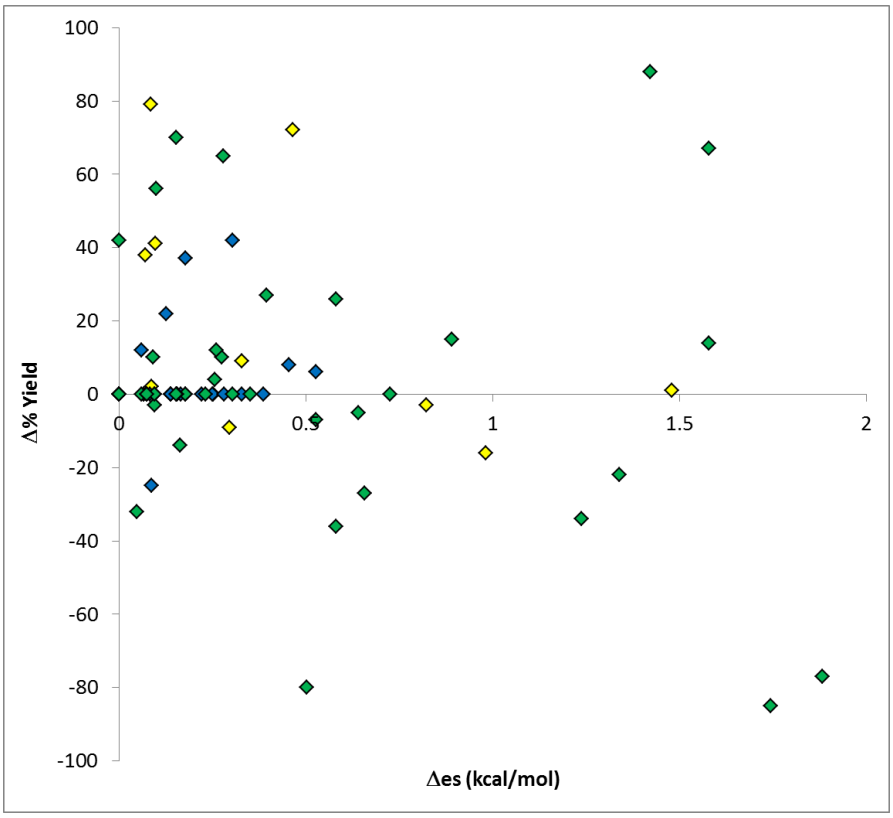

Legend

Yellow = phenol tethers = C-G

Blue = benzylic tethers = I-P

Green = mixed benzyl-phenol tethers (C-G) + (I-P)

	Diastereomeric SALs Set A							Diastereomeric SALs Set B									
Entry	(S,S) Tether	(R,R) Tether	%ee product XS1	%R	%S	ΔΔG‡ (kcal/mol)	Yield (%)	(S,S) Tether	(R,R) Tether	%ee product XS1	%R	%S	ΔΔG‡ (kcal/mol)	Yield (%)	Δ(ΔΔG‡) Set A - Set B	Abs Δ(ΔΔG‡) Δ es (kcal/mol)	Δ (% Yield)
1	C	D	65	17.5	82.5	-0.92	37	D	C	69	15.5	84.5	-1.00	35	0.09	0.09	2
2	C	E	75	12.5	87.5	-1.15	85	E	C	84	8	92	-1.45	94	0.29	0.29	-9
3	C	F	80	10	90	-1.30	70	F	C	82	9	91	-1.37	32	0.07	0.07	38
4	C	G	65	17.5	82.5	-0.92	63	G	C	60	20	80	-0.82	22	-0.10	0.10	41
5	D	E	68	16	84	-0.98	93	E	D	64	18	82	-0.90	14	-0.08	0.08	79
6	D	F	22	39	61	-0.26	11	F	D	90	5	95	-1.74	10	1.48	1.48	1
7	D	G	0	50	50	0.00	0	G	D	60	20	80	-0.82	3	0.82	0.82	-3
8	E	F	27	36.5	63.5	-0.33	9	F	E	0	50	50	0.00	0	-0.33	0.33	9
9	E	G	84	8	92	-1.45	100	G	E	68	16	84	-0.98	28	-0.46	0.46	72
10	F	G	0	50	50	0.00	0	G	F	68	16	84	-0.98	16	0.98	0.98	-16
11	I	J	91	4.5	95.5	-1.81	100	J	I	92	4	96	-1.88	100	0.07	0.07	0
12	I	K	93	3.5	96.5	-1.96	100	K	I	90	5	95	-1.74	100	-0.22	0.22	0
13	I	L	92	4	96	-1.88	100	L	I	90	5	95	-1.74	100	-0.14	0.14	0
14	I	M	88	6	94	-1.63	100	M	I	88	6	94	-1.63	100	0.00	0.00	0
15	I	N	90	5	95	-1.74	100	N	I	92	4	96	-1.88	100	0.14	0.14	0
16	I	O	92	4	96	-1.88	100	O	I	94	3	97	-2.06	100	0.18	0.18	0
17	I	P	93	3.5	96.5	-1.96	100	P	I	91	4.5	95.5	-1.81	100	-0.16	0.16	0
18	J	K	93	3.5	96.5	-1.96	100	K	J	91	4.5	95.5	-1.81	100	-0.16	0.16	0
19	J	L	91	4.5	95.5	-1.81	100	L	J	92	4	96	-1.88	100	0.07	0.07	0
20	J	M	90	5	95	-1.74	100	M	J	92	4	96	-1.88	100	0.14	0.14	0
21	J	N	91	4.5	95.5	-1.81	100	N	J	93	3.5	96.5	-1.96	100	0.16	0.16	0
22	J	O	92	4	96	-1.88	100	O	J	93	3.5	96.5	-1.96	100	0.08	0.08	0
23	J	P	87	6.5	93.5	-1.58	100	P	J	93	3.5	96.5	-1.96	100	0.39	0.39	0
24	K	L	86	7	93	-1.53	100	L	K	94	3	97	-2.06	94	0.53	0.53	6
25	K	M	74	13	87	-1.13	100	M	K	87	6.5	93.5	-1.58	92	0.45	0.45	8
26	K	N	88	6	94	-1.63	100	N	K	92	4	96	-1.88	100	0.25	0.25	0
27	K	O	90	5	95	-1.74	100	O	K	89	5.5	94.5	-1.68	88	-0.06	0.06	12
28	K	P	91	4.5	95.5	-1.81	100	P	K	94	3	97	-2.06	100	0.25	0.25	0
29	L	M	88	6	94	-1.63	100	M	L	80	10	90	-1.30	100	-0.33	0.33	0
30	L	N	90	5	95	-1.74	100	N	L	87	6.5	93.5	-1.58	100	-0.16	0.16	0
31	L	O	92	4	96	-1.88	100	O	L	87	6.5	93.5	-1.58	58	-0.30	0.30	42
32	L	P	93	3.5	96.5	-1.96	100	P	L	89	5.5	94.5	-1.68	100	-0.28	0.28	0
33	M	N	86	7	93	-1.53	75	N	M	84	8	92	-1.45	100	-0.09	0.09	-25
34	M	O	91	4.5	95.5	-1.81	100	O	M	89	5.5	94.5	-1.68	78	-0.13	0.13	22
35	M	P	94	3	97	-2.06	100	P	M	92	4	96	-1.88	63	-0.18	0.18	37
36	N	O	91	4.5	95.5	-1.81	100	O	N	90	5	95	-1.74	100	-0.07	0.07	0
37	N	P	93	3.5	96.5	-1.96	100	P	N	93	3.5	96.5	-1.96	100	0.00	0.00	0
38	O	P	94	3	97	-2.06	100	P	O	94	3	97	-2.06	100	0.00	0.00	0
39	I	C	96	2	98	-2.31	100	C	I	87	6.5	93.5	-1.58	100	-0.73	0.73	0
40	I	D	85	7.5	92.5	-1.49	76	D	I	77	11.5	88.5	-1.21	11	-0.28	0.28	65
41	I	E	91	4.5	95.5	-1.81	100	E	I	87	6.5	93.5	-1.58	100	-0.23	0.23	0
42	I	F	80	10	90	-1.30	56	F	I	92	4	96	-1.88	92	0.58	0.58	-36
43	I	G	89	5.5	94.5	-1.68	100	G	I	86	7	93	-1.53	30	-0.15	0.15	70
44	J	C	94	3	97	-2.06	100	C	J	92	4	96	-1.88	100	-0.18	0.18	0
45	J	D	92	4	96	-1.88	100	D	J	80	10	90	-1.30	74	-0.58	0.58	26
46	J	E	91	4.5	95.5	-1.81	100	E	J	90	5	95	-1.74	100	-0.07	0.07	0
47	J	F	92	4	96	-1.88	98	F	J	37	31.5	68.5	-0.46	10	-1.42	1.42	88
48	J	G	90	5	95	-1.74	100	G	J	85	7.5	92.5	-1.49	96	-0.26	0.26	4
49	C	K	93	3.5	96.5	-1.96	100	K	C	94	3	97	-2.06	100	0.09	0.09	0
50	C	L	86	7	93	-1.53	93	L	C	94	3	97	-2.06	100	0.53	0.53	-7
51	C	M	80	10	90	-1.30	53	M	C	70	15	85	-1.03	43	-0.27	0.27	10
52	C	N	93	3.5	96.5	-1.96	100	N	C	91	4.5	95.5	-1.81	100	-0.16	0.16	0
53	C	O	89	5.5	94.5	-1.68	73	O	C	70	15	85	-1.03	100	-0.66	0.66	-27
54	C	P	94	3	97	-2.06	97	P	C	93	3.5	96.5	-1.96	100	-0.09	0.09	-3
55	K	D	86	7	93	-1.53	79	D	K	88	6	94	-1.63	23	0.10	0.10	56
56	K	E	86	7	93	-1.53	100	E	K	92	4	96	-1.88	100	0.35	0.35	0
57	K	F	57	21.5	78.5	-0.77	19	F	K	83	8.5	91.5	-1.41	24	0.64	0.64	-5
58	K	G	87	6.5	93.5	-1.58	100	G	K	85	7.5	92.5	-1.49	90	-0.09	0.09	10
59	D	L	0	50	50	0.00	23	L	D	92	4	96	-1.88	100	1.88	1.88	-77
60	D	M	0	50	50	0.00	0	M	D	0	50	50	0.00	0	0.00	0.00	0
61	D	N	0	50	50	0.00	0	N	D	78	11	89	-1.24	34	1.24	1.24	-34
62	D	O	87	6.5	93.5	-1.58	11	O	D	20	40	60	-0.24	33	-1.34	1.34	-22
63	D	P	0	50	50	0.00	0	P	D	40	30	70	-0.50	80	0.50	0.50	-80
64	L	E	91	4.5	95.5	-1.81	100	E	L	65	17.5	82.5	-0.92	85	-0.89	0.89	15
65	L	F	87	6.5	93.5	-1.58	67	F	L	0	50	50	0.00	0	-1.58	1.58	67
66	L	G	92	4	96	-1.88	100	G	L	85	7.5	92.5	-1.49	73	-0.39	0.39	27
67	E	M	90	5	95	-1.74	100	M	E	89	5.5	94.5	-1.68	100	-0.06	0.06	0
68	E	N	86	7	93	-1.53	100	N	E	89	5.5	94.5	-1.68	100	0.15	0.15	0
69	E	O	92	4	96	-1.88	100	O	E	87	6.5	93.5	-1.58	100	-0.30	0.30	0
70	E	P	92	4	96	-1.88	100	P	E	91	4.5	95.5	-1.81	100	-0.07	0.07	0
71	M	F	87	6.5	93.5	-1.58	14	F	M	0	50	50	0.00	0	-1.58	1.58	14
72	M	G	88	6	94	-1.63	100	G	M	82	9	91	-1.37	88	-0.26	0.26	12
73	F	N	86	7	93	-1.53	20	N	F	87	6.5	93.5	-1.58	52	0.05	0.05	-32
74	F	O	86	7	93	-1.53	25	O	F	82	9	91	-1.37	39	-0.16	0.16	-14
75	F	P	0	50	50	0.00	0	P	F	90	5	95	-1.74	85	1.74	1.74	-85
76	N	G	90	5	95	-1.74	100	G	N	90	5	95	-1.74	58	0.00	0.00	42
77	G	O	94	3	97	-2.06	100	O	G	93	3.5	96.5	-1.96	100	-0.09	0.09	0
78	G	P	92	4	96	-1.88	100	P	G	91	4.5	95.5	-1.81	100	-0.07	0.07	0

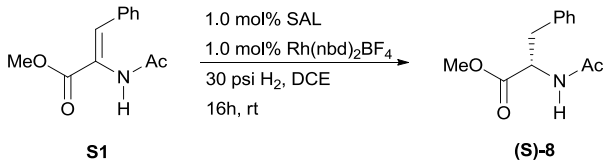

S1 (S)-8

(R,R)-Bisoxazoline linked tethers

(S,S)-Bisoxazoline linked tethers		C	D	E	F	G	I	J	K	L	M	N	O	P
C	ee (%)	73	68	80	84	72			89	86	88	83	80	77
	yield (%)	2	6	8	11	2			100	21	24	7	5	4
D	ee (%)		74	86	75	0				82	88	86	86	87
	yield (%)		9	36	5	0				48	17	3	2	3
E	ee (%)			89	84	92					92	85	90	89
	yield (%)			38	5	96					73	95	100	100
F	ee (%)				85	85						86	84	88
	yield (%)				13	4						11	7	6
G	ee (%)					0							93	80
	yield (%)					0							18	30
I	ee (%)	93	86	89	88	88	87	89	90	87	89	87	89	88
	yield (%)	96	100	100	100	100	100	100	100	100	80	100	100	93
J	ee (%)	91	87	91	88	89		90	91	88	91	89	91	89
	yield (%)	100	85	100	70	100		100	100	100	100	100	100	100
K	ee (%)		90	88	83	91			91	87	80	87	88	86
	yield (%)		95	100	7	100			100	90	16	100	100	100
L	ee (%)			89	88	90				89	88	88	91	86
	yield (%)			92	54	100				100	27	100	100	100
M	ee (%)				70	91					86	86	88	84
	yield (%)				5	100					100	89	100	20
N	ee (%)					90						84	86	84
	yield (%)					7						16	7	30
O	ee (%)												92	83
	yield (%)												10	36
P	ee (%)													83
	yield (%)													50

LEGEND

- 0-29
- 30-69
- 70-89
- 90-94
- 95-100

Screening protocol procedures scale-up reaction

The following procedure is typical. To a solution of BINOL tether ((*S*,*S*)-**I**) (3.7 mg, 5.1 μmol) and BINOL tether ((*R*,*R*)-**C**) (3.8 mg, 5.1 μmol) in dicloromethane (DCM, 1.0 mL) was added a solution of diethyl zinc (0.10 mL, 5.6 μmol) dropwise and 3 2 mm glass beads. The resulting mixture was stirred on an orbital shaker (ca 125 revolutions/min) for 30 minutes and then concentrated in vacuo to afford (BINOL)SAL **Zn(IC)** which was diluted with dichloroethane (DCE, 2.0 mL) and used without further purification. A solution of $Rh(nbd)_2BF_4$ (1.9 mg, 5.1 μmol) in DCM (0.20 mL) was added dropwise and

the resulting mixture was stirred for 30 minutes at ambient temperature under N_2. A solution of *N*-(1-(4-chlorophenyl)vinyl)acetamide (1.0×10^2 mg, 5.1×10^2 mmol) in DCE was then added and the vial was placed into a hydrogenated chamber. The chamber was purged with hydrogen gas (5 x 20 psi) and then pressurized to 30 psi H_2 and lightly shaken (ca 125 revolutions/minute) at ambient temperature for 16 hours. The hydrogen pressure was released, and the crude reaction mixture was concentrated and purified by flash chromatography on silica gel using EtOAc/Hexanes (1:5) as the eluent yielding (*S*)-*N*-(1-(4-chlorophenyl)ethyl)acetamide (98% yield) as a white solid: gas chromatography on a CP-Chirasil-Dex CB column (I.D. = 0.25 mm) using a temperature program of 140-200^{o}C at 1^{o}C/min) show 95% ee; $[\alpha]_D$ = -152 (c = 0.5, EtOH)[The configurations were assigned from comparing optical rotations with the reported values]; ^{1}H NMR (400 MHz, $CDCl_3$) δ 7.33-7.25 (4H, m), 5.76 (1H, bs), 5.11 (1H, m), 2.00 (3H, s), 1.48 (3H, d, J = 6.92 Hz); ^{13}C NMR (100 MHz) δ 169.11, 141.79, 133.06, 128.77, 127.58, 48.20, 23.41, 21.69.

Synthesis of key compounds

Synthetic route for S2-BINOL

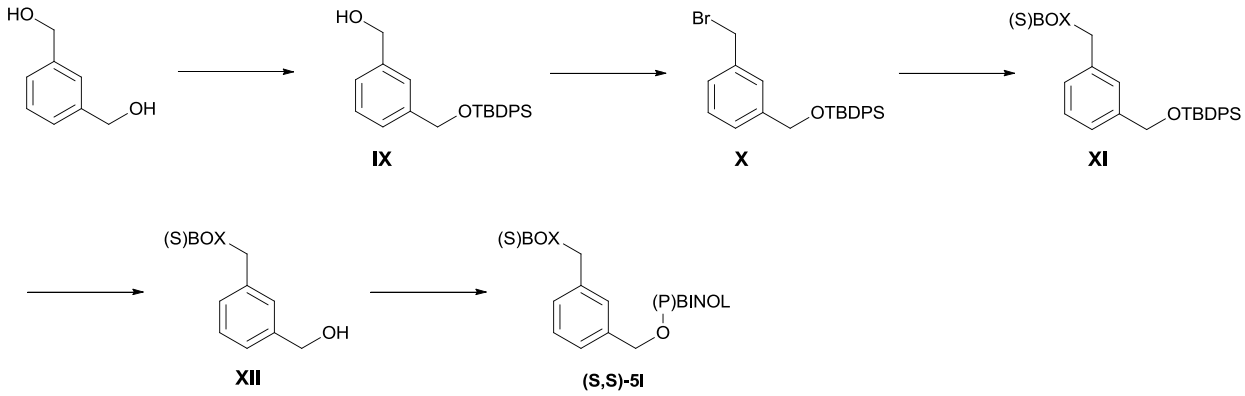

Preparation of IX

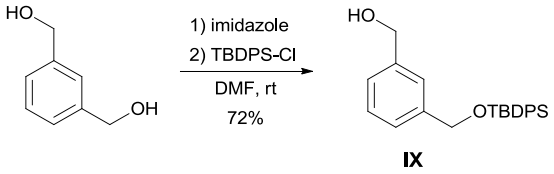

To 1,3-benzene dimethanol (10.0 g, 72.4 mmol) and imidazole (19.7 g, 289 mmol) was added DMF (150 mL) under N_2. The reaction mixture was stirred (15 minutes) at room temperature then cooled (0^oC) and TBDPS-Cl (21.4 mL, 72.4 mmol) was added dropwise over 5 minutes. The reaction mixture was allowed to warm to room temperature overnight. $NaHCO_3$ (satd.) was added (100 mL) and the mixture was extracted with diethyl ether (3 x 100 mL). The organic extracts were combined, dried with magnesium sulfate, filtered, and concentrated. Flash chromatography on silica gel (25:75 ethyl acetate:hexanes) affords **IX** (19.7 g, 72.3 %) as a white solid. TLC: Rf 0.30 (25:75 ethyl acetate:hexanes); ^1H NMR (400 MHz, d-$CHCl_3$) δ 7.81-7.78 (4H, m), 7.53-7.32 (10H,

m), 4.87 (1H, s), 4.71 (1H, s), 2.10 (1H, s), 1.20 (9H, s); ^{13}C NMR (100 MHz, d-$CHCl_3$) δ 141.44, 140.88, 135.68, 133.52, 129.82, 128.58, 127.83, 125.64, 125.41, 124.70, 65.52, 65.38, 26.95, 19.41 IR (neat) 3330, 3064, 2856, 1600-1500, 1107 cm^{-1}; HRMS (ESI): Calcd. For $C_{24}H_{28}O_2Si$ $(M+Na)^+$: 399.1756, found 399.1769 m/z.

Preparation of X

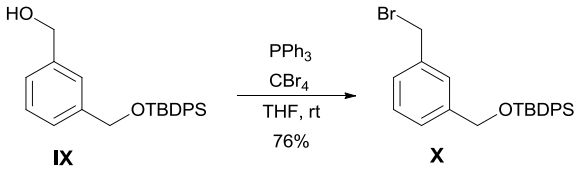

IX **X**

IX (10.0 g, 26.7 mmol) and PPh_3 (6.98g, 26.7 mmol) was dissolved in THF (150 mL) , stirred (15 minutes), then cooled (0^oC). A solution of CBr_4 (8.81 g, 26.7 mmol) in THF (15 mL) was added dropwise. The reaction mixture was allowed to warm to room temperature overnight (16 h). The precipitate was removed by filtration through celite, washed with THF (2 x 50 mL), and the combined organic washes were concentrated. Flash chromatography on silica gel (5:95 ethyl acetate:hexanes) affords **X** (8.90 g, 76%) as a colorless oil. TLC: Rf 0.70 (5:95 ethyl acetate:hexanes); ^{1}H NMR (400 MHz, d-$CHCl_3$) δ 7.87-7.85 (4H, m), 7.58-7.38 (10H, m), 4.92 (2H, s), 4.60 (2H, s), 1.27 (9H, s); ^{13}C NMR (100 MHz, d-$CHCl_3$) δ 141.88, 137.80, 135.73, 133.48, 129.93, 128.86, 127.94, 127.71, 126.820, 126.23, 65.35, 33.85, 27.04, 19.49; IR (neat) 2958, 2852, 1103, 1070 cm^{-1}; HRMS (ESI): Calcd. For $C_{24}H_{27}OSiBr$ (M+H): 461.0912, found 461.0912 m/z.

Preparation of (S,S)-XI

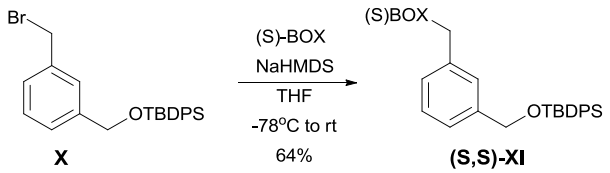

X **(S,S)-XI**

To a cooled solution (-78°C) of (S,S)-bisoxazoline [(S)-BOX] (5.0 g, 16.3 mmol) in THF (150 mL), NaHMDS (1M in THF, 17.1 mL) was added dropwise over the course of 1 h, and stirred at -78°C for 2 hours. A solution of **X** (7.17g, 16.3 mmol) in THF (15 mL) was added dropwise to the reaction mixture and slowly allowed to warm to room temperature overnight. The reaction was quenched with the addition of NH_4Cl (satd) and extracted with CH_2Cl_2 (3 x 100 mL). The combined organic extracts were dried with $MgSO_4$, filtered, and concentrated. Flash chromatography on silica gel (33:33:33 ethyl acetate: hexanes: CH_2Cl_2) afforded **(S,S)-XI** (6.94 g, 64%) as a light yellow oil. TLC: Rf 0.85 (6:94 methanol:dichloromethane); Optical rotation: $[\alpha]_D^{20} = -17.1^o$ (c 0.5, CH_3Cl); ^1H NMR (400 MHz, d-$CHCl_3$) δ 7.80-7.78 (4H, m), 7.52-7.27 (18H, m), 7.05-7.03 (2H, m), 5.28 (2H, t, J = 8.52 Hz), 4.85 (2H, s), 4.72 and 4.71 (2H, overlapping t, J = 8.12, 8.12 Hz), 4.24-4.21 (1H, m), 4.20-4.11 (2H, m), 3.60-3.48 (2H, m), 1.21 (9H, s) ppm; ^{13}C NMR (100 MHz, d-$CHCl_3$) δ 165.55, 165.52, 142.18, 142.13, 141.47, 137.99, 135.66, 135.55, 129.81, 128.80, 128.76, 128.70, 128.66, 127.84, 127.78, 127.65, 127.55, 126.87, 126.74, 126.70, 126.52, 124.52, 41.51, 36.02, 26.99, 19.43 ppm.; IR (neat) 2951, 2849, 1653, 1108, 1067 cm^{-1}; HRMS (ESI): Calcd. For $C_{43}H_{44}N_2O_3Si$ (M+Na): 665.3199, found 665.3208 m/z.

Preparation of (S,S)-XII

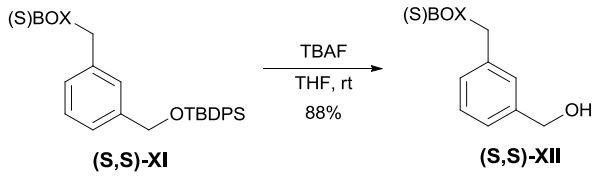

(S,S)-XI **(S,S)-XII**

To a solution of **(S,S)-XI** (6.90 g, 10.4 mmol) in THF (100 mL) was added dropwise TBAF (1.0M in THF, 10.4 mL). The solution was stirred at room temperature for 16 h. Water (35 mL) was added and the mixture was extracted with CH_2Cl_2 (3 x 60 mL). The combined organic extracts were dried ($MgSO_4$), filtered, and concentrated. Flash chromatography on silica gel (7:93 methanol:CH_2Cl_2) affords **(S,S)-XII** (3.91 g, 88%) as a sticky white foam. TLC: Rf 0.4 (6:94 methanol:dichloromethane); Optical rotation: $[\alpha]_D^{20}$ = -21.6^o (c 0.5, CH_3Cl); ^{1}H NMR (400 MHz, d-$CHCl_3$) δ 7.35-7.21 (10H, m), 7.23-7.21 (2H, m), 7.01-6.99 (2H, m), 5.21 and 5.19 (2H, overlapping t, J =8.40, 7.92 Hz), 4.71-4.63 (4H, m), 4.18 (1H, t, J = 8.24 Hz), 4.11-4.04 (2H, m), 3.48-3.39 (2H, m); ^{13}C NMR (100 MHz, d-$CHCl_3$) δ 165.52, 165.50, 141.93, 141.87, 139.71, 137.09, 129.25, 128.71, 128.63, 127.65, 127.58, 127.23, 126.69, 126.68, 75.43, 75.23, 69.49, 64.80, 41.41, 35.53; IR (neat) 3243, 1658, 1555-1148, 1019 cm^{-1}; HRMS (ESI): Calcd. For $C_{27}H_{26}N_2O_3$ (M+H): 449.1841, found 449.1833 m/z.

Preparation of BINOL tether (S,S)-5I and BINOL tether (R,R)-5C

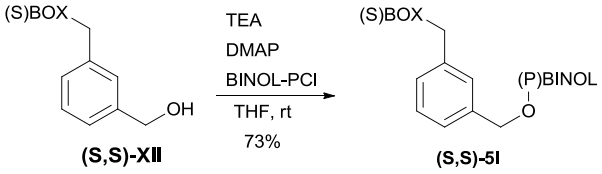

(S,S)-XII **(S,S)-5I**

PCl_3 (3.66 mL, 41.9 mmol) was added dropwise to (R)-BINOL (500 mg, 1.75 mmol) at room temperature, followed by the dropwise addition of a catalytic amount of N-methyl

pyrrolidine (4 drops). The reaction mixture was heated to 74^{o}C for 1.0 h. (Careful monitoring of the temperature was done to ensure no racemization). The crude reaction mixture was concentrated. Toluene was added (3x20 mL) and subsequently removed under reduced pressure to remove excess PCl_3 affording BINOL-PCl without further purification. The freshly prepared BINOL-PCl was dissolved in THF(10 mL) and added to a solution of **(S,S)-XII** (596 mg, 1.40 mmol), catalytic DMAP (8.53 mg, 6.99 x 10-2 mmol), and TEA (2.42 mL, 17.5 mmol) in THF (15 mL). The reaction mixture was stirred overnight at room temperature. The crude mixture was filtered through celite, and the precipitate was washed with THF (3 x 5 mL). The filtrate was concentrated, and flash chromatography on silica gel (33:33:33 ethyl acetate: dichloromethane: hexanes) affords **(S,S)-5I** (758 mg, 73%) as a white foam. Optical rotation: $[\alpha]_D^{20}$ = -164^{o} (c 0.5, CH_3Cl); ^{1}H NMR (400 MHz, d-$CHCl_3$) δ 7.91-7.81 (4H, m), 7.44-7.08 (20 H, m), 6.90-6.88 (2H, m), 5.12 and 5.10 (2H, overlapping t, J = 10.1 Hz and 9.92 Hz), 4.87 and 4.62 (2H, ddd, J_1 = 7.72, 12.32 Hz, J_2 = 7.92, 12.32 Hz), 4.59-4.54 (2H, m), 4.06 (1H, t, J = 8.16 Hz), 3.99-3.91 (2H, m), 3.36 and 3.30 (2H, ddd, J_1 = 7.80, 13.9 Hz, J_2 = 8.56, 13.89 Hz); ^{13}C NMR (100 MHz, d-$CHCl_3$) δ 165.34 ($J_{C,P}$ = 8.44 Hz), 153.91, 148.82, 147.45, 141.98 (JC,P = 5.82 Hz), 138.23, 137.83, 133.34, 132.91, 132.83, 131.82, 131.63, 131.32, 130.46, 130.18, 128.81, 128. 73, 128.68, 128.63, 128.39, 128.26, 127.57, 127.51, 127.01, 126.66, 126.62, 126.29, 125.93, 125.09, 124.93,122.78, 121.88, 121.56, 117.90, 75.36, 75.14, 69.60, 69.58, 66.82, 62.34, 41.41, 35.78; ^{31}P NMR (162 MHz, d-$CHCl_3$) δ 139.0 ppm ; IR (neat) 3040, 1653, 1589-1328, 1021, 939 cm^{-1}; HRMS (ESI): Calcd. For $C_{47}H_{37}N_2O_5P$ (M+H): 741.2513, found 741.2540 m/z.

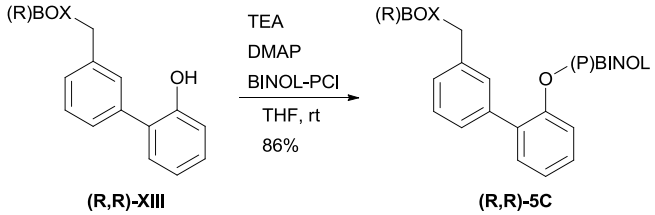

(R,R)-5C was prepared in the same manner starting with **(R,R)-XIII** (702 mg, 1.40 mmol) affording **(R,R)-5C** (879 mg, 78%) as a white foam. Optical rotation: $[\alpha]_D^{20}$ = -78^o (c 0.5, CH_3Cl); ^{1}H NMR 7.95-7.49 (4H, m), δ 7.47-7.02 (26 H, m), 5.19 and 5.17 (2H, overlapping t, *J* = 10.5, 10.4 Hz), 4.67-4.58 (2H, m), 4.14-4.04 (3H, m), 3.52-3.49 (2H, m); ^{13}C NMR (100 MHz, d-$CHCl_3$) δ 165.52 ($J_{C,P}$ = 11.04 Hz), 152.94, 148.77, 148.66, 147.72, 147.66, 147.00, 142.00, 138.03, 137.86, 133.90, 133.85, 133.62, 132.80, 132.46, 131.62, 131.37, 131.19, 130.99, 130.54, 130.41, 130.12, 129.87, 129.35, 128.64, 128.54, 128.41, 128.37, 128.34, 128.13, 127.53, 127.49, 127.25, 127.06, 126.93, 126.68, 126.65, 126.56, 126.47, 126.32, 126.11, 124.93, 124.70, 124.42, 123.82, 122.64, 121.78, 121.68, 121.13, 120.99, 118.14, 74.26 ($J_{C,P}$ = 17.9 Hz), 69.57, 41.33, 35.89; 31P NMR (162 MHz, d-$CHCl_3$) δ 144.8 ppm; IR (neat) 3028, 1646, 1585-1348, 1197, 956 cm^{-1}; HRMS (ESI): Calcd. For $C_{52}H_{39}N_2O_5$ (M+H): 803.2675, found 803.2709 m/z.

Characterization of (BINOL)SAL Zn(IC)

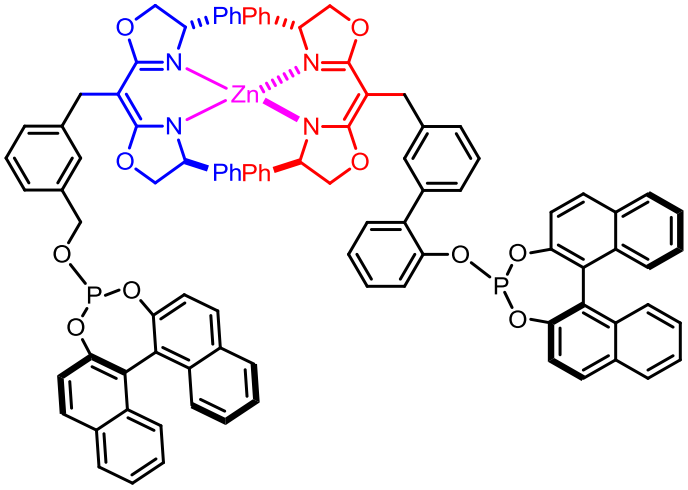

Optical rotation: $[\alpha]_D^{20}$ = -92° (c 0.5, CH_3Cl); ^{1}H NMR δ 8.00-7.89 (9H, m), 7.56-6.96 (47 H, m), 5.10-5.05 (1H, m), 4.87-4.82 (1H, m), 4.05-3.96 (4H, m), 3.83-3.78 (6H, m), 3.67 (2H, s), 3.32-3.24 (4H, m); ^{13}C NMR (100 MHz, d-$CHCl_3$) δ 169.85, 169.69, 152.91, 148.83, 147.90, 147.23, 145.33, 144.14, 137.14, 130.43, 130.08, 129.92, 128.40, 128.83, 127.94, 127.55, 127.18, 127.06, 126.92, 126.29, 126.21, 124.89, 121.97, 121.91, 121.72, 118.91, 72.92, 65.39; ^{31}P NMR (162 MHz, d-$CHCl_3$) δ 147.5 and 144.0 ppm; IR (neat) 3028, 2933, 1646, 1197 cm^{-1}; HRMS (ESI): Calcd. For $C_{99}H_{74}N_4O_{10}P_2Zn$ (M+H): 1605.4250, found 1605.4299 m/z.

BINOL-OPh (**L5**)

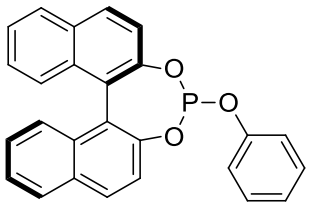

TLC: Rf = 0.80 (10:90 EtOAc:hexanes); melting point: 95-100 °C (decomposition); Optical rotation: $[\alpha]_D^{20}$ = -142.4° (c 0.5, CH_3Cl); ^{1}H NMR δ 8.02-7.99 (4H, m), □ 7.66-

7.23 (12H, m); ^{13}C NMR (100 MHz, d-$CHCl_3$) δ 151.18, 147.22, 147.10, 132.78, 132.47, 131.76, 131.31, 130.61, 129.97, 129.89, 128.46, 128.40, 126.79, 126.69, 126.46, 126.36, 125.32, 125.16, 124.48, 121.64, 120.41, 120.31; ^{31}P NMR (162 MHz, d-$CHCl_3$) δ 145.1; IR (neat) 2909, 2894, 1388-1201, 1069 cm^{-1}.

BINOL-POBn (**L6**)

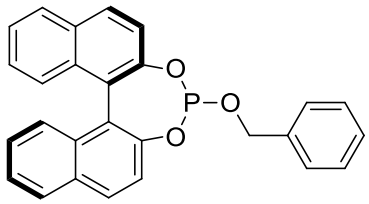

TLC: Rf = 0.75 (8:92 EtOAc:hexanes); melting point: 125-130 °C (decomposition); Optical rotation: $[\alpha]_D^{20}$ = -440° (c 0.5, CH_3Cl); ^{1}H NMR δ 8.08-7.96 (4H, m), 7.61-7.284 (12 H, m), 5.04 and 4.82 (2H, dd, J_1 = 12.19 Hz, 8.01 Hz, J_2 = 12.19 Hz, 8.31 Hz); ^{13}C NMR (100 MHz, d-$CHCl_3$) δ 148.7, 148.6, 147.5, 137.4, 137.3, 132.8, 132.5, 131.6, 131.1, 130.5, 130.2, 128.5, 128.4, 128.4, 128.1, 127.6, 126.7, 126.3, 126.3, 125.1, 125.0, 124.0, 124.0, 122.6, 121.8, 121.8, 121.5, 64.7, 66.7; ^{31}P NMR (162 MHz, d-$CHCl_3$) δ 140.8 ppm; IR (neat) 3044, 1589-1319, 939 cm^{-1}.

Preparation of BINOL(n-alkyl series) L4a–L4d

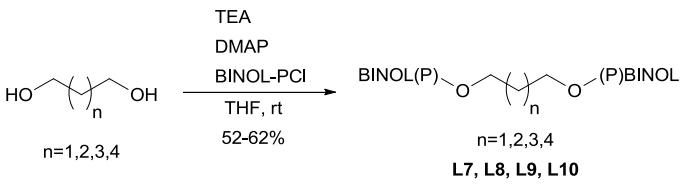

PCl_3 (3.66 mL, 41.9 mmol) was added dropwise to (R)-BINOL (500 mg, 1.75 mmol) at room temperature followed by the dropwise addition of a catalytic amount of N-methyl pyrrolidine (4 drops). The reaction mixture was heated to 74^{o}C for 1.0 h. (Careful monitoring of the temperature was done to ensure no racemization). The crude reaction mixture was concentrated. Toluene was added (3x20 mL) and subsequently removed under reduced pressure to remove excess PCl_3 affording BINOL-PCl without further purification. 1,3-propanediol (86.4 mg, , 1.14 mmol) in THF (15 mL) was added TEA (0.728 mL, 3.41 mmol). The solution was stirred for 15 minutes and the freshly prepared BINOL-PCl was dissolved in THF (10 mL) and added slowly to the reaction flask at room temperature. The reaction mixture was stirred overnight at room temperature. The crude mixture was filtered through celite, and the precipitate was washed with THF (3 x 5 mL). The filtrate was concentrated under reduced pressure. Flash chromatography on silica gel (5:95 ethyl acetate : hexanes) affords alkyl n3BINOL ligand **L7** (419 mg, 52.4%) as a white foam. Melting point: 92-95°C (decomposition); Optical rotation: $[\alpha]_D^{20}$ = -4.6^{o} (c 0.5, CH_3Cl); ^{1}H NMR (400 MHz, d-$CHCl_3$) δ 8.01-7.88 (8H, m), 7.53-7.27 (16H, m), 4.06 and 3.90 (4H, m), 1.85 (2H, m) ppm; ^{13}C NMR (100 MHz, d-$CHCl_3$) δ 148.76 ($J_{C,P}$ = 5.08 Hz), 147.52, 132.85, 132.61, 131.55, 131.02, 130.43, 130.12, 128.39, 128.35, 127.03, 126.29, 126.24, 125.07, 124.90, 122.61, 121.87, 121.56, 61.18 ($J_{C,P}$ = 6.07), 32.21 ppm; ^{31}P NMR (162 MHz, d-$CHCl_3$) δ 140.42 ppm; IR (neat) 3049, 1589-1319, 927 cm^{-1}; HRMS (ESI): Calcd. For $C_{43}H_{30}O_6P_2$(M+H): 705.1596, found 705.1609 m/z.

n4-alkyl BINOL **L8** was prepared according to the general procedure starting with 1,4-butane diol (102 mg, 1.14 mmol) affording the product (489 mg, 59.9%) as a white foam. Melting point: 95-98°C (decomposition); Optical rotation: $[\alpha]_D^{20}$ = -4.0° (c 0.5, CH_3Cl); ^{1}H NMR (400 MHz, d-$CHCl_3$) δ 8.03-7.92 (8H, m), 7.57-7.28 (16H, m), 4.01 and 3.81 (4H, m), 1.70 (4H, m) ppm; ^{13}C NMR (100 MHz, d-$CHCl_3$) δ 148.75 ($J_{C,P}$ = 5.1 Hz), 147.59, 132.87, 132.66, 131.57, 131.03, 130.45, 130.07, 128.41, 128.36, 127.03, 126.30, 126.27, 125.08, 124.92, 124.15, 124.10, 122.73, 122.71, 121.90, 121.59, 64.63 ($J_{C,P}$ = 6.07), 27.30 ppm; ^{31}P NMR (162 MHz, d-$CHCl_3$) δ 141.06 ppm; IR (neat) 3050, 1592-1322, 940 cm^{-1}; HRMS (ESI): Calcd. For $C_{44}H_{32}O_6P_2$(M+H): 719.1752, found 719.1772 m/z.

n5-alkyl BINOL **L9** was prepared according to the general procedure starting with 1,5-pentane diol (118 mg, 1.14 mmol) affording the product (502 mg, 60.31%) as a white foam. Melting point: 102-109°C (decomposition); Optical rotation: $[\alpha]_D^{20}$ = -3.4° (c 0.5, CH_3Cl); ^{1}H NMR (400 MHz, d-$CHCl_3$) δ 8.01-7.89 (8H, m), 7.54-7.26 (16H, m), 3.96 and 3.77 (4H, m), 1.63-1.54 (4H, m), 1.46-1.40 (2H, m) ppm; ^{13}C NMR (100 MHz, d-$CHCl_3$) δ 148.7 ($J_{C,P}$ = 5.1 Hz), 132.8, 132.6, 131.5, 131. 0, 130.4, 130.0, 128.4, 128.3, 127.0, 126.3, 126.2, 125.0, 124.9, 124.1, 122.7, 121.9, 121.6, 65.0 ($J_{C,P}$ = 6.13), 30.5 ($J_{C,P}$ = 4.1 Hz), 21.9 ppm; ^{31}P NMR (162 MHz, d-$CHCl_3$) 141.4; IR (neat) 3043, 1585-1319, 944 cm^{-1}; HRMS (ESI): Calcd. For $C_{45}H_{34}O_6P_2$(M+H): 733.1909, found 733.1909 m/z.

n6-alkyl BINOL **L10** was prepared according to the general procedure starting with 1,6-hexane diol (134 mg, 1.14 mmol) affording the product (528 mg, 62.3%) as a white foam. Melting point: 104-110°C (decomposition); Optical rotation: $[\alpha]_D^{20}$ = -2.6° (c 0.5, CH_3Cl); ^{1}H NMR (400 MHz, d-$CHCl_3$) δ 8.01-7.90 (8H, m), 7.55-7.26 (16H, m), 3.95 and 3.77 (4H, m), 1.65 (4H, m), 1.32 (4H, m); ^{13}C NMR (100 MHz, d-$CHCl_3$) δ 148.92, 147.61 ($J_{C,P}$ = 2.08 Hz), 132.9, 132.7, 131.5, 131.0, 130.4, 13.0, 128.4, 128.3, 127.0, 126.3, 126.2, 125.0, 124.9, 124.2, 122.8, 121. 9, 121.6, 65.1 ($J_{C,P}$ = 6.6 Hz), 30.9, ($J_{C,P}$ = 4.0 Hz), 25.20 ppm; ^{31}P NMR (162 MHz, d-$CHCl_3$) δ 141.9; IR (neat) 3039, 1584-1319, 940 cm^{-1}; HRMS (ESI): Calcd. For $C_{46}H_{36}O_6P_2$(M+H): 747.2065, found 747.2043 m/z.

2.12 References

1. Knowles, W. S. Asymmetric hydrogenations (Nobel Lecture). *Angew. Chem. , Int. Ed.* **2002**, *41*, 1998-2007.

2. Horner, L.; Siegel, H.; Buethe, H. Hydrogen transfer. XXII. Asymmetric catalytic hydrogenation with an optically active phosphinerhodium complex in homogeneous solution. *Angew. Chem. Int. Ed. Engl.* **1968**, *7*, 942.

3. Kagan, H. B.; Dang-Tuan-Phat Asymmetric catalytic reduction with transition metal complexes. I. Catalytic system of rhodium(I) with (-)-2,3-0-isopropylidene-2,3-dihydroxy-1,4-bis(diphenylphosphino)butane, a new chiral diphosphine. *J. Amer. Chem. Soc.* **1972**, *94*, 6429-6433.

4. Pena, D.; Minnaard, A. J.; de Vries, J. G.; Feringa, B. L. Highly Enantioselective Rhodium-Catalyzed Hydrogenation of β-Dehydroamino Acid Derivatives Using Monodentate Phosphoramidites. *J. Am. Chem. Soc.* **2002**, *124*, 14552-14553.

5. Gavrilov, K. N.; Bondarev, O. G.; Polosukhin, A. I. Chiral phosphites as ligands in asymmetric metal complex catalysis and synthesis of coordination compounds. *Russ. Chem. Rev.* **2004**, *73*, 671-699.

6. Jerphagnon, T.; Renaud, J.; Bruneau, C. Chiral monodentate phosphorus ligands for rhodium-catalyzed asymmetric hydrogenation. *Tetrahedron: Asymmetry* **2004**, *15*, 2101-2111.

7. de Vries, J. G.; Lefort, L. The combinatorial approach to asymmetric hydrogenation: phosphoramidite libraries, ruthenacycles, and artificial enzymes. *Chem. - Eur. J.* **2006**, *12*, 4722-4734.

8. Minnaard, A. J.; Feringa, B. L.; Lefort, L.; de Vries, J. G. Asymmetric Hydrogenation Using Monodentate Phosphoramidite Ligands. *Acc. Chem. Res.* **2007**, *40*, 1267-1277.

9. Eberhardt, L.; Armspach, D.; Harrowfield, J.; Matt, D. BINOL-derived phosphoramidites in asymmetric hydrogenation: can the presence of a functionality in the amino group influence the catalytic outcome? *Chem. Soc. Rev.* **2008**, *37*, 839-864.

10. Bruneau, C.; Renaud, J. In *In Monophosphinites, -aminophosphinites, -phosphonites, -phosphites and -phosphoramidites.* Section Title: Organometallic and Organometalloidal Compounds; 2008; Vol. 1, pp 36-69.

11. Teichert, J. F.; Feringa, B. L. Phosphoramidites: Privileged Ligands in Asymmetric Catalysis. *Angew. Chem. , Int. Ed.* **2010**, *49*, 2486-2528.

12. van Leeuwen, P. W. N. M.; Kamer, P. C. J.; Claver, C.; Pamies, O.; Dieguez, M. Phosphite-containing ligands for asymmetric catalysis. *Chem. Rev. (Washington, DC, U. S.)* **2011**, *111*, 2077-2118.

13. Chan, A. S. C.; Pluth, J. J.; Halpern, J. Identification of the enantioselective step in the asymmetric catalytic hydrogenation of a prochiral olefin. *J. Am. Chem. Soc.* **1980**, *102*, 5952-5954.

14. Chua, P. S.; Roberts, N. K.; Bosnich, B.; Okrasinski, S. J.; Halpern, J. The origins of the enantioselection in asymmetric catalytic hydrogenation of amino acid precursors. *J. Chem. Soc. , Chem. Commun.* **1981**, 1278-1280.

15. Brown, J. M.; Parker, D. Mechanism of asymmetric hydrogenation. Rhodium complexes formed by unsaturated carboxylic acids, carboxylates, and carboxamides. *J. Org. Chem.* **1982**, *47*, 2722-2730.

16. Brown, J. M.; Parker, D. Mechanism of asymmetric homogeneous hydrogenation. Rhodium-catalyzed reductions with deuterium and hydrogen deuteride. *Organometallics* **1982**, *1*, 950-956.

17. Halpern, J. Mechanism and stereoselectivity of asymmetric hydrogenation. *Science (Washington, D. C. , 1883-)* **1982**, *217*, 401-407.

18. Landis, C. R.; Halpern, J. Asymmetric hydrogenation of methyl (Z)-α-acetamidocinnamate catalyzed by [1,2-bis(phenyl-o-anisoyl)phosphino)ethane]rhodium(I): kinetics, mechanism and origin of enantioselection. *J. Am. Chem. Soc.* **1987**, *109*, 1746-1754.

19. Schmidt, T.; Baumann, W.; Drexler, H.; Arrieta, A.; Heller, D.; Buschmann, H. About the Crystal Structure of [Rh((S,S)-DIPAMP)((Z)-2-benzoylamino-3-(3,4-dimethoxyphenyl)-methyl Acrylate)]BF_4: Major or Minor Catalyst-Substrate Complex?. *Organometallics* **2005**, *24*, 3842-3848.

20. Giernoth, R.; Heinrich, H.; Adams, N. J.; Deeth, R. J.; Bargon, J.; Brown, J. M. PHIP Detection of a Transient Rhodium Dihydride Intermediate in the Homogeneous Hydrogenation of Dehydroamino Acids. *J. Am. Chem. Soc.* **2000**, *122*, 12381-12382.

21. Gridnev, I. D.; Higashi, N.; Asakura, K.; Imamoto, T. Mechanism of Asymmetric Hydrogenation Catalyzed by a Rhodium Complex of (S,S)-1,2-Bis(tert-butylmethylphosphino)ethane. Dihydride Mechanism of Asymmetric Hydrogenation. *J. Am. Chem. Soc.* **2000**, *122*, 7183-7194.

22. Imamoto, T.; Yashio, K.; Crepy, K. V. L.; Katagiri, K.; Takahashi, H.; Kouchi, M.; Gridnev, I. D. P-Chiral Tetraphosphine Dirhodium Complex as a Catalyst for Asymmetric Hydrogenation: Synthesis, Structure, Enantioselectivity, and Mechanism. Stereoselective Formation of a Dirhodium Tetrahydride Complex and Its Reaction with Methyl (Z)-α-Acetamidocinnamate. *Organometallics* **2006**, *25*, 908-914.

23. Gridnev, I. D.; Imamoto, T.; Hoge, G.; Kouchi, M.; Takahashi, H. Asymmetric Hydrogenation Catalyzed by a Rhodium Complex of (R)-(tert-Butylmethylphosphino)(di-tert-butylphosphino)methane: Scope of Enantioselectivity and Mechanistic Study. *J. Am. Chem. Soc.* **2008**, *130*, 2560-2572.

24. Landis, C. R.; Hilfenhaus, P.; Feldgus, S. Structures and Reaction Pathways in Rhodium(I)-Catalyzed Hydrogenation of Enamides: A Model DFT Study. *J. Am. Chem. Soc.* **1999**, *121*, 8741-8754.

25. Feldgus, S.; Landis, C. R. Large-Scale Computational Modeling of [Rh(DuPHOS)]+-Catalyzed Hydrogenation of Prochiral Enamides: Reaction Pathways and the Origin of Enantioselection. *J. Am. Chem. Soc.* **2000**, *122*, 12714-12727.

26. Feldgus, S.; Landis, C. R. Origin of Enantioreversal in the Rhodium-Catalyzed Asymmetric Hydrogenation of Prochiral Enamides and the Effect of the α-Substituent. *Organometallics* **2001**, *20*, 2374-2386.

27. Donoghue, P. J.; Helquist, P.; Wiest, O. Ligand and Substrate Effects on the Mechanism of Rhodium-Catalyzed Hydrogenation of Enamides. *J. Org. Chem.* **2007**, *72*, 839-847.

28. Donoghue, P. J.; Helquist, P.; Norrby, P.; Wiest, O. Prediction of Enantioselectivity in Rhodium Catalyzed Hydrogenations. *J. Am. Chem. Soc.* **2009**, *131*, 410-411.

29. Gridnev, I. D.; Imamoto, T. Mechanism of enantioselection in Rh-catalyzed asymmetric hydrogenation. The origin of utmost catalytic performance. *Chem. Commun. (Cambridge, U. K.)* **2009**, 7447-7464.

30. Etayo, P.; Vidal-Ferran, A. Rhodium-catalyzed asymmetric hydrogenation as a valuable synthetic tool for the preparation of chiral drugs. *Chem. Soc. Rev.* **2013**, *42*, 728-754.

31. Takacs, J. M.; Reddy, D. S.; Moteki, S. A.; Wu, D.; Palencia, H. Asymmetric Catalysis Using Self-Assembled Chiral Bidentate P,P-Ligands. *J. Am. Chem. Soc.* **2004**, *126*, 4494-4495.

32. Takacs, J. M.; Chaiseeda, K.; Moteki, S. A.; Reddy, D. S.; Wu, D.; Chandra, K. Rhodium-catalyzed asymmetric hydrogenation using self-assembled chiral bidentate ligands. *Pure Appl. Chem.* **2006**, *78*, 501-509.

33. Moteki, S. A.; Takacs, J. M. Exploiting self-assembly for ligand-scaffold optimization: substrate-tailored ligands for efficient catalytic asymmetric hydroboration. *Angew. Chem. , Int. Ed.* **2008**, *47*, 894-897.

34. Moteki, S. A.; Toyama, K.; Liu, Z.; Ma, J.; Holmes, A. E.; Takacs, J. M. Two-stage optimization of a supramolecular catalyst for catalytic asymmetric hydroboration. *Chem. Commun. (Cambridge, U. K.)* **2012**, *48*, 263-265.

35. Thacker, N. C.; Moteki, S. A.; Takacs, J. M. Ligand Scaffold Optimization of a Supramolecular Hydrogenation Catalyst: Analyzing the Influence of Key Structural Subunits on Reactivity and Selectivity. *ACS Catal.* **2012**, *2*, 2743-2752.

36. Takacs, J. M.; Hrvatin, P. M.; Atkins, J. M.; Reddy, D. S.; Clark, J. L. The selective formation of neutral, heteroleptic zinc(II) complexes via self-discrimination of chiral bisoxazoline racemates and pseudoracemates. *New J. Chem.* **2005**, *29*, 263-265.

37. Atkins, J. M.; Moteki, S. A.; DiMagno, S. G.; Takacs, J. M. Single Enantiomer, Chiral Donor-Acceptor Metal Complexes from Bisoxazoline Pseudoracemates. *Org. Lett.* **2006**, *8*, 2759-2762.

38. Reetz, M. T.; Sell, T.; Meiswinkel, A.; Mehler, G. A new principle in combinatorial asymmetric transition-metal catalysis: Mixtures of chiral monodentate P ligands. *Angew. Chem. , Int. Ed.* **2003**, *42*, 790-793.

39. Reetz, M. T. Combinatorial transition-metal catalysis: mixing monodentate ligands to control enantio-, diastero-, and regioselectivity. *Angew. Chem. , Int. Ed.* **2008**, *47*, 2556-2588.

40. Woodmansee, D. H.; Pfaltz, A. Asymmetric hydrogenation of alkenes lacking coordinating groups. *Chem. Commun. (Cambridge, U. K.)* **2011**, *47*, 7912-7916.

41. Roseblade, S. J.; Pfaltz, A. Iridium-Catalyzed Asymmetric Hydrogenation of Olefins. *Acc. Chem. Res.* **2007**, *40*, 1402-1411.

42. Lightfoot, A.; Schnider, P.; Pfaltz, A. Enantioselective hydrogenation of olefins with iridium-phosphanodihydrooxazole catalysts. *Angew. Chem. , Int. Ed.* **1998**, *37*, 2897-2899.

43. Reetz, M. T.; Mehler, G.; Bondarev, O. Chiral diphosphites and diphosphoramidites as cheap and efficient ligands in Rh-catalyzed asymmetric olefin hydrogenation. *Chem. Commun. (Cambridge, U. K.)* **2006**, 2292-2294.

44. Moteki, S. Developing a supramolecular catalyst for asymmetric hydroboration. 2008.

45. Gridnev, I. D.; Fan, C.; Pringle, P. G. New insights into the mechanism of asymmetric hydrogenation catalyzed by monophosphonite-rhodium complexes. *Chem. Commun. (Cambridge, U. K.)* **2007**, 1319-1321.

46. Miyashita, A.; Yasuda, A.; Takaya, H.; Toriumi, K.; Ito, T.; Souchi, T.; Noyori, R. Synthesis of 2,2'-bis(diphenylphosphino)-1,1'-binaphthyl (BINAP), an atropisomeric chiral bis(triaryl)phosphine, and its use in the rhodium(I)-catalyzed asymmetric hydrogenation of α-(acylamino)acrylic acids. *J. Am. Chem. Soc.* **1980**, *102*, 7932-7934.

47. Halpern, J.; Riley, D. P.; Chan, A. S. C.; Pluth, J. J. Novel coordination chemistry and catalytic properties of cationic 1,2-bis(diphenylphosphino)ethanerhodium(I) complexes. *J. Am. Chem. Soc.* **1977**, *99*, 8055-8057.

48. Wassenaar, J.; Jansen, E.; van Zeist, W.; Bickelhaupt, F. M.; Siegler, M. A.; Spek, A. L.; Reek, J. N. H. Catalyst selection based on intermediate stability measured by mass spectrometry. *Nat. Chem.* **2010**, *2*, 417-421.

49. Lewis, C. A.; Miller, S. J. Site-selective derivatization and remodeling of erythromycin A by using simple peptide-based chiral catalysts. *Angew. Chem. , Int. Ed.* **2006**, *45*, 5616-5619.

50. Lewis, C. A.; Chiu, A.; Kubryk, M.; Balsells, J.; Pollard, D.; Esser, C. K.; Murry, J.; Reamer, R. A.; Hansen, K. B.; Miller, S. J. Remote Desymmetrization at Near-Nanometer Group Separation Catalyzed by a Miniaturized Enzyme Mimic. *J. Am. Chem. Soc.* **2006**, *128*, 16454-16455.

51. Lewis, C. A.; Gustafson, J. L.; Chiu, A.; Balsells, J.; Pollard, D.; Murry, J.; Reamer, R. A.; Hansen, K. B.; Miller, S. J. A Case of Remote Asymmetric Induction in the Peptide-Catalyzed Desymmetrization of a Bis(phenol). *J. Am. Chem. Soc.* **2008**, *130*, 16358-16365.

52. Lewis, C. A.; Longcore, K. E.; Miller, S. J.; Wender, P. A. An Approach to the Site-Selective Diversification of Apoptolidin A with Peptide-Based Catalysts. *J. Nat. Prod.* **2009**, *72*, 1864-1869.

53. Fowler, B. S.; Laemmerhold, K. M.; Miller, S. J. Catalytic Site-Selective Thiocarbonylation and Deoxygenation of Vancomycin Reveal Hydroxyl-Dependent Conformational Effects. *J. Am. Chem. Soc.* **2012**, *134*, 9755-9761.

54. Pathak, T. P.; Miller, S. J. Site-Selective Bromination of Vancomycin. *J. Am. Chem. Soc.* **2012**, *134*, 6120-6123.

55. Han, S.; Miller, S. J. Asymmetric Catalysis at a Distance: Catalytic, Site-Selective Phosphorylation of Teicoplanin. *J. Am. Chem. Soc.* **2013**, *135*, 12414-12421.

56. Kolb, H. C.; Finn, M. G.; Sharpless, K. B. Click chemistry: diverse chemical function from a few good reactions. *Angew. Chem. , Int. Ed.* **2001**, *40*, 2004-2021.

57. Prier, C. K.; Rankic, D. A.; MacMillan, D. W. C. Visible Light Photoredox Catalysis with Transition Metal Complexes: Applications in Organic Synthesis. *Chem. Rev. (Washington, DC, U. S.)* **2013**, *113*, 5322-5363.

58. Bonnet, S.; Collin, J.; Sauvage, J. A Ru(terpy)(phen)-incorporating ring and its light-induced geometrical changes. *Chem. Commun. (Cambridge, U. K.)* **2005**, 3195-3197.

CHAPTER THREE: UNEXPECTED REACTION PATHWAYS IN THE OXIME-DIRECTED RHODIUM-CATALYZED ASYMMETRIC HYDROBORATION

3.1 Introduction

The asymmetric hydroboration reaction, the net addition of B-H to a prochiral alkene, is a valuable synthetic transformation due in large measure to the versatile nature of the organoborane product's carbon-boron bond; chiral organoboranes undergo an expanding number of stereospecific functional group transformations converting the C-B bond to C-O, C-C, C-N, C-X (X = halide), or C-H (Figure 1).[1-6] Recent studies on the formation of carbon-carbon bonds is of particular note. Ohmura, Awano, and Suginome reported the coupling of α-(acylamino)benzyl boronic esters with aryl bromides with inversion of configuration.[3] The high degree of enantiospecificity is attributed to the coordination of amide to boron hindering the approach of palladium from one of the faces. In a complementary strategy, Crudden and co-workers showed that cross-couplings of secondary boronate esters precede with retention of configuration.[4] Other recently reported transformations are also quite impressive. For example, Aggarwal and co-workers found that C-B bonds could be transformed selectively to carbon-halide bonds with inversion of configuration.[5] Several of the substrates examined in this study retained 99-100% of their enantiomeric purity. Miura and co-workers recently reported an *in situ* conversion of an aminoboronate to a diamine with retention of configuration.[6] These transformations illustrate the value in selective approaches chiral organoboronates.

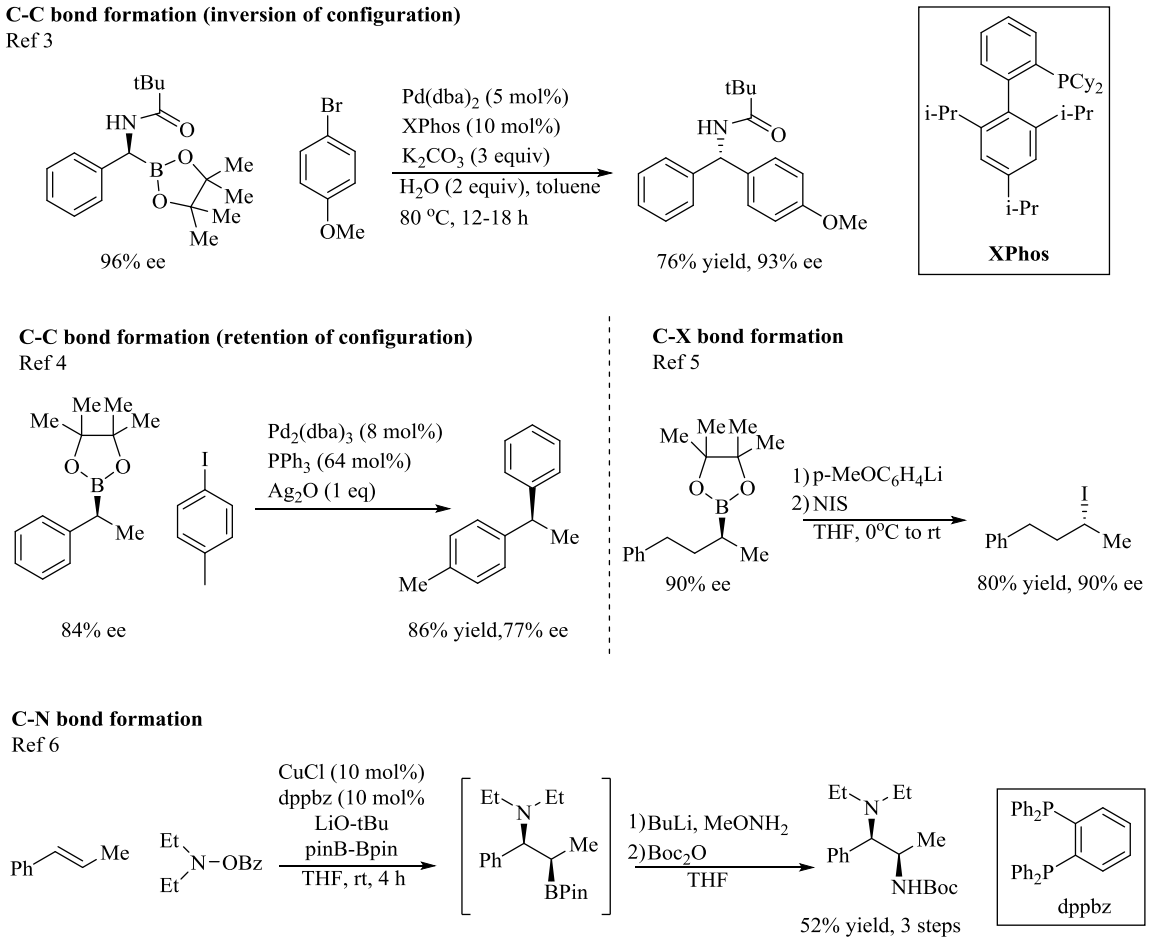

Figure 1 Representative bond transformations for the versatile C-B bond

Below are several methods for preparation of chiral organoboranes. (Figure 2). The oldest preparative method is the asymmetric hydroboration of an alkene with a stoichiometric equivalent of chiral borane; this will be discussed in detail in section 3.2 (vide infra). Alternatively, the catalytic asymmetric hydroboration (CAHB) is a powerful method to induce asymmetry from a chiral catalyst rather than the borane itself.[7-12] CAHB has a long history, and after a period of relative dormancy, recent results, obtained for new classes of substrates and simple chiral catalysts, have reinvigorated the field.

Takacs and co-workers found that simple TADDOL-derived monophosphites and phosphoramidites were effective ligands for the Rh-CAHB of a series of *para*-substituted styrene derivatives affording 90-95% ee; while the yields of the branched isomer (62-79%) were moderate due to formation of the competing linear isomer, it was significant that, in contrast to prior dogma, both electron-donating and electron-withdrawing substituents were sucessful.[13] The low regioselectivity problem was later solved by using TADDOL-derived supramolecular catalysts to give greater than 90% yields of chiral branched isomers in high enantiomeric excess.[14,15] Alternative strategies began to emerge. For example, chiral organoboranes can be prepared in high enantiomeric purity by copper-catalyzed borylative conjugate additions to α,β-unsaturated esters using diboranes.[16] Hall and co-workers presented an alternative approach with a copper-catalyzed hydride addition to β-boronyl-β-alkyl-α,β-unsaturated esters.[17] In a related approach, the asymmetric hydrogenation of vinyl boronates has proven to be quite effective with rhodium[18] and iridium[19,20] catalysts.

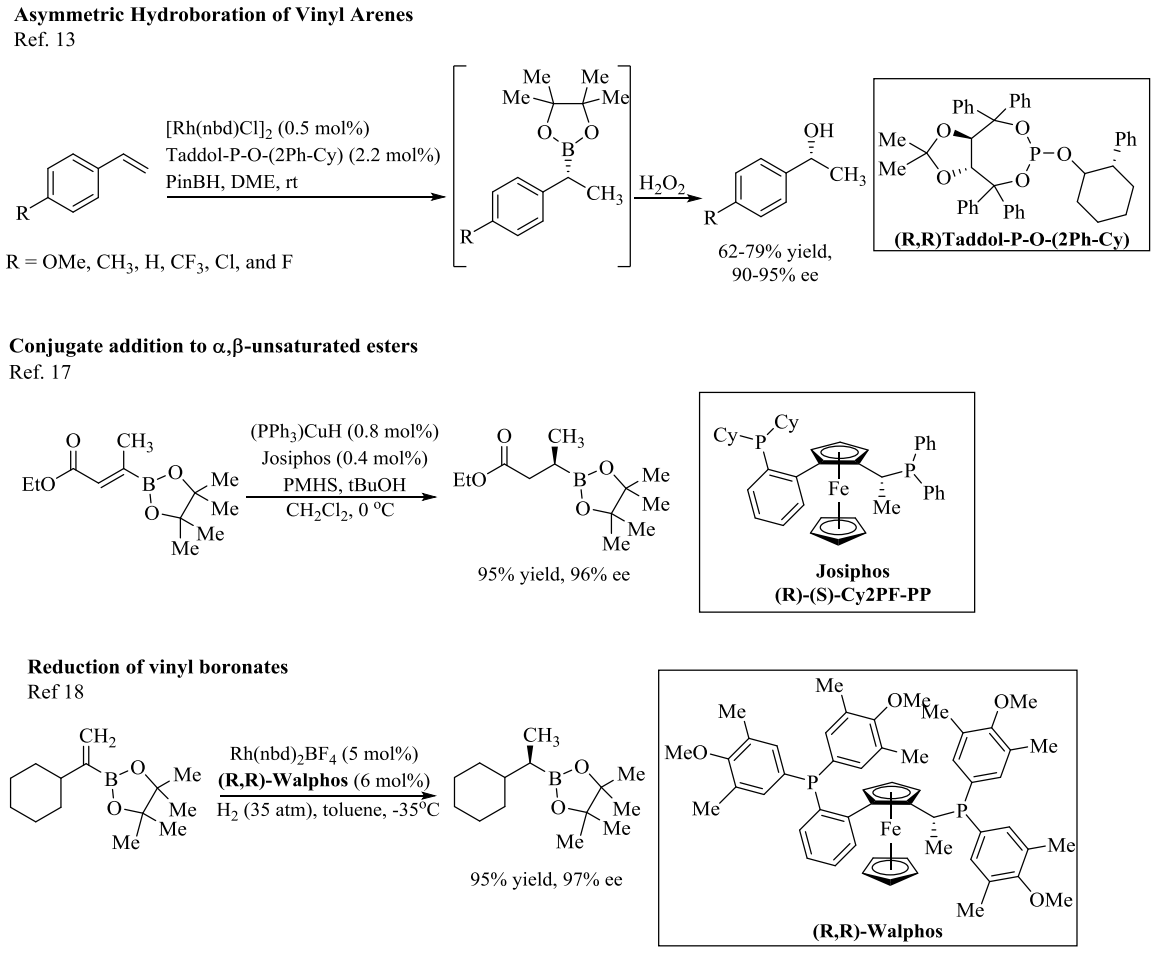

Figure 2 Representative methods for formation of chiral C-B bond

3.2 The challenging hydroboration of 1,1-disubstituted alkenes

The stoichiometric asymmetric hydroboration reaction was first reported by Brown and Zweifel for the selective hydroboration of cis-alkenes (99% ee) with diisopinocampheylborane (Ipc_2BH) (Figure 2).[21-23] This landmark achievement proved for the first time chiral reagents could achieve such high enantioselectivity. The limitations of using Ipc_2BH include limited substrate generality (low enantioselectivity

for trans-, tri-, and 1,1-disubstituted alkenes) and problematic reagent stability due to the competing dehydroboration. Substrate generality was improved with the development of monoisopinocampheylborane ($IPcBH_2$); this reagent increased the enantioselectivity to more useful values for trans-disubstituted (73% ee) and trisubstituted alkenes (53% ee).[24,25] Masamune and co-workers developed a C_2-symmetric borolane (DMB) giving excellent selectivity for *cis*- or *trans*-disubstittued and trisubstituted alkenes (97-99% ee).[26] However, DMB is both relatively unstable and its synthesis of DMB requires seven steps decreasing its practicality. Nonetheless, the one class of disubstituted alkenes for which there was no effective asymmetric hydroboration reagent was the 1,1-disubstituted series (i.e., methylidene substrates); this is attributed to difficulty in differentiation between the prochiral enantiotopic faces.[27] Recently, Soderquist reported a novel chiral borane derived from 10-substituted-9-borabicyclo[3.3.2]decanes which afforded quite good selectivity for some 1,1-disubstituted alkenes; however, there are two significant drawbacks with this reagent.[28] (1) Synthesis of the chiral borane requires four linear steps from β-methoxy-9-BBN including a chiral resolution. (2) Good selectivity for 1,1-disubstituted alkenes was achieved only when the was a significant difference in steric demand between the alkene substituents, for example, methyl versus *tert*-butyl.

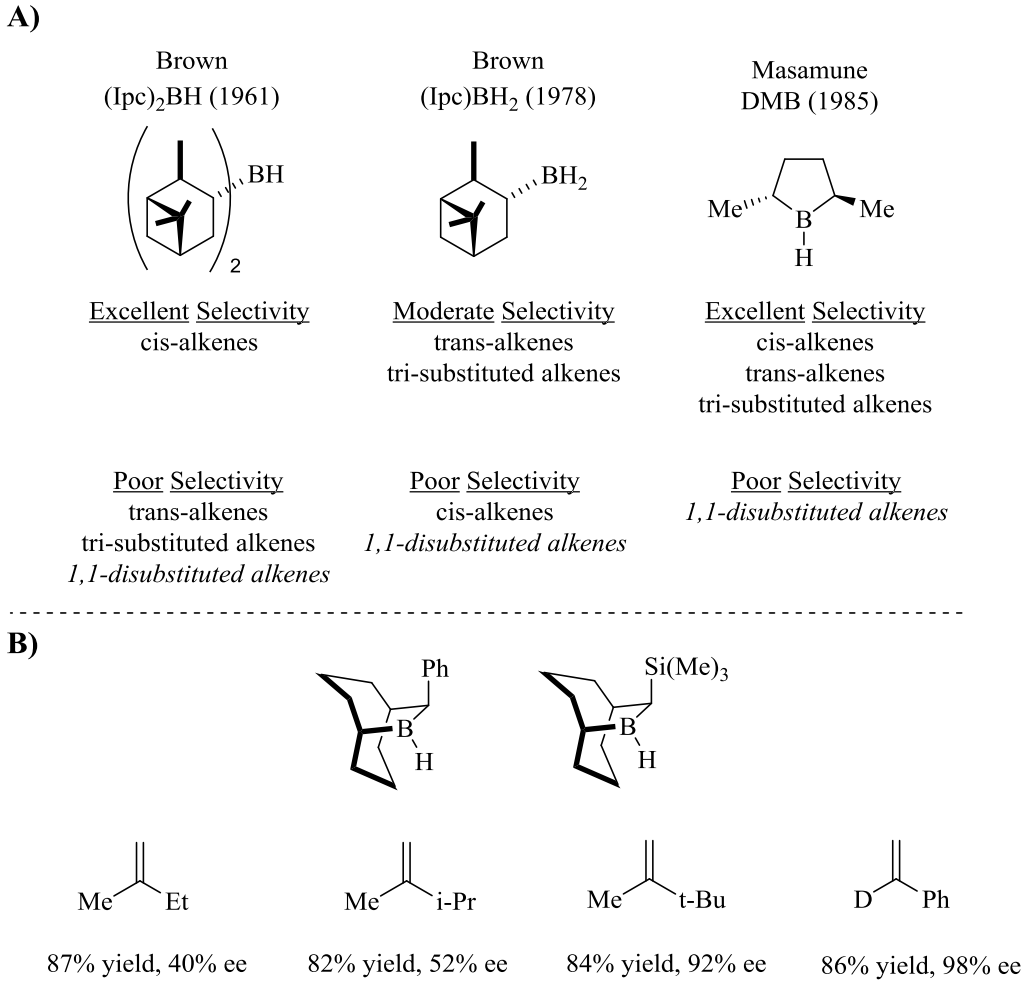

Figure 3 Chiral boranes for the asymmetric hydroboration reaction. A) The first generation of chiral boranes were effective for all but the 1,1-disubstituted series. B) Soderquist developed a series of bicyclic boranes giving high selectivity for hydroboration of 1,1-disubstitued alkenes that possess sterically-biased olefin substituents.

Thus while significant progress has been made, problems remain when using stoichiometric chiral boranes to achieve high selectivity. Chiral boranes may require multiple difficult steps for preparation and do not have long shelf lives. CAHB using a chiral metal catalyst with a racemic or achiral borane is, in principle, a more practical

approach, especially if it is feasible to design a library of catalysts screened against simple to prepare boranes for the various classes of alkenes.[7-12] .

The discovery of catalyzed hydroboration originated from the observation by Kono and Ito that 4,4,6-trimethyl-1,3,2-dioxaborinane (tmdBH) or catecholborane (catBH) readily undergoes oxidative addition to $Rh(PPh_3)_3Cl$ (Wilkinson's Catalyst) at room temperature (Figure 4).[29] Subsequently, it was found tmdBH[30] and catBH[31] only react with alkenes at elevated temperatures with little to no reaction at room temperature. The metal-catalyzed variant was first realized by Männig and Nöth with their report of the rhodium catalyzed hydroboration of alkenes with Wilkinson's catalyst and catBH at room temperature.[32] They showed that the rhodium-catalyzed hydroboration preferred alkenes over ketones, which suggested this approach could be tolerant of other functional groups.

Kono and Ito's discovery of oxidative addition of borane to $Rh(PPh_3)_3Cl$ (Ref 29)

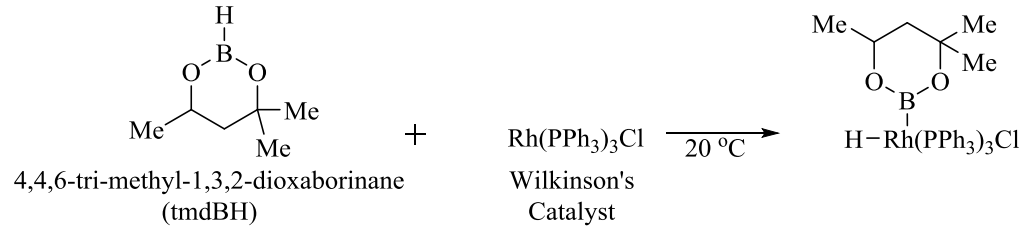

Uncatalyzed reaction of catecholborane with olefins (Ref 31)

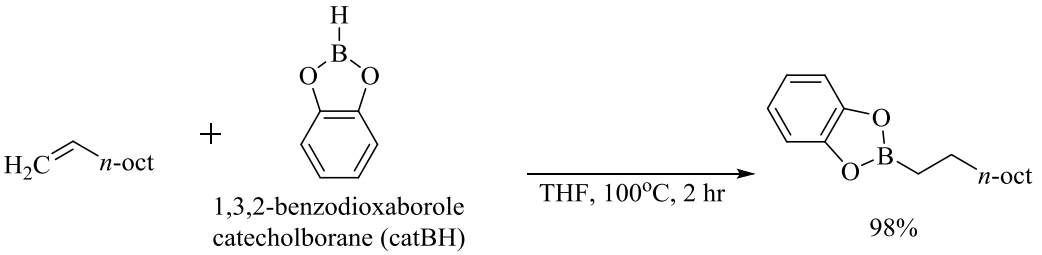

Mannig and Noth report first example of catalyzed hydroboration (Ref 32)

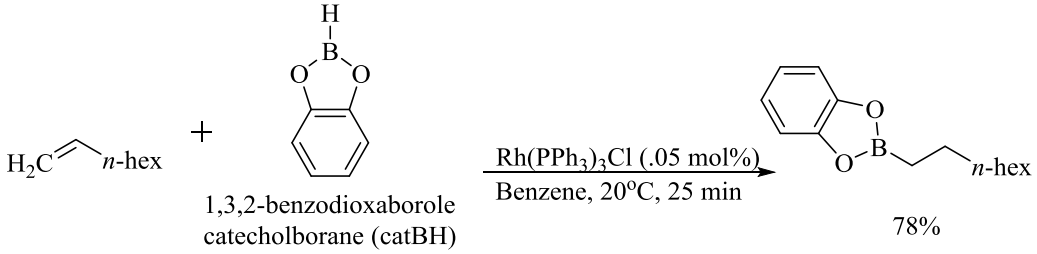

Figure 4 Discovery of oxidative addition of borane to Wilkinson's catalyst led to development of metal catalyzed hydroboration

The generally accepted mechanism for the Rh-catalyzed hydroboration was proposed by Mannig and Noth with a representative mechanism shown (Figure 5).[32] $Rh(PPh_3)_3Cl$ must first disassociate a ligand to open a coordination site affording intermediate **A**, which upon alkene coordination forms intermediate **B**. Oxidative addition of borane (intermediate **C**) followed by migratory insertion may form either a branched alkyl-Rh

intermediate (**D**) or a linear alkyl-Rh species (**D'**). Reductive elimination affords the corresponding alkyl-borane product while regenerating the active catalytic species **A**.

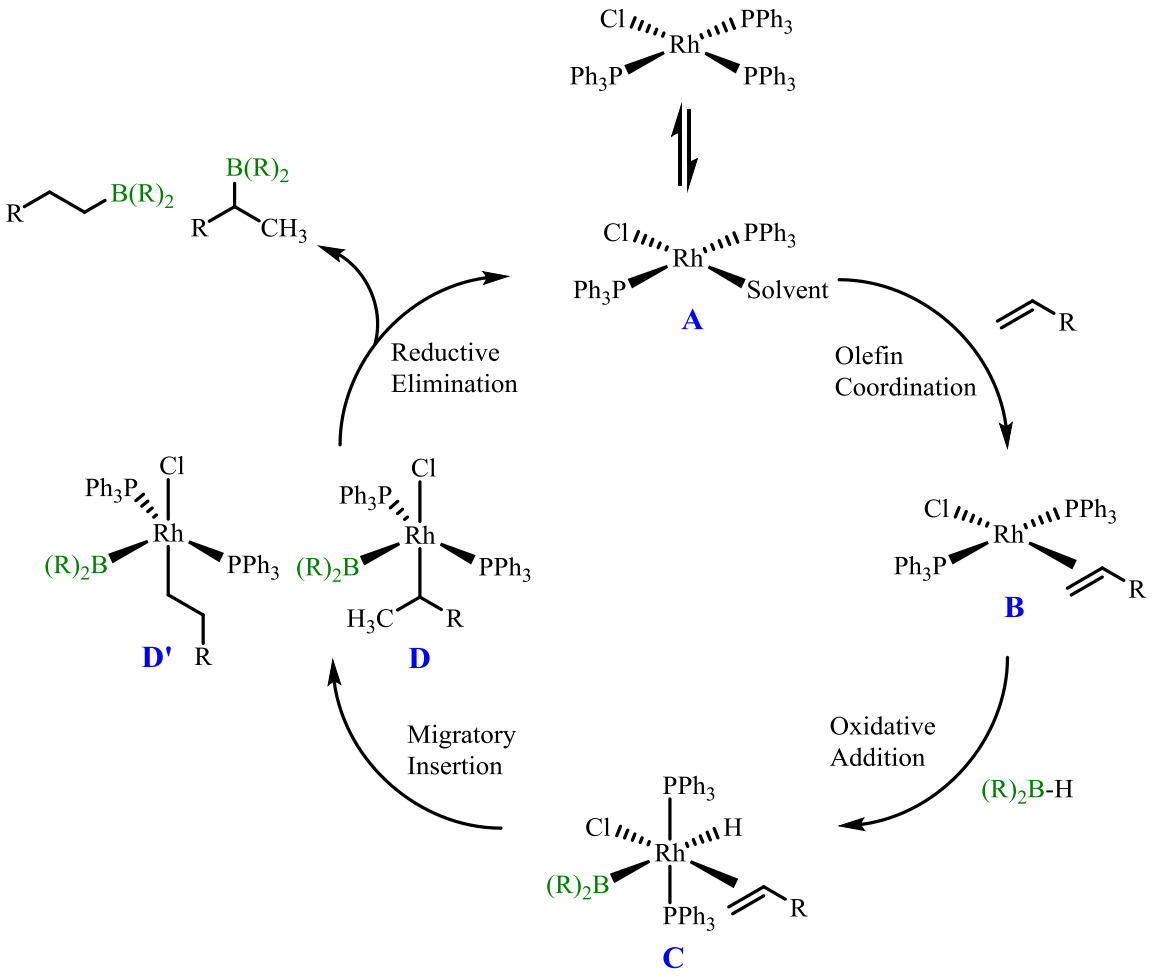

Figure 5 Proposed mechanism for Rh-catalyzed hydroboration with Wilkinson's catalyst

It has been a challenge to achieve high selectivity from the catalyzed asymmetric hydroboration reaction (CAHB) of 1,1-disubstitued alkenes (Figure 6). Sato, Miyaura, and Suzuki reported a cationic Rh-BINAP catalyst and catecholborane afforded moderate selectivity in the Rh-CAHB of α-methyl styrene.[33] Mazet and Gérard reported an iridium *P,N*-ligated catalyst which gave excellent selectivity using pinacolborane (92% ee).[34]

Pinacolborane was selected over catecholborane, because the corresponding pinacolboronate esters are easier to isolate. To highlight the impact of ligand choice, when BINAP is substituted for the optimized chiral *P,N*-ligand, no reaction occurs. Hoveyda recently reported the hydroboration of α-methyl styrene (87% ee) using a copper catalyst ligated with a chiral N-heterocyclic carbene (NHC) and dipinacolborane ($B_2(pin)_2$).[35] In this example, the $B_2(pin)_2$ reacts with (NHC)Cu-alkoxide forming (NHC)Cu-BPin. Enantioselective Cu-B addition to the 1,1-disubstituted alkene forms an organocopper intermediate. Protonolysis regenerates the copper alkoxide forming hydroboration products. Aside from the directed examples discussed in section 3.3, a major limitation in the CAHB of 1,1-disubstiuted alkenes is the lack of substrate scope' In the recent examples cited above, for example, only α-methyl substituted vinylarene derivatives are reported. This is perhaps not surprising; the difference in size between the aryl and the methyl substituents likely helps differentiate the enantiotopic faces of the pi-system.

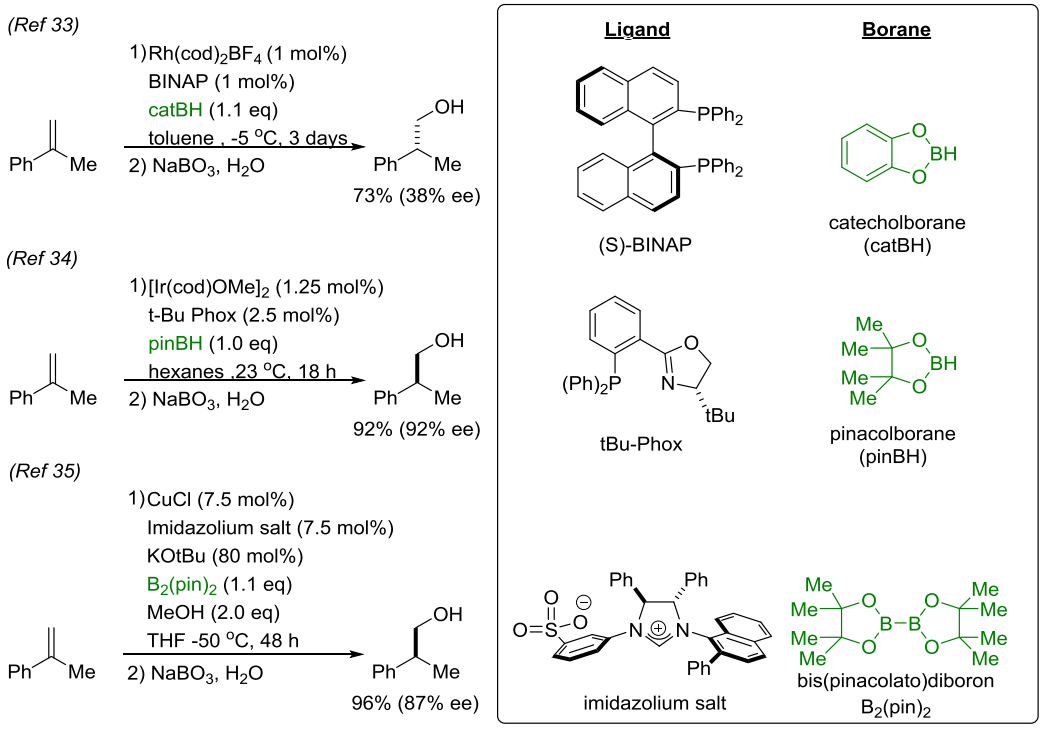

Figure 6 CAHB of α-methyl styrene

3.3 Directed hydroboration

An alternative strategy that proves useful in expanding the substrate scope beyond simple sterics uses a coordinating functional group to direct the catalytically-active metal to the prochiral alkene. A cationic metal with an open coordination site is able to bind to the directing group and the alkene; two-point binding has long been proven effective for the Rh-catalyzed asymmetric hydrogenation (Rh-CAH) and a wide variety of other directed reactions.[36] Evans, Fu, and Hoveyda pioneered the field of amide-directed hydroboration of β,γ-unsaturated acyclic alkenes catalyzed by achiral rhodium and iridium complexes (Figure 7).[37,38] Excellent regioselectivity was observed when two considerations were met: (1) A secondary amide is required to prevent reduction of the

amide in the presence of catBH. (2) Excess catBH is required since the borane decomposes under the reaction conditions.[39] (This will be discussed furthermore in section 3.4).

(Ref 38)

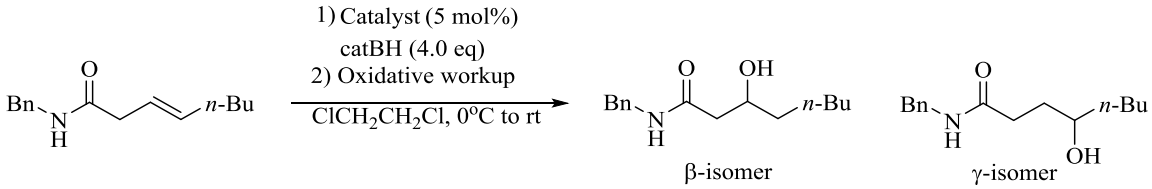

Entry	Catalyst	yield (%)	Regioselectivity (β:γ)
1	$[Rh(nbd)(dppb)]BF_4$	74	20:1
2	$[Ir(cod)(Pcy_3)(py)]PF_6$	73	99:1

Figure 7 First example of a directed catalytic hydroboration

A simple modification of the catalyzed hydroboration mechanism adapted for two-point binding substrates is shown below. Starting with a disolvated Rh(I) complex **A**, coordination of a substrate with a directing group (DG) and alkene affords Rh(I) complex **B**. Oxidative addition of borane (X_2B-H where X = a diol derivative such as pinacol, catechol, etc.) gives Rh(III) complex **C**. Migratory insertion of the alkene gives the Rh(III)-alkyl complex **D** which undergoes reductive elimination expelling the alkyl borane and regenerating active catalyst **A**. One can consider possible deviations from this simplified catalytic mechanism at several stages during the cycle. For example, oxidative addition of X_2B-H can place either the H or the boron in the apical position in the perspective drawn below potentially leading to diastereomeric intermediates. Which

diastereomer is formed may dictate whether the alkene migratory insertion occurs into the Rh-H or Rh-BX_2bond. Secondly, if reductive elimination step is slow or disfavored, a competing β-hydride elimination pathway can give undesired byproducts.[40-43] Our group has recently submitted a publication (now accepted) on a collaborative computational study evaluating the different reaction pathways for the amide-directed Rh-catalyzed hydroboration.

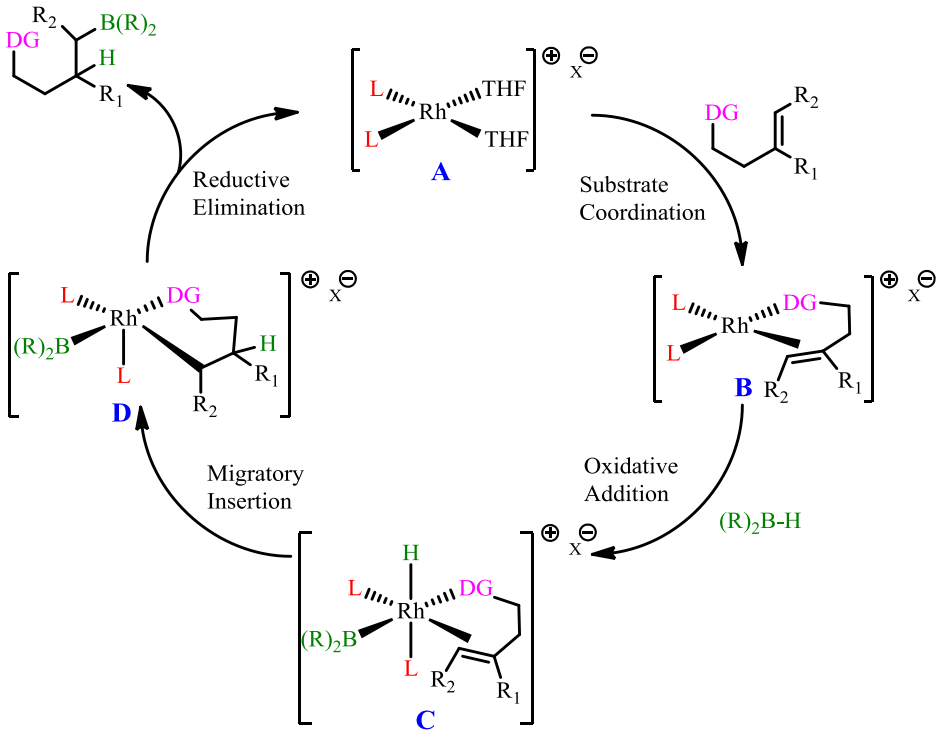

Figure 8 Proposed mechanism for 2-point binding hydroboration. DG = directing group, L = ligating group, $(R)_2B$-H = borane

Takacs et al envisaged that a chiral rhodium catalyst could potentially be effective for the directed CAHB of β,γ-unsaturated amides. Previously, Takacs and co-workers found TADDOL-based phosphites and phosphoramidites gave high enantioselectivity in the

CAHB of styrene derivatives with pinacolborane (Figure 2).[44] While the reactions went to near completion, the desired yields were only moderate due to formation of the undesired linear isomer. It was proposed that the amide's directing ability should negate this regioselectivity problem. They found that Rh-CAHB of acyclic β,γ-unsaturated substrates using chiral TADDOL and BINOL-derived monophosphite and phosphoramidite ligands were effective for certain β,γ-unsaturated di- or trisubstituted alkenes directed by amides[45,46] including published work not reported in this thesis which I carried out, as well as Weinreb amides.[47] The successful results from directed hydroboration of di- and trisubstituted alkenes prompted exploration of the challenging class of 1,1-disubstituted alkenes (i.e., methylidene substrates). Aniline-derived amides and tert-butyl esters were quite effective in the Rh-CAHB of 1,1-disubstituted β,γ-unsaturated methylidene substrates.[48] Regioselectivity favored *gamma*- over *beta*-substitution ranged from 5:1 to 20:1 with good yields for *gamma*-borylated product (53%-78%) and excellent enantioselectivity (91-94% ee).

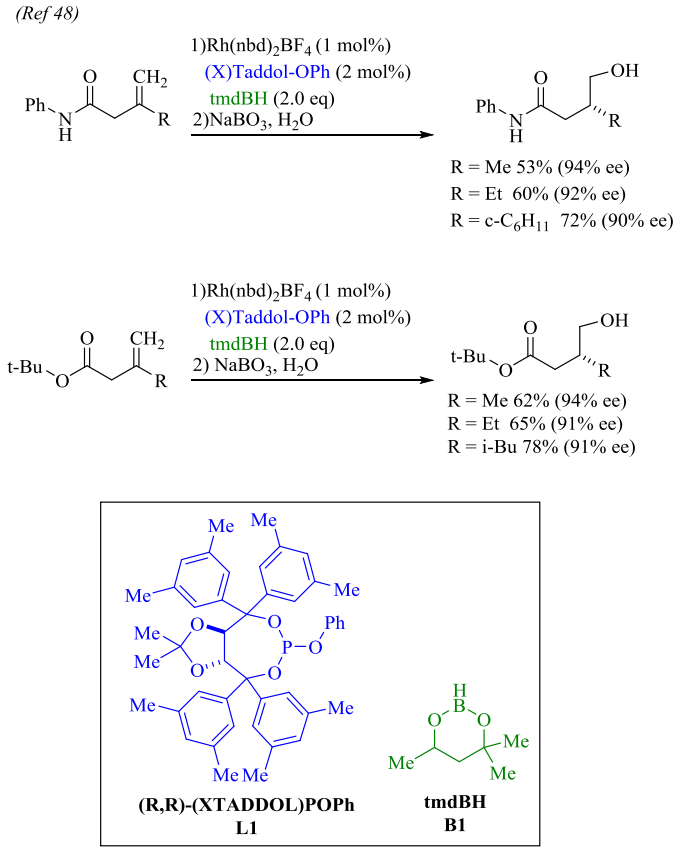

Figure 9 Directed CAHB of 1,1-disubstituted alkenes

Studies into the CAHB of Oxime Ethers: Results and Discussion

A note to the readers: the following portion of this chapter outlines our findings into an unexpected and unusually facile C-H insertion and its role in the oxime-directed Rh-catalyzed hydroboration. Our current understanding of the reaction is as follows:

- *Reduced products are not formed directly from H_2 and Rh(I).* The Rh-catalyzed hydroboration is susceptible to influence of H_2 on the reaction mechanism.
- *Ortho-metallation is only detected with a proximal alkene that reacts*. Saturated substrates do not readily *ortho*-metallate under standard reaction conditions.

Substitution of the alkene for alternate directing groups does not facilitate C-H insertion.

- *The mechanism by which oxime-directed hydroboration products are formed is dependent upon the nature of the borane*. With catecholborane, the reaction pathway is oxidative addition, migratory insertion, and reductive elimination. With tmdBH, the hydroboration products are likely formed from a dehydrogenative borylation followed by reduction.
- *The source of the "H-H" addition in the reduced products is not straightforward*. During Rh-catalyzed hydroboration, isotopically-labelled boranes (>90% D incorporation) lose deuterium before transfer to the reacting alkene; the B-D is exchanged for B-H, presumably from the THF solvent.

3.4 Oxime-directed hydroboration

Amides are relatively stable and often require relatively harsh reactions conditions to refunctionalize in the presence of other sensitive functionalities; this makes their presence less synthetically useful. Oximes are more labile than amides and have the benefit of an extra heteroatom for further functionalization (Figure 10); in addition, oximes are much less common, and a route to their enantioselective synthesis may offer new possibilities for synthesis. For example, the nitrogen protecting group may be removed forming hydroxylamines or the labile O-N bond may be cleaved giving alcohols. Together with the possibilities for subsequent functionalization of the C-B

bond, investigating their CAHB chemistry seemed to be a potentially useful endeavor.

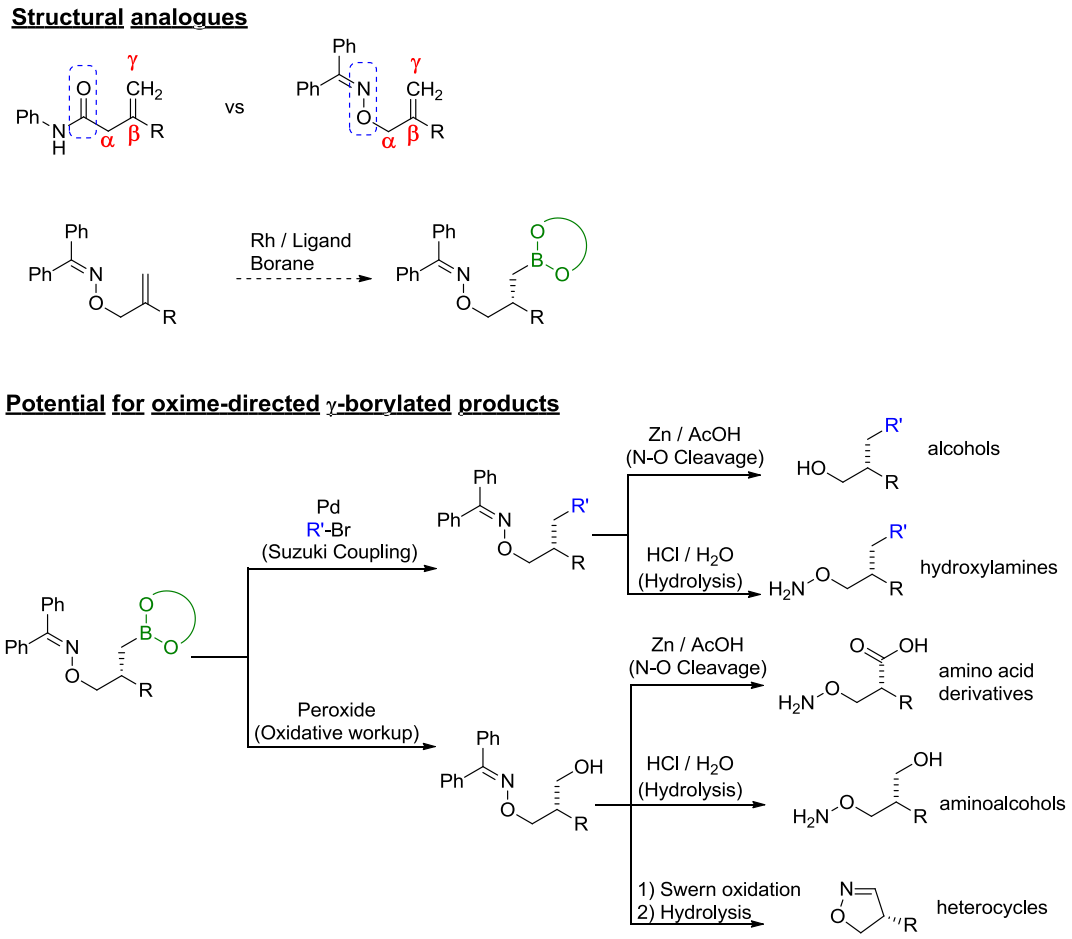

Figure 10 Hydroboration of β,γ unsaturated oximes provide access to wide variety of products

Oxime-directed catalysis to β,γ-unsaturated alkenes can be effective. Recently, Sanford and co-workers reported an oxime-directed Pd-catalyzed dihydroxylation of a β,γ-unsaturated alkene (Figure 11).[49] Using chiral aliphatic oximes, the Pd-catalyzed diastereoselective dihydroxylation of β,γ-unsaturated alkenes gave up to 80% diastereomeric excess.

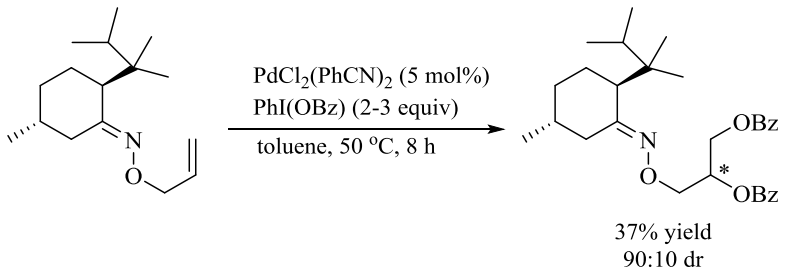

Figure 11 Oxime-directed dioxygenation of β,γ-unsaturated alkenes

While the hydroboration of 1,1-disubstituted-β,γ-unsaturated phenyl amide derivatives precedes smoothly affording the γ-isomer as the major product (53% yield), a significant amount of reduction product (22%) was also isolated (Figure 9).[48] It was presumed that this reduced product was the result of a competing side reaction wherein a Rh(III) dihydride catalyst was formed; it is believed the H_2 is its source having been formed by catalyzed borane decomposition or through spontaneous disproportionation (Scheme 1)[39] or a nucleophile-promoted pathway.[50] Typically, these pathways can be avoided if the alkene is more reactive than the borane decomposition, but for slow-reacting or coordinating substrates these pathways become more of a concern. With two-point directing substrates, an excess of borane is required to get complete conversion of starting materials suggesting the directing groups may promote borane disproportionation.

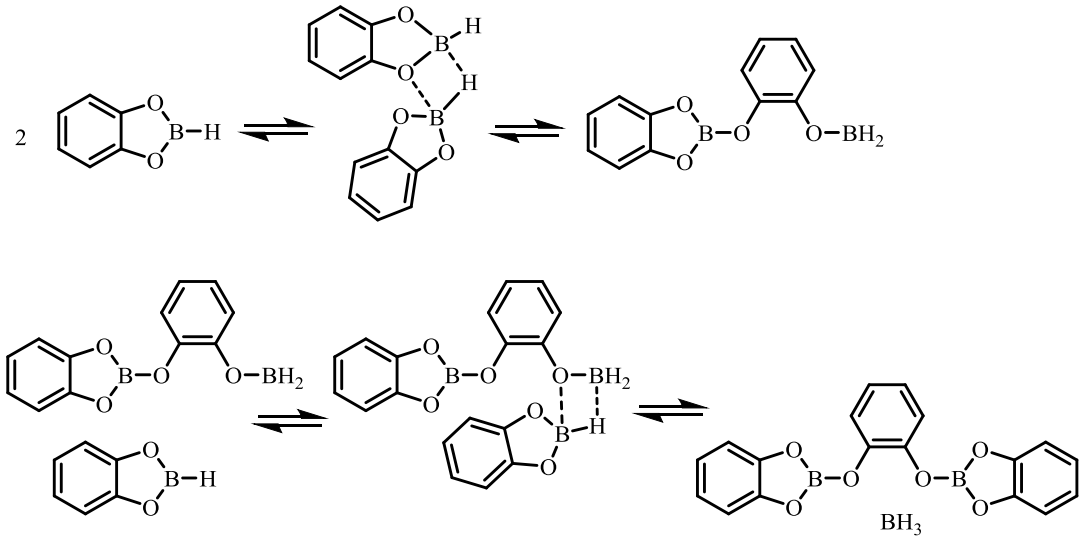

Scheme 1 Spontaneous disproportionation of catecholborane. Adapted with permission from *Inorg. Chem*. **1962**, *1*, 744-748 ©2014 American Chemical Society

3.5 The initial reactions of a simple oxime substrate were patterned after the amide substrates examined previously and initially seemed promising.

1,1-disubstituted-β,γ-unsaturated oxime **1**, originally prepared and investigated preliminarily by Mr. Andrew Geis, was subjected to Rh-CAHB under the identical reaction conditions used for the structurally similar 1,1-disubstituted-β,γ-unsaturated *N*-phenyl amide discussed previously with $Rh[(xTaddol)POPh]_2BF_4$ as the catalyst (Figure 12). Starting material was consumed after 16 h, but γ-alcohol **4** was isolated in only 6% yield. Preliminary studies had indicated by chiral HPLC that oxime **1** underwent CAHB with high enantioselectivity; however that turned out to be wrong. I confirmed that the enantiomers did not resolve upon chiral HPLC or chiral GC with the columns available. Fortunately, derivatizing with Mosher's acid chloride, (S)-methoxy-α-(trifluomethyl)phenylacetyl chloride, gave diastereomeric esters that

could be used to determine the diastereomeric excess by ^{19}F NMR; unfortunately, it was low (12% de).[51,52] Two products in which the alkene had been reduced accounted for about 90% of the mass recovered in the reaction; these two products were formed in a 1:2 ratio and were isolated and characterized. The minor of the two reduced product was the typical reduced product seen from net H_2 reduction of the alkene; the major reduced product was missing an aromatic proton and an unusual singlet accounting for one exchangeable hydrogen at δ 11.2 ppm was seen. NMR and high-resolution mass spectrometry analysis helped me to determine the product is the *ortho*-hydroxylated product **3**. We hypothesized this occurred through directed C-H activation followed by boryl substitution. Under oxidative workup conditions, borylated product was converted to the *ortho*-hydroxy derivative. [Readers note that the terms *ortho*-metallation and *ortho*-borylation will be used in the discussion below based on the observed formation of the *ortho*-hydroxy product.] Attempts to isolate the borylated product for further characterization were unsuccessful; the *ortho*-borylated and *gamma*-borylated products co-eluted and were inseparable. Changing the catalyst to one using a phosphoramidite ligand (XTADDOL)PN(Me)Ph afforded the γ-alcohol as the major product (57%), but the enantioselectivity, although improved, was still low (33% ee by MTPA-derivatization) and the undesired reduced material was obtained in 41% yield.

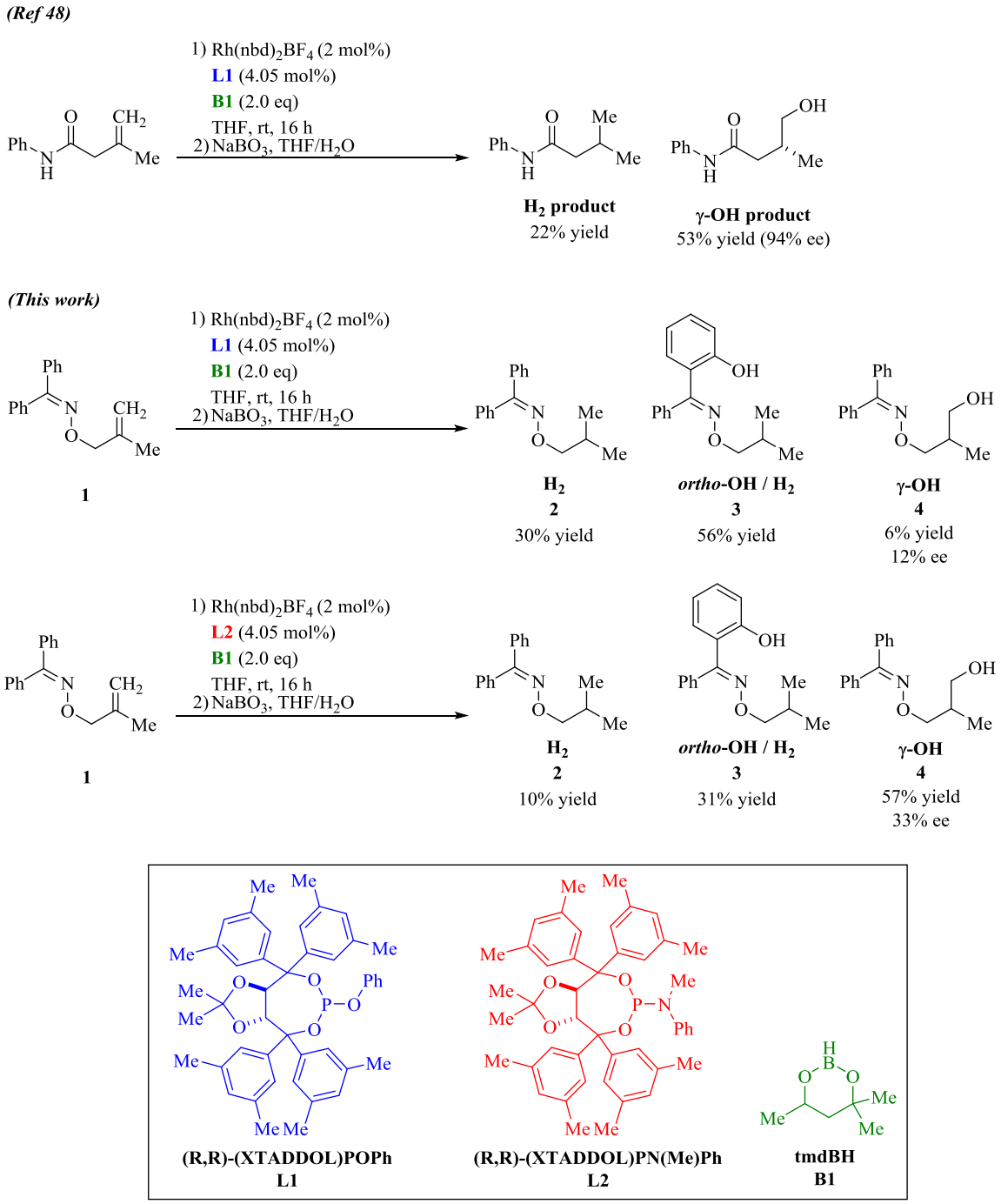

Figure 12 Hydroboration of β,γ-unsaturated oximes afford *gamma*-hydroxylated and reduced products

Since the often (annoying) competing reduction is now a major competing pathway with oxime substrates, it was postulated that *ortho*-metallation could be responsible for the increased yields of reduced material. However, a simpler explanation is that borane decomposition forms H_2 which is scavenged by Rh(I) to promote the Rh-catalyzed hydrogenation. The stoichiometry of the reagents used in the reaction indicates that the borane could in principle provide enough H_2 to account for the reduced products (Figure 13). For example, the γ-borylated product requires consumption of one equivalent of borane. H_2 can be formed from 2 sources: (1) decomposition of two equivalents of borane gives one equivalent diborane and one equivalent H_2; and/or (2) the *ortho*-borylated material arises from H/B exchange with liberation of one H_2.

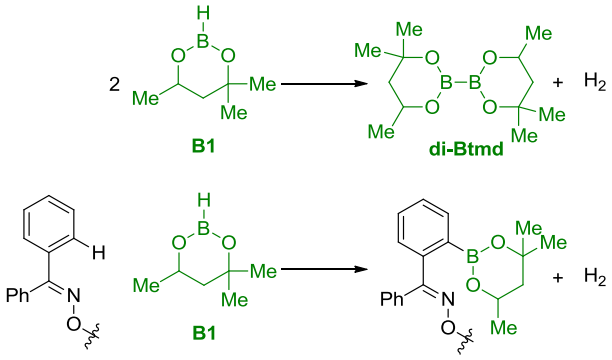

Figure 13 Possible sources of H_2 from borane decomposition and ortho-borylation

3.6 Proof of the structure of the ortho-hydroxylated material 3 by alternative synthesis

To confirm the structure of ortho-hydroxylated product **3**, an alternate synthetic scheme was developed (Figure 14). Starting from commercially available 2-

hydroxybenzophenone, the oxime was formed in good yield. Alkylation with 1-bromo-2-methyl propane afforded *ortho*-hydroxylated ether **3** whose spectral characterization proved identical to that isolated from the hydroboration reaction. The intramolecular hydrogen bonding of the *ortho*-hydroxy group suppresses intermolecular hydrogen exchange giving a sharp concentration independent singlet in the HNMR spectrum with an unusually far downfield chemical shift (δ 11.2 ppm).

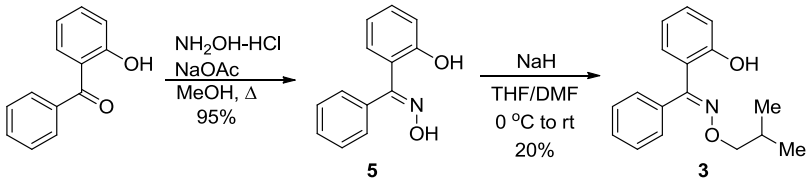

Figure 14 Synthetic proof of ortho-hydroxylated product

3.7 The observed *ortho*-hydroxylation to form 3 occurs at room temperature, but such mild conditions for C-H activation are not common in the literature.

The field of C-H activation chemistry has expanded rapidly over the past 10 years and continues to grow with an ever increasing number of new organometallic catalysts [53-63] and organocatalysts.[64] Nonetheless, metal-catalyzed C-H activation is rarely observed to be facile at room temperature; heating is usually required for efficient *ortho*-metallation.[63] There are only a few reports of Rh(III) catalyzed C-H activation at room temperature; out of over 150 reports, only 5 were accomplished at room temperature (Figure 15).[65-69] A survey of the directing groups reported for C-H activation found *N*-phenyl amides directed the rhodium-catalyzed C-H activation captured by an alkene, imine, or halide at 60-130 °C.[65,70-72] If elevated temperatures are required, then it is

perhaps not surprising, that we did not observe the potential corresponding *ortho*-metallation/borylation in our prior studies of amide-directed CAHB using N-phenyl amide substrates. Relevant to the chemistry described in this chapter, oximes have been used as directing groups for C-H activation with Pd[73,74] and Rh[75,76], but all of these reports required harsh conditions (>60 °C) to effect reaction.

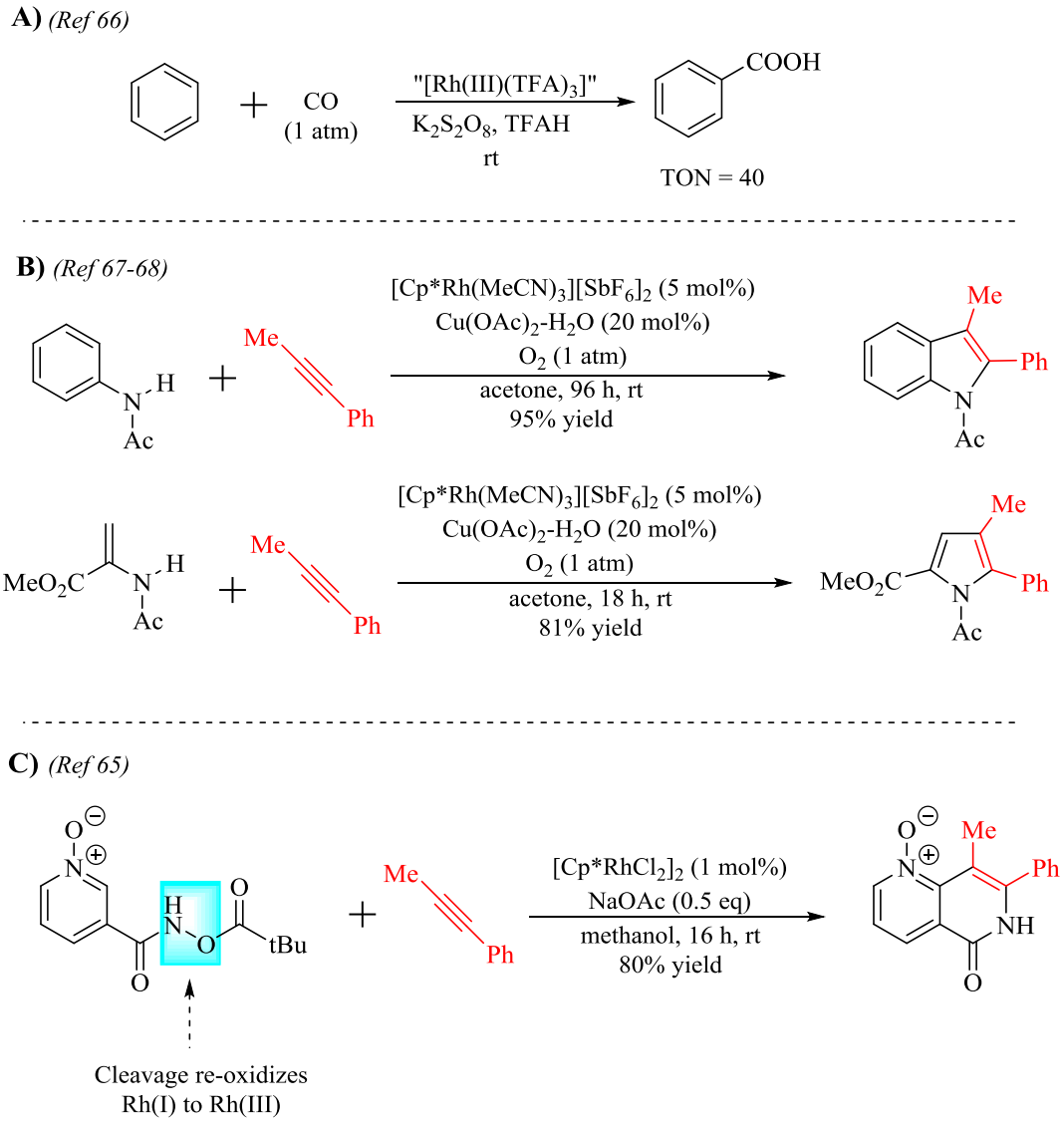

Figure 15 Examples of Rh-catalyzed C-H activation at room temperature. A) Carboxylation of arenes; B) Indoline and Pyrrole Synthesis; C) Using a self-oxidizing directing group

3.8 The reduced product is not formed simply by rhodium-catalyzed alkene hydrogenation

The simplest way to account for the formation of reduced alkene products is that Rh(I) scavenges adventitious H_2 that is formed from borane decomposition, and the alkene simply undergoes rhodium-catalyzed hydrogenation; this is the generally assumed origin of reduced products in CAHB. If this is the case for the oxime substrate, then the *ortho*-borylation occurs via an independent pathway (vide infra). In testing the rhodium-catalyzed hydrogen, we were surprised to find that running the reaction under a hydrogen atmosphere (H_2 balloon) with the rhodium catalyst but no borane present did not reduce the alkene (Table 1, entry 1). While this result doesn't rule out the possibility that a Rh(III)-dihydride is responsible for alkene reduction, it does suggest the dihydride is not formed directly from Rh(I) and H_2.

tmdBH is needed to effect alkene hydrogenation. The reaction was again run under a hydrogen atmosphere, but this time limiting amounts of tmdBH were present. With as little as 0.4 equivalents of tmdBH, exclusive formation of the reduced product **2** was found; neither hydroxylated product (i.e., **3** or **4**) were formed in appreciable amounts (Table 1, entry 3). With 2.0 equivalents of tmdBH (i.e., the normal reaction conditions except under a hydrogen atmosphere), both **3** and **4** were present, but in amounts substantially below that seen in the absence of the hydrogen atmosphere (Table 1, entry 4). Surprisingly, similar effects are not seen for the analogous CAHBs using catecholborane (catBH) under a H_2 atmosphere (Table 1, entries 5-7). This result is confirmed when CAHBs using catBH afforded similar yields under H_2 atmosphere or N_2 atmosphere (Table 1, entry 8 vs 9).

.

Table 1: Borane as an additive influences the hydrogenation reaction

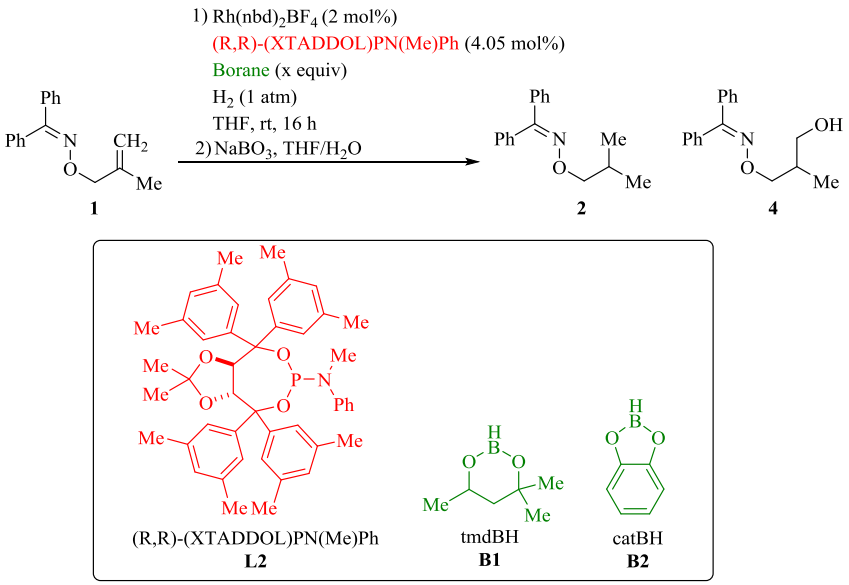

Entry	Borane (equivalent)	Starting Material Remaining (%)	H_2 product (%)	γ-OH (%)
1	0 equiv	100	0	0
2	tmdBH (0.2 equiv)	50	50	0
3	tmdBH (0.4 equiv)	5	95	0
4	tmdBH (2.0 equiv)	0	61	21
5	catBH (0.2 equiv)	94	1	0
6	catBH (0.4 equiv)	92	2	3
7	catBH (2.0 equiv)	0	8	58
8[a]	catBH (2.0 equiv)	0	6	63

[a]Reaction under a N_2 atmosphere without added H_2.

A proposed mechanism to account for the formation of the hydrogenation product is described below (Figure 16A). Oxidative addition of a borane (X_2BH) to to Rh(I)(Ligand)$_2$ (intermediate **B**) produces Rh(III)H(Ligand)$_2$BR$_2$ (intermediate **C**). As H_2 is introduced, σ-bond metathesis between the Rh-B and H-H would regenerate X_2BH (the borane is effectively a co-catalyst) and form Rh-dihydride **D**. (A more detailed

explanation of the possible mechanism is in Section 3.15.) Migratory insertion followed by reductive elimination forms the reduced product. Perira and Srebnik exploit a similar "crossover" strategy in the Rh-catalyzed addition of CCl_4 to alkenes using a sub-stoichiometric amount of pinBH (Figure 16B) to promote the reaction pathway.[77]

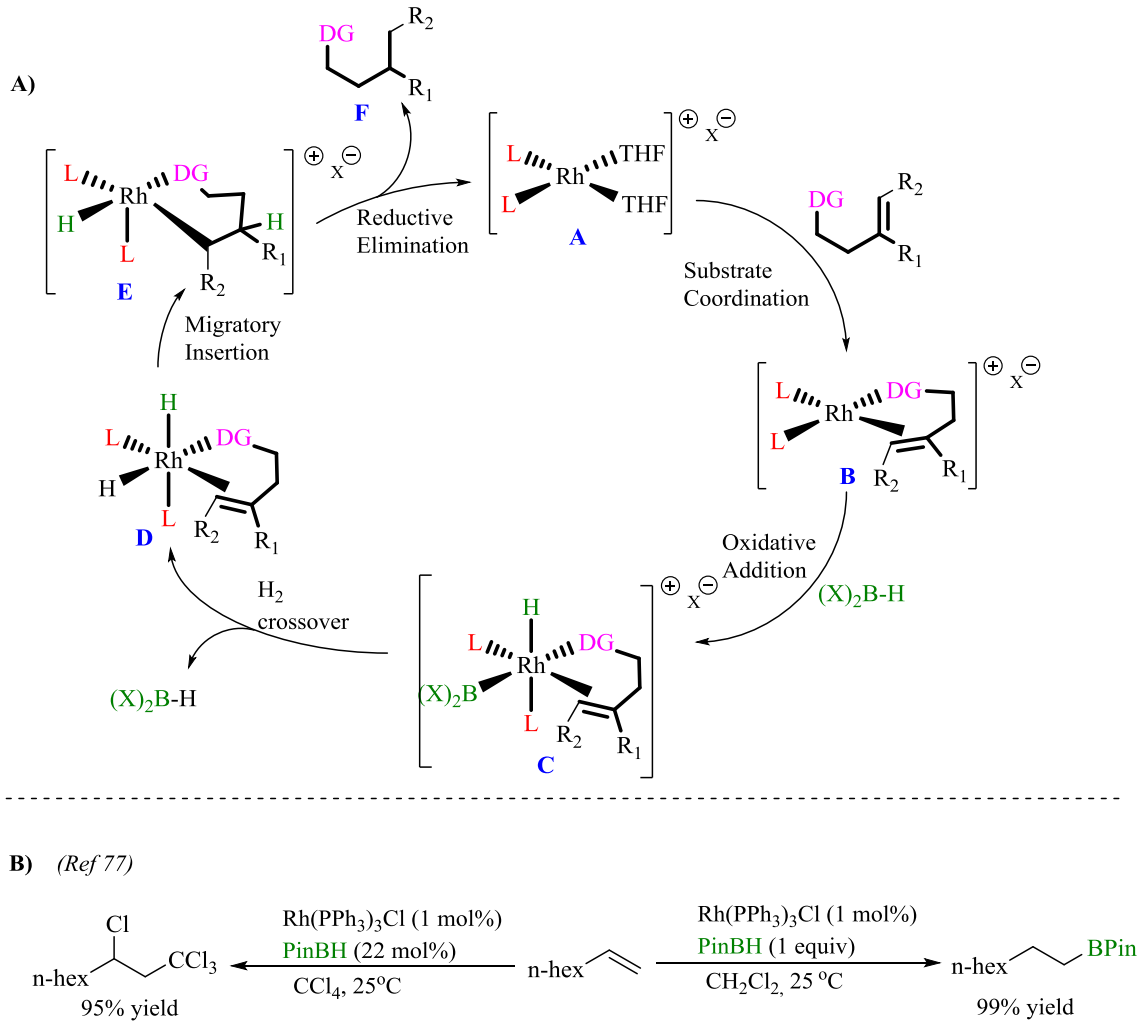

Figure 16: A) Proposed mechanism for role of borane activation for active reduction of alkenes B) Crossover occurs readily with Wilkinson's catalyst and pinBH in CCl_4

3.9 The choice of borane has a large effect on the product distribution obtained in the Rh-CAHB of β,γ-unsaturated oximes

β,γ-unsaturated oxime **1** was screened with boranes differing only in diol backbone. tmdBH and pinBH are similar electronically and sterically, yet give substantially different product ratios in the Rh-CAHB of **1** (Table 2). The new complication arises in that pinBH gives poor regioselectivity for hydroboration of the alkene; that is, competing formation of the β-alcohol **6** lowers the yield of desired γ-alcohol **4**. CatBH affords only 7% total reduced material, and less than 1% of *ortho*-hydroxlation **3**; the latter suggests that C-H activation is disfavored by catBH. Overall, the desired γ-alcohol is the predominant product with catBH (63% yield), but the enantioselectivity is poor (ca 6% ee).

Table 2 Nature of borane affects the hydroboration greatly

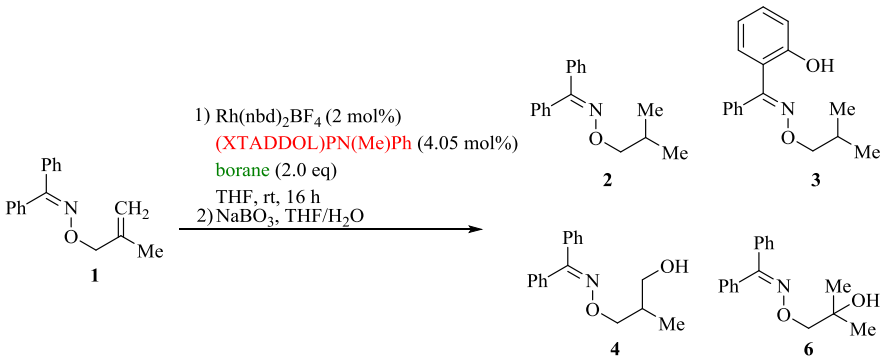

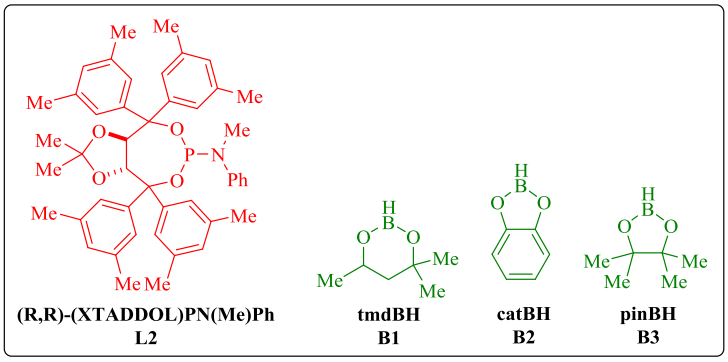

Entry	Borane	Starting Material Remaining **1**(%)	H_2 product **2** (%)	*o*-OH / H_2 **3** (%)	β-OH **6** (%)	γ-OH **4** (%)
1	tmdBH **B1**	0	10	31	0	58 (33% ee)
2	pinBH **B3**	14	24	8	16	30 (11% ee)
3	catBH **B2**	0	6	1	7	63 (6% ee)

3.10 Are the reduced products formed via the same pathway as chiral γ-products?

If a short-lived catalytic species is responsible for the formation of reduced product **2**, its rate of formation would likely differ from that of the other products over the course of the reaction; that is what is found (Figure 16). After completion of borane addition at 0

°C, the reaction mixture was stirred at 0 °C for 30 minutes and then allowed to warm to room temperature. Aliquots were removed and quenched by oxidative workup. The crude products were extracted and purified by flash chromatography. Their isolated yields are shown below (Figure 17). The majority of reduced product **2** is formed within the first 30 minutes at 0 °C. Meanwhile, the *ortho*-borylated product **3** and γ-borylated product **4** were formed, roughly in parallel, over the remaining course of the reaction. This result suggests reduced product **2** may be formed from a pathway independent of the *ortho*-borylated and gamma borylated products. It is not clear how the proposed mechanism in Figure 15 accommodates this conclusion since the reduction stops shortly into the reaction; one possibility is that a limited amount of hydrogen remains or is generated after the initial phase of the reaction.

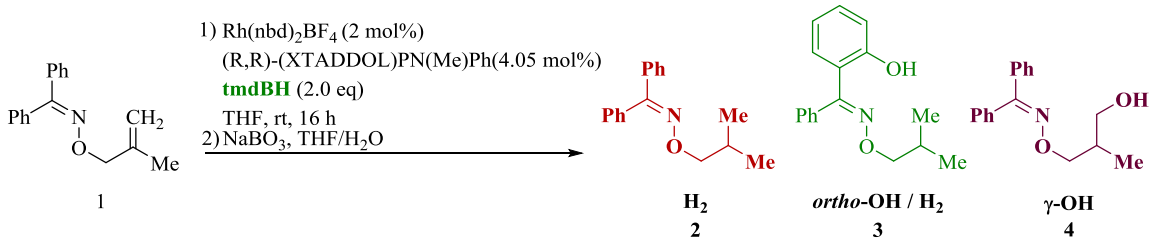

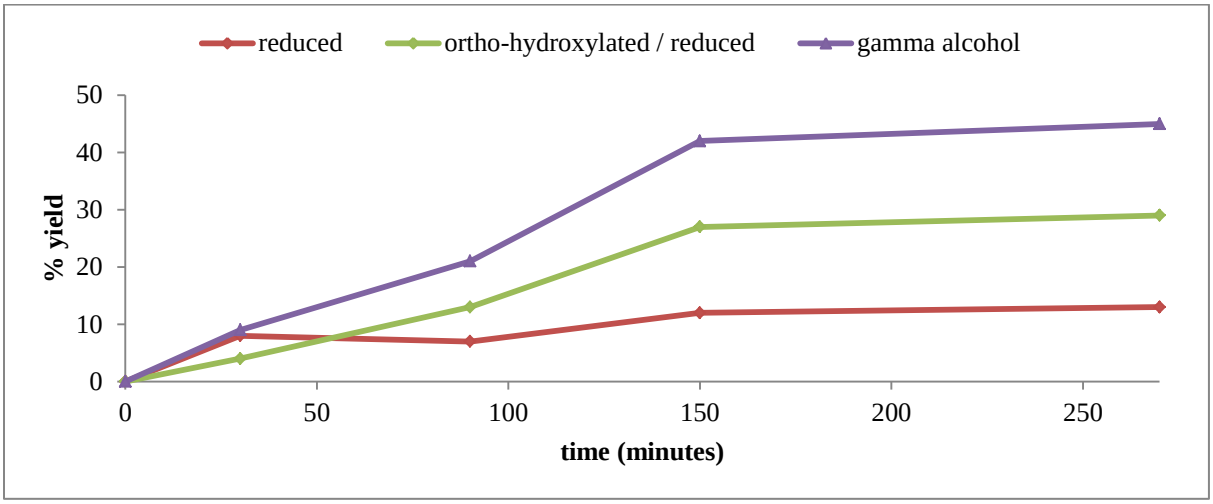

Figure 17 Rate reaction for oxime directed hydroboration indicates *ortho*-hydroxylated product and gamma-hydroxy product are formed concurrently

3.11 The size of the vinyl substituent has only a small effect on the product distribution, but improves the selectivity.

Previous studies in the amide-directed CAHB of methylidene substrates found that substrates in which the vinyl methyl substituent is replaced by a larger, more sterically-demanding substituent gave increased yields of γ-borylated product with decreased formation of reduced products.[48] To probe this, two substrates were prepared, one bearing an isobutyl substituent and another with a cyclohexyl group. Unfortunately, the substituents had little impact on the observed product distributions (Table 3). However,

there was one significant benefit, the level of enantioselectivity increased as high as 70% ee giving some hope that a superior catalyst could ultimately be obtained. Perhaps increasing the size of the substituent helps to further differentiate the enantiotopic faces of the alkene.

Table 3 Changing the vinyl substituent increases the enantioselectivity but total reduced products remain relatively unaffected

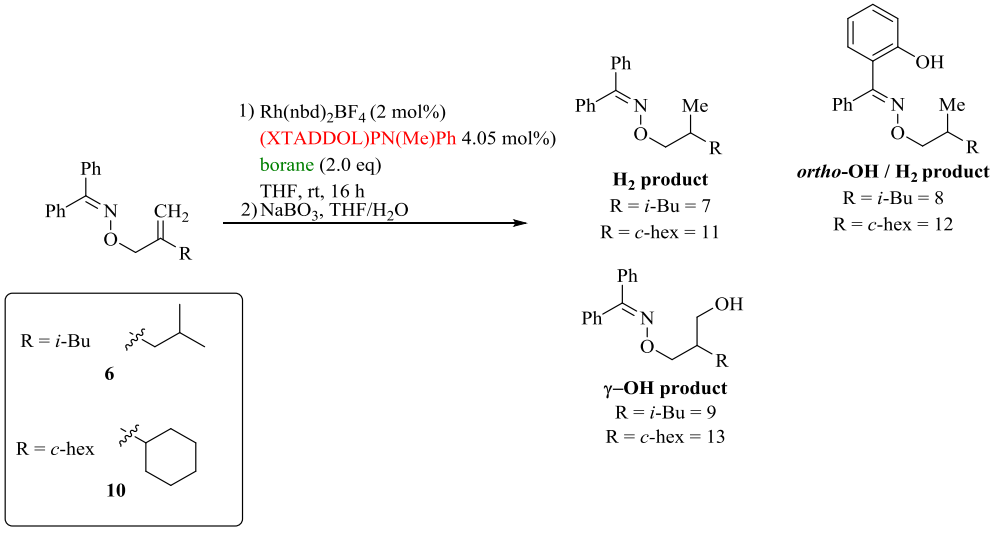

Entry	Borane	R = substituent	H_2 product (%)	*o*-OH / H_2 (%)	β-OH (%)	γ-OH (%) / (% ee)
1	tmdBH	Isobutyl	16	29	0	52 (60)
2	catBH	Isobutyl	0	0	0	16 (0)
3	tmdBH	Cyclohexyl	28	11	0	60 (40)
4	catBH	cyclohexyl	5	2	7	52 (70)

3.12 The alkene is essential for efficient *ortho*-metallation/borylation and the formation of 3.

Having gathered some information on the formation of reduced product **2**, we turned our attention to the formation of the *ortho*-borylated and reduced product **3**. The C-H insertion could occur either before, during, or after reaction with the alkene. As the *ortho*-borylated material with the alkene intact has never been observed, it is presumed that C-H insertion must occur during the hydroboration reaction. To test this, the reduced product **2** was synthesized and subjected to hydroboration conditions. Only 3% of the *ortho*-hydroxylated product **3** was isolated after workup. While not conclusive evidence that *ortho*-metallation requires the alkene be present, for example, one could imagine that *ortho*-metallation occurs but hydrogen is delivered back to its original position, the results obtained starting from **2** coupled with the evidence presented for its formation by an independent pathway is strongly suggestive that **2** is not converted to **3** under the reaction conditions (Figure 18).

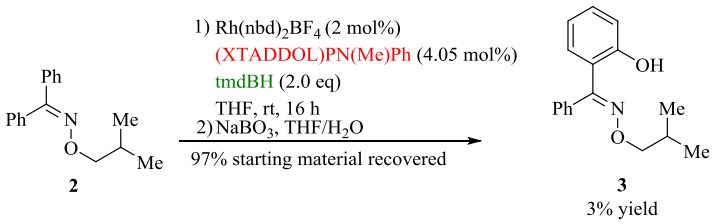

Figure 18 *Ortho*-borylation not promoted in saturated oxime

Is norbornadiene involved in the catalytic cycle? Norbornadiene (nbd) is a common diene ligand used with metal precursors in catalysis; due to the strain in the pi-systems,

the diene ligand is thought to rapidly react via CAHB and thus be an innocuous bystander in the hydroboration reaction of interest. However, olefin ligands have the ability to participate in catalytic reactions;[78,79] for example, norbornene has a substantial role in catalysis in the palladium-catalyzed Catellani reaction.[80-82] In the Catellani reaction, norbornene is thought to form a palladacycle intermediate which upon reductive elimination and depalladation reforms norbornene. Hence, norbornene is part of the catalytic cycle or at the very least serves as a co-catalyst in that reaction. In a similar vein, Hua, Nguyen, Scaggs, and Jeon found phosphorus ligating groups and norbornene cooperatively participated in the diastereoselective rhodium-catalyzed intramolecular alkene hydrosilyation reaction (Figure 19).[83] When norbornene was used as a sub-stoichiometric additive, excellent yield and diastereoselectivity were observed. The proposed mechanistic cycle involves norbornene acting as a hydride shuttle.

If norbornadiene were responsible for C-H activation and subsequent formation of *ortho*-borylated product **3**, replacement with an alternative diene ligand should result in a change in yield. When Rh(1,5-cyclooctadiene)$_2$BF$_4$ was used, there was no change in reduced or borylated yields. Furthermore, norbornene rapidly undergoes CAHB.[84] This suggests that while norbornadiene is expected to undergo CAHB, it should otherwise not interfere in the reaction of **1**.

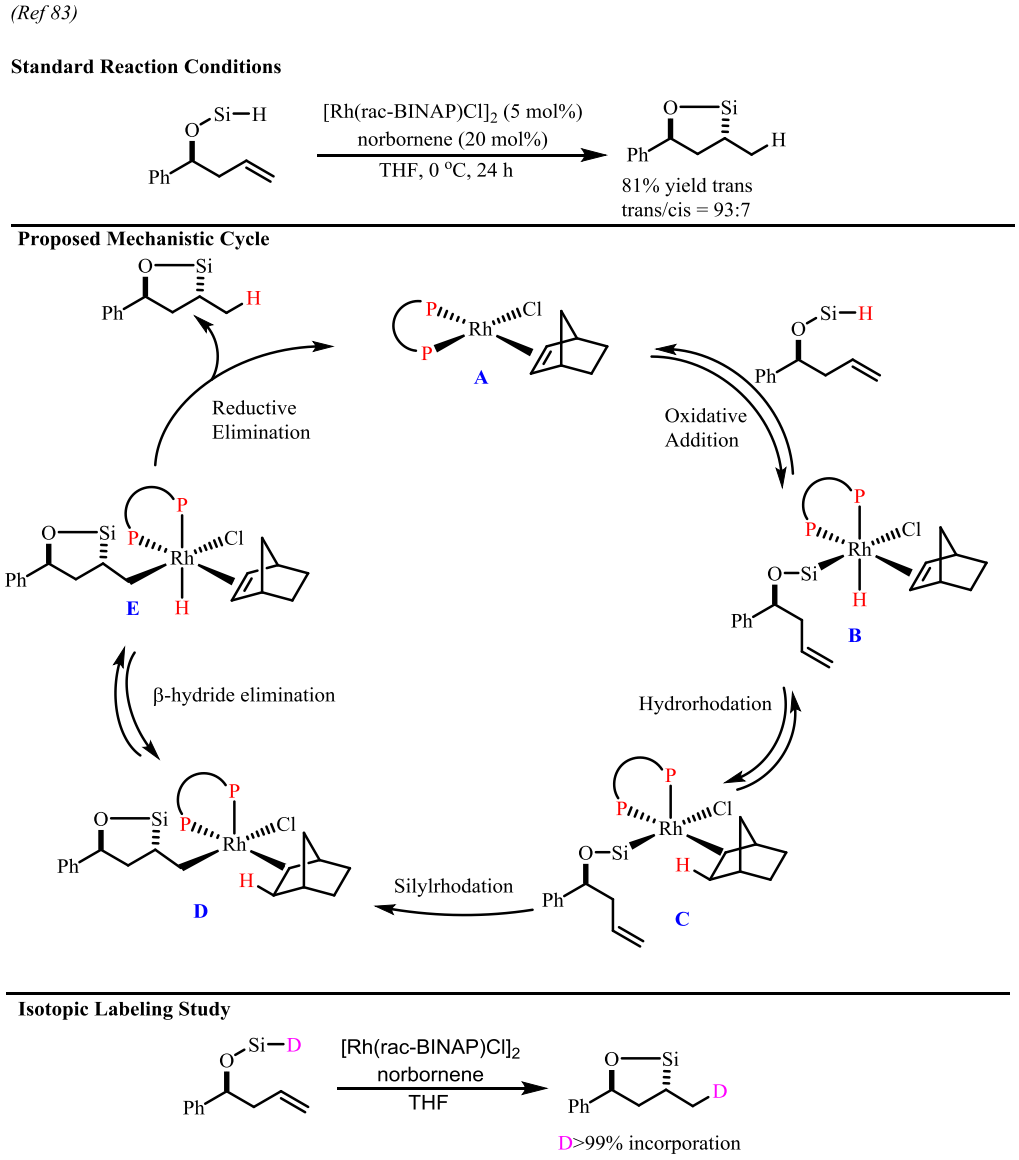

Figure 19 Norbornene-mediated rhodium-catalyzed intramolecular alkene hydrosilylation reactions

Is an active catalyst, not just the catalyst precursor and tmdBH, needed for ortho-borylation of ***2****?* C-H activation using rhodium catalysts may proceed through either a rhodium(I) intermediate, which oxidatively adds to the *ortho*-C-H bond, or a Rh(III) intermediate via transmetallation or some variant of sigma-bond metathesis.[57] While

reduced product **2** is not efficiently converted to *ortho*-borylated product **3** under the typical reaction conditions, it is possible the some rhodium intermediate along the reaction pathway can more efficiently effect the reaction. To explore whether generation of a Rh(III)-alkyl species in the presence of saturated oxime **2** could facilitate *ortho*-metallation, a fast-reacting sacrificial substrate was added. Norbornene was used in previous studies as a sacrificial substrate to consume a non-selective catalyst during the Rh-CAHB reaction.[84] Adding 0.3 equivalents of norbornene to the attempted reaction of **2** did not increase the yield of the *ortho*-hydroxylated product **3** (Figure 20).

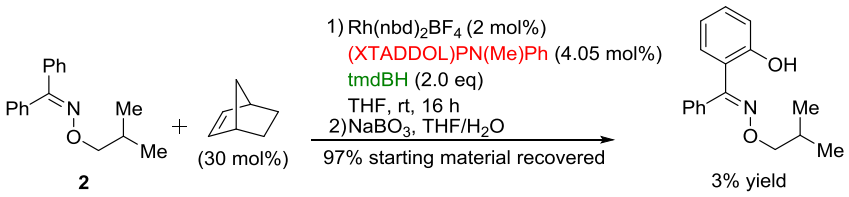

Figure 20 Formation of Rh(III) through sacrificial substrate does not increase yield of ortho-borylated material

Alternative weak directing groups do not promote ortho-borylation suggesting that an intermediate along the pathway in which the alkene reacts leads to the attendant ortho-metallation. If the alkene substituent is required to promote *ortho*-metallation/borylation, then one can consider two possible modes; either *ortho*-C-H insertion occurs from an intermediate formed during hydroboration of the alkene, or the alkene simply serves as a weak directing group to promote *ortho*-C-H insertion. To explore the latter possibility, the analogous ester and alkyne substrates were prepared (Figure 21). When treated under the standard catalytic conditions, no *ortho*-borylated products were obtained from these

substrates. This suggests an intermediate along the pathway in which the alkene reacts to form a Rh(III)-alkyl intermediate, leads to the attendant *ortho*-metallation.

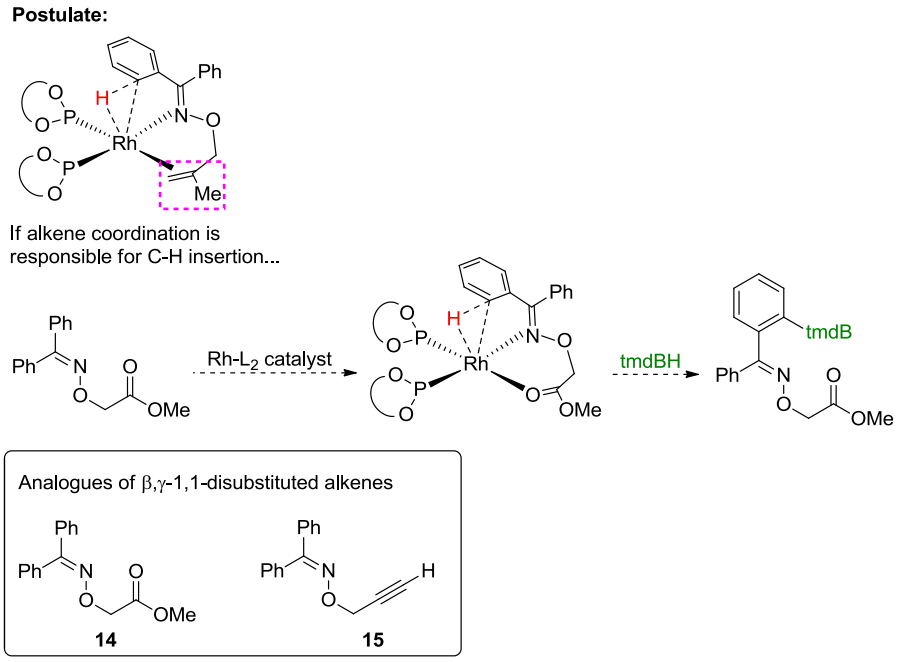

Figure 21 Determination whether alkene could act as directing group for agostic C-H interaction

The 1,1-γ,δ-unsaturated derivative was used to determine the effect of distancing the alkene by one carbon from the directing group. Evans, Fu, and Hoveyda saw a reduction in reaction rate as the amide-directing groups were extended farther from the alkenes.[85] We observed a similar decrease in reactivity with only 31% δ-OH product isolated after 16 hours (Figure 22). *Ortho*-borylated product was not observed under these reaction conditions, although a substantial quantity of reduced product was isolated.

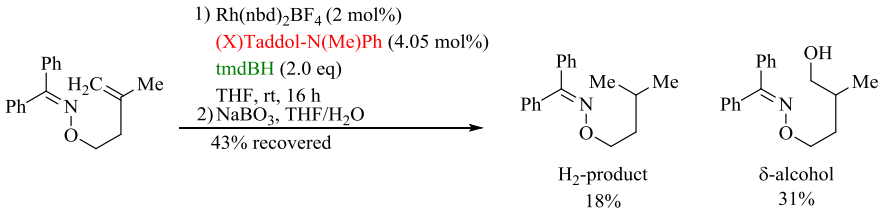

Figure 22 γ,δ-unsaturated oxime affords δ-alcohol in high regioselectivity with no *ortho*-borylation

3.13 The proximal aryl group is necessary for effective hydroboration.

The oxime ether derived from benzophenone was initially chosen for these investigations because it (1) provided a convenient chromophore for UV-Vis detection, and (2) it was thought that the sterically demanding aryl substituents might enhance the facial bias of the alkene pi-system. However, since *ortho*-borylation was a problem, it seemed reasonable to keep the chromophore, but move it away from the metal center (Figure 23). Two 2-phenylisobutyraldehye oxime derivatives were therefore prepared. It was expected that the phenyl substituent would be oriented away from the alkene to avoid unfavorable steric interactions, and the methyl groups would reside in a staggered confirmation relative to the nitrogen lone pair. Unfortunately, these substrates proved inactive to hydroboration under conditions previously optimized for the benzophenone derived oximes. Only starting material was recovered with no sign of reduction or hydroboration.

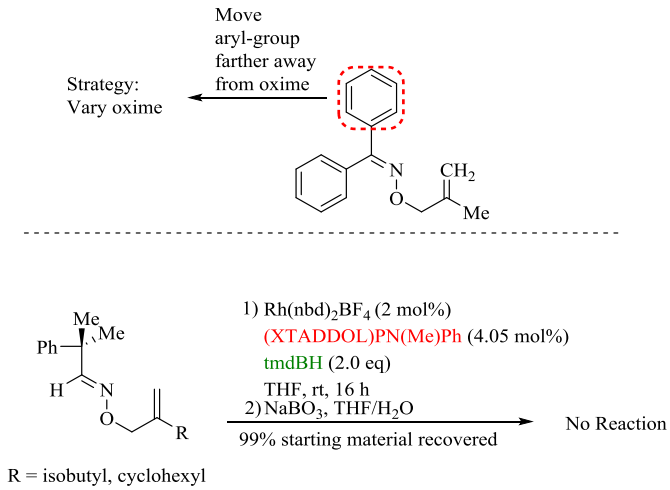

Figure 23 Moving the problematic phenyl group eliminates *ortho* C-H from borylation

3.14 Deuterium-labeling reveals near quantitative ortho-metallation during tmdBH-promoted rhodium-catalyzed reduction of 1 to 2 under a H_2 atmosphere.

At this point we decided to look at the reactions of deuterium-labeled substrate **1**, first focusing on reaction conditions that exclusively promote reduction of the alkene (i.e., reaction under a hydrogen atmosphere). The preparation of benzophenone-d^{10} was straightforward (Scheme 2). Bromobenzene-d^5 was converted to the aryl Grignard. Addition to 1,1'-carbonyldiimimidazole (CDI) affords benzophenone-d^{10} upon aqueous workup. Benzophenone-d^{10} was used to prepare the β,γ-unsaturated substrate **16**-d^{10} (the labeled version of **1**) and a saturated analogue **18**-d^{10} (a labeled version of **2**) for further mechanistic studies.

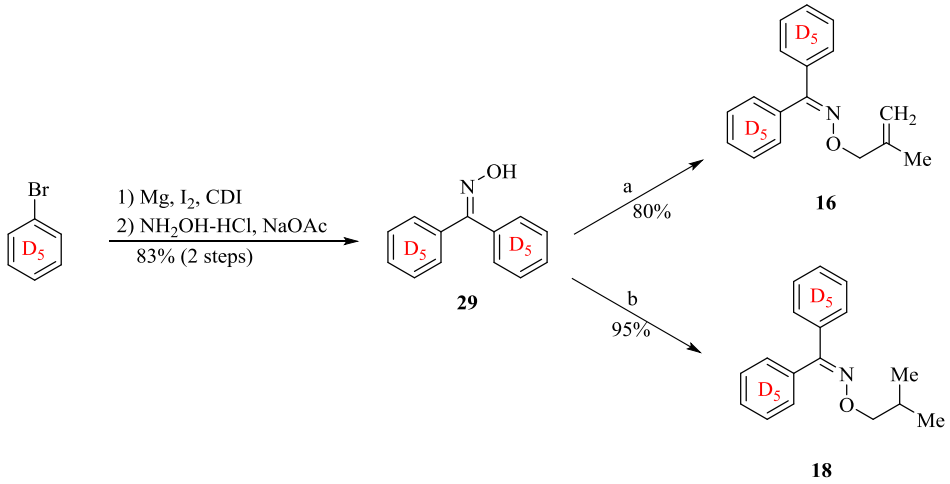

Scheme 2 Preparation of deuterated analogues for mechanistic studies. a) NaH, 3-Cl-2-Me-1-propene, TBAI; b) NaH, 1-Br-2-Me-propane, TBAI.

Unexpected deuterium scrambling is observed for the reaction run under a hydrogen atmosphere. β,γ-Unsaturated substrate **16**-d^{10} was subjected to the tmdBH-promoted hydrogenation conditions described above for substrate **1** (2 mol% $[(nbd)Rh((XTADDOL)PN(Me)Ph)_2]BF_4$, 0.4 equivalents tmdBH, 1 atm H_2) (Figure 24). The crude product was filtered through a short plug of silica gel to remove trace metals. ^{1}H NMR analysis showed a newly formed singlet at δ 7.52 ppm which was tentatively assigned the *ortho*-H shown in Figure 24. The two hydrogens α to the oxime, a doublet at δ 4.00 pm, were used as the internal standard to quantitate deuterium incorporation in the reduced product **17**. Based on this standard, one *ortho*-deuterium was exchanged for hydrogen to the extent of 83% in the **17**; *ortho*-metallation is occurring much more frequently than initially thought. Most of the deuterium liberated by H/D-exchange is transferred to the alkene. Approximately 57% is transferred from the phenyl ring to the γ-carbon of what was the alkene; a smaller amount of deuterium (approximately 12%) was

transferred to what was the β-carbon of the alkene. Only ca 14% of deuterium originally on the phenyl ring is missing, presumably lost as H-D under these reaction conditions.

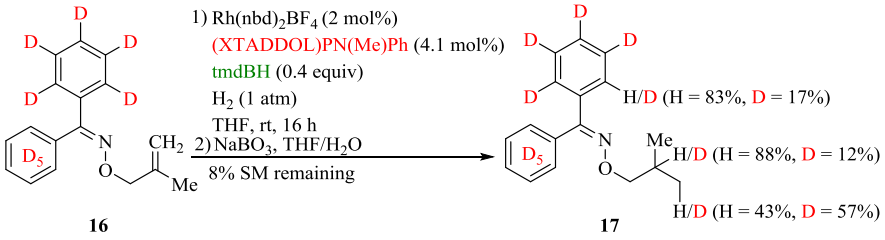

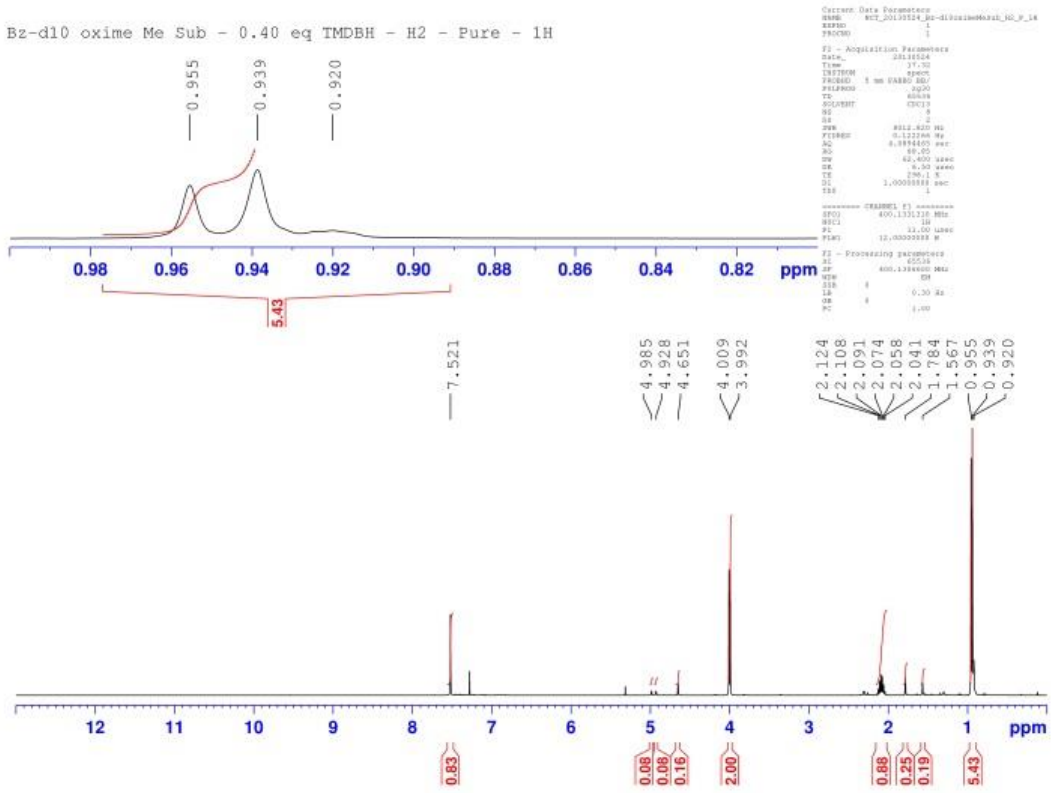

Figure 24 Rh-catalyzed hydrogenation of β,γ-Unsaturated substrate **16**-d^{10}

The reduced product is stable under the reaction conditions; labelled reduction product ***18***-d^{10} *does not undergo H/D-exchange.* The role of the alkene in the H/D-

exchange was explored next. In an atmosphere of with a large excess H_2, exchange of H/D should occur frequently for an *ortho*-metallated intermediate if oxidative addition were occurring without alkene participation (Figure 25). Saturated analogue **18**-d^{10} was added to a H_2 atmosphere, but no H/D exchange was observed. This result suggests for C-H (or C-D) activation to occur, a β,γ unsaturated alkene, borane, and an *ortho* C-H (or C-D) must be present.

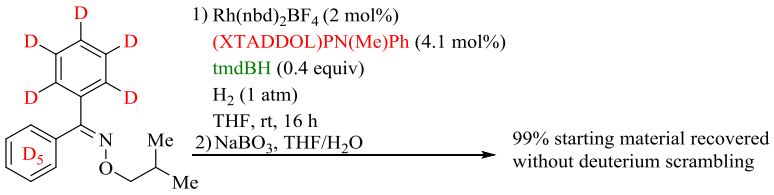

18

Figure 25 *Ortho*-metallation not observed with labeled saturated substrate under H_2 atmosphere

Chelation-assisted oxidative addition could explain the C-D/C-H exchange and deuterium scrambling in a pathway independent from hydroboration (Figure 25), but this proposed mechanism is not supported by experiment. Chelation-assisted C-H activation has frequently been proposed in unrelated C-H metallation chemistry using rhodium(I) catalysts [57,86,87] This could in principle explain the observed deuterium scrambling in **17** as follows. Two-point coordination of the substrate to Rh(I) species followed by oxidative addition of the *ortho* C-D would generate a Rh(III) intermediate. Migratory insertion of the coordinated alkene into the Rh-D bond delivers deuterium generating an Rh(III)-alkyl intermediate. β-Hydride elimination leaves deuterium on either the alkene or the methyl substituent scrambling deuterium in the starting **16**-d^{10}. Reductive

elimination generates an aryl C-H while regenerating the rhodium(I) catalyst.

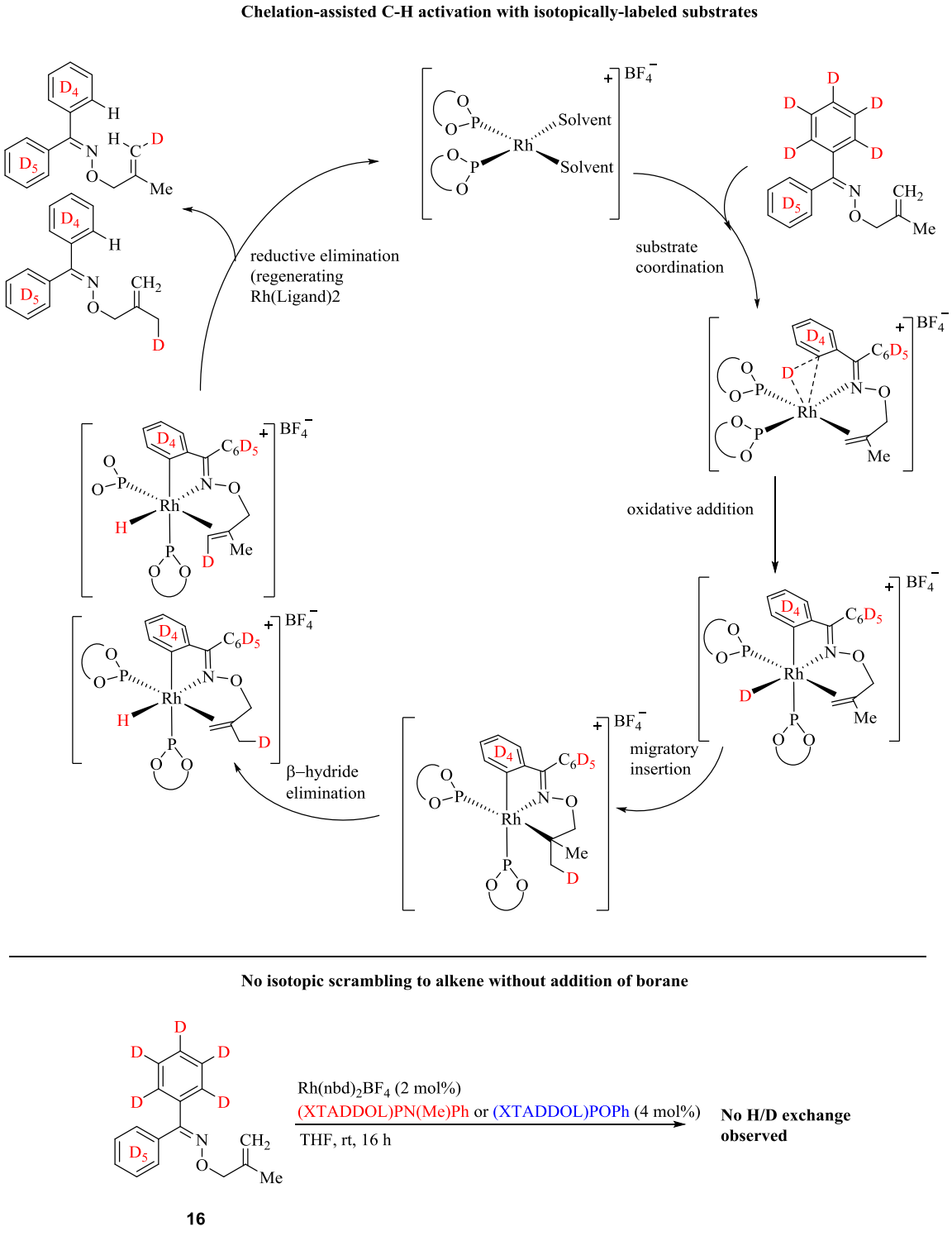

Figure 26 *Ortho*-metallation is not observed without the addition of borane.

Deuterium is not scrambled in the starting material, ***16****-d*^{10}. To test the possible mechanism shown in Figure 26, β,γ-unsaturated analogue **16**-*d*^{10} was treated in separate experiments with 2 mol% [(nbd)Rh((XTADDOL)PN(Me)Ph)$_2$]BF$_4$ and with 2 mol% [(nbd)Rh((XTADDOL)POPh)$_2$]BF$_4$; the mixtures were stirred under N_2 for 16 hours. No deuterium/hydrogen exchange was observed for **16**-*d*^{10}. Increasing the catalyst loading to 20 mol% showed no evidence for deuterium scrambling. In addition, a small amount (8%) of **16**-*d*^{10} was observed from the reaction mixture described in Figure 24. Analyzing its ^{1}H NMR spectrum showed no deuterium exchange or loss (NMR data: δ 4.98 (1H), 4.93 (1H), 4.65 (2H), 1.78(3H) ppm). From the experiments described above, we conclude that neither the starting material nor the reduced product undergo H/D-scrambling to account for **17**; furthermore, the mechanism for facile *ortho*-metallation H/D-exchange requires tmdBH and does not proceed independent of alkene reduction.

3.15 Even in the absence of added hydrogen, *ortho*-metallation is virtually quantitative during concomitant Rh-CAHB

The results obtained in the reaction of ***16****-d*^{10}. Having first focused on the reaction of β,γ-unsaturated substrate **16**-*d*^{10} under conditions that promote exclusive reduction of the alkene (i.e., reaction under a hydrogen atmosphere), we now return to reaction conditions that promote Rh-CAHB. **16**-*d*^{10} was reacted under an inert atmosphere as described above for substrate **1** (2 mol% [(nbd)Rh((XTADDOL)PN(Me)Ph)$_2$]BF$_4$ and 2 eq tmdBH). Ignoring the isotope distribution, the labeled and unlabeled substrates give

virtually identical product distributions (Figure 27). Surprisingly, we find evidence for *ortho*-metallation and H/D-exchange, not only for the reduced product as was found for reaction under a hydrogen atmosphere, but for all three products! The isotope distribution for the reduced product **19** differs in small, but perhaps important ways, from **17** described above. One *ortho*-deuterium is replaced by hydrogen virtually quantitatively, and the deuterium is cleanly incorporated into a methyl group in **19**. The *ortho*-borylated and alkene reduced product **20** similarly shows clean redistribution of one *ortho*-deuterium to a methyl group, but with incorporation of boron in the *ortho*-position. In this case, a second *ortho*-deuterium is partially exchanged for hydrogen. We will consider the distribution of the deuterium for the major product, the expected hydroboration product **21** later, but note here that one *ortho*-deuterium is replaced by hydrogen virtually quantitatively.

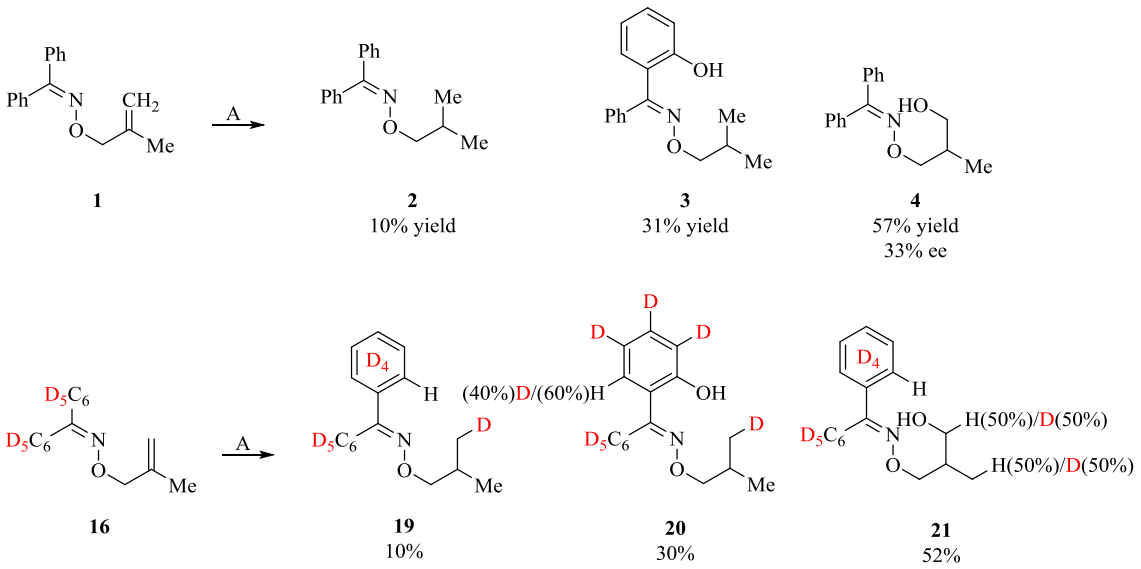

Figure 27 Hydroboration of β,γ-Unsaturated substrate 16-d^{10} reveals D-transfer A) Reaction conditions: 2 mol% $Rh(nbd)_2BF_4$, 4.1 mol% (XTADDOL)PN(Me)Ph, 2.0 equiv tmdBH, THF, rt, 16 h. Oxidative workup: $NaBO_3$, THF/H_2O

Proposed mechanisms to account for the redistribution of deuterium in ***16****-d*^{10} *are discussed below.* Deuterium exchange of the *ortho*-C-D/C-H must be associated with hydroboration of β,γ-unsaturated alkene. We propose the pathways diverge as the stage where X_2B-H undergoes oxidative addition to the rhodium-substrate complex (Figure 28, steps A and A'). Step A ultimately leads to formation of *ortho*-borylated product, while the diastereomeric pathway through the step labeled A' leads to γ-borylated product; this is based on the proximity of the pi-system to the Rh-H bond. In pathway A, migratory insertion of hydride to the β-position leads to an intermediate with rhodium bound to the γ-carbon. In pathway A', migratory insertion forms a β-Rh intermediate. Two pathways can help explain the deuterium incorporation on the γ-borylated products as will be discussed in further detail below.

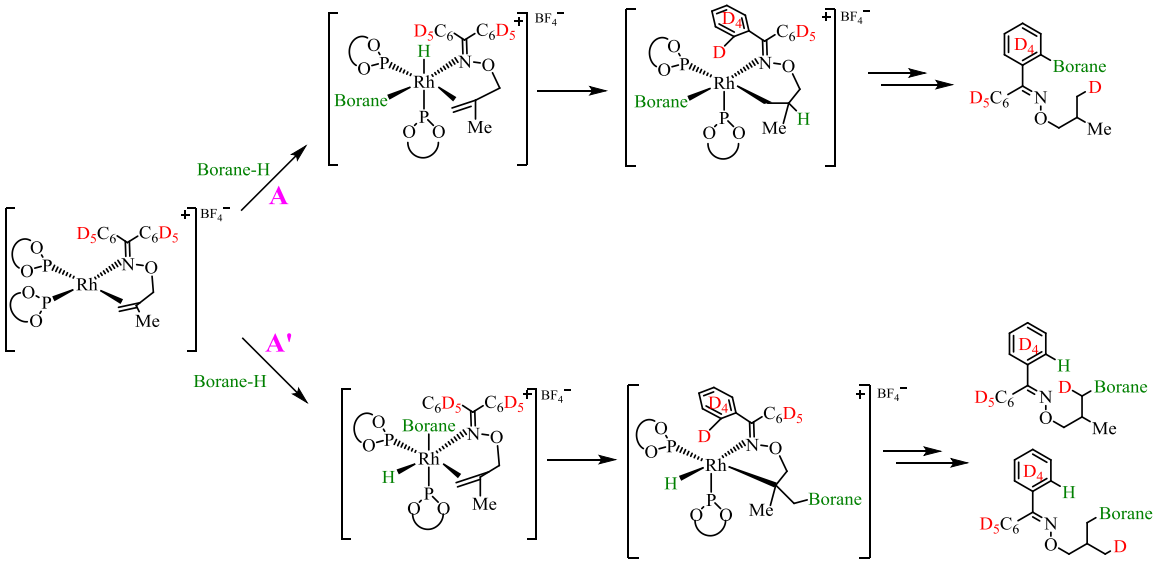

Figure 28 Proposed mechanism for formation of *ortho*-borylated **3** and γ-borylated **4** accounting for deuterium scrambling to substituent

*Formation of ortho-borylated product **3**.* The details for a proposed mechanism to rationalize the formation of *ortho*-borylated product **3** is shown below (Figure 29). Coordination of substrate is followed by oxidative addition of tmdBH (Figure 29, steps A and B). After migratory insertion, the rhodium bound to the γ-carbon may be situated such that it has an agostic interaction with the *ortho* C-D predisposing it towards σ-bond metathesis (Figure 29, steps C and D).[88] σ-bond metathesis substitutes the boron for deuterium on the *ortho*-carbon; reductive elimination can then account for deuterium incorporation on the γ-carbon (Figure 29, step E).

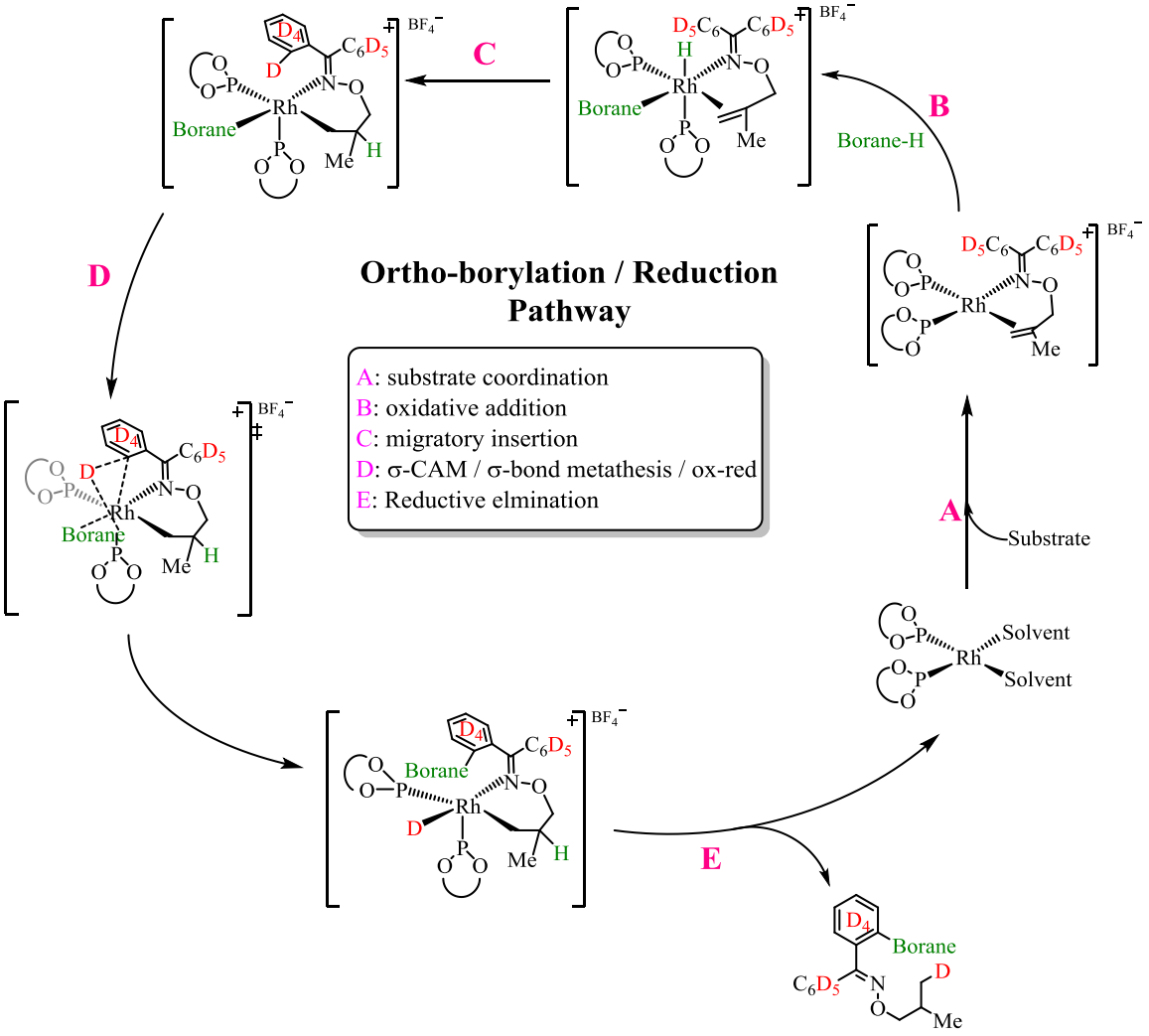

Figure 29 Proposed mechanism for borylated/reduced products

The proposed mechanism seems to account for several of the unusual observations made for this reaction. It accounts for the reduction of the alkene as well as the *ortho*-borylation and the fact that experimentally, no *ortho*-borylated product with the alkene intact has been found. It suggests that the mild C-H activation may be due to the unique electronics of the rhodium-alkyl intermediate, an intermediate that is unlike those in the vast majority rhodium-catalyzed C-H activation reactions. The need for a rhodium-alkyl

intermediate might explain the ineffectiveness of alternative directing groups. It may also account for why the nature of the borane is critical; recall, catBH does not promote *ortho*-metallation. Similarly, why substrates in which the aryl C-H is more distal or the alkene is more remote might not favor a structure having a strong agostic interaction with the *ortho* C-D predisposing it toward σ-bond metathesis.

Precedence for increased reactivity from an ortho-metallated hydrogenation catalyst species has recently been described. Pfaltz and co-workers demonstrated an *ortho*-metallated iridium catalyst was efficient in the asymmetric hydrogenation of aliphatic imines (Figure 30).[88] Iridium P,N-ligated catalyst **Pfaltz-L1** rapidly converted to the metallocycle **Pfaltz-L2** at 0 °C in the presence of phenyl methyl ketimine under a H_2 atmosphere (1 bar). The *ortho*-metallocycle was observed by NMR; attempts to isolate failed due to decomposition. Generally, alkyl ketimines suffer from low reactivity to hydrogenation relative to aryl ketimines; Pfaltz speculated the poor reactivity from aliphatic ketimines could be due to inability to form catalytically active *ortho*-metallocycle complexes. Ir-catalyzed asymmetric hydrogenation of cyclohexyl methyl ketimine with **Pfaltz-L2** did indeed give higher reactivity than the parent catalyst **Pfaltz-L1**.

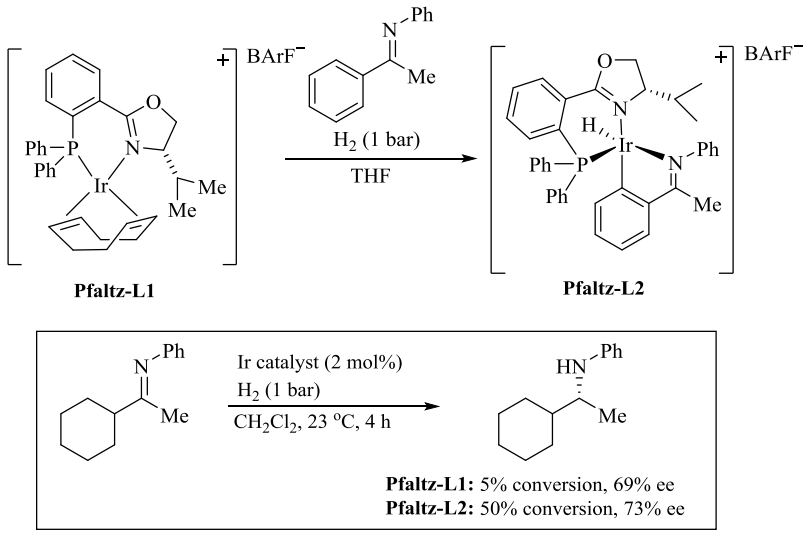

Figure 30 Pfaltz's discovery of an *ortho*-iridacycle with improved catalyst efficiency in the iridium-catalyzed asymmetric hydrogenation of dialkyl ketimines.

The Rh-BX_2/C-D σ-bond metathesis is a particularly interesting aspect of the proposed mechanism. Whether rhodium is formally oxidized to the Rh(V) oxidation state or whether the Rh(III) intermediate reacts through a σ-bond metathesis has been the subject of recent debate.[89,90] For example, hydride exchange in the rhodium-catalyzed hydrosilyation reaction has been studied by Vyboishchikov and Nikonov.[91] Rh(V)-silyl hydride complexes were isolated and characterized.[92-97] DFT calculations on a series of silyl hydride complexes formally assigned as Rh(V) complexes were found to have varying degrees of interligand Si-H interactions (Figure 31). This finding led the authors to eliminate a classical oxidative addition as the mechanism; instead the interaction was considered "sophisticated" and "multicentral."

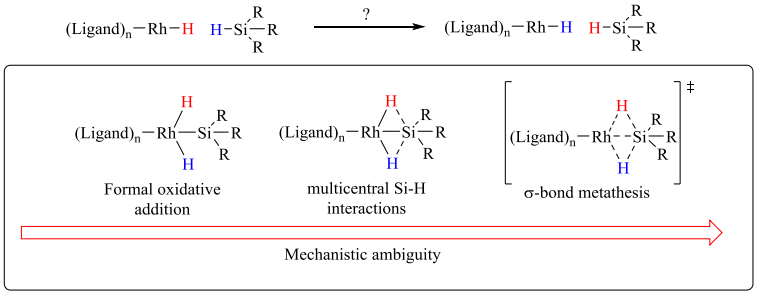

Figure 31 Four-centered intermediates may be a better description than discrete Rh(V) complexes in Rh-H/Si-H exchange reactions

Recently, an alternative to traditional σ-bond metathesis, σ-complex assisted metathesis (σ-CAM), has been suggested.[89] While σ-bond metathesis occurs in a single concerted step, σ-CAM is said to proceeds through multiple rearrangements of σ-ligands leading to bond metathesis. Hall and Hartwig proposed catalytic cycles supported by DFT calculations that involve σ-CAM for the borylation of alkanes; this was supported by experimental observation of key intermediates associated with multiple ligand exchanges (Figure 32A).[98] Adapting this to the oxime-directed hydroboration would involve formation of a tmdB-D intermediate that subsequently reacts to form the *ortho*-borylated β-Rh species (Figure 32B).

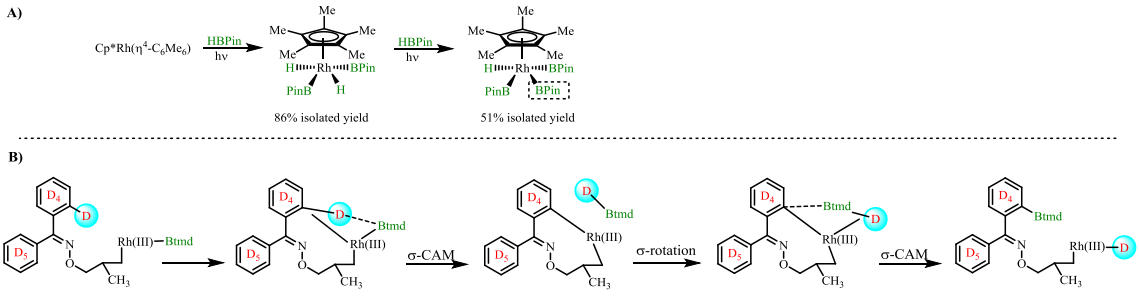

Figure 32 σ-CAM mechanism for *ortho*-borylation and deuterium exchange. A) Hartwig observed formation of tris-borated Rh complexes likely formed from σ-CAM. B) Proposed mechanism for σ-CAM in oxime-directed CAHB.

*Returning to the redistribution of deuterium for the major product in the expected hydroboration product **21***. γ-alcohol **21** also showed quantitative replacement of deuterium at the *ortho*-position of the aromatic ring by hydrogen and complete transfer of deuterium to the propenyl moiety. Curiously, the deuterium incorporation added to two positions on what was the propenyl moiety in a 50:50 ratio. This seems indicative of a pseudo symmetric intermediate or an isomerization reaction. The latter seems more reasonable and a proposed mechanism accounting for the observed redistribution of deuterium is described below (Figure 33).

*Formation of ortho-borylated product **21***. The proposed mechanism for the formation of **21** is more difficult to formulate than that accounting for the formation of **3**. As suggested in the previous mechanism, the catalytic cycle is initiated by oxidative addition of tmdBH to the rhodium-complexed substrate (Figure 33, steps A and B). This cycle differs from that described in Figure 29 in that we propose migratory insertion of the alkene into the Rh-BX_2 bond affording a β-rhodium(III)-alkyl intermediate. We need to once again, suppose a strong agostic interaction, in this case involving the *ortho*-C-D and Rh(III)-D bond (Figure 33, steps C and D). After σ-bond metathesis (or σ-CAM), competing β-hydride elimination is apparently preferred over reductive elimination. This gives either the β,γ-unsaturated vinyl boronate or alkene and a rhodium dihydride (i.e., H-Rh-D). Stepwise readdition of H and D to the two isomeric alkenes could afford the observed products with deuterium placed appropriately.

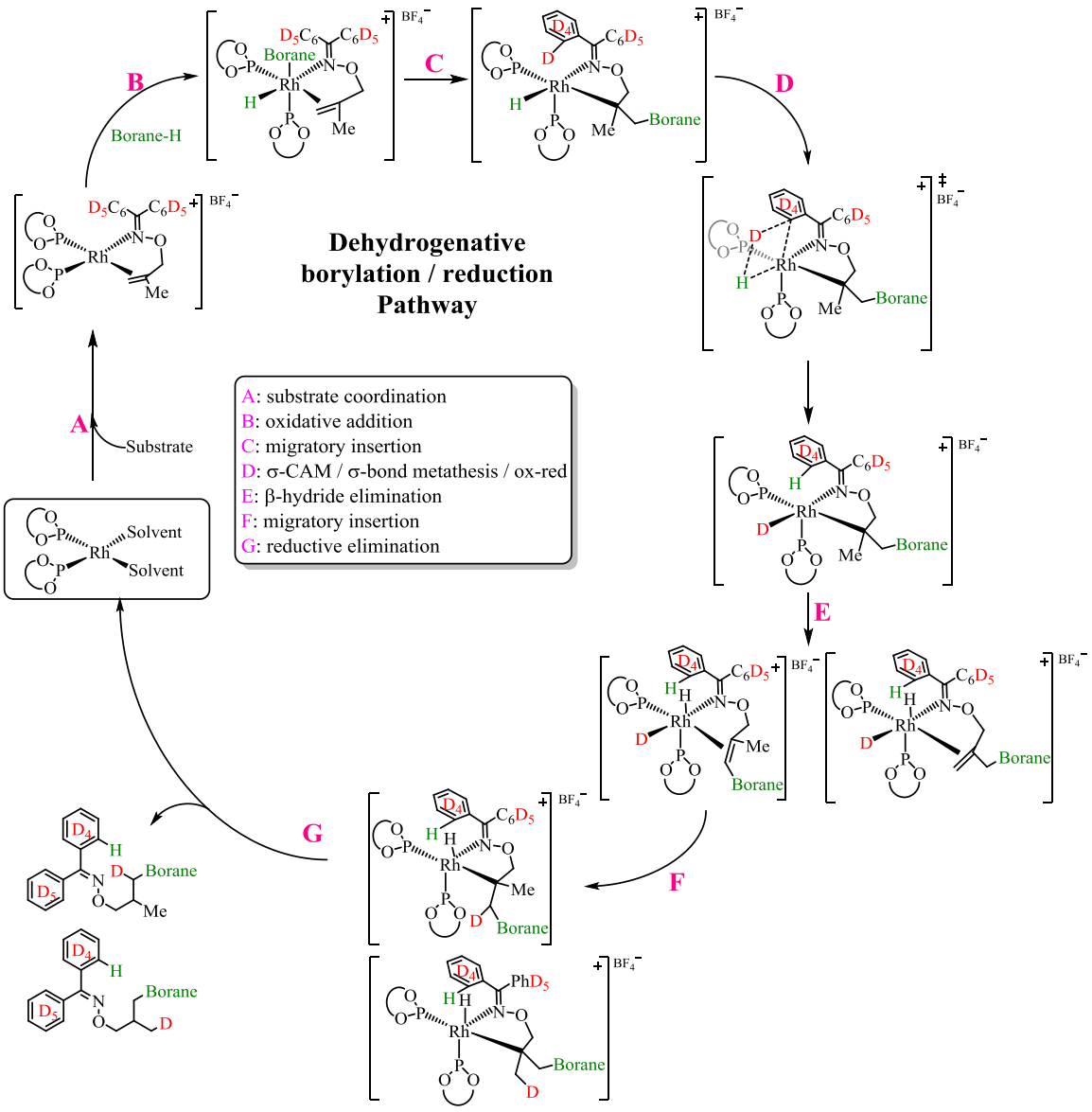

Figure 33 Proposed mechanism for deuterium transfer to both gamma carbons in formation of gamma alcohols

Dehydrogenative borylations. Figure 33 suggests that the γ-borylated products do not come from the envisaged mechanism for two-point binding hydroboration, but instead via a dehydrogenative borylation/reduction; the latter pathway has precedence in the literature. Dehydrogenative borylation has been reported for directed and non-directed

systems.[40-43] For example, Westcott and co-workers found the hydroboration of enamides proceeds through a dehydrogenative borylation followed by hydrogenation (Figure 34).[43] The vinyl boronate (the product from dehydrogenative borylation) was isolated in 15% yield along with the net hydroboration product (i.e., 70% of the reduced boronate ester). To distinguish between a classical hydroboration mechanism and the two-step dehydrogenative borylation/hydrogenation mechanism, a trisubstituted enamine resistant to hydrogenation was used; hydroboration of 1-pyrrolidino-1-cyclopentene gave 80% conversion to the vinyl boronate (observed by NMR).

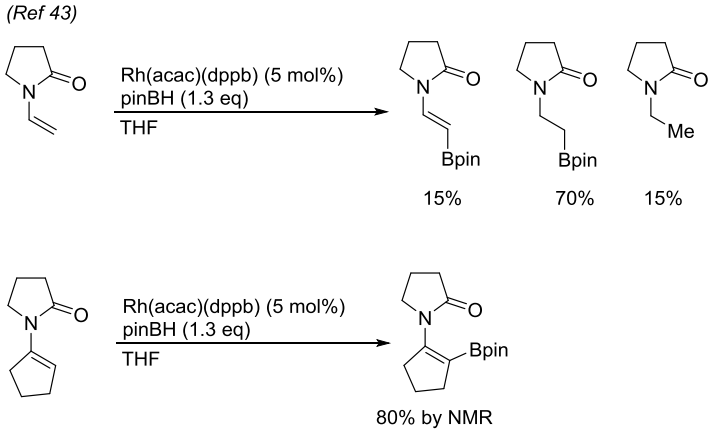

Figure 34 Dehydrogenative borylation and subsequent reduction reported by Westcott and co-workers

The dehydrogenative borylation/hydrogenation mechanism is admittedly not a perfect fit for the oxime-directed Rh-CAHB. We have not found the signature vinyl boronate (or the corresponding aldehyde upon oxidation) in crude reaction mixtures. ^{11}B NMR analysis of the crude product mixtures before oxidative workup show peaks corresponding to trace amounts of unreacted tmdBH, the *ortho*- and *gamma*-borylated products, and borane degradation products (tris-tmdB);[39] there are no peaks

corresponding to what one would expect for a vinyl boronate. Finally, there isn't a compelling explanation at this stage for the facile reduction of the presumed vinyl boranate with hydrogen.

The nature of the borane had a significant impact on the propensity to ortho-metallate. Treating β,γ-unsaturated substrate **16**-d^{10} with 2 mol% [(nbd)Rh((XTADDOL)PN(Me)Ph)$_2$]BF_4 and 2 equivalents catBH (in place of tmdBH) gives γ-alcohol **22** in low yield (20%), but no H/D exchange is not observed in **22** or the recovered starting material (Figure 35). This suggests either a very different mechanism (perhaps the standard two-point binding CAHB mechanism) as a consequence of a lowered tendency for σ-bond metathesis as a function of borane. To explore whether lack of *ortho*-H/D exchange is due to the non-catalyzed hydroboration by catBH, attempted hydroboration using only catBH resulted in 1-2% γ-alcohol

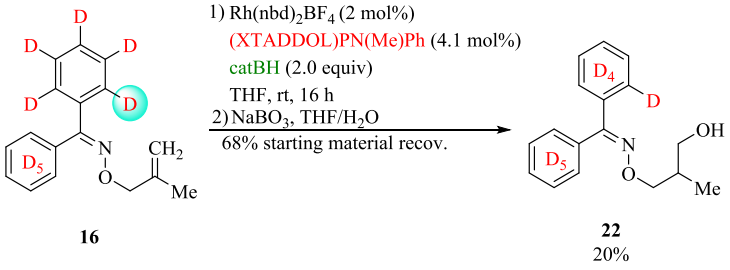

Figure 17 Catecholborane produces products with no H/D exchange

To summarize, tmdBH and catBH both form the γ-alcohol in comparable yields but labeling studies suggest different mechanisms account for unlabeled product formation (58% and 63%). From the deuterium distribution, tmdBH may form the product through a dehydrogenative borylation followed by H_2 (or HD) reduction; catBH affords the

product through the expected oxidative addition / reductive elimination pathway (Figure 36).

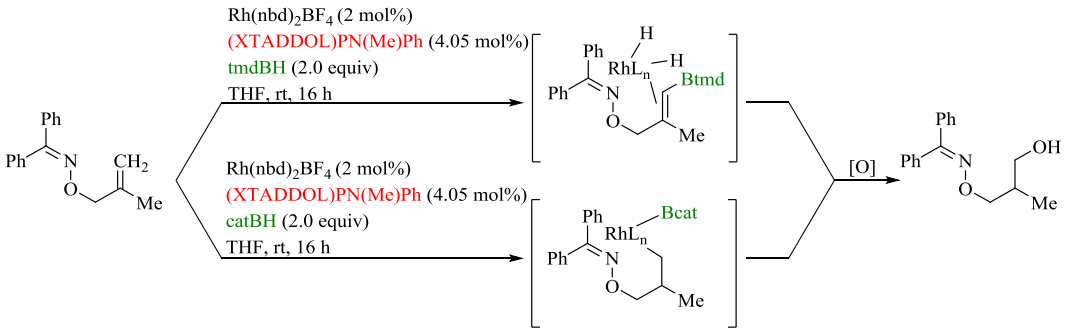

Figure 18 The nature of the borane determines how the γ-borylated products are formed.

3.16 Competition and double labeling experiments indicate little or no crossover

The deuterium transfer observed in **21** seems to suggest that the deuterium is transferred intramolecularly, although it must be noted that there is a net loss of deuterium in **20**, so there must be intermolecular pathways as well. To further probe the question of whether deuterium is mostly transferred inter- or intramolecularly, a series of competition and double labeling experiments were carried out. First, β,γ-unsaturated substrate **6** and saturated analogue **2** were combined under the standard Rh-CAHB conditions with tmdBH (Figure 37). It was possible to isolate most of the reactions products via flash chromatography, but unfortunately, the oxidized isobutyl derivative and the reduced starting material **2** proved inseparable. However, ^{1}H NMR analysis of the inseparable mixture indicates that saturated substrate **2** remains unchanged. We therefore conclude that presence of the saturated substrate does not affect the yield of γ-alcohol formation (52%).

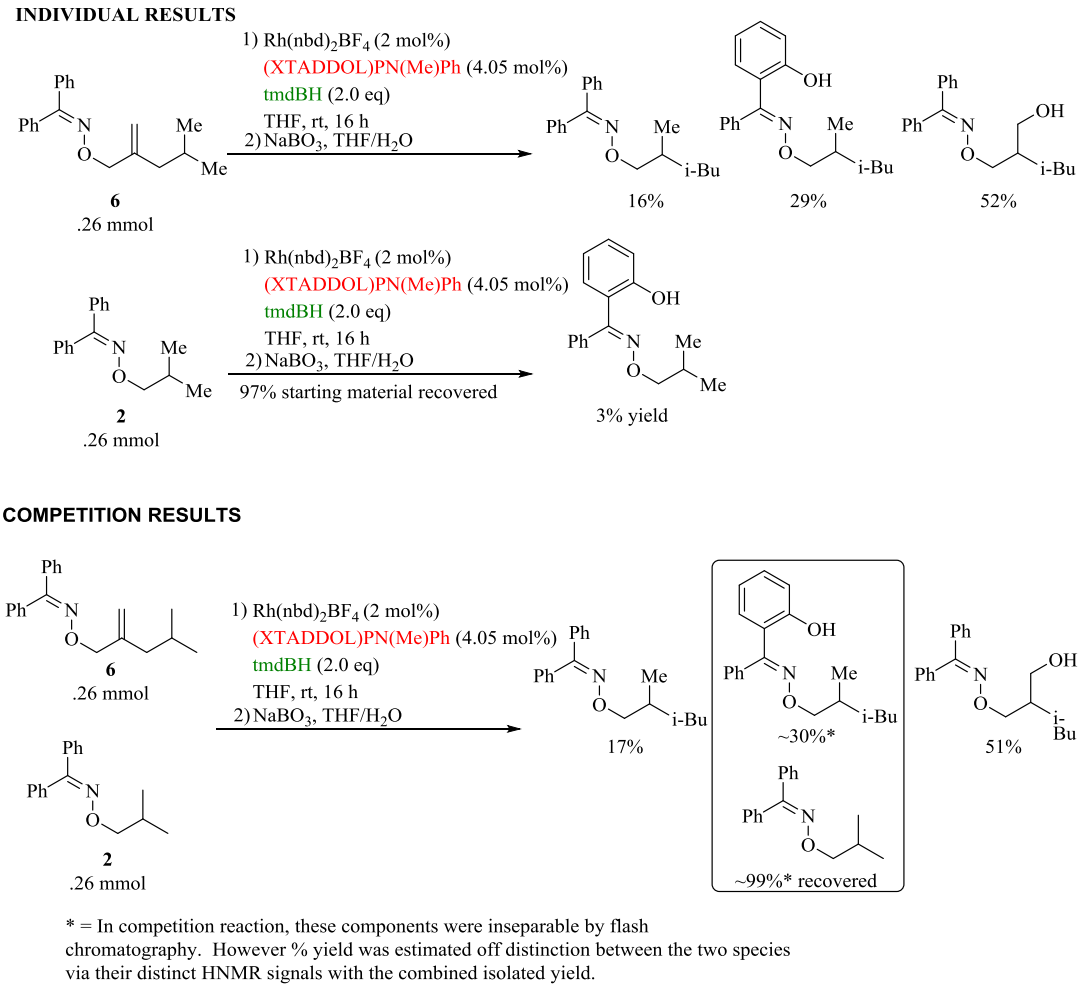

Figure 19 Competition reaction between a saturated and unsaturated substrate produces no crossover in hydroboration products

The next series of experiments are double labeling experiments looking for deuterium crossover from isotopically labeled to unlabeled substrates; this would confirm whether the *ortho*-metallation liberated some undetermined, as of yet, deuterated intermediate. Chromatographic conditions were found to separate the hydroboration products derived from **1** (vinyl methyl substitutent) and **10** (cyclohexyl substituent). For comparison purposes, β,γ-unsaturated substrates **16**-d^{10} and **10** were individually reacted under the

standard standard Rh-CAHB conditions with 2 mol% $[(nbd)Rh((XTADDOL)PN(Me)Ph)_2]BF_4$ and 2 equivalents tmdBH; each giving a mixture of reduced product, *ortho*-borylated and reduced product, and the expected γ-alcohol hydroboration product (Figure 38). A 1:1 mixture of **16**-d^{10} and **10** were similarly reacted and the products separated after oxidation. While some differences can be noted, the mixture of substrates gave results that were overall quite similar to the individual experiments. First and foremost, the yields of γ-alcohol (i.e., **21** and **13**) were unchanged in the competition reaction compared to the individual reactions, and most importantly, no deuterium crossover was found between labeled and unlabeled substrates. The ortho-borylated/reducted products **12** and **20** were also essentially unchanged in yield, the distribution of deuterium was unchaged in **20**, and **12** did not pick up any deuterium via crossover. The reduced products **19** and **11** behaved quite differently. The isotopically labeled **19** was obtained in somewhat lower yield under the completion conditions (i.e., 3% versus 10%), although given the complex mixture obtain, it is not clear how significant that difference is; its deuterium distribution is, however, unchanged. Reduced product **11** (7% yield compared to 28% performed in the individual reaction) surprisingly incorporates one deuterium via aryl H/D-exchange. In addition, recovered **10** (7%) is now doubly deuterated on the alkene; note that the latter could not be separated from the starting material so its assignment is tentative but might be taken as evidence of the previously described dehydrogenative borylation/reduction pathway. The source of the deuterium which transfers to the unlabeled material is likely from *ortho*-borylated product **20** since, as in its individual experiment, a total of 1.6 deuterium atoms

undergo H/D-exchange, of which 1 is transferred intramolecularly. It seems remarkable, but totaling the deuterated crossover products accounts for essentially all of the 0.6 deuterium atoms lost in forming **20**.

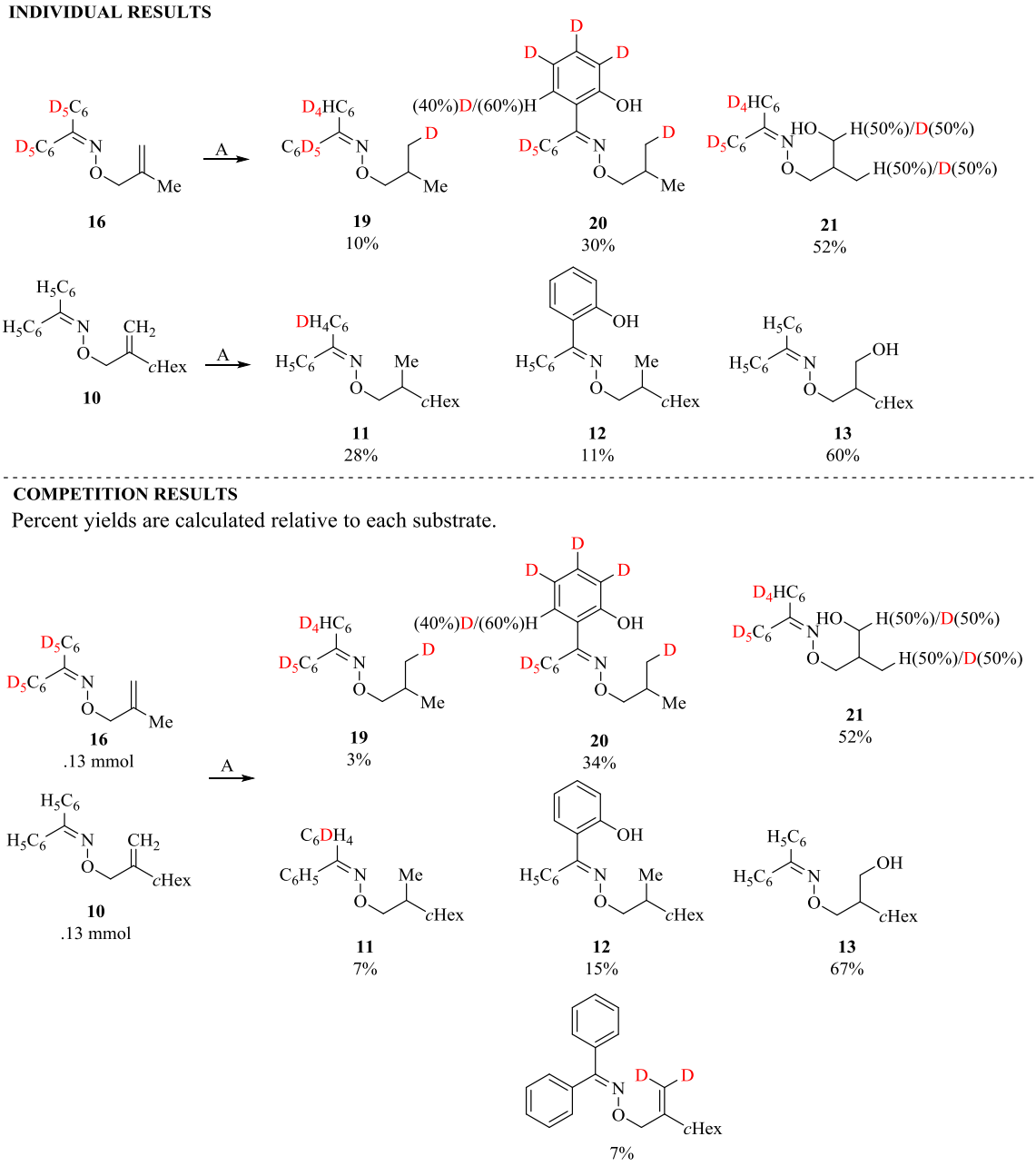

Figure 20 Competition experiment with labeled and unlabeled substrates reveal no crossover in gamma-alcohol formation - only reduced. Reaction conditions **A**: 2 mol% $Rh(nbd)_2BF_4$, 4.1 mol% (XTADDOL)PN(Me)Ph, 2.0 equiv tmdBH, THF, rt, 16 h. Oxidative workup: $NaBO_3$, THF/H_2O

One possible explanation for presence of deuterium on the alkene in recovered **10** is a decreased rate of hydrogenation; recall no recovered starting material had shown the wash in of deuterium into substrate **1**. Experimentally, this indeed seems to be the case. Attempted rhodium-catalyzed hydrogenation of **10** using the standard reaction conditions with 0.4 equivalents tmdBH and a hydrogen atmosphere, **10** affords only 54% of the reduced product **11**; in contrast, **1** gives the reduced product quantitatively under these conditions (Figure 39).

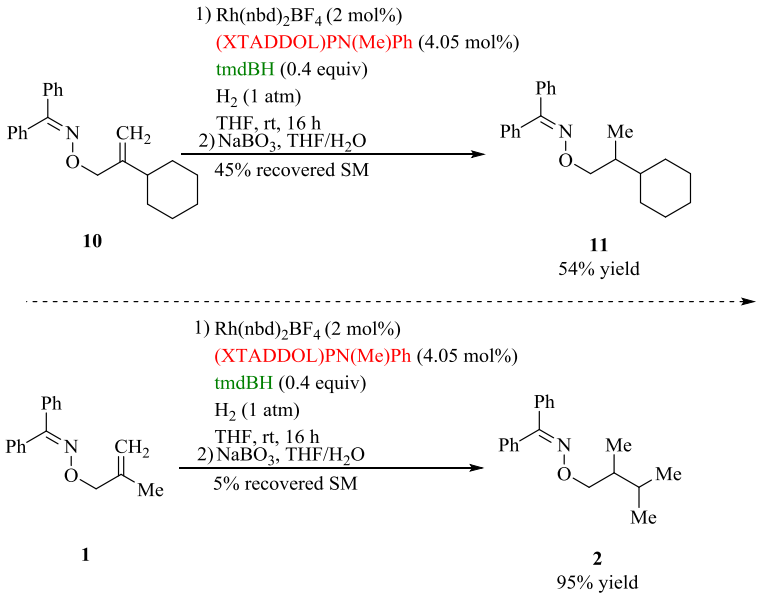

Figure 21 Hydrogenation with cyclohexyl substituent has reduced reactivity compared to methyl substituent

Due to the slow reduction of **10**, we wondered whether a labeled oxime derivative with a cyclohexyl alkene substituent would also show exchange of the vinyl hydrogens. β,γ-Unsaturated substrate **23**-d^{10} was synthesized and treated under Rh/tmdBH/H_2-hydrogenation conditions using 2% [(nbd)Rh((XTADDOL)PN(Me)Ph)$_2$]BF_4, 0.4

equivalents tmdBH under a H_2 atmosphere (Figure 40). The reduced product was isolated with 82% *ortho*-D substitution; this is comparable to the 83% ortho-D exchange from β,γ-unsaturated substrate **10**-d^{10} under identical reaction conditions in a H_2 atmosphere (Figure 24). The ^{1}H NMR spectrum is shown below with deuterium incorporation at the γ-methyl (δ 0.87 ppm) (Figure 40).

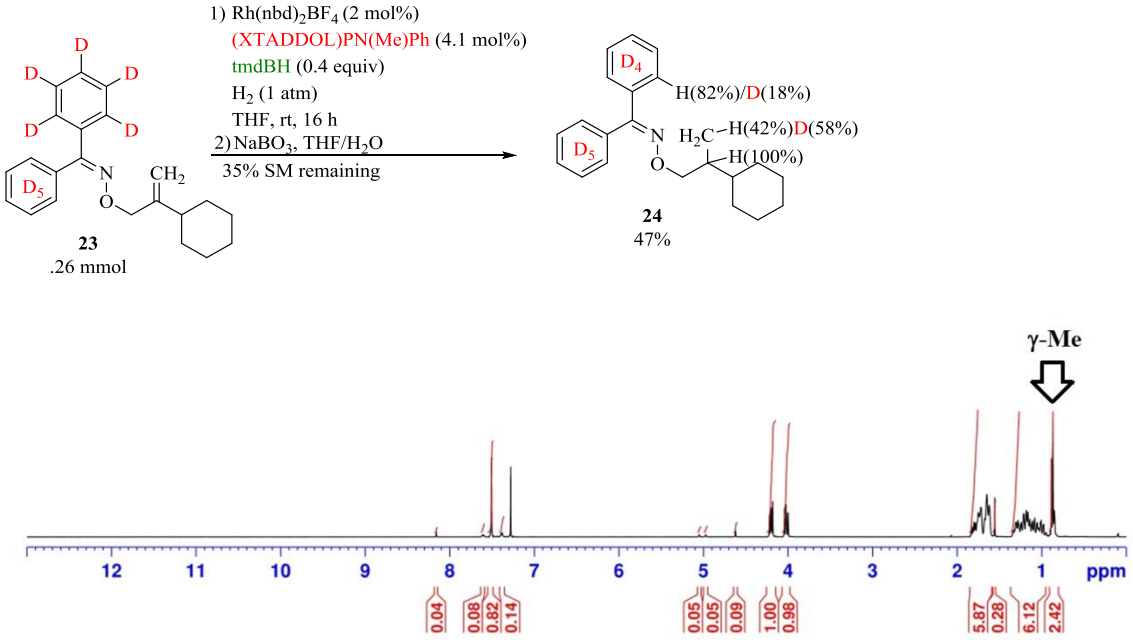

Figure 40 Hydrogenation β,γ-unsaturated substrate **23**-d^{10} incorporates deuterium into the products. H NMR of portion of isolated reduced product

Rh-CAHB of β,γ-unsaturated substrate **23**-d^{10} affords a product distribution not too dissimilar from its unlabeled isomer **10** (Figure 41) and all reaction products show quantitative ortho-H/D exchange. There are some subtle differences in the redistribution of that deuterium. The reduced products incorporated one deuterium on the γ-methyl as before, but the γ-alcohol **25** incorporates only 50% deuterium on the methyl substituent and no deuterium is incorporated on the β-carbon or the cyclohexyl ring; this differs from

16-d^{10} for which there was complete deuterium transfer to two positions in the product. Whether this has significance to the mechanism is not clear

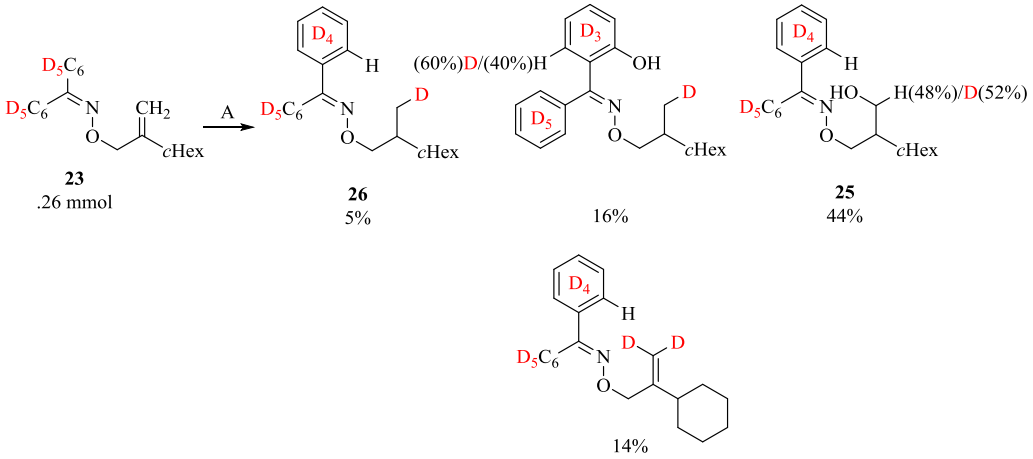

Figure 41 Hydroboration of d^{10}-labeled benzophenone oxime with cyclohexyl substituent gives deuterium incorporation onto the product

3.17 Synthesis of deuterium-labeled boranes and the unusual loss of label in the oxime-directed Rh-CAHB.

Deuterated boranes are commonly used for exploring the mechanism of the hydroboration reaction, and we sought to carry out studies with tmdBD to compare to those described above; however, this proved to be problematic. While there are several reports of the preparation of deuterated borane reagents, many authors using such reagents do not isotopic purity of the borane used. The most common methods for preparing deuterated boranes is via the reaction of BD_3-THF or $PhN(Et)_2$-BD_3[99,100] with the diol backbone of choice. In our hands reacting with the 2-methyl-2,4-pentadiol, we find up to 20% tmdBH contaminates the tmdBD after distillation. Since BD_3 is prepared

from 99% D-incorporated $NaBD_4$, we attribute the source of hydrogen to exchange from the diol.

To address this problem, two routes were recently reported to facilitate H/D exchange using iridium catalysts and D_2 (Figure 42). Hartwig and co-workers reported an iridium catalyst reported to reduce dipinacolborane (B_2pin_2) to pinBD in 80% yield.[101] Alternatively, Nolan and co-workers reported low catalyst loadings (0.1 mol% Ir catalyst) for the deuteration of boranes under relatively mild conditions 10 atm D_2.[102] Nolan's approach was reported for a series of boranes structurally similar to those used in our research, so this approach was attempted first.

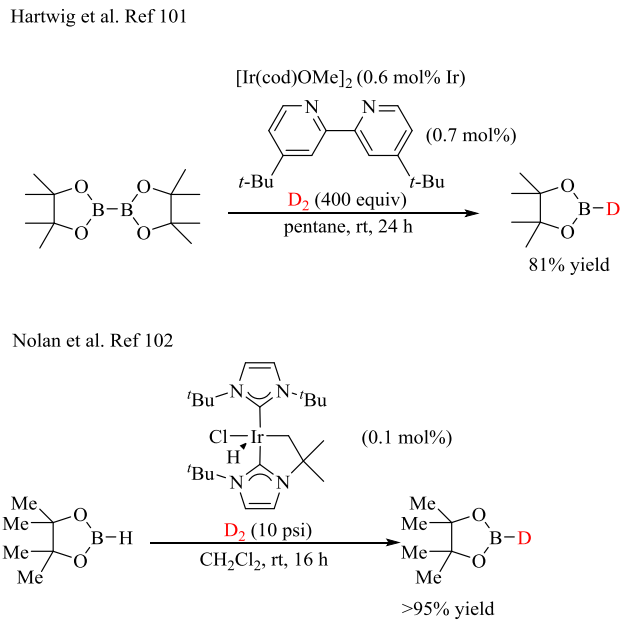

Figure 42 Preparation of tmdB-D with a high degree of isotopic purity

Nolan's iridium-NHC catalyst was prepared as described in Figure 43.[103] The catalyst is labile, so only small quantities of catalyst (<100 mg) were prepared used fresh. Repeating Nolan's deuteration conditions (0.1 mol% catalyst loading with 10 psi D_2)

afforded tmdBD with approximately 86% deuterium incorporation as determined by ^{1}H NMR analysis. Fortunately, increasing the catalyst loading to 0.3 mol% and the D_2 pressure to 30 psi improved the H/D-exchange; isotopic incorporation of greater than 90% D was achieved as estimated from ^{1}H NMR and ^{11}B NMR (Figure 43).

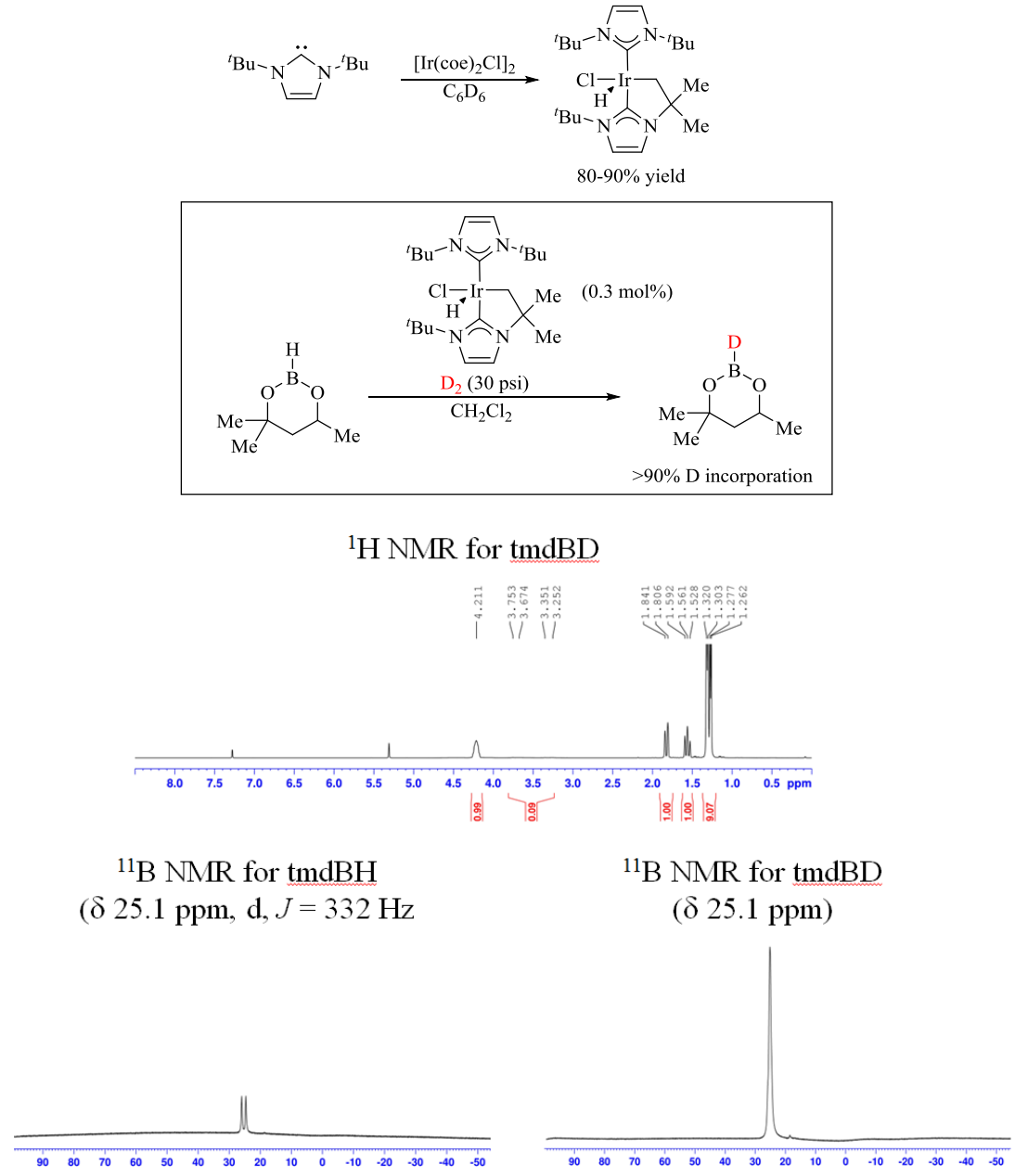

Figure 43 Ir-NHC catalyst affords deuterated tmdBD

The reaction of β,γ-unsaturated substrate **1** with 2 equivalents of freshly prepared tmdBD under the standard reaction conditions (2 mol% $[(nbd)Rh((XTADDOL)PN(Me)Ph)_2]BF_4$ catalyst in THF) gave quite unexpected results (Figure 44). While the yields of the now expected reduced, *ortho*-hydroxylated and reduced, and γ-alcohol hydroboration products were comparable to those obtained with tmdBH, there is little to no deuterium incorporation on the β or γ-substituents. Only the *ortho*-hydroxylated and reduced product has a low percentage (ca. 35%) of deuterium incorporation at the β-position of the reduced material. In contrast, neither the reduced product nor the γ-alcohol had deuterium incorporated at the β or γ-positions. Furthermore, aryl H/D-exchange was also low; only about 50% deuterium incorporation was observed for the reduced and hydroboration products.

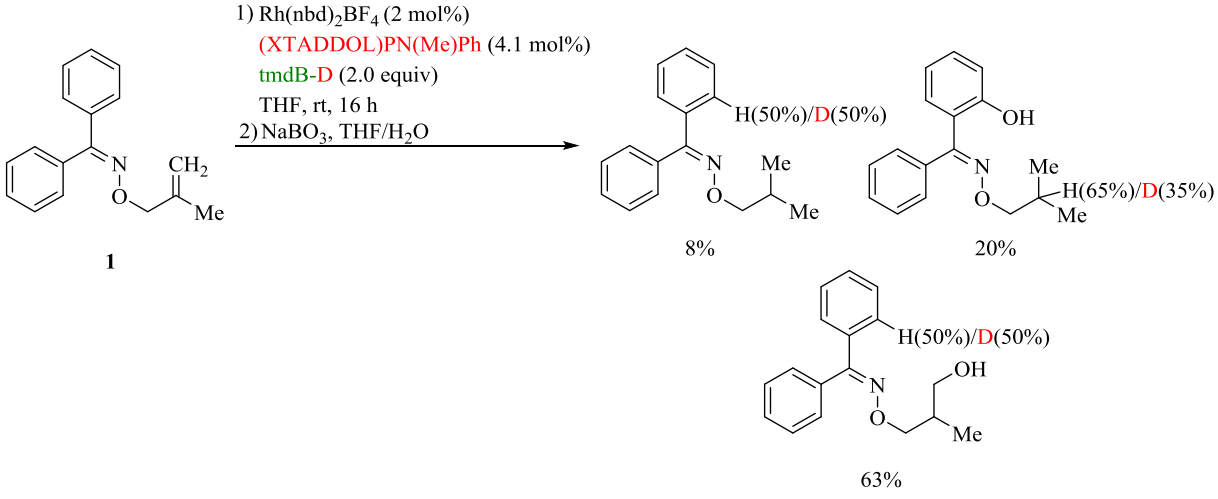

Figure 44 CAHB with labeled borane reveals a loss of deuterium label in the hydroboration products.

The source of the hydrogen to account for lost deuterium is puzzling and currently a topic under investigation in the Takacs labs. Finding the source of the hydrogen is important. The competing formation of reduced products compromises the efficiency of our CAHB reactions, and not only ours, those of other researchers, too. Thus far, it has been assumed that the reduced products arise from H_2 produced in the decomposition of the borane. The decomposition of tmdBD should generate D_2, but we find no deuterium incorporation into the reduced product and the regioselective incorporation of 35% deuterium in the *ortho*-borylated and reduced product above is not consistent with hydrogenation by D_2. Why would the latter reaction be regioselective, if the deuterium comes from D_2? The source of reduction seems in reality be more complicated than a simple scavenging of available H_2 or D_2; it is time to get that story sorted out.

As for potential sources of hydrogen, we know is that the mass balance accounts for ca 90% of the material, largely eliminating substrate decomposition as a viable source of hydrogen. Hydrogen involved in reduction must come from a source previously believed to be innocuous; the likely sources are ligand, diene (i.e., norbornadiene or 1,5-cylooctadiene), or solvent (tetrahydrofuran). The substoichiometric amounts of ligand and diene available do not seem to be a viable source of hydrogen, but there is some precedent suggesting that THF could be an option. Yi and Leung reported that a rhodium(III)-alkyl complex catalyzed the H/D-exchange of THF from D_2O, albeit at high temperature and long reaction times (135 °C, 40 h) (Figure 45).[104] For the oxime-directed CAHB, experiments in deuterated solvents are currently underway to investigate whether THF is the source of H.

(*Ref 104*)

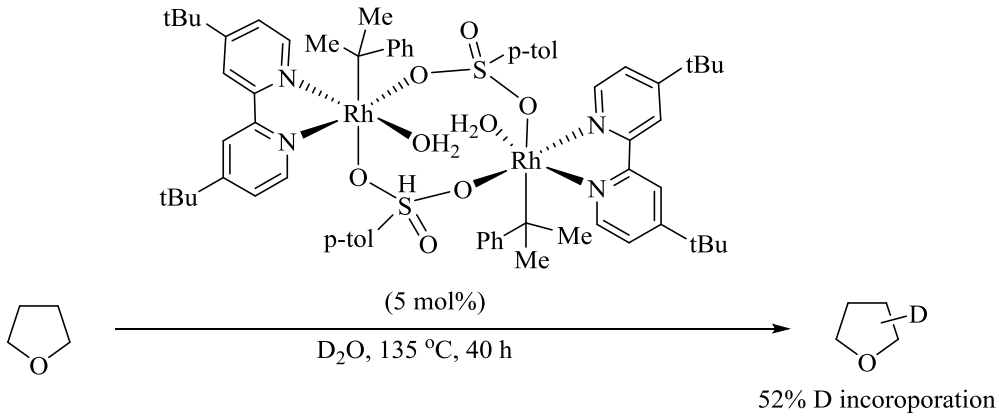

Figure 45 Deuteration of THF with a Rh(III) catalyst. Adapted from Ref 104 with permission from John Wiley and Sons.

Others in the Takacs lab have picked up the study of oxime ethers at this point. To prevent aryl-H/D exchange, acetone-, cyclohexyl, and cyclopentyl-derived oxime ethers are currently under investigation (Figure 46).

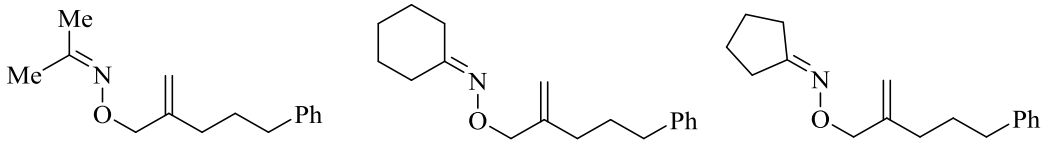

Figure 46 Next generation of functionalized oximes for the directed CAHB.

3.18 Conclusions and Future Directions

At this point in the studies, the mechanistic understanding of oxime-directed Rh-CAHB is still not complete. However, many important observations have been found for planning future studies. Isolation of the *ortho*-hydroylated material proved Rh-catalyzed *ortho*-metallation transpired. Had the C-H not been functionalized, this reaction pathway

may have gone unnoticed. The proximity of the alkene to the *ortho*-H was key for *ortho*-metallation to occur. β,γ-unsaturated alkenes were required for *ortho*-metallation to occur suggesting a Rh(III)-alkyl intermediate is likely involved. Subsequent labelling studies of the benzophenone oximes revealed metallation to be selective. Deuterium transfer to the reacting alkene was observed in both reduction and hydroboration products. In contrast, deuterium-labeled borane afforded hydroboration products missing deuterium incorporation suggesting the borane-D(H) was lost before migratory insertion of the alkene. More importantly, this loss of deuterium gives mechanistic evidence for the source of reduced product formation; Reduction during Rh-CAHB may turn out to be more sophisticated than a simple H_2 reduction. This has broad implications not only to future labeling studies, but to sequestering the troublesome reduction step encountered in various organic transformations.

For future studies, either the hydroboration or the C-H activation could be further optimized. To exploit the hydroboration reaction, varying the borane or the ligating groups could lead to higher yields of desired hydroboration products. Takacs et al previously reported that the influence of the borane has a substantial role in selectivity and reactivity for Rh-CAHB.[47] Exploration of boranes may provide a catalyst system capable of avoiding C-H activation as was found with Rh-CAHB with catecholborane. Screening monodentate and bidentate ligands with various electronic and steric properties may dissuade the reaction from progressing through the undesired C-H activation pathway.

A more interesting approach is taking advantage of the C-H activation. Additives could be used to trap the *ortho*-metalated species for further product functionalization. For example, reactions run under a carbon monoxide atmosphere could form aldehydes. Furthermore, *ortho*-D was transferred quantitatively to the γ-substituents in the Rh-CAHB of deuterium-labeled oximes. If fluorine were substituted for deuterium, fluorine transfer generates a new stereocenter with a net addition of H-F to the alkene (Figure 47).

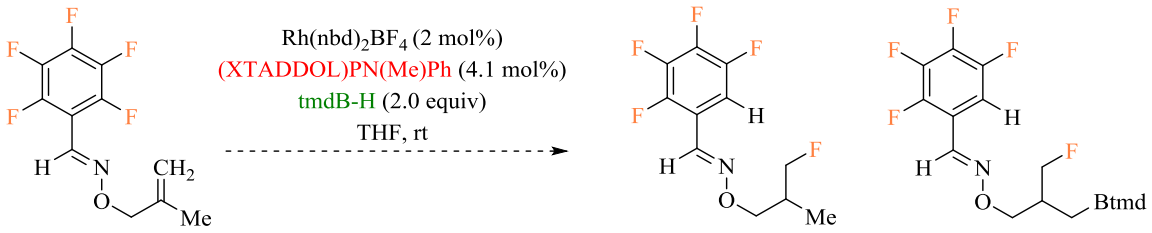

Figure 47 Rh-CAHB of flourinated benzaldehydes may reveal valuable transformations

In conclusion, this ongoing study has demonstrated the complexity of the Rh-CAHB. The mechanism may vary from depending on the choice of directing group, catalyst, borane, and proximity of directing group to the alkene. While selectivity and yields obtained in these studies were modest, the *ortho*-metallation under mild conditions may be further exploited in future studies. The largest contribution from this challenging study was observation of reduction products being formed through an indirect hydrogenation or hydroboration. Further insight into the reduction mechanism and source of H_2 could prove generally beneficial to organometallic catalysis.

3.19 Experimental

Reactions were carried out under a dry nitrogen atmosphere. Tetrahydrofuran (THF) was freshly distilled from sodium metal and benzophenone. Dichloromethane (DCM), methanol (MeOH), benzene, and toluene were dried with 4Å molecular sieves. All synthesized compounds were purified using flash chromatography with the indicated solvents on Silica Gel 60 Geduran®. Thin layer chromatography analyses were performed on Silica Gel HLF (250 microns) precoated analytical plates and visualized with use of handheld short wavelength UV light, vanillin stain (ethanol, H_2SO_4, and vanillin), or ninhydrin stain (ethanol, acetic acid, and ninhydrin). NMR spectra were recorded on a 400 MHz spectrometer using $CHCl_3$ (δ 7.27 ppm), $CDCl_3$ (δ 77.0 ppm), DMSO (δ 2.54 ppm), or d_6-DMSO (δ 40.45 ppm). Peaks are expressed as m (unresolved multiplet), q (quartet), t (triplet), d (doublet), s (singlet), bs (broad singlet). IR spectra were recorded by FT-IR using the ATR technique (ZnSe). Optical rotations were measured in solutions, 1.0 g/100 mL $CHCl_3$ unless indicated otherwise and recorded using a Rudolph Autopol III automatic polarimeter. HRMS analyses were performed by the Nebraska Center for Mass Spectrometry.

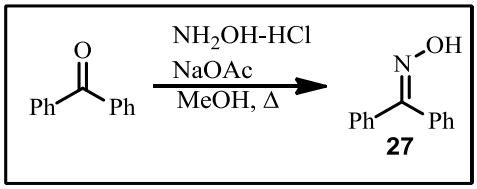

27

A mixture of benzophenone (5.00 g, 27.4 mmol), hydroxylamine hydrochloride (2.48 g, 35.7 mmol), and sodium acetate (2.92 g, 35.7 mmol) in MeOH (100 mL) was placed in 250 mL round-bottomed flask with a reflux condensor. The reaction mixture was heated

to reflux for 4 hours. The reaction mixture was cooled to room temperature. The crude reaction mixture was concentrated under reduced pressure. The remaining solid was re-dissolved in EtOAc (100 mL) and washed with water (3 x 30 mL). The organic extract was dried with Na_2SO_4, filtered, and concentrated yielding a white solid. The solid was recrystallized from ethyl acetate/hexanes and dried under white vacuum affording **27** (4.87 g, 90%) as a white powder-like solid (mp 138-140 °C). TLC analysis (30:70 ethyl acetate/hexanes) showed a spot at Rf 0.3; ^{1}H NMR (400 MHz, $CDCl_3$) δ 9.29 (1H, s), 7.54-7.36 (10H, m); ^{13}C NMR (100 MHz, $CDCl_3$) δ 158.0, 136.2, 132.7, 129. 6, 129.3, 129.2, 128.4, 128.3, 127.9; IR (neat) 3419 (N=OH), 3074 (Aromatic C-H) cm^{-1}

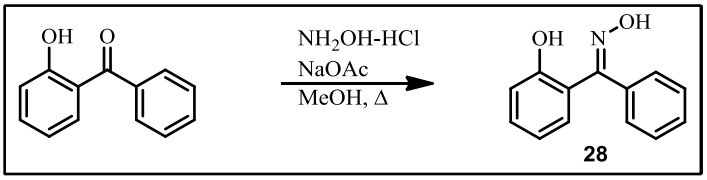

2-hydroxy-benzophenone (1 g, 5.04 mmol) was converted to 2-hydroxybenzophenone oxime **28** using the procedure for benzophenone oxime **27** affording **28** (989 mg, 92%) as a white powder. TLC analysis (70:30 ethyl acetate/hexanes) showed a spot at Rf 0.2; ^{1}H NMR (400 MHz, $CDCl_3$) δ 11.24 (1H, s), 7.57-7.52 (3 H, m), 7.38-7.35 (2H, m), 7.31-7.30 (2H, m), 7.28-7.25 (2H, m), 7.06-7.03 (1H, m), 6.91-6.85 (1H, m), 6.78 (1H, t, *J* = 7. 9 Hz); ^{13}C NMR (100 MHz, $CDCl_3$) δ 162.3, 126.1, 157.9, 139.4, 131.1, 131.0, 131.0, 130.8, 130.8, 130.7, 129.3, 126.2, 128.5, 128.5, 128.5, 128.4, 127.9, 119.1, 119.1, 118.7, 118.6, 117.1, 117.1 IR (neat) 3377 (N-OH), 3311 (ArOH), 3031 (Aromatic C-H) cm^{-1}

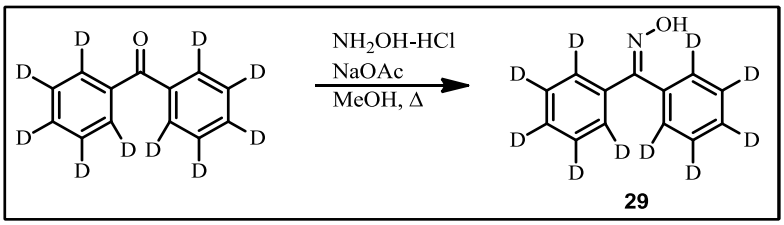

D_{10}-benzophenone (5.29 g, 27.5 mmol) was converted to D10-benzophenone oxime **29** using the procedure for benzophenone oxime **27** affording **29** (5.23 g, 92%) as a white powder. TLC analysis (30:70 ethyl acetate/hexanes) showed a spot at Rf 0.3; ^{1}H NMR (400 MHz, $CDCl_3$) δ 9.44 (1H, s), 7.52-7.34 (.06 H, m); ^{13}C NMR (100 MHz, $CDCl_3$) δ 157.9, 136.1, 132.5, 129.3, 129.2, 129.1, 128.9, 128.7, 128.1, 128.0, 127.9, 127.8, 127.7, 127.5, 127.3; IR (neat) 3233 (N-OH) cm^{-1}; HRMS (EI): Calcd. For $C_{13}HD_{10}NO$ (M): 207.1468, found 207.1464 m/z.

Preparation of allylic alcohols

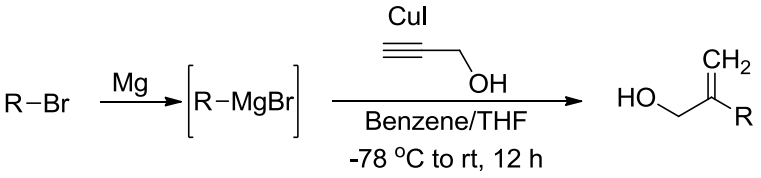

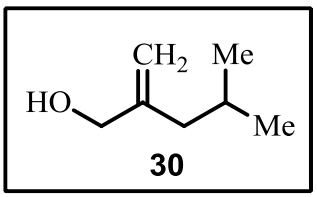

A mixture of magnesium (14.3 g, 589 mmol) and iodine (catalytic) in THF (10 mL) was placed in a 500 mL 3-neck round-bottomed flask with a reflux condenser and addition funnel. 2-methyl-1-bromo-propane (80.6 g, 589 mmol) in 200 mL THF was added to the addition funnel and slowly added to magnesium solution with applied heat until reaction

initation. Rate of addition was adjusted to safely maintain reflux. To a separate 1 L round bottomed flask was added propargyl alcohol (10.0 g, 178 mmol) and copper iodide (34.0 g, 178 mmol). The reaction mixture was purged with N_2 three times. A 1:1 mixture of THF/benzene (400 mL) was added to the copper iodide flask and the reaction mixture was cooled to -78 °C. The solution of isopropenylmagnesium bromide was added dropwise. The reaction was allowed to warm to room temperature and stirred overnight. The crude reaction mixture was washed with NH_4Cl (satd) (100 mL) and extracted with EtOAc (3 x 100 mL). The organic extracts were combined and washed with brine (1 x 50 mL). The organic extract was dried with $MgSO_4$, filtered, concentrated yielding an orange oil. Flash chromatography on silica gel (30:70 EtOAc/hexanes) afforded **30** (12.8 g, 62%) as a clear oil. TLC analysis (25:75 ethyl acetate/hexanes) showed a spot at Rf 0.3; ^{1}H NMR (400 MHz, $CDCl_3$) δ 5.07 (1H, s), 4.87 (1 H, s), 4.07 (2H, d, *J* = 6.0 Hz), 1.97-1.73 (1H, m), 0.91 (3H, d, *J* = 6.6 Hz); ^{13}C NMR (100 MHz, $CDCl_3$) δ 147.9, 110.3, 65.9, 42.8, 26.3, 22.5; IR (neat) 3376 (OH), 3051 (alkene C-H),2961 (C-H), 1773 (C=C), 976 (C-O) cm^{-1}

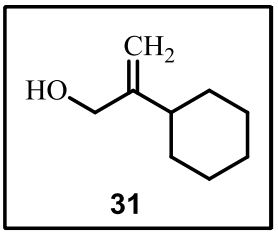

31

Cyclohexyl bromide (102 g, 743 mmol) was converted to cyclohexyl substituted allylic alcohol **31** using the procedure for **30** affording **31** (15.5 g, 56%) as a clear oil. TLC analysis (30:70 ethyl acetate/hexanes) showed a spot at Rf 0.3; ^{1}H NMR (400 MHz, $CDCl_3$) δ 9.44 (1H, s), 7.52-7.34 (.06 H, m); ^{13}C NMR (100 MHz, $CDCl_3$) δ 157.9,

136.1, 132.5, 129.3, 129.2, 129.1, 128.9, 128.7, 128.1, 128.0, 127.9, 127.8, 127.7, 127.5, 127.3; IR (neat) 3300 (OH), 2921 (alkene C-H), 2838 (C-H), 1639 (C=C), 1010 (C-O) cm^{-1}

Preparation of Allylic Carbonates

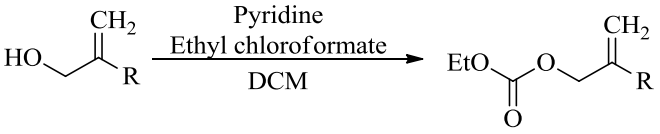

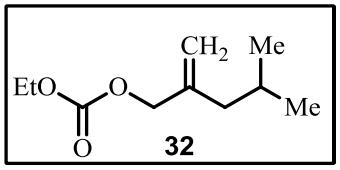

To a cooled solution (0 °C) of isobutyl allylic alcohol **30** (10.0 g, 87.6 mmol) and DMAP (535 mg, 4.38 mmol) in DCM (150 mL) was slowly added pyridine (13.9 g, 175 mmol). Ethyl chloroformate (11.4 g, 105 mmol) was added dropwise over the course of 15 minutes. The reaction mixture was allowed to warm to room temperature overnight. The reaction mixture was washed with water (3 x 25 mL). The organic extracts were dried with Na_2SO_4, filtered, and concentrated yielding a faint yellow oil. The crude reaction mixture was purified via flash chromatography on silica gel (30:70 DCM/hexanes) afforded **32** (15.0 g, 92%) as a clear oil. TLC analysis (30:70 DCM/hexanes) showed a spot at Rf 0.5; ^{1}H NMR (400 MHz, $CDCl_3$) δ 5.11 (1H, s), 4.95 (1 H, s), 4.22 (2H, q, *J* = 7.2 Hz), 1.98 (2H, d, *J* = 7.2 Hz), 1.82-1.76 (1H, m), 1.33 (3H, t, *J* = 7.1 Hz), 0.89 (6H, d, *J* = 9.8 Hz); ^{13}C NMR (100 MHz, $CDCl_3$) δ 155.1, 142.3, 113.8, 69.9, 64.0, 42.8, 26.2,

22.4, 14.3; IR (neat) 2954 (C-H stretch), 1739 (C=O stretch), 1649 (C=C stretch), 1250 (C-O stretch) cm^{-1}

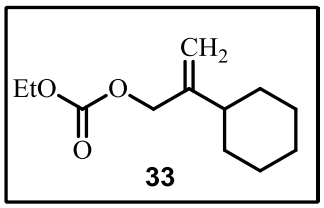

33

Cyclohexyl allylic alcohol **31** (13.6 g, 88.2 mmol) was converted to cyclohexyl substituted ethyl carbonate **31** using the procedure for **32** affording **33** (17.8 g, 95%) as a clear oil. TLC analysis (30:70 DCM/hexanes) showed a spot at Rf 0.6; ^{1}H NMR (400 MHz, $CDCl_3$) δ 5.06 (1H, s), 4.97 (1 H, s), 4.62 (2H, s), 4.23 (2H, q, *J* = 6.4 Hz), 1.98 (1H, t, *J* = 11.5 Hz), 1.84-1.69 (5H, m), 1.35-1.17 (8H, m); ^{13}C NMR (100 MHz, $CDCl_3$) δ 155.1, 148.7, 111.1, 69.4, 64.0, 41.2, 32.1, 26.6, 26.2, 14.3; IR (neat) 2928 (C-H stretch), 1744 (C=O stretch), 1721 (C=C stretch), 1237 (C-O stretch)cm^{-1}

Preparation of unsaturated and saturated substrates

Substrates were alkylated with oximes via 2 methods: *Method A* (Alkylation) or *Method B* (Pd-catalyzed substitution)

Method A: Alkylation

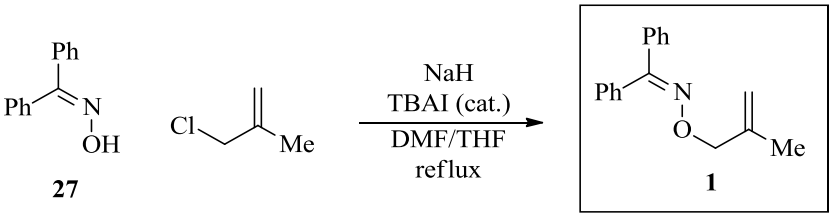

27 **1**

To a cooled solution of benzophenone oxime (2.00g, 10.1 mmol) and catalytic t-butyl ammonium iodide (187 mg, 0.51 mmol) in a mixture of 1:1 DMF/THF (100 mL) was added dry NaH (316 mg, 13.2 mmol). 3-chloro-2-methyl-1-propene (1.19g, 13.2 mmol) was added dropwise. The reaction mixture was stirred for 30 minutes at 0 °C. The septum was removed and an oven-dried reflux condenser flushed with N_2 was added to the round bottom flask. The reaction mixture was heated at 70 °C for 4 hours. The reaction mixture was cooled to 0 °C and water was added dropwise (2 mL). A 3:1 Et_2O/water was added to the reaction mixture. The organic extracts were dried with Na_2SO_4, filtered, and concentrated affording a yellow oil. The crude reaction mixture was purified via flash chromatography on silica gel (30:70 DCM/hexanes) afforded **1** (2.14 g, 84%) TLC analysis (30:70 DCM/hexanes) showed a spot at Rf 0.6; ^{1}H NMR (400 MHz, $CDCl_3$) δ 7.52-7.32 (10H, m), 4.97 (1H, s), 4.92 (1H, s), 4.64 (1H, s), 1.77 (3H, s); ^{13}C NMR (100 MHz, $CDCl_3$) δ 156.7, 142.1, 136.6, 133.5, 129.2, 128.8, 128.2, 128.1, 127.9, 112.2, 78.24, 19.7; IR (neat) 3054 (C-H aromatic stretch), 2908 (C-H aliphatic), 1652 (C=C stretch), 1501 (C=N stretch), 1441 (N-O stretch), 979 (C-O stretch) cm^{-1}

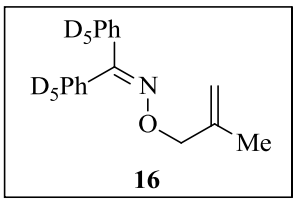

16

D_{10}-benzophenone oxime **29** (2 g, 9.65 mmol) was converted to isotopically labeled benzophenone oxime **16** using the procedure for **1** affording **16** (2.02 g, 80%) as a white

powder. TLC analysis (70:30 DCM/hexanes) showed a spot at Rf 0.5; ^{1}H NMR (400 MHz, $CDCl_3$) δ 4.97 (1H, s), 4.92 (1H, s), 4.64 (2H, s), 1.77 (3H, s); ^{13}C NMR (100 MHz, $CDCl_3$) δ 142.11, 112.24, 78.24, 19.66; IR (neat) 2910 (C-H aliphatic), 1659 (C=C stretch), 1438 (N-O stretch), 982 (C-O stretch) cm^{-1}

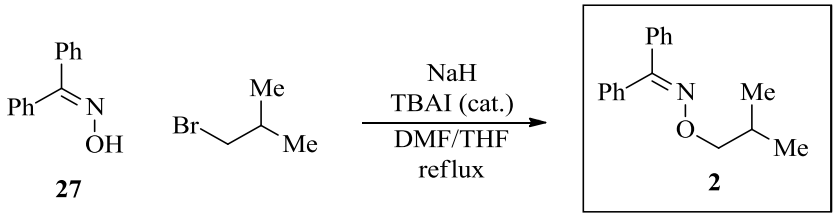

To a cooled solution of benzophenone oxime **27** (2.00g, 10.1 mmol) and catalytic t-butyl ammonium iodide (187 mg, 0.51 mmol) in a mixture of 1:1 DMF/THF (100 mL) was added dry NaH (316 mg, 13.2 mmol). 1-bromo-2-methylpropane (1.72 g, 13.2 mmol) was added dropwise. The reaction mixture was stirred for 30 minutes at 0 °C. The septum was removed and an oven-dried reflux condenser flushed with N_2 was added to the round bottom flask. The reaction mixture was heated at 70 °C for 4 hours. The reaction mixture was cooled to 0 °C and water was added dropwise (2 mL). A 3:1 Et_2O/water was added to the reaction mixture. The organic extracts were dried with Na_2SO_4, filtered, and concentrated affording a yellow oil. The crude reaction mixture was purified via flash chromatography on silica gel (30:70 DCM/hexanes) afforded 2 (2.24 g, 92%) as a clear oil. TLC analysis (30:70 DCM/hexanes) showed a spot at Rf 0.6; ^{1}H NMR (400 MHz, $CDCl_3$) δ 7.51-7.31 (10H, m), 3.98 (2H, d, J = 6.8 Hz), 2.12-2.02 (1H, m), 0.93 (6H, d, J = 6.7 Hz); ^{13}C NMR (100 MHz, $CDCl_3$) δ 156.1, 136.44, 135.6, 129.3, 129.1, 128.6, 128.2, 128.0, 127.8, 81.2, 28.1, 19.2; IR (neat) 3054 (C-H

aromatic stretch), 2958 (C-H aliphatic), 1588 (C=N stretch), 1438 (N-O stretch), 996 (C-O stretch) cm^{-1}

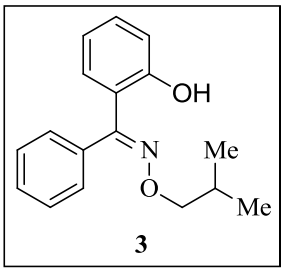

3

2-hydroxylbenzophenone oxime **28** (500 mg, 2.34 mmol) was converted to ortho-hydroxylated oxime **3** using the procedure for **2** affording **3** (126m g, 20%) as a clear oil. TLC analysis (10:90 EtOAc/hexanes) showed a spot at Rf 0.7; ^{1}H NMR (400 MHz, $CDCl_3$) δ 11.2 (1H, s), 7.52-7.47 (3H, m), 7.32-7.24 (3H, m), 7.03 (1H, d, *J* = 8.9 Hz), 6.84-6.77 (1H, m), 6.73 (1H, t, *J* = 8.0 Hz), 3.94 (2H, d, *J* = 6.9 Hz), 2.10-2.00 (1H, m), 0.90 (2H, d, *J* = 6.72 Hz); ^{13}C NMR (100 MHz, $CDCl_3$) δ 160.3, 158.2, 132.0, 130.7, 130.5, 128.9, 128.4, 128.3, 118.8, 118.8, 117.1, 81.5, 27.9, 19.0; IR (neat) 3055 (C-H aromatic stretch), 2958 (C-H aliphatic), 1588 (C=N stretch), 1438 (N-O stretch), 996 (C-O stretch) cm^{-1}

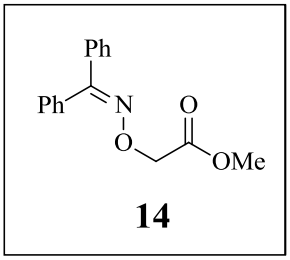

14

Methyl-2-(((diphenylmethylene)amino)oxy) acetate (methyl ester analogue **14**) Methyl bromoacetate (814 mg, 5.3 mmol) and benzophenone oxime 27 (1.0 g, 5.1 mmol) were

converted to methyl ester **14** (784 mg, 61%) as a colorless oil using the procedure for benzophenone alkylation for **2**. TLC analysis (30:70 EtOAc/hexanes) showed a spot at Rf 0.7; ^{1}H NMR (400 MHz, $CDCl_3$) δ 7.51-7.32 (10H, m), 4.76 (2H, s), 3.80 (3H, s); ^{13}C NMR (100 MHz, $CDCl_3$) δ 170.6, 158.5, 136.02, 133.0, 129.6, 129.4, 129.1, 128.2, 128.2, 128.1, 71.0, 51.9; IR (neat) 3070(C-H aromatic stretch), 2945 (C-H aliphatic), , 1747 (C=O), 1435 (N-O stretch), 1084 (C-O stretch) cm^{-1}

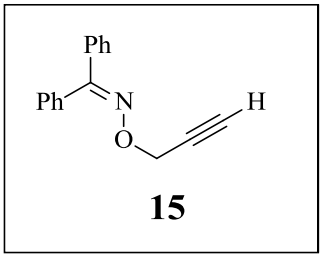

15

Benzophenone O-prop-2-yn-1-yl-oxime (alkyne analogue **15**) Propargyl bromide (633 mg, 5.32 mmol) and benzophenone oxime **27** (1.0 g, 5.1 mmol) were converted to β,γ-alkyne **15** (924 mg, 77%) as a colorless oil using the procedure for benzophenone alkylation for **2**. TLC analysis (30:70 EtOAc/hexanes) showed a spot at Rf 0.9; ^{1}H NMR (400 MHz, $CDCl_3$) δ 7.55-7.34 (10H, m), 4.80 (2H, d, *J* = 2.4 Hz), 2.49 (1H, t, *J* = 2.3 Hz); ^{13}C NMR (100 MHz, $CDCl_3$) δ 158.3, 136.2, 133.0, 129.6, 129.4, 129.0, 128.3, 128.2, 128.1, 80.0, 74.4, 62.0; IR (neat) 3280 (sp C-H stretch), 2910 (C-H aliphatic), 1446 (N-O stretch), 1011 (C-O stretch) cm^{-1}

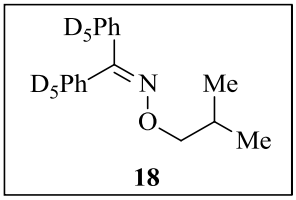

18

D_{10}-benzophenone oxime **29** (500 mg, 2.41 mmol) was converted to isotopically labeled benzophenone oxime **18** using the procedure for **2** affording **18** (604 mg, 95%) as a colorless oil. TLC analysis (70:30 DCM/hexanes) showed a spot at Rf 0.5; ^{1}H NMR (400 MHz, $CDCl_3$) δ 3.98 (2H, d, *J* = 6.8 Hz), 2.11-2.02 (1H, m), 0.93 (6H, d, *J* = 6.7 Hz); ^{13}C NMR (100 MHz, $CDCl_3$) δ 81.2, 28.1, 19.2

Method B: Pd-catalyzed substitution

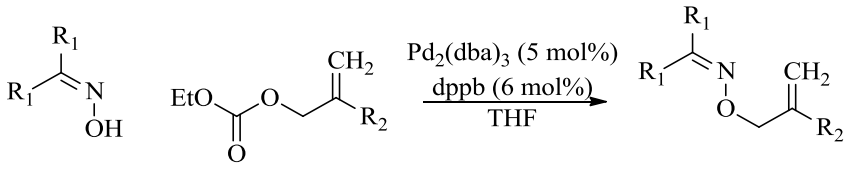

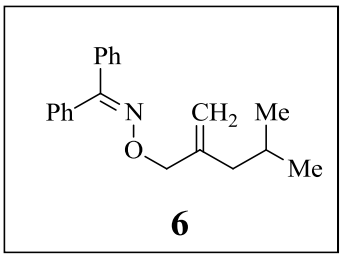

To a mixture of benzophenone oxime **27** (2.00 g, 10.1 mmol), Pd_2(dba)3 (194 mg, 0.21 mmol), and dppb (216 mg, 0.51 mmol) in THF (40 mL) was added isobutyl carbonate **32** (1.58 g, 8.47 mmol). The reaction mixture was stirred overnight at room temperature. The reaction mixture was concentrated in vacuo and purified via flash chromatography on silica gel (20:80 DCM/hexanes) affording **6** (2.33 g, 94%) as a clear oil. TLC analysis (10:90 EtOAc/hexanes) showed a spot at Rf 0.9; ^{1}H NMR (400 MHz, $CDCl_3$) δ 7.52-7.32 (10H, m), 5.03 (1H, s), 4.89 (1H, s), 4.65 (2H, s), 1.96-1.84 (2H, m), 1.83-1.74 (1H, m), 0.88 (6H, d, *J* = 6.5 Hz); ^{13}C NMR (100 MHz, $CDCl_3$) δ 156.7, 144.8, 136.6, 133.5,

129.2, 128.7, 128.2, 128.0, 127.9, 112.9, 77.3, 43.3, 26.0, 22.5; IR (neat) 3058 (C-H aromatic stretch), 2951 (C-H aliphatic), 1655 (C=C stretch), 1488 (C=N stretch), 1437 (N-O stretch), 969 (C-O stretch) cm^{-1}

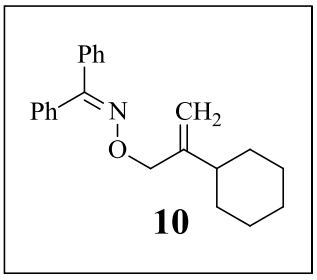

10

Cyclohexyl carbonate **33** (1.80 g, 8.46 mmol) was converted to β,γ-unsaturated cyclohexyl substrate **10** using the procedure for **6** affording **10** (2.48 g, 92%) as a clear oil. TLC analysis (10:90 EtOAc/hexanes) showed a spot at Rf 0.9; ^{1}H NMR (400 MHz, $CDCl_3$) δ 7.49-7.31 (10H, m), 4.97 (1H, s), 4.89 (1H, s), 4.71 (1H, s), 1.95 (1H, t, J = 11.3 Hz), 1.80-1.67 (5H, m), 1.32-1.11 (5H, m); ^{13}C NMR (100 MHz, $CDCl_3$) δ 156.7, 151.0, 136.6, 133.6, 129.2, 128.7, 128.2, 128.0, 127.9, 109.9, 76.9, 41.4, 32.2, 26.8, 26.3; IR (neat) 3084 (C-H aromatic stretch), 2925 (C-H aliphatic), 1642 (C=C stretch), 1441 (N-O stretch), 976 (C-O stretch) cm^{-1}

Typical reduction reaction procedure with sub-stoichiometric tmdBH addition

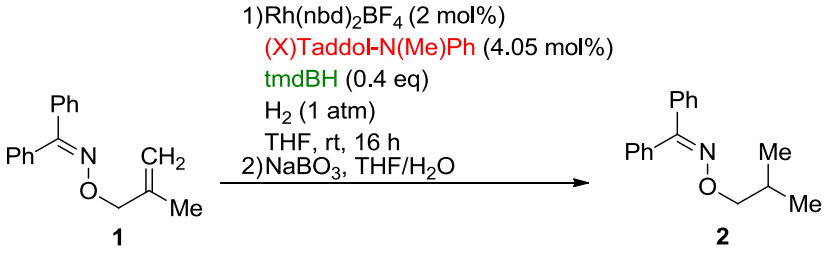

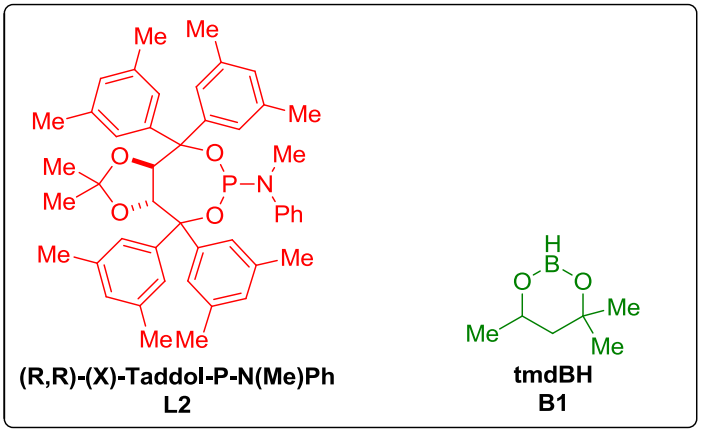

To a vial containing $Rh(nbd)_2BF_4$ (3.0 mg, 7.93 μmol) was added **L2** (11.4 mg, 16.0 μmol) in THF (1 mL) and stirred for 1 hour for complexation (solution changes from colorless to yellow instantaneously). A 1 mL aliquot of the resulting $Rh[(\mathbf{L2})_2(nbd)]BF_4$ solution was added to a 50 mL round bottom flask with stir bar. The resulting yellow solution was added β,γ-unsaturated oxime **1** (66.3 mg, 0.11 mmol) as a solution in THF (2 mL). The reaction mixture was stirred for 30 minutes at RT and then cooled in an ice bath. To the cooled solution (0 °C) was added dropwise (over the course of 2 minutes) a solution of 4,4,6-trimethyl-1,3,2-dioxaborinane (tmdBH, **B1**, 13.5 mg, 0.53 mmol) in THF (1 mL). The reaction vessel was evacuated and added a H2 balloon. The mixture was allowed to warm to room temperature and stirred for 16 hours. The reaction mixture was added a 1:3 water/THF mixture (4 mL). $NaBO_3$-monohydrate (300 mg, 300 mmol)

was added and the reaction mixture was stirred vigorously. After a 6 hour stir, the resultant mixture was extracted with EtOAc (3 x 15 mL) and the combined organic extracts were dried with Na_2SO_4, filtered, and concentrated under reduced pressure. The crude reaction mixture was purified via flash chromatography on silica gel (30:70 DCM/hexanes) afforded **2** as a colorless oil.

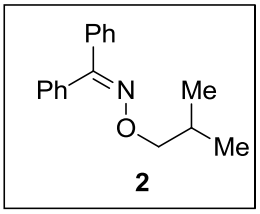

2

Benzophenone O-isobutyl oxime (Reduced product **2**) TLC analysis (10:90 EtOAc/hexanes) showed a spot at Rf 0.9; ^{1}H NMR (400 MHz, $CDCl_3$) δ 7.51-7.31 (10H, m), 3.98 (2H, d, *J* = 6.8 Hz), 2.12-2.02 (1H, m), 0.93 (6H, d, *J* = 6.7 Hz); ^{13}C NMR (100 MHz, $CDCl_3$) δ 156.1, 136.44, 135.6, 129.3, 129.1, 128.6, 128.2, 128.0, 127.8, 81.2, 28.1, 19.2; IR (neat) 3054 (C-H aromatic stretch), 2958 (C-H aliphatic), 1588 (C=N stretch), 1438 (N-O stretch), 996 (C-O stretch) cm^{-1}

Typical hydroboration reaction

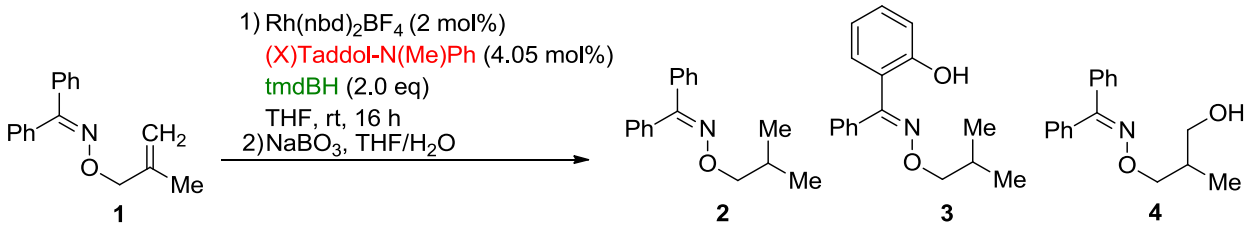

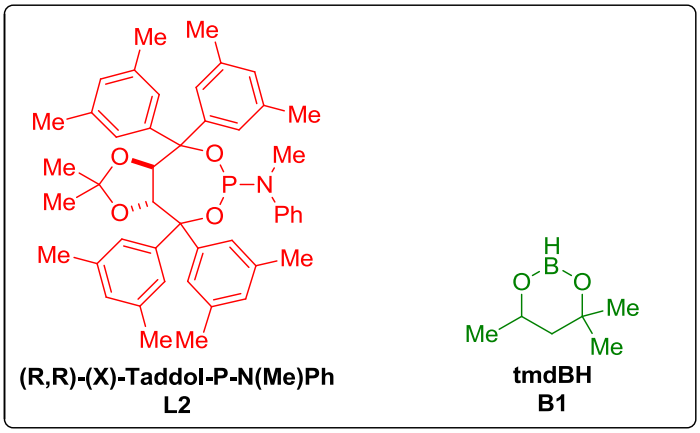

To a vial containing $Rh(nbd)_2BF_4$ (3.0 mg, 7.93 μmol) was added **L2** (11.4 mg, 16.0 μmol) in THF (1 mL) and stirred for 1 hour for complexation (solution changes from colorless to yellow instantaneously). A 1 mL aliquot of the resulting $Rh[(\mathbf{L2})_2(nbd)]BF_4$ solution was added to a 50 mL round bottom flask with stir bar. The resulting yellow solution was added β,γ-unsaturated oxime **1** (66.3 mg, 0.26 mmol) as a solution in THF (2 mL). The reaction mixture was stirred for 30 minutes at RT and then cooled in an ice bath. To the cooled solution (0 °C) was added dropwise (over the course of 20 minutes) a solution of 4,4,6-trimethyl-1,3,2-dioxaborinane (tmdBH, **B1**, 67.6 mg, 0.53 mmol) in THF (1 mL). The mixture was allowed to warm to room temperature and stirred for 4 hours. Afterwards, the reaction mixture was concentrated and reduced product **2** was separated via flash chromatography on silica gel (20:80 EtOAc/hexanes) as a clear oil.

The inseparable ortho-borylated and γ-borylated products were concentrated and added a 1:3 water/THF mixture. $NaBO_3$-monohydrate (300 mg, 300 mmol) was added and the reaction mixture was stirred vigorously. After a 6 hour stir, the resultant mixture was extracted with EtOAc (3 x 15 mL) and the combined organic extracts were dried with Na_2SO_4, filtered, and concentrated under reduced pressure. The crude reaction mixture was purified via flash chromatography on silica gel (20:80 EtOAc/hexanes) afforded **3** and **4** as colorless oils.

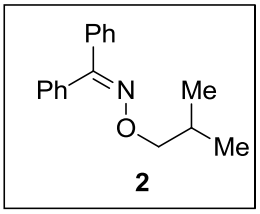

2

Benzophenone O-isobutyl oxime (Reduced product **2**) β,γ-unsaturated substrate **1** (66.3 mg, 0.24 mmol) was converted to reduced product **2** (6.8 mg, 10%) as a colorless oil. TLC analysis (10:90 EtOAc/hexanes) showed a spot at Rf 0.9; ^{1}H NMR (400 MHz, $CDCl_3$) δ 7.51-7.31 (10H, m), 3.98 (2H, d, *J* = 6.8 Hz), 2.12-2.02 (1H, m), 0.93 (6H, d, *J* = 6.7 Hz); ^{13}C NMR (100 MHz, $CDCl_3$) δ 156.1, 136.44, 135.6, 129.3, 129.1, 128.6, 128.2, 128.0, 127.8, 81.2, 28.1, 19.2; IR (neat) 3054 (C-H aromatic stretch), 2958 (C-H aliphatic), 1588 (C=N stretch), 1438 (N-O stretch), 996 (C-O stretch) cm^{-1}

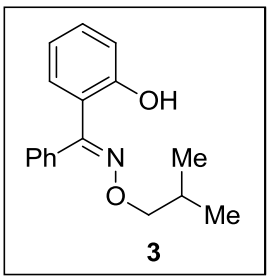

3

(2-hydroxyphenyl)(phenyl methanone O-isobutyl oxime (Ortho-hydroxylated and reduced product **3**) β,γ-unsaturated substrate **1** (66.3 mg, 0.24 mmol) was converted to ortho-hydroxylated / reduced product **3** (22.3 mg, 31%) as a colorless oil. TLC analysis (10:90 EtOAc/hexanes) showed a spot at Rf 0.8; ^{1}H NMR (400 MHz, $CDCl_3$) δ 11.2 (1H, s), 7.52-7.47 (3H, m), 7.32-7.24 (3H, m), 7.03 (1H, d, *J* = 8.9 Hz), 6.84-6.77 (1H, m), 6.73 (1H, t, *J* = 8.0 Hz), 3.94 (2H, d, *J* = 6.9 Hz), 2.10-2.00 (1H, m), 0.90 (2H, d, *J* = 6.7 Hz); ^{13}C NMR (100 MHz, $CDCl_3$) δ 160.3, 158.2, 132.0, 130.7, 130.5, 128.9, 128.4, 128.3, 118.8, 118.8, 117.1, 81.5, 27.9, 19.0; IR (neat) 3055 (C-H aromatic stretch), 2958 (C-H aliphatic), 1588 (C=N stretch), 1438 (N-O stretch), 996 (C-O stretch) cm^{-1}

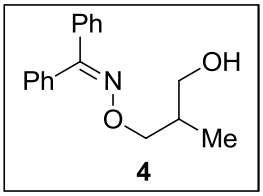

4

Benzophenone O-(3-hydroxy-2-methylpropyl) oxime (gamma-hydroxyl product **4**) β,γ-unsaturated substrate **1** (66.3 mg, 0.24 mmol) was converted to gamma-hydroxylated product **3** (40.7 mg, 57%) as a colorless oil. TLC analysis (30:70 EtOAc/hexanes) showed a spot at Rf 0.3; ^{1}H NMR (400 MHz, $CDCl_3$) δ 7.50-7.33 (10H, m), 4.29 and 4.13 (2H, ddd, J_1 = 4.6= Hz, J_2 = 7.5 Hz), 3.64-3.52 (2H, m), 2.18-2.11 (1H, m), 2.01 (1H, t, J = 5.5 Hz), 0.94 (3H, d, J = 7.0 Hz); ^{13}C NMR (100 MHz, $CDCl_3$) δ 157.2, 136.1, 133.3, 129.5, 128.9, 128.9, 128.3, 128.2, 127.8, 77.9, 66.3, 35.8, 13.5; IR (neat) 3360 (O-H stretch), 3041 (C-H aromatic stretch), 2924 (C-H aliphatic), 1585 (C=N stretch), 1434 (N-O stretch), 989 (C-O stretch) cm^{-1}

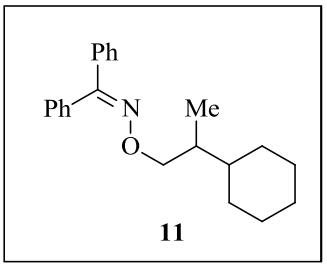

11

Benzophenone O-2-cyclohexylpropyl oxime (reduced product **11**) β,γ-unsaturated substrate **10** (84.4 mg, 0.24 mmol) was converted to reduced product **11** (25.0 mg, 28%) as a colorless oil using the procedure for typical Rh-CAHB described for **1**. TLC analysis (30:70 EtOAc/hexanes) showed a spot at Rf 0.9; ^{1}H NMR (400 MHz, $CDCl_3$) δ 7.52-7.33 (10H, m), 4.20 and 4.02 (2H, dd, J_1 = 6.0 Hz, J_2 = 10.2 Hz), 1.80-1.62 (6H, m), 1.30-1.08 (6H, m), 0.88 (3H, d, J = 6.9 Hz); ^{13}C NMR (100 MHz, $CDCl_3$) δ 156.2, 136.7, 133.6, 129.3, 129.1, 128.9, 128.6, 128.2, 127.9, 127.8, 78.3, 40.0, 37.8, 30.8, 28.9, 26.9, 26.8, 26.7, 13.7; IR (neat) 3058 (C-H aromatic stretch), 2921 (C-H aliphatic), 1588 (C=N stretch), 1443 (N-O stretch), 980 (C-O stretch) cm^{-1}

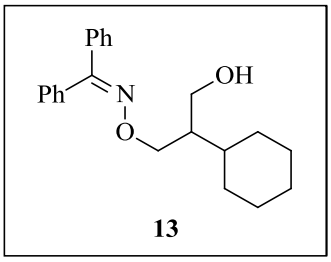

13

Benzophenone O-2-cyclohexyl-3-hydroxypropyl oxime (gamma-hydroxyl product **13**) β,γ-unsaturated substrate **10** (84.4 mg, 0.24 mmol) was converted to gamma-hydroxylated product **13** (53.5 mg, 60%) as a colorless oil using the procedure for typical Rh-CAHB described for **1**. Chiral HPLC analysis (Chiralcel OD, 70:30 hexanes:isopropanol) showed peaks at 7.82 min and 8.47 min; TLC analysis (30:70

EtOAc/hexanes) showed a spot at Rf 0.3; ^{1}H NMR (400 MHz, $CDCl_3$) δ 7.51-7.33 (10H, m), 4.44-4.31 (2H, unresolved ddd), 3.68 (2H, t, *J* = 6.4 Hz), 2.01 (1H, t, *J* = 5.5 Hz), 0.94 (3H, d, *J* = 7.0 Hz), 2.07-2.03 (1H, m), 1.75-1.00 (13 H, m); ^{13}C NMR (100 MHz, $CDCl_3$) δ 157.4, 136.0, 133.3, 129.5, 129.0, 128.8, 128.3, 128.3, 127.8, 75.7, 63.5, 46.0, 36.9, 30.7, 30.5, 26.7, 26.6, 26.5; IR (neat) 3360 (O-H stretch), 3058 (C-H aromatic stretch), 2917 (C-H aliphatic), 1490 (C=N stretch), 1441 (N-O stretch), 981 (C-O stretch) cm^{-1}

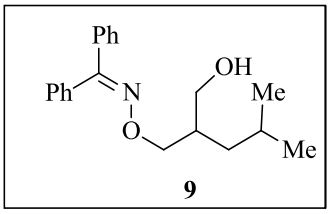

9

Benzophenone O-(2-hydroxymethyl)-4-methylpentyl oxime (gamma hydroxylated product **9**) β,γ-unsaturated substrate **6** (77.5 mg, 0.24 mmol) was converted to gamma-hydroxylated product **3** (40.7 mg, 57%) as a colorless oil. Chiral HPLC analysis (Chiralcel OD, 70:30 hexanes:isopropanol) showed peaks at 9:01 min and 9:55; min TLC analysis (30:70 EtOAc/hexanes) showed a spot at Rf 0.3; ^{1}H NMR (400 MHz, $CDCl_3$) δ 7.51-7.34 (10H, m), 4.35 and 4.14 (2H, ddd, J_1 = 4.0 Hz, J_2 = 10.8 Hz), 3.64-3.63 (1H, m), 3.57-3.51 (1H, m), 2.12(1H, t, *J* = 5.5 Hz,), 2.04-2.02 (1H, m), 1.71-1.64 (1H, m), 1.21-1.11 (2H, m), 0.97-0.93 (6H, m); ^{13}C NMR (100 MHz, $CDCl_3$) δ 157.3, 136.0, 133.2, 129.5, 129.0, 128.9, 128.3, 128.3, 127.8, 77.0, 65.1, 38.5, 37.2, 25.3, 22.9, 22.8; IR (neat) 3376 (O-H stretch), 3081 (C-H aromatic stretch), 2961 (C-H aliphatic), 1595 (C=N stretch), 1448 (N-O stretch), 976 (C-O stretch) cm^{-1}

MTPA characterization of gamma alcohol for enantiomeric excess assignment

Determination of enantiomeric excess of **4** could not be determined with with chiral HPLC columns. Synthesis of the corresponding diastereomers from (S)-(+)-α-Methoxy-α-trilfluoromethylphenylacetyl chloride (S)-MTPA-Cl allows for NMR determination of the diastereomeric excess.

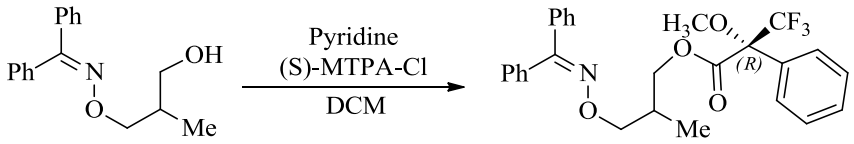

4 **4-(R)MTPA**

(2R)-3-(((diphenylmethylene)amino)oxy)-2-methylpropyl-3,3,3-trifluoro-2-methoxy-2-phenylpropanoate (4-(R)-MTPA. To a vial containing gamma-hydroxylated product 4 (5.0 mg, 18.6 μmol) and excess triethylamine (3 drops) was added DCM (3 mL). (S)-MTPA-Cl (25.0 μmol, 0.25 mL of a freshly prepared 0.1 M solution in toluene) was added dropwise under N_2. DMAP (1.86 mmol, 0.1 mL from a freshly prepared 0.1 M stock solution in DCM) was added and the resulting reaction mixture was stirred at room temperature for 4 hours. The salt was filtered with a small silica plug which was subsequently flushed with EtOAc (2 x 1 mL). The combined organic filtrates were concentrated in vacuo. The crude reaction mixture was purified via flash chromatography on silica gel (10:90 EtOAc/hexanes) which afforded **4-(R)-MTPA** (8.8 mg, 98 %) as a colorless oil. TLC analysis (10:90 EtOAc/hexanes) showed a spot at Rf 0.8; ^{1}H NMR (400 MHz, $CDCl_3$) δ 7.48-7.28 (15H, m), 4.35-4.23 (2H, m), 4.17-4.02 (2H, m) 3.55 (3H, s), 2.42-2.36 (1H, bs), 0.99 (3H, t, J = 7.6 Hz); ^{13}C NMR (100 MHz,

$CDCl_3$) δ 166.6, 157.2, 157.1, 136.3, 133.3, 132.3, 129.6, 129.4, 129.1, 129.0, 128.8, 128.4, 128.3, 128.1, 128.1, 127.8, 127.4, 124.8, 121.9, 84.6, 75.4, 68.1, 55.4, 32.8, 13.8; ^{19}F NMR (357.5 MHz, $CDCl_3$) δ -71.56, -71.64 ; IR (neat) 3038 (C-H aromatic stretch), 2924 (C-H aliphatic), 1742 (C=O), 1451 (N-O stretch), 1000 (C-O stretch) cm^{-1}

Rh-CAHB of deuterated benzophenone derivatives with tmdB-H

Using a procedure for typical Rh-CAHB with deuterium-labeled substrate **16** and tmdBH, the products isolated as described below.

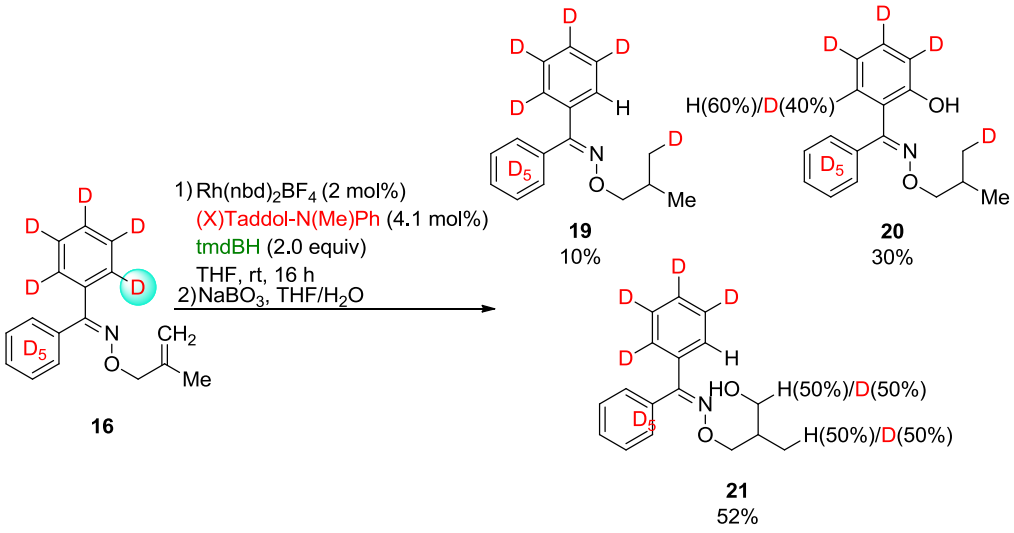

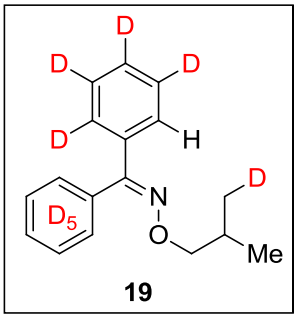

(D9H)-Benzophenone O-isobutyl oxime (reduced product 1**9**) β,γ-unsaturated substrate **16** (69.1 mg, 0.24 mmol) was converted to reduced product **19** (6.82 mg, 10%) as a colorless oil. TLC analysis (30:70 EtOAc/hexanes) showed a spot at Rf 0.9; ^{1}H NMR (400 MHz, $CDCl_3$) δ 7.50 (1H, s), 3.98 (2H, d, J = 6.7 Hz), 2.11-2.02 (1H, m), 0.94-0.90 (5H, m); ^{13}C NMR (100 MHz, $CDCl_3$) δ 127.7, 81.2, 28.0, 19.2

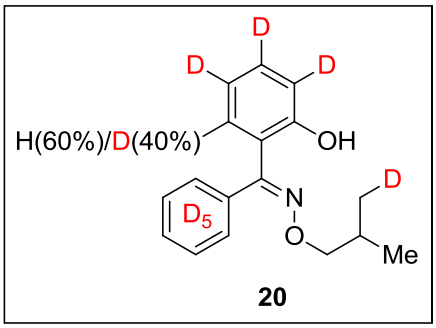

20

(2-hydroxyphenyl)(phenyl methanone O-isobutyl oxime (ortho-hydroxylated and reduced product **19**) β,γ-unsaturated substrate **16** (69.1 mg, 0.24 mmol) was converted to ortho-hydroxylated product **20** (22.2 mg, 30%) as a colorless oil. TLC analysis (30:70 EtOAc/hexanes) showed a spot at Rf 0.85; ^{1}H NMR (400 MHz, $CDCl_3$) δ 11.2 (1H, s), 6.83 (0.6H, s), 3.94 (2H, d, J = 6.9 Hz), 2.09-1.99 (1H, m), 0.91-0.88 (4.7H, m); ^{13}C NMR (100 MHz, $CDCl_3$) δ 160.3, 158.2, 131.8, 130.4, 128.3, 128.0, 127.8, 127.5, 118.8, 118.7, 81.5, 27.9, 27.8, 19.0, 18.9, 18.7, 18.5; IR (neat) 3085 (O-H phenol), 2920 (C-H aliphatic), 1585 (C=N stretch), 1441 (N-O stretch), 1025 (C-O stretch) cm^{-1}

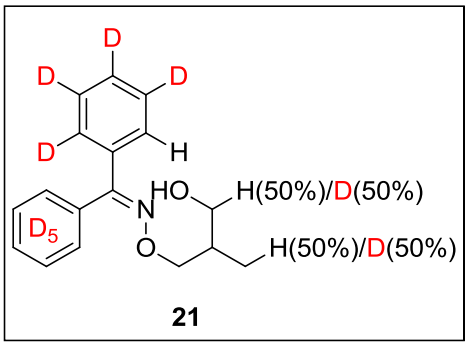

21

Benzophenone O-(2-hydroxymethyl)-4-methylpentyl oxime(gamma-hydroxylated product **21**) β,γ-unsaturated substrate **16** (69.1 mg, 0.24 mmol) was converted to gamma-hydroxylated product **21** (38.7 mg, 52%) as a colorless oil. TLC analysis (30:70 EtOAc/hexanes) showed a spot at Rf 0.5; ^{1}H NMR (400 MHz, $CDCl_3$) δ 7.49 (1H, s), 4.30 and 4.13 (2H, ddd, J_1 = 4.5 Hz, J_2 = 10.9 Hz), 3.62-3.53 (1.5H, m), 2.17-2.10 (1H, m), 2.04 (1H, bs), 0.95-0.92 (2.5H, m); ^{13}C NMR (100 MHz, $CDCl_3$) δ 127.7, 77.9, 66.3, 35.8, 13.5; IR (neat) 3339 (O-H stretch), 2924 (C-H aliphatic), 1595 (C=N stretch), 1454 (N-O stretch), 972 (C-O stretch) cm^{-1}

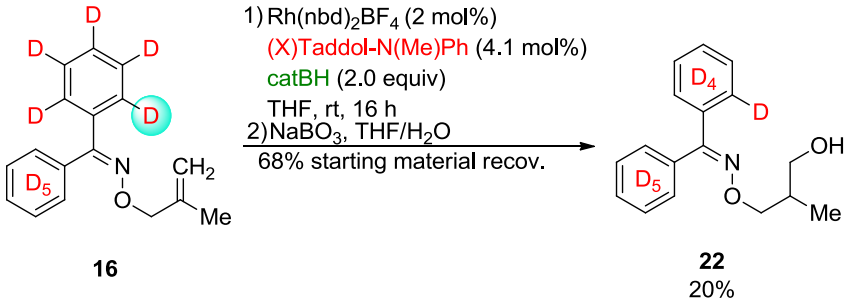

16 **22** 20%

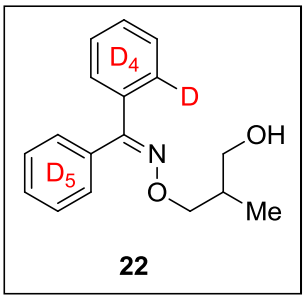

22

D10-Benzophenone O-(2-hydroxymethyl)-4-methylpentyl oxime(gamma-hydroxylated product **21**) β,γ-unsaturated substrate **16** (69.1 mg, 0.24 mmol) was converted to gamma-hydroxylated product **22** (15.1 mg, 20%) as a colorless oil. TLC analysis (30:70 EtOAc/hexanes) showed a spot at Rf 0.5; ^{1}H NMR (400 MHz, $CDCl_3$) δ 4.30 and 4.13 (2H, ddd, J_1 = 4.6 Hz, J_2 = 10.9 Hz), 2.18-2.10 (1H, m), 2.03 (1H, bs), 0.94 (3H, d, J = 7.0 Hz); ^{13}C NMR (100 MHz, $CDCl_3$) δ 157.1, 136.0, 133.0, 77.9, 66.3, 35.8, 13.5. ; IR (neat) 3342 (O-H stretch), 2931 (C-H aliphatic), 1588 (C=N stretch), 1451 (N-O stretch), 969 (C-O stretch) cm^{-1}

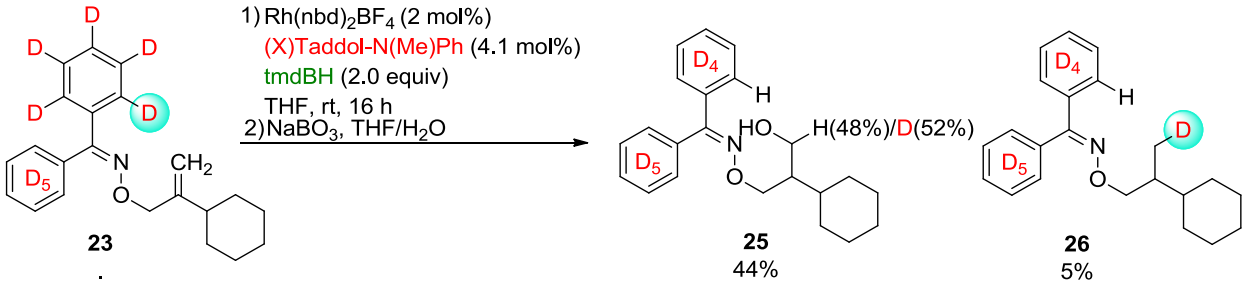

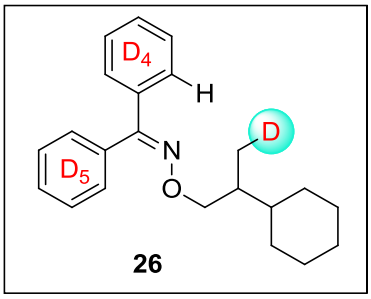

(D9H)Benzophenone O-2-cyclohexylpropyl oxime (reduced product **26**) β,γ-unsaturated substrate **23** (87.0 mg, 0.24 mmol) was converted to reduced product **19** (4.60 mg, 5%) as a colorless oil. TLC analysis (30:70 EtOAc/hexanes) showed a spot at Rf 0.9; ^{1}H NMR (400 MHz, $CDCl_3$) δ 7.50 (1H, s), 4.11 (2H, dd, J_1 = 5.8 Hz, J_2 = 10.3 Hz), 1.81-1.57 (6H, m), 1.31-0.97 (7H, m), 0.88-0.85 (2H, m); ^{13}C NMR (100 MHz, $CDCl_3$) δ 127.7, 78.3, 33.9, 37.8, 37.8, 30.7, 28.8, 26.9, 26.8, 26.7, 13.7, 13.6; IR (neat) 2914 (C-H aliphatic), 1587 (C=N stretch), 1428 (N-O stretch), 972 (C-O stretch) cm^{-1}

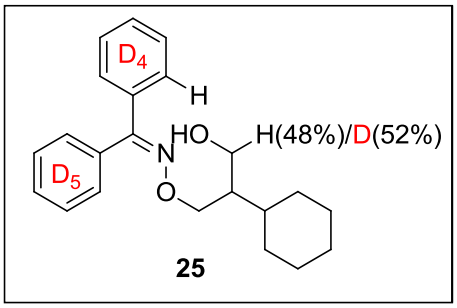

25

(D9H)Benzophenone O-2-cyclohexyl-3-hydroxypropyl oxime (gamma hydroxylated product **25**) β,γ-unsaturated substrate **23** (87.0 mg, 0.24 mmol) was converted to gamma-hydroxylated product **19** (40.2 mg, 44%) as a colorless oil. TLC analysis (30:70 EtOAc/hexanes) showed a spot at Rf 0.5; ^{1}H NMR (400 MHz, $CDCl_3$) δ 7.50 (1H, s), 4.20 and 4.02 (2H, ddd, J_1 = 3.8 Hz, J_2 = 10.6 Hz), 3.70-3.66 (1.4H, m), 2.29-2.22 (0.5H, m), 2.06-2.02 (1H, m), 1.75-1.58 (6H, m), 1.44-1.40 (1H, m), 1.28-1.02 (5.5 H, m); ^{13}C NMR (100 MHz, $CDCl_3$) δ 157.4, 133.0, 127.7, 75.7, 63.5, 46.0, 36.9, 30.7, 30.5, 26.4, 26.6, 26.5; IR (neat) 3358 (O-H stretch), 3062 (aromatic C-H), 2926 (C-H aliphatic), 1575 (C=N stretch), 1450 (N-O stretch), 972 (C-O stretch) cm^{-1}

Synthesis of tmdB-D

Labeled-boranes prepared with an iridium catalyst and D_2 were reported by Nolan et al.[103] The catalyst was readily prepared from commercially available tBu NHC and $[Ir(coe)_2Cl]_2$.

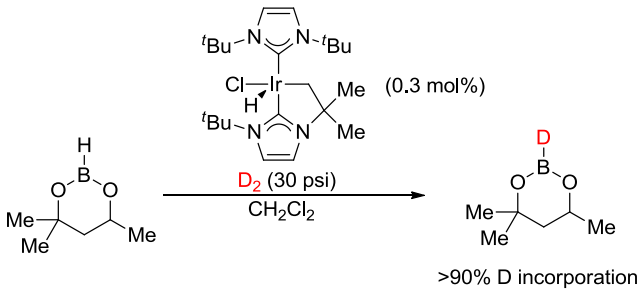

Ten open-faced vials, each with several glass beads to aid in stirring, were each added tmdBH (0.19 g, 1.48 mmol) in DCM (0.2 mL). A stock solution of Ir[t-BuNHC] catalyst was prepared by dissolving catalyst (28.8 mg, 49.0 μmol) in DCM (2.2 mL) creating a .022 M solution. To each open-faced reaction vial was added freshly prepared Ir[t-BuNHC] stock solution (0.2 mL, 4.4 μmol). The reaction vials were loaded into a high pressure chamber. The chamber was charged with D_2 (30 psi) and lightly shaken (ca 100 revolutions/min) at ambient temperature for 24 h, at which point the deuterium pressure was released. The reaction mixtures were combined into one vial and carefully concentrated under reduced pressure at 0 °C. Bulb-to-bulb distillation (1 atm, 180 °C) afforded tmdB-D (1.1 g, 58%) as a colorless oil. ^{1}H NMR (400 MHz, $CDCl_3$) δ 4.21 (1H), 1.82 (1H, d, J = 14 Hz), 1.56 (1H, t, *J* = 12.4 Hz), 1.32-1.26 (9H, m); ^{13}C NMR (100 MHz, $CDCl_3$) δ 71.0, 64.7, 46.2, 31.0, 28.2, 23.0; ^{11}B NMR (128 MHz, $CDCl_3$) δ 25.1 (s)

^{11}B NMR for tmdBH
(δ 25.1 ppm, d, J = 332 Hz

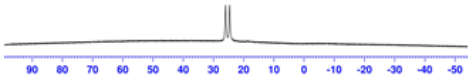

^{11}B NMR for tmdBD
(δ 25.1 ppm)

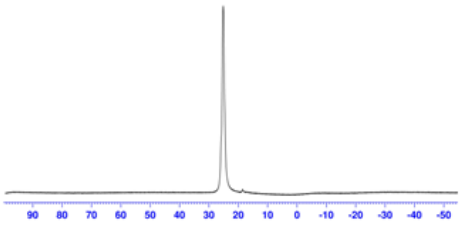

3.20 References

1. Scott, H. K.; Aggarwal, V. K. Highly Enantioselective Synthesis of Tertiary Boronic Esters and their Stereospecific Conversion to other Functional Groups and Quaternary Stereocentres. *Chem. - Eur. J.* **2011**, *17*, 13124-13132.

2. Crudden, C. M.; Glasspoole, B. W.; Lata, C. J. Expanding the scope of transformations of organoboron species: carbon-carbon bond formation with retention of configuration. *Chem. Commun. (Cambridge, U. K.)* **2009**, 6704-6716.

3. Ohmura, T.; Awano, T.; Suginome, M. Stereospecific Suzuki-Miyaura Coupling of Chiral Î±-(Acylamino)benzylboronic Esters with Inversion of Configuration. *J. Am. Chem. Soc.* **2010**, *132*, 13191-13193.

4. Imao, D.; Glasspoole, B. W.; Laberge, V. S.; Crudden, C. M. Cross Coupling Reactions of Chiral Secondary Organoboronic Esters With Retention of Configuration. *J. Am. Chem. Soc.* **2009**, *131*, 5024-5025.

5. Larouche-Gauthier, R.; Elford, T. G.; Aggarwal, V. K. Ate Complexes of Secondary Boronic Esters as Chiral Organometallic-Type Nucleophiles for Asymmetric Synthesis. *J. Am. Chem. Soc.* **2011**, *133*, 16794-16797.

6. Matsuda, N.; Hirano, K.; Satoh, T.; Miura, M. Regioselective and stereospecific copper-catalyzed aminoboration of styrenes with bis(pinacolato)diboron and O-benzoyl-N,N-dialkylhydroxylamines. *J. Am. Chem. Soc.* **2013**, *135*, 4934-4937.

7. Vogels, C. M.; Westcott, S. A. Recent advances in organic synthesis using transition metal-catalyzed hydroborations. *Curr. Org. Chem.* **2005**, *9*, 687-699.

8. Carroll, A.; O'Sullivan, T. P.; Guiry, P. J. The development of enantioselective Rhodium-catalyzed hydroboration of olefins. *Adv. Synth. Catal.* **2005**, *347*, 609-631.

9. Brown, J. M.; Nguyen, B. N. In *In Stereoselective hydroboration and diboration of carbon-carbon double bonds.* Section Title: Organometallic and Organometalloidal Compounds; 2011; Vol. 1, pp 295-324.

10. Guiry, P. J.; Saunders, C. P. The development of bidentate P,N ligands for asymmetric catalysis. *Adv. Synth. Catal.* **2004**, *346*, 497-537.

11. Beletskaya, I.; Pelter, A. Hydroborations catalyzed by transition metal complexes. *Tetrahedron* **1997**, *53*, 4957-5026.

12. Burgess, K.; Ohlmeyer, M. J. Transition-metal promoted hydroborations of alkenes, emerging methodology for organic transformations. *Chem. Rev.* **1991**, *91*, 1179-1191.

13. Moteki, S. A.; Wu, D.; Chandra, K. L.; Reddy, D. S.; Takacs, J. M. TADDOL-derived phosphites and Phosphoramidites for Efficient Rhodium-Catalyzed Asymmetric Hydroboration. *Org. Lett.* **2006**, *8*, 3097-3100.

14. Moteki, S. A.; Takacs, J. M. Exploiting self-assembly for ligand-scaffold optimization: substrate-tailored ligands for efficient catalytic asymmetric hydroboration. *Angew. Chem. , Int. Ed.* **2008**, *47*, 894-897.

15. Moteki, S. A.; Toyama, K.; Liu, Z.; Ma, J.; Holmes, A. E.; Takacs, J. M. Two-stage optimization of a supramolecular catalyst for catalytic asymmetric hydroboration. *Chem. Commun. (Cambridge, U. K.)* **2012**, *48*, 263-265.

16. Jerphagnon, T.; Pizzuti, M. G.; Minnaard, A. J.; Feringa, B. L. Recent advances in enantioselective copper-catalyzed 1,4-addition. *Chem. Soc. Rev.* **2009**, *38*, 1039-1075.

17. Ding, J.; Hall, D. G. Preparation of chiral secondary boronic esters via copper-catalyzed enantioselective conjugate reduction of β-boronyl-β-alkyl α,β-unsaturated esters. *Tetrahedron* **2012**, *68*, 3428-3434.

18. Moran, W. J.; Morken, J. P. Rh-Catalyzed Enantioselective Hydrogenation of Vinyl Boronates for the Construction of Secondary Boronic Esters. *Org. Lett.* **2006**, *8*, 2413-2415.

19. Paptchikhine, A.; Cheruku, P.; Engman, M.; Andersson, P. G. Iridium-catalyzed enantioselective hydrogenation of vinyl boronates. *Chem. Commun. (Cambridge, U. K.)* **2009**, 5996-5998.

20. Gazic Smilovic, I.; Casas-Arce, E.; Roseblade, S. J.; Nettekoven, U.; Zanotti-Gerosa, A.; Kovacevic, M.; Casar, Z. Iridium-Catalyzed Chemoselective and

Enantioselective Hydrogenation of (1-Chloro-1-Alkenyl) Boronic Esters. *Angew. Chem. , Int. Ed.* **2012**, *51*, 1014-1018, S1014/1-S1014/129.

21. Brown, H. C.; Zweifel, G. Hydroboration as a convenient procedure for the asymmetric synthesis of alcohols of high optical purity. *J. Am. Chem. Soc.* **1961**, *83*, 486-487.

22. Zweifel, G.; Ayyangar, N. R.; Brown, H. C. Hydroboration. XVII. An examination of several representative dialkylboranes as selective hydroborating agents. *J. Am. Chem. Soc.* **1963**, *85*, 2072-2076.

23. Zweifel, G.; Ayyangar, N. R.; Munekata, T.; Brown, H. C. Hydroboration. XX. Reaction of diisopinocampheylborane with representative 2-methyl-1-alkenes. A convenient synthesis of optically active 2-methyl-1-alkanols. *J. Am. Chem. Soc.* **1964**, *86*, 1076-1079.

24. Brown, H. C.; Schwier, J. R.; Singaram, B. Simple synthesis of monoisopinocampheylborane of high optical purity. *J. Org. Chem.* **1978**, *43*, 4395-4397.

25. Brown, H. C.; Singaram, B. Hydroboration. 68. Chiral synthesis via organoboranes. 1. A simple procedure to achieve products of essentially 100% optical purity in hydroboration of alkenes with monoisopinocampheylborane. Synthesis of boronic esters and derived products of very high enantiomeric purities. *J. Am. Chem. Soc.* **1984**, *106*, 1797-1800.

26. Masamune, S.; Kim, B. M.; Petersen, J. S.; Sato, T.; Veenstra, S. J.; Imai, T. Organoboron compounds in organic synthesis. 1. Asymmetric hydroboration. *J. Am. Chem. Soc.* **1985**, *107*, 4549-4551.

27. Thomas, S. P.; Aggarwal, V. K. Asymmetric hydroboration of 1,1-disubstituted alkenes. *Angew. Chem. , Int. Ed.* **2009**, *48*, 1896-1898.

28. Gonzalez, A. Z.; Roman, J. G.; Gonzalez, E.; Martinez, J.; Medina, J. R.; Matos, K.; Soderquist, J. A. 9-Borabicyclo[3.3.2]decanes and the Asymmetric Hydroboration of 1,1-Disubstituted Alkenes. *J. Am. Chem. Soc.* **2008**, *130*, 9218-9219.

29. Kono, H.; Ito, K.; Nagai, Y. Oxidative addition of 4,4,6-trimethyl-1,3,2-dioxaborinane and benzo[1,3,2]dioxaborole to tris(triphenylphosphine)halorhodium. *Chem. Lett.* **1975**, 1095-1096.

30. Woods, W. G.; Strong, P. L. 4,4,6-Trimethyl-1,3,2-dioxaborinane. A stable dialkoxyborane. *J. Am. Chem. Soc.* **1966**, *88*, 4667-4671.

31. Brown, H. C.; Gupta, S. K. 1,3,2-Benzodioxaborole, a convenient monofunctional hydroborating agent. Simple new synthesis of alkaneboronic esters and acids from olefins via hydroboration. *J. Amer. Chem. Soc.* **1971**, *93*, 1816-1818.

32. Maennig, D.; Noeth, H. Catalytic hydroboration with rhodium complexes. *Angew. Chem.* **1985**, *97*, 854-855.

33. Sato, M.; Miyaura, N.; Suzuki, A. Rhodium(I)-catalyzed asymmetric hydroboration of alkenes with 1,3,2-benzodioxaborole. *Tetrahedron Lett.* **1990**, *31*, 231-234.

34. Mazet, C.; Gerard, D. Highly regio- and enantioselective catalytic asymmetric hydroboration of α-substituted styrenyl derivatives. *Chem. Commun. (Cambridge, U. K.)* **2011**, *47*, 298-300.

35. Corberan, R.; Mszar, N. W.; Hoveyda, A. H. NHC-Cu-Catalyzed Enantioselective Hydroboration of Acyclic and Exocyclic 1,1-Disubstituted Aryl Alkenes. *Angew. Chem. , Int. Ed.* **2011**, *50*, 7079-7082, S7079/1-S7079/50.

36. Landis, C. R.; Halpern, J. Asymmetric hydrogenation of methyl (Z)-α-acetamidocinnamate catalyzed by [1,2-bis(phenyl-o-anisoyl)phosphino)ethane]rhodium(I): kinetics, mechanism and origin of enantioselection. *J. Am. Chem. Soc.* **1987**, *109*, 1746-1754.

37. Evans, D. A.; Fu, G. C. Amide-directed, iridium-catalyzed hydroboration of olefins: documentation of regio- and stereochemical control in cyclic and acyclic systems. *J. Am. Chem. Soc.* **1991**, *113*, 4042-4043.

38. Evans, D. A.; Fu, G. C.; Hoveyda, A. H. Rhodium(I)- and iridium(I)-catalyzed hydroboration reactions: scope and synthetic applications. *J. Am. Chem. Soc.* **1992**, *114*, 6671-6679.

39. Rose, S. H.; Shore, S. G. Boron heterocycles. I. Preparation and properties of 1,3,2-dioxaborolane. *Inorg. Chem.* **1962**, *1*, 744-748.

40. Caballero, A.; Sabo-Etienne, S. Ruthenium-catalyzed hydroboration and dehydrogenative borylation of linear and cyclic alkenes with pinacolborane. *Organometallics* **2007**, *26*, 1191-1195.

41. Brown, J. M.; Lloyd-Jones, G. C. Vinylborane Formation in Rhodium-Catalyzed Hydroboration of Vinylarenes. Mechanism versus Borane Structure and Relationship to Silation. *J. Am. Chem. Soc.* **1994**, *116*, 866-878.

42. Westcott, S. A.; Marder, T. B.; Baker, R. T. Transition metal-catalyzed addition of catecholborane to Î±-substituted vinylarenes: hydroboration vs dehydrogenative borylation. *Organometallics* **1993**, *12*, 975-979.

43. Geier, M. J.; Vogels, C. M.; Decken, A.; Westcott, S. A. The transition metal catalyzed hydroboration of enamines. *J. Organomet. Chem.* **2009**, *694*, 3154-3159.

44. Moteki, S. A.; Wu, D.; Chandra, K. L.; Reddy, D. S.; Takacs, J. M. TADDOL-derived phosphites and Phosphoramidites for Efficient Rhodium-Catalyzed Asymmetric Hydroboration. *Org. Lett.* **2006**, *8*, 3097-3100.

45. Smith, S. M.; Thacker, N. C.; Takacs, J. M. Efficient amide-directed catalytic asymmetric hydroboration. *J. Am. Chem. Soc.* **2008**, *130*, 3734-3735.

46. Smith, S. M.; Takacs, J. M. Amide-Directed Catalytic Asymmetric Hydroboration of Trisubstituted Alkenes. *J. Am. Chem. Soc.* **2010**, *132*, 1740-1741.

47. Smith, S. M.; Uteuliyev, M.; Takacs, J. M. Catalytic asymmetric hydroboration of β,γ-unsaturated Weinreb amides: striking influence of the borane. *Chem. Commun. (Cambridge, U. K.)* **2011**, *47*, 7812-7814.

48. Smith, S. M.; Hoang, G. L.; Pal, R.; Khaled, M. O. B.; Pelter, L. S. W.; Zeng, X. C.; Takacs, J. M. γ-selective directed catalytic asymmetric hydroboration of 1,1-disubstituted alkenes. *Chem. Commun. (Cambridge, U. K.)* **2012**, *48*, 12180-12182.

49. Neufeldt, S. R.; Sanford, M. S. Asymmetric Chiral Ligand-Directed Alkene Dioxygenation. *Org. Lett.* **2013**, *15*, 46-49.

50. Westcott, S. A.; Blom, H. P.; Marder, T. B.; Baker, R. T.; Calabrese, J. C. Nucleophile promoted degradation of catecholborane: consequences for transition metal-catalyzed hydroborations. *Inorg. Chem.* **1993**, *32*, 2175-2182.

51. Dale, J. A.; Dull, D. L.; Mosher, H. S. α-Methoxy-α-trifluoromethylphenylacetic acid, a versatile reagent for the determination of enantiomeric composition of alcohols and amines. *J. Org. Chem.* **1969**, *34*, 2543-2549.

52. Ward, D. E.; Rhee, C. K. A simple method for the microscale preparation of Mosher's acid chloride. *Tetrahedron Lett.* **1991**, *32*, 7165-7166.

53. Giri, R.; Shi, B.; Engle, K. M.; Maugel, N.; Yu, J. Transition metal-catalyzed C-H activation reactions: diastereoselectivity and enantioselectivity. *Chem. Soc. Rev.* **2009**, *38*, 3242-3272.

54. Thansandote, P.; Lautens, M. Construction of Nitrogen-Containing Heterocycles by C-H Bond Functionalization. *Chem. - Eur. J.* **2009**, *15*, 5874-5883.

55. McGlacken, G. P.; Bateman, L. M. Recent advances in aryl-aryl bond formation by direct arylation. *Chem. Soc. Rev.* **2009**, *38*, 2447-2464.

56. Chiusoli, G. P.; Catellani, M.; Costa, M.; Motti, E.; Della Ca', N.; Maestri, G. Catalytic C-C coupling through C-H arylation of arenes or heteroarenes. *Coord. Chem. Rev.* **2010**, *254*, 456-469.

57. Colby, D. A.; Bergman, R. G.; Ellman, J. A. Rhodium-catalyzed C-C bond formation via heteroatom-directed C-H bond activation. *Chem. Rev. (Washington, DC, U. S.)* **2010**, *110*, 624-655.

58. Lyons, T. W.; Sanford, M. S. Palladium-Catalyzed Ligand-Directed C-H Functionalization Reactions. *Chem. Rev. (Washington, DC, U. S.)* **2010**, *110*, 1147-1169.

59. Hopkinson, M. N.; Gee, A. D.; Gouverneur, V. AuI/AuIII Catalysis: An Alternative Approach for C-C Oxidative Coupling. *Chem. - Eur. J.* **2011**, *17*, 8248-8262.

60. Sun, C.; Li, B.; Shi, Z. Direct C-H Transformation via Iron Catalysis. *Chem. Rev. (Washington, DC, U. S.)* **2011**, *111*, 1293-1314.

61. Boorman, T. C.; Larrosa, I. Gold-mediated C-H bond functionalisation. *Chem. Soc. Rev.* **2011**, *40*, 1910-1925.

62. Yeung, C. S.; Dong, V. M. Catalytic Dehydrogenative Cross-Coupling: Forming Carbon-Carbon Bonds by Oxidizing Two Carbon-Hydrogen Bonds. *Chem. Rev. (Washington, DC, U. S.)* **2011**, *111*, 1215-1292.

63. Wencel-Delord, J.; Droege, T.; Liu, F.; Glorius, F. Towards mild metal-catalyzed C-H bond activation. *Chem. Soc. Rev.* **2011**, *40*, 4740-4761.

64. Pan, S. C. Organocatalytic C-H activation reactions. *Beilstein J. Org. Chem.* **2012**, *8*, 1374-1384, No. 159.

65. Huckins, J. R.; Bercot, E. A.; Thiel, O. R.; Hwang, T.; Bio, M. M. Rh(III)-Catalyzed C-H Activation and Double Directing Group Strategy for the Regioselective Synthesis of Naphthyridinones. *J. Am. Chem. Soc.* **2013**, *135*, 14492-14495.

66. Grushin, V. V.; Marshall, W. J.; Thorn, D. L. A new, highly selective Rh(III) catalytic system for carboxylation of arenes via C-H activation under mild conditions. *Adv. Synth. Catal.* **2001**, *343*, 161-165.

67. Huestis, M. P.; Chan, L.; Stuart, D. R.; Fagnou, K. The Vinyl Moiety as a Handle for Regiocontrol in the Preparation of Unsymmetrical 2,3-Aliphatic-Substituted Indoles and Pyrroles. *Angew. Chem. , Int. Ed.* **2011**, *50*, 1338-1341, S1338/1-S1338/146.

68. Stuart, D. R.; Alsabeh, P.; Kuhn, M.; Fagnou, K. Rhodium(III)-Catalyzed Arene and Alkene C-H Bond Functionalization Leading to Indoles and Pyrroles. *J. Am. Chem. Soc.* **2010**, *132*, 18326-18339.

69. Zeng, R.; Wu, S.; Fu, C.; Ma, S. Room-Temperature Synthesis of Trisubstituted Allenylsilanes via Regioselective C-H Functionalization. *J. Am. Chem. Soc.* **2013**, *135*, 18284-18287.

70. Schroeder, N.; Wencel-Delord, J.; Glorius, F. High-Yielding, Versatile, and Practical [Rh(III)Cp*]-Catalyzed Ortho Bromination and Iodination of Arenes. *J. Am. Chem. Soc.* **2012**, *134*, 8298-8301.

71. Hesp, K. D.; Bergman, R. G.; Ellman, J. A. Rhodium-Catalyzed Synthesis of Branched Amines by Direct Addition of Benzamides to Imines. *Org. Lett.* **2012**, *14*, 2304-2307.

72. Quinones, N.; Seoane, A.; Garcia-Fandino, R.; Mascarenas, J. L.; Gulias, M. Rhodium(iii)-catalyzed intramolecular annulations involving amide-directed C-H activations: synthetic scope and mechanistic studies. *Chem. Sci.* **2013**, *4*, 2874-2879.

73. Chan, C.; Zhou, Z.; Chan, A. S. C.; Yu, W. Pd-Catalyzed Ortho-C-H Acylation/Cross Coupling of Aryl Ketone O-Methyl Oximes with Aldehydes Using tert-Butyl Hydroperoxide as Oxidant. *Org. Lett.* **2010**, *12*, 3926-3929.

74. Ren, Z.; Mo, F.; Dong, G. Catalytic Functionalization of Unactivated sp3 C-H Bonds via exo-Directing Groups: Synthesis of Chemically Differentiated 1,2-Diols. *J. Am. Chem. Soc.* **2012**, *134*, 16991-16994.

75. Tsai, A. S.; Brasse, M.; Bergman, R. G.; Ellman, J. A. Rh(III)-catalyzed oxidative coupling of unactivated alkenes via C-H activation. *Org. Lett.* **2011**, *13*, 540-542.

76. Zhao, P.; Wang, F.; Han, K.; Li, X. Rhodium(III)-Catalyzed Cyclization-Olefination of N-Acetoxyl Ketoimine-Alkynes. *Org. Lett.* **2012**, *14*, 3400-3403.

77. Pereira, S.; Srebnik, M. Transition Metal-Catalyzed Hydroboration of and CCl4 Addition to Alkenes. *J. Am. Chem. Soc.* **1996**, *118*, 909-910.

78. Feng, X.; Du, H. Synthesis of Chiral Olefin Ligands and their Application in Asymmetric Catalysis. *Asian J. Org. Chem.* **2012**, *1*, 204-213.

79. Glorius, F. Chiral olefin ligands - New "Spectators" in asymmetric catalysis. *Angew. Chem. , Int. Ed.* **2004**, *43*, 3364-3366.

80. Jiao, L.; Bach, T. Palladium-catalyzed direct 2-alkylation of indoles by norbornene-mediated regioselective cascade C-H activation. *J. Am. Chem. Soc.* **2011**, *133*, 12990-12993.

81. Jiao, L.; Herdtweck, E.; Bach, T. Pd(II)-Catalyzed Regioselective 2-Alkylation of Indoles via a Norbornene-Mediated C-H Activation: Mechanism and Applications. *J. Am. Chem. Soc.* **2012**, *134*, 14563-14572.

82. Catellani, M.; Motti, E.; Della Ca, N. Catalytic Sequential Reactions Involving Palladacycle-Directed Aryl Coupling Steps. *Acc. Chem. Res.* **2008**, *41*, 1512-1522.

83. Hua, Y.; Nguyen, H. H.; Scaggs, W. R.; Jeon, J. Ligand-Controlled, Norbornene-Mediated, Regio- and Diastereoselective Rhodium-Catalyzed Intramolecular Alkene Hydrosilylation Reactions. *Org. Lett.* **2013**, *15*, 3412-3415.

84. Smith, S. M.; Takacs, J. M. Remarkable Levels of Enantioswitching in Catalytic Asymmetric Hydroboration. *Org. Lett.* **2010**, *12*, 4612-4615.

85. Evans, D. A.; Fu, G. C.; Hoveyda, A. H. Rhodium(I)- and iridium(I)-catalyzed hydroboration reactions: scope and synthetic applications. *J. Am. Chem. Soc.* **1992**, *114*, 6671-6679.

86. Jun, C.; Moon, C. W.; Lee, D. Chelation-assisted carbon-hydrogen and carbon-carbon bond activation by transition metal catalysts. *Chem. - Eur. J.* **2002**, *8*, 2422-2428.

87. Lenges, C. P.; Brookhart, M. Addition of Olefins to Aromatic Ketones Catalyzed by Rh(I) Olefin Complexes. *J. Am. Chem. Soc.* **1999**, *121*, 6616-6623.

88. Schramm, Y.; Barrios-Landeros, F.; Pfaltz, A. Discovery of an iridacycle catalyst with improved reactivity and enantioselectivity in the hydrogenation of dialkyl ketimines. *Chem. Sci.* **2013**, *4*, 2760-2766.

89. Perutz, R. N.; Sabo-Etienne, S. The sigma-CAM mechanism: sigma complexes as the basis of sigma-bond metathesis at late-transition-metal centers. *Angew. Chem. , Int. Ed.* **2007**, *46*, 2578-2592.

90. Balcells, D.; Clot, E.; Eisenstein, O. C-H Bond Activation in Transition Metal Species from a Computational Perspective. *Chem. Rev. (Washington, DC, U. S.)* **2010**, *110*, 749-823.

91. Vyboishchikov, S. F.; Nikonov, G. I. Rhodium Silyl Hydrides in Oxidation State +5: Classical or Nonclassical?. *Organometallics* **2007**, *26*, 4160-4169.

92. Taw, F. L.; Bergman, R. G.; Brookhart, M. Silicon-Hydrogen Bond Activation and Formation of Silane Complexes Using a Cationic Rhodium(III) Complex. *Organometallics* **2004**, *23*, 886-890.

93. Cook, K. S.; Incarvito, C. D.; Webster, C. E.; Fan, Y.; Hall, M. B.; Hartwig, J. F. Rhodium silyl boryl hydride complexes: Comparison of bonding and the rates of elimination of borane, silane, and dihydrogen. *Angew. Chem. , Int. Ed.* **2004**, *43*, 5474-5477.

94. Nagashima, H.; Tatebe, K.; Ishibashi, T.; Nakaoka, A.; Sakakibara, J.; Itoh, K. Unusual Rate Enhancement in the $RhCl(PPh_3)_3$-Catalyzed Hydrosilylation by Organosilanes Having Two Si-H Groups at Appropriate Distances: Mechanistic Aspects. *Organometallics* **1995**, *14*, 2868-2879.

95. Duckett, S. B.; Perutz, R. N. Thermal and photochemical reactions of rhodium(trialkylsilyl) hydride complexes: NMR and bonding of poly(silyl)(hydride) complexes. *J. Chem. Soc. , Chem. Commun.* **1991**, 28-31.

96. Duckett, S. B.; Haddleton, D. M.; Jackson, S. A.; Perutz, R. N.; Poliakoff, M.; Upmacis, R. K. Photochemical oxidative addition reactions of (Î·5-cyclopentadienyl)bis(ethene)rhodium with dihydrogen and trialkylsilanes: formation and isolation of rhodium(III) and rhodium(V) hydrides. *Organometallics* **1988**, *7*, 1526-1532.

97. Fernandez, M. J.; Bailey, P. M.; Bentz, P. O.; Ricci, J. S.; Koetzle, T. F.; Maitlis, P. M. Synthesis, x-ray, and low-temperature neutron-diffraction study of a rhodium(V) complex: dihydridobis(triethylsilyl)(pentamethylcyclopentadienyl)rhodium. *J. Am. Chem. Soc.* **1984**, *106*, 5458-5463.

98. Hartwig, J. F.; Cook, K. S.; Hapke, M.; Incarvito, C. D.; Fan, Y.; Webster, C. E.; Hall, M. B. Rhodium Boryl Complexes in the Catalytic, Terminal Functionalization of Alkanes. *J. Am. Chem. Soc.* **2005**, *127*, 2538-2552.

99. Smith, S. M.; Takacs, J. M. Remarkable Levels of Enantioswitching in Catalytic Asymmetric Hydroboration. *Org. Lett.* **2010**, *12*, 4612-4615.

100. Kikuchi, T.; Nobuta, Y.; Umeda, J.; Yamamoto, Y.; Ishiyama, T.; Miyaura, N. Practical synthesis of pinacolborane for one-pot synthesis of unsymmetrical biaryls via aromatic C-H borylation-cross-coupling sequence. *Tetrahedron* **2008**, *64*, 4967-4971.

101. Wei, C. S.; Jimenez-Hoyos, C. A.; Videa, M. F.; Hartwig, J. F.; Hall, M. B. Origins of the Selectivity for Borylation of Primary over Secondary C-H Bonds Catalyzed by Cp*-Rhodium Complexes. *J. Am. Chem. Soc.* **2010**, *132*, 3078-3091.

102. Nelson, D. J.; Egbert, J. D.; Nolan, S. P. Deuteration of boranes: catalyzed versus non-catalysed processes. *Dalton Trans.* **2013**, *42*, 4105-4109.

103. Scott, N. M.; Dorta, R.; Stevens, E. D.; Correa, A.; Cavallo, L.; Nolan, S. P. Interaction of a Bulky N-Heterocyclic Carbene Ligand with Rh(I) and Ir(I). Double C-H Activation and Isolation of Bare 14-Electron Rh(III) and Ir(III) Complexes. *J. Am. Chem. Soc.* **2005**, *127*, 3516-3526.

104. Yi, X.; Chan, K.; Huang, E. K.; Sau, Y.; Williams, I. D.; Leung, W. C-H Activation with iridium(III) and rhodium(III) alkyl complexes containing a 2,2'-bipyridyl ligand. *Eur. J. Inorg. Chem.* **2010**, 2369-2375.

CHAPTER FOUR: SYNTHESIS OF D-CYCLOSERINE AND ^{13}C-LABELED D-CYCLOSERINE

4.1 Tuberculosis - A constantly evolving worldwide threat

In 1993, the World Health Organization (WHO) declared tuberculosis (TB) a global public health emergency with 7-8 million reported cases resulting in a staggering 1.3-1.6 million deaths.[1] TB is caused by bacillus *Mycobacterium tuberculosis*. Current drug treatment from TB has led to a mortality rate reduction of 41% since 1990. Two obstacles slowing the WHO's target of 50% reduction by 2015 are (1) the co-infection with HIV makes treatment more difficult and (2) effective treatment to multidrug-resistant (MDR-TB) and extensively drug-resistant (EDR-TB) strains remains elusive. In 2011, one in five reported TB cases was classified as MDR-TB. With the numbers of drug-resistant strains increasing, the demand for new drug treatments will remain.

D-Cycloserine (DCS) is a second-line drug for the treatment of TB. While the mechanism of action is not fully understood, it is believed to serve as a D-alanine mimic, which competitively inhibits the D-alanine pathway of peptidoglycan biosynthesis.[2] Finding therapeutic targets that inhibit the D-alanine pathway is believed to be important,[3] because *M. tuberculosis* is comprised of a lipid rich structure comprised of a D-alanine cross-linked peptidoglycan backbone.[4] This backbone gives the cell wall its tensile strength, and thus inhibition of the cross-linking leads to less virulent strains.

In a collaboration with Professors Robert Powers (UNL-Chemistry) and Raul Barletta (UNL Veterinary and Biomedical Sciences) experiments were proposed to elucidate on the mechanism of action for DCS. To carry out these experiments, an effective route for

an isotopically labeled derivative was needed to prepare sufficient quantities for metabolic experiments. The synthesis of DCS has been reported in both the unlabeled[5,6] and labeled[7,8] forms. However, these routes were not suitable for producing ^{13}C-labeled DCS starting from commercially available ^{13}C-labeled serine, the latter is typically sold only in milligram quantities. During the preparation of our manuscript, several other synthetic routes were published on the synthesis of D-cycloserine from D-serine.[9,10] While these methods may have been effective, several considerations argued against their use. (1) The isotopically labeled racemic serine is much less expensive than the enantiomerically pure form. (2) When using isotopically labeled D-serine as the starting material, the α-stereocenter must be carefully monitored throughout the synthesis for unwanted racemization. Additionally, our route employed a late stage resolution that allowed access to both enantiomers of the labeled cycloserine for subsequent experiments. Herein, the synthetic route that will be described was used to produce both unlabeled and ^{13}C-labeled DCS starting from 250 mg of the corresponding DL-serine.

4.2 Synthesis of DL-Cycloserine

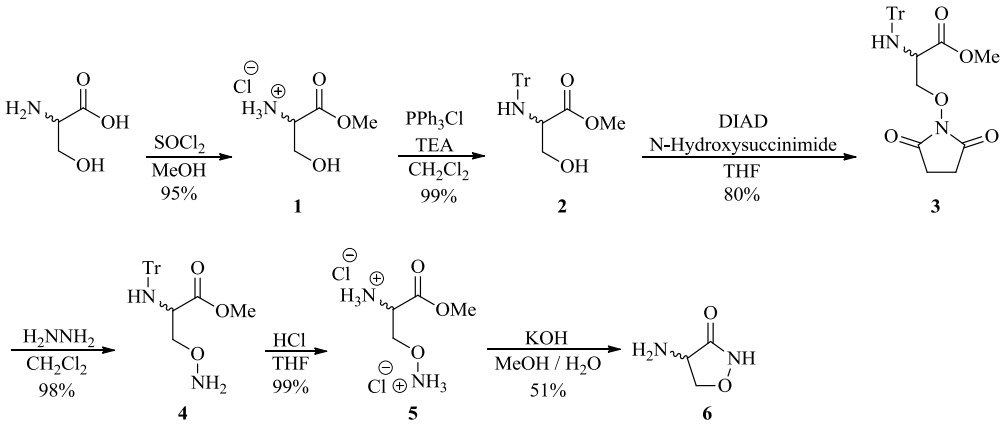

Scheme 1 Synthesis of DL-cycloserine

DL-serine was converted to the corresponding methyl ester upon treatment with $SOCl_2$ in MeOH. The Mitsunobu reaction with serine derivatives can be challenging due to a competing elimination reaction. Cherney and Wang reported that a bulky amino-protecting group is required for sufficient conversion.[11] A trityl group was chosen due to its relative ease of installation and removal; the latter effected by either H_2 or acid. The diisopropyl azodicarboxylate (DIAD) promoted Mitsunobu reaction with trityl-protected serine methyl ester proceeded smoothly affording the desired hydroxy succinimide derivative **3** in 80% yield.

Two common methods for succinimide deprotection use either hydrazine[12,13] in protic solvents or methyl hydrazine[14] in polar solvents at elevated temperatures. Treatment of **3** with hydrazine in refluxing EtOH led to hydrazine attack on the methyl ester. Conversely, deprotection in EtOH at room temperature afforded hydroxyl amine **4** in only 35% yield with trityl-protected cycloserine being the major product formed. Originally optimistic that this could be an entry into the DCS synthesis, attempts at trityl deprotection by acid or hydrogenation catalyzed by Pd/C only led to decomposition of the cycloserine – likely resulting from N-O bond cleavage.[15] Fortunately, treating **3** with hydrazine in CH_2Cl_2 affords the deprotected hydroxylamine derivative **4** in near quantitative yield. Addition of dry HCl (3M in Et_2O) affords the doubly-protonated salt **5**, a similar intermediate to that used in the original DCS synthesis reported by Stammer.[5,6] Using the reaction conditions, with respect to concentration and equivalents base, Stammer's report gave a low yield of (DL)-cycloserine in our hands. This is likely the result of the high solubility of cycloserine in H_2O. Optimization of reaction conditions found a 2:1 mixture of MeOH / H_2O with 3 equivalents base gave (DL)-

cycloserine **6** in moderate yields (51%). The high solubility of cycloserine in water can be explained by its zwitterionic nature. The IR spectra of **6** has a strong C-O stretch at 1527 cm^{-1}, while the C=O stretch is absent in the spectrum.

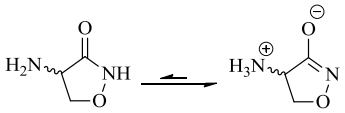

Figure 1 Equilibrium favors zwitterionic form of cycloserine

4.3 Corrected resolution of DCS with L-tartaric acid

The first synthesis of DCS reported addition of L-tartaric acid to DL-cycloserine facilitated precipitation of the desired DCS/D-tartrate salt. However, when the salt formation was practiced with commercially available DCS, no precipitation occurred upon addition of D-tartaric acid (Figure 2). Conversely, addition of one equivalent of L-tartaric acid to DCS led to spontaneous precipitation of a fine white crystalline powder. After filtration, this powder was identified to be the DCS/L-Tartrate salt **7**. The optical rotation of the isolated DCS/L-Tartrate salt **7** ($[a]_D^{20}$ = +43.2) is identical to that previously reported for the DCS/D-tartrate salt.[6] We conclude that the literature report was made in error. Additionally, when one equivalent of L-tartaric acid was added to the water soluble DCS/D-tartrate salt, compound **7** slowly precipitated from the solution. This latter observation suggested that both enantiomers of the cycloserine could be resolved through sequential salt formation, crystallization, and filtration.

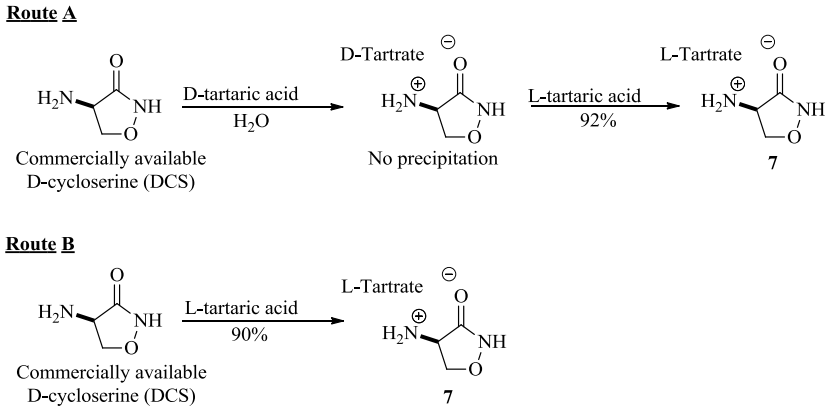

Figure 2 Resolution of D-cycloserine with L-tartaric acid

Given the literature, we were somewhat surprised by the solubility of the cycloserine/tartrate salts; it proved to be somewhat problematic and required careful optimization of the reaction conditions. As expected, addition of D-tartaric acid to DCS does not precipitate a salt either at 0.78 M or 2.61 M (Figure 3, entries A and C). However, when L-tartaric acid is added to duplicate aqueous solutions of DCS/D-tartrate salt, DCS-L-tartrate salt spontaneously precipitates out of solution at higher concentrations but not at the more dilute conditions (Figure 3, entry B and D); even after stirring for 24 h, no salt precipitation was observed for the dilute sample at 0.78 M.

Figure 3 Resolution of DCS is concentration dependent in water. A) DCS, D-tartaric acid (0.78 M) ; B) DCS, D-tartaric acid, L-tartaric acid (0.78 M); C) DCS, D-tartaric acid (2.61 M); D) DCS, D-tartaric acid, L-tartaric acid (2.61 M)

4.4 Resolution of (DL)-cycloserine

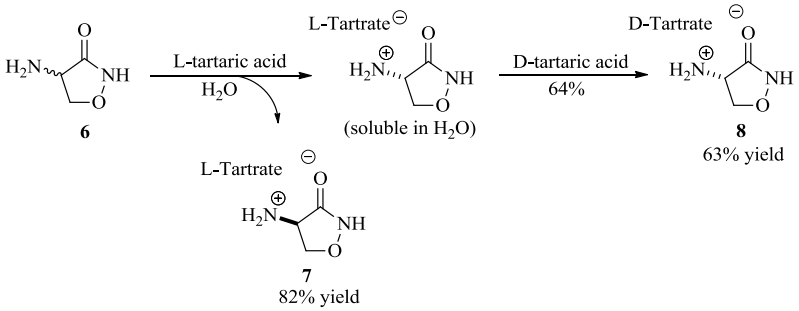

Figure 4 Sequential resolution of DL-cycloserine

After addition of L-tartaric acid to DL-cycloserine **6**, the DCS/L-tartrate salt **7** precipitated and was separated by filtration and then dried under vacuum. To the filtrate was added D-tartaric acid and the resulting solid precipitate was filtered affording LCS/D-tartrate salt **8**. The two salts have nearly identical but opposite optical rotations

($[a]_D^{20}$ = +43.2 and -42.8, c = 0.7 H_2O respectively) as to be expected for an effective resolution. Ion exchange chromatography on Amberlite® IR-120 PLUS resin followed by lyophlization of the eluents afforded DCS and L-cycloserine (LCS) with a minimal amount of unidentified impurities. Careful recrystallization of the resolved cycloserine affords DCS **9** and L-cycloserine **10** in 64-65% yield. The moderate yields are likely the resulting from the high solubility of cycloserine in water during the recrystallization. The degree of optical rotation of synthesized **9** matches that of commercially purchased DCS ($[a]_D^{20}$ = +120.3° (c = 1.0, H_2O)).

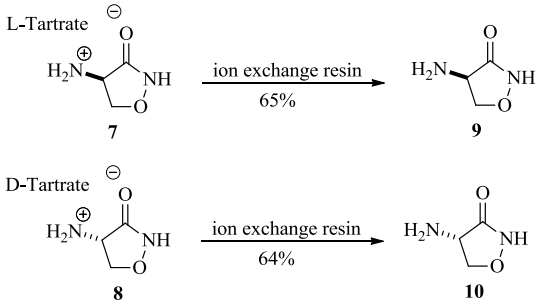

Figure 5 Ion exchange resin effectively removes tartrate

4.5 Synthesis of isotopically labeled DCS

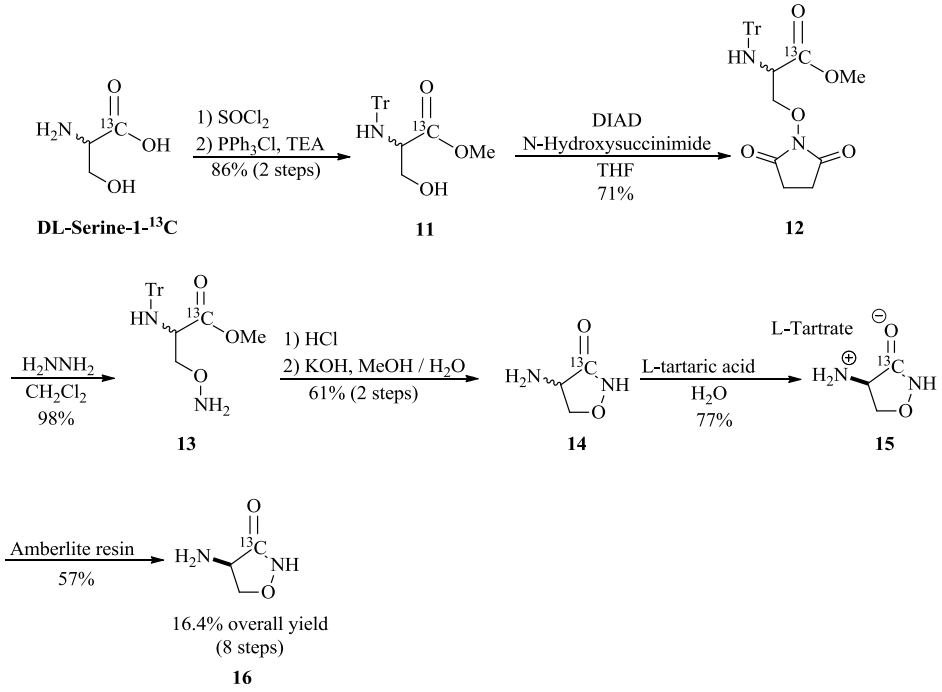

Scheme 2 Synthesis of D-cycloserine-1-^{13}C

Starting from isotopically labeled DL-serine-1-^{13}C, D-cycloserine-1-^{13}C **16** was synthesized in 16.4% overall yield. Yields for each step were comparable to that of the unlabeled material. ^{1}H NMR, ^{13}C NMR, and high-resolution mass spectrometry were used to characterize the isotopically-labeled material.

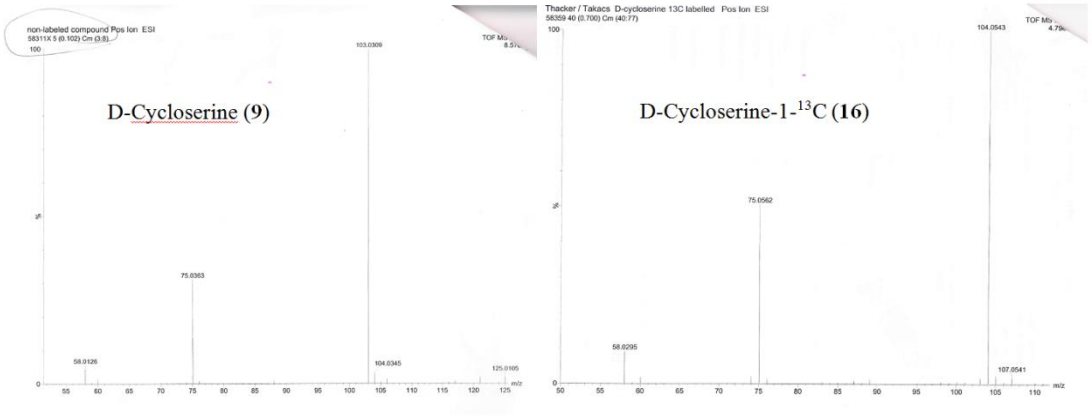

Figure 6 High resolution mass spectrometry finds peaks for unlabeled DCS (**9**) and ^{13}C-labeled DCS (**16**)

4.6 Experimental

Reactions were carried out under a dry nitrogen atmosphere. Dichloromethane (DCM), tetrahydrofuran (THF), and methanol (MeOH) were freshly distilled under the following conditions: DCM from calcium hydride, THF from sodium metal and benzophenone, and MeOH from Mg. All synthesized compounds were purified using flash chromatography with the indicated solvents using EMD Silica Gel 60 Geduran®. Thin layer chromatography analyses were performed on Analtech Silica Gel HLF (250 microns) precoated analytical plates and visualized with use of handheld short wavelength UV light, vanillin stain (ethanol, H_2SO_4, and vanillin), or ninhydrin stain (ethanol, acetic acid, and ninhydrin). NMR spectra were recorded on a 400 MHz Bruker Advance NMR spectrometer using $CHCl_3$ (δ 7.27 ppm), $CDCl_3$ (δ 77.0 ppm), DMSO (δ 2.54 ppm), or d_6-DMSO (δ 40.45 ppm). Peaks are expressed as m (unresolved multiplet),

q (quartet), t (triplet), d (doublet), s (singlet), bs (broad singlet). IR spectra were recorded using an Avatar 360 FT-IR. Optical rotations were measured in solutions, 1.0 g/100 mL H_2O unless indicated otherwise, and recorded using an Autopol III automatic polarimeter. HRMS analyses were performed by the Nebraska Center for Mass Spectrometry.

Synthesis of D-cycloserine

DL-Serine methyl ester hydrochloride (1). To a cooled (0 °C) solution of DL-serine (250 mg, 2.38 mmol) in MeOH (2 mL) was added dropwise $SOCl_2$ (0.17 mL, 2.4 mmol). The solution was stirred for 16 h at room temperature, at which point it was concentrated with rotary evaporation. To the resulting oil, hexanes were added (3 mL), and the solution was concentrated. The resulting solid was then recrystallized from MeOH/Et_2O to afford **1** (352 mg, 95%) as a white crystalline solid (mp 124–126 °C (decomp.)). ^{1}H NMR (400 MHz, d_6-DMSO) d 8.64 (3H, bs), 5.64 (1H, s), 4.08 (1H, t, J = 7 Hz), 3.83 (2H, s), 3.74 (3H, s); ^{13}C NMR (100 MHz, d_6-DMSO) d 168.93, 59.89, 54.84, 53.18; IR (ATR) 3381 (OH stretch), 3023 (N-H stretch), 1736 (CO_2CH_3 stretch), 1499 (C-H bend), 1245 (C-N stretch) cm^{-1}.

DL-Methyl 3-hydroxy-2-(tritylamino)propanoate (2). To a cooled (0 °C) solution of **1** (350 mg, 2.25 mmol) in DCM (10 mL) was added dropwise triethylamine (0.69 mL, 4.9 mmol) over the course of 5 minutes. Triphenylmethyl chloride (659 mg, 2.36 mmol) in DCM (2.5 mL) was then added over the course of 15 minutes. The resulting cold reaction mixture was stirred (2 h), and then warmed to room temperature overnight. The reaction mixture was washed (1 x 10 mL $NaHCO_3$) and extracted with DCM (3 x 15

mL). The organic extracts were combined and washed with brine (1 x 5 mL). The organic extract was dried with $MgSO_4$, filtered, and concentrated yielding a white solid. This solid was recrystallized from ethyl acetate/hexanes and dried under high vacuum affording **2** (804 mg, 99%) as a white powder-like solid (mp 135–137 °C). TLC analysis (30:70 ethyl acetate/hexanes) showed a spot at R_f 0.3; ^{1}H NMR (400 MHz, $CDCl_3$) d 7.56–7.53 (6H, m), 7.34–7.25 (6H, m), 7.24–7.22 (3H, m), 3.79–3.75 (1H, m), 3.65–3.57 (2H, m), 3.33 (3H, s); ^{13}C NMR (100 MHz, $CDCl_3$) d 174.0, 145.7, 128.8, 128.0, 126.7, 71.0, 65.0, 57.9, 52.0; IR (ATR) 3465 (OH stretch), 3309 (N-H stretch), 1720 (CO_2CH_3 stretch), cm^{-1}.

DL-*O*-(1,3-dihydro-2,5-dioxo-1-pyrolidinyl)-*N*-(triphenylmethyl) methyl ester (3). A solution containing PPh_3 (580 mg, 2.22 mmol), *N*-hydroxysuccinimide (255 mg, 2.22 mmol), and **2** (800 mg, 2.22 mmol) in THF (10 mL) was prepared. The reaction mixture was purged with N_2 three times. The reactants were stirred for 10 minutes to dissolve most of the solid (some solid was not dissolved). The reaction was cooled to 0 °C, and DIAD (0.46 mL, 2.22 mmol) was added dropwise over 3 minutes. The reaction was allowed to warm to room temperature and stirred overnight. The crude reaction mixture was concentrated under reduced pressure. Flash chromatography on silica gel (20:80 acetone/hexanes) afforded **3** (813 mg, 80%) as a white powder-like solid (mp 156–159 °C). TLC analysis (30:70 acetone/hexanes) showed a spot at R_f 0.30; ^{1}H NMR (400 MHz, $CDCl_3$) d 7.56–7.55 (6H, m), 7.31–7.27 (6H, m), 7.23–7.22 (3H, m), 4.42 and 4.01 (2H, dd, J_1 = 9.1 Hz, 4.0 Hz, J_2 = 9.1 Hz, 5.8 Hz), 3.70–3.65 (1H, m), 3.36 (3H, s), 3.12 (1H, d, J =10 Hz), 2.64 (4H, s); ^{13}C NMR (100 MHz, $CDCl_3$) d 172.5, 170.6, 145.6,

128.8, 128.0, 126.6, 79.0, 71.2, 55.7, 52.2, 25.4; IR (ATR) 3658 (N-H stretch), 2977 (C-H aromatic stretch), 1722 (CO_2CH_3 stretch), cm^{-1}; HRMS (ESI) calcd. For $C_{27}H_{26}N_2O_5$ (M+H):459.1920, found 459.1914 m/z.

DL-Methyl-γ-aminooxy-α-amino(triphenylmethyl)butyrate (4). To a cooled (0 °C) solution of **3** (810 mg, 1.77 mmol) in DCM (5 mL) was slowly added hydrazine (0.16 mL, 5.09 mmol). The resulting solution was stirred at 0 °C for an additional 30 minutes and then allowed to warm to room temperature overnight. The reaction mixture was filtered through Celite® and concentrated. Flash chromatography on silica gel (3:97 methanol/dichloromethane) afforded **4** (664 mg, 98%) as a colorless oil. TLC analysis (8:92 methanol/dichloromethane) showed a spot at R_f 0.35; ^1H NMR (400 MHz, $CDCl_3$) d 7.64–7.62 (6H, m), 7.36–7.33 (6H, m), 7.27–7.24 (3H, m), 5.50 (2H, s), 4.11 (1H, dd, *J* = 10.2 Hz, 4.8 Hz), 3.84–3.77 (1H, d overlapping with 1H), 3.29 (3H, s), 2.89 (1H, d, *J* = 10.1 Hz) ; ^{13}C NMR (100 MHz, $CDCl_{3)}$ d 174.4, 146.0, 128. 9, 128.0, 126.7, 78.1, 71.0, 55.8, 51.8; IR (ATR) 3313 (N-H stretch), 3056 (C-H aromatic stretch), 1726 (CO_2CH_3 stretch) cm^{-1}; HRMS (ESI) calcd. For $C_{23}H_{24}N_2O_3$ (M+Na):399.1685, found 399.1695 m/z.

DL-β-aminoxyalanine methyl ester dihydrochloride (5). To a cooled solution 0 °C of **4** (658 mg, 1.75 mmol) in THF (5 mL) was added dropwise 3.0 M HCl in diethyl ether (2.62 mL, 7.87 mmol). The resulting mixture was allowed to warm to room temperature and stirred overnight. The reaction mixture was filtered and the precipitate was washed

with THF (4 x 10 mL THF) and dried under vacuum affording **5** (358 mg, 99%) as a white fluffy solid (mp 144–146 °C (decomp.)). ^{1}H NMR (400 MHz, d_6-DMSO) d 11.80–7.80 (5H, bs), 4.61–4.59 (1H, m), 4.56–4.47 (2H, m), 3.76 (3H, s) ^{13}C NMR (100 MHz, d_6-DMSO) d 164.3, 71.7, 53.7, 51.3; IR (ATR) 2848 (N-H stretch), 2639 (ON-H stretch), 1740 (CO_2CH_3 stretch) cm^{-1}; HRMS (ESI) calcd. For $C_4H_{11}N_2O_3$ (M+H): 135.0770, found 135.0769 m/z.

DL-Cycloserine (6). To a cooled (0 ^{o}C) solution of **5** (350 mg, 1.69 mmol) in MeOH/water (0.5 mL/0.1 mL) was added KOH (332 mg, 5.92 mmol) in water (0.4 mL) dropwise over a period of 10 minutes. The pH was carefully monitored and kept between 11-11.5. The solution was stirred for 30 minutes at 0 °C and 30 minutes at room temperature. The reaction solution was cooled (0 °C) and 2 mL of a mixture of isopropyl alcohol/ethanol (50:50) was added. The reaction mixture was then stirred for 10 minutes and filtered. The solids were washed with 0.5 mL of a mixture of cold isopropyl alcohol/ethanol (50:50). The filtrate was cooled (0 °C) and the pH of the solution was adjusted to 6.0 with the addition of glacial acetic acid. The precipitation occurred over 30 minutes at 0 ^{o}C once the pH reached 6.0. The supernatant liquid was removed and the remaining precipitate was washed (1 x 0.5 mL of isopropyl alcohol/ethanol (50:50)) and then diethyl ether (1 x 1 mL). The solid was dried under high vacuum yielding **6** (88.0 mg, 51%) as a white powder-like solid (mp 146–149 °C (decomp.)). ^{1}H NMR (400 MHz, d_6-DMSO) d 5.50–4.75 (3H, bs), 4.46–4.39 (1H, m), 3.79–3.72 (2H, m); ^{13}C NMR (100 MHz, d_6-DMSO) d 174.9, 75.5, 54.1; IR (ATR) 3399 (NH_3 stretch), 1536 (C-O stretch) cm^{-1}.

D-Cycloserine-L-Tartrate (7) and L-Cycloserine-D-Tartrate (9). To a cooled (0 °C) solution of **6** (80.0 mg, 0.784 mmol) in H_2O (0.3 mL) was added L-Tartaric Acid (118 mg, 0.784 mmol) in H_2O (0.2 mL). A white solid precipitated immediately and the reaction mixture was stirred for 30 minutes at 0 ^oC. The supernatant liquid was transferred to a clean vial. The crystalline precipitate was washed with cold water (1 x 1 mL) and cooled acetone (1 x 1 mL). The solid was dried under high vacuum affording D-Cycloserine-L-Tartrate **7** (82.0 mg, 82%) as a white crystalline powder. The supernatant liquid was cooled (0 °C) and D-Tartaric acid (80.0 mg, 0.784 mmol) was added. The reaction mixture was stirred for 30 minutes at 0 °C, and cold acetone (1 x 1 mL) was added. The supernatant liquid was decanted , and the white precipitate was washed with cold water (1 x 1 mL). The water was decanted off. The solid was then washed with cold acetone (0 °C, 1 x 1 mL) and dried under vacuum affording L-Cycloserine-D-Tartrate **8** (62.2 mg, 63%) as a white crystalline solid. **7**: mp 158–160 °C (decomp.); Optical rotation: $[a]_D^{20}$ = +43.2° (c 0.7, H_2O); ^1H NMR (400 MHz, d_6-DMSO) d 8.48–6.83 (7H, bs), 4.49 (1H, t, J = 8.08 Hz), 4.17 (1H, s), 3.99 and 3.90 (2H, dd, J_1 = 9.7 Hz, 7.9 Hz, J_2 = 9.7 Hz, 8.3 Hz); ^{13}C NMR (100 MHz, d_6-DMSO) d 174.34, 170.95, 73.38, 52.73; IR (ATR) 3322 (N-H stretch), 3036 (OH stretch), 2786 (CO_2H stretch), 1683 (C=O stretch) cm^{-1}. **9**: mp 158–160 °C (decomp.); Optical rotation: $[a]_D^{20}$ = - 42.8° (c 0.7, H_2O); ^1H NMR (400 MHz, d_6-DMSO) d 8.48–6.83 (7H, bs), 4.49 (1H, t, J=8.08 Hz), 4.17 (1H, s), 3.99 and 3.90 (2H, dd, J_1 = 9.7 Hz, 7.9 Hz, J_2 = 9.7 Hz, 8.3 Hz); ^{13}C NMR (100 MHz, d_6-DMSO) d 174.3, 171.0, 73.4, 52.7; IR (ATR) 3322 (N-H stretch), 3036 (OH stretch), 2786 (CO_2H stretch), 1683 (C=O stretch) cm^{-1}.

D-Cycloserine (9). L-Tartrate salt **7** (75.0 mg, 0.297 mmol) was dissolved in water (0.5 mL) and added to a short plug of Amberlite® IR-120 PLUS ion exchange resin (ca 1.0 g, sodium form). The column was washed with water (ca. 2.0 mL) until the effluent tested negative to ninhydrin stain. D-Cycloserine **9** was then eluted with 2% aq. NH_4OH (ca 10 mL) until the effluent test negative to ninhydrin stain. The latter eluent was lyophilized, and the white flaky solid dissolved in 4% aq. NH_4OH (0.1 mL) and a mixture of ethanol/isopropanol (50:50, 1.0 mL). The solution was cooled (0 °C) and glacial acetic acid added dropwise until the solution reached pH 6; a precipitate formed over the course of ca. 30 minutes. The precipitate was washed with ether and dried affording D-Cycloserine (**9)** (19.7 mg, 65%) as a white powder-like solid (mp 146–149 °C (decomp.)). $[a]_D^{20}$ = +120.3° (c 1.0, H_2O); ^{1}H NMR (400 MHz, d_6-DMSO) d 5.50–4.75 (3H, bs), 4.46–4.39 (1H, m), 3.79–3.72 (2H, m); ^{13}C NMR (100 MHz, d_6-DMSO) d 174.9, 75.5, 54.1; IR (ATR) 3040 (NH_3 stretch), 1528 (C-O stretch) cm^{-1}.

L-Cycloserine (10). D-Tartrate salt **8** (58.0 mg, 0.23 mmol) was converted to L-Cyloserine (**11**) using the general procedure described for tartrate salt **9** giving **10** (15.3 mg, 64%) as a white powder-like solid (mp 146–149 °C (decomp.)). $[a]_D^{20}$ = -118.4° (c 1.0, H_2O); ^{1}H NMR (400 MHz, d_6-DMSO) d 5.50–4.75 (3H, bs), 4.46–4.39 (1H, m), 3.79–3.72 (2H, m); ^{13}C NMR (100 MHz, d_6-DMSO) d 174.9, 75.5, and 54.1; IR (ATR) 1938 (NH_3 stretch), 1528 (C-O stretch) cm^{-1}.

Synthesis of labeled D-Cycloserine-1-^{13}C

DL-Methyl-3-hydroxy-2-(tritylamino)propanoate-1-^{13}C (**11**). Commercially available DL-Serine-1-^{13}C (250 mg, 2.36 mmol) was converted to DL-Serine-1-^{13}C methyl ester hydrochloride using the procedure for unlabeled material (**1**). This material was used immediately without subsequent purification. DL-Serine-1-^{13}C methyl ester hydrochloride was converted to DL-Methyl-3-hydroxy-2-(tritylamino)propanoate-1-^{13}C (**11**) using the procedure for unlabeled material (**2**) affording **11** (738 mg, 86% over 2 steps) as a white powder. ^{1}H NMR (400 MHz, $CDCl_3$) d 7.53–7.51 (6H, m), 7.32–7.28 (5H, m), 7.24–7.21 (3H, m), 3.78–3.72 (1H, m), 3.64–3.55 (2H, m), 3.32 (3H, d, *J* = 3.8 Hz), 3.05-2.96 (1H, m), 2.37 (1H, t, *J* = 12.56 Hz); ^{13}C NMR (100 MHz, $CDCl_3$) d 174.0; HRMS (ESI) cald. For $^{13}CC_{22}H_{23}NO_3$ (M+Na): 385.1609, found 385.1612 m/z.

DL-*O*-(1,3-Dihydro-2,5-dioxy-1-pyrolidinyl)-*N*-(triphenylmethyl)-1-^{13}C methyl ester (**12**). **11** (733 mg, 2.02 mmol) was converted to DL-*O*-(1,3-Dihydro-2,5-dioxy-1-pyrolidinyl)-*N*-(triphenylmethyl)-1-^{13}C methyl ester (**12**) using the procedure for unlabeled material (**3**) affording **12** (660 mg, 71%) as a white powder. ^{1}H NMR (400 MHz, $CDCl_3$) d 7.56–7.53 (6H, m), 7.31–7.26 (6H, m), 7.23–7.18 (3H, m), 4.44–4.40 (1H, m), 4.03–3.98 (1H, m), 3.70–3.63 (1H, m), 3.35 (3H, d, *J* = 3.8 Hz), 3.10 (1H, dd, J_1 = 10.0 Hz, J_2 = 3.8 Hz), 2.69 (4H, s); ^{13}C NMR (100 MHz, $CDCl_3$) d 172.6; HRMS (ESI) cald. For $^{13}CC_{26}H_{26}N_2O_5$ (M+Na): 482.1773, found 482.1781 m/z.

DL-Methyl-γ-Aminooxy-α-amino(triphenylmethyl)butyrate-1-^{13}C (13). **12** (653 mg, 1.42 mmol) was converted to DL-Methyl-γ-Aminooxy-α-

amino(triphenylmethyl)butyrate-1-^{13}C (**13**) using the procedure for unlabeled material (**4**) affording **13** (526 mg, 98%) as a colorless oil. ^{1}H NMR (400 MHz, $CDCl_3$) d 7.55–7.52 (6H, m), 7.31–7.26 (6H, m), 7.23–7.18 (3H, m), 5.47 (2H, bs), 4.06–4.01 (1H, m), 3.77–3.68 (2H, m), 3.24 (3H, d, J = 3.8 Hz), 3.78 (1H, bs); ^{13}C NMR (100 MHz, $CDCl_3$) d 174.3; HRMS (ESI) cald. For $^{13}CC_{22}H_{24}N_2O_3$ (M+Na): 400.1718, found 400.1727 m/z.

DL-Cycloserine-1-^{13}C (**14**). **13** (520 mg, 1.38 mmol) was converted to the Di-HCl salt using the procedure for unlabeled material (**5**) and used without further purification. Di-HCl salt of **13** was then converted to DL-Cycloserine-1-^{13}C (**14**) using the procedure for unlabeled material (**6**) affording **14** (87.2 mg, 61% over 2 steps) as a white powder. ^{1}H NMR (400 MHz, d_6-DMSO) d 4.44–4.36 (1H, m), 3.76–3.69 (2H, m); ^{13}C NMR (100 MHz, d_6-DMSO) d 175.0; HRMS (ESI) cald. For $^{13}CC_2H_6N_2O_2$ (M+H): 104.0541, found 104.0542 m/z.

D-Cycloserine-1-^{13}C-L-Tartrate (**15**). **14** (80.3 mg, 0.787 mmol) was converted to D-Cycloserine-1-^{13}C-L-Tartrate (**15**) using the procedure for unlabelled material (**8**) affording **15** (76.7 mg, 77%) as a white crystalline powder. ^{1}H NMR (400 MHz, d_6-DMSO) d 4.46 (1H, s), 4.05 (2H, s), 3.80 (2H, s); ^{13}C NMR (100 MHz, d_6-DMSO) d 174.2; HRMS (ESI) cald. For $^{13}CC_6H_{12}N_2O_8$ (M+H): 254.0705, found 254.0700 m/z.

D-Cycloserine-1-^{13}C (16). **15** (73 mg, 0.288 mmol) was converted to D-Cycloserine-1-^{13}C (**16**) using the procedure for unlabelled material (**9**) affording **16** (16.9 mg, 57%) as a white powder. ^{1}H NMR (400 MHz, d_6-DMSO) d 4.43–4.40 (1H, m), 3.76–3.71 (2H, m),

3.60–3.10 (3H, bs); ^{13}C NMR (100 MHz, d_6-DMSO) d 175.0; HRMS (ESI) cald. For $^{13}CC_2H_6N_2O_2$ (M+H): 104.0541, found 104.0543 m/z.

4.7 References

1. Floyd, K. Global Tuberculosis Report 2012. *http://apps.who.int/iris/bitstream/10665/75938/1/9789241564502_eng.pdf* (accessed September 10, 2013).

2. Bruning, J. B.; Murillo, A. C.; Chacon, O.; Barletta, R. G.; Sacchettini, J. C. Structure of the Mycobacterium tuberculosis D-alanine:D-alanine ligase, a target of the antituberculosis drug D-cycloserine. *Antimicrob. Agents Chemother.* **2011**, *55*, 291-301.

3. Almeida Da Silva, P. E.; Palomino, J. C. Molecular basis and mechanisms of drug resistance in Mycobacterium tuberculosis: classical and new drugs. *J. Antimicrob. Chemother.* **2011**, *66*, 1417-1430.

4. Neuhaus, F. C. The enzymic synthesis of D-alanyl-D-alanine. II. Kinetic studies on D-alanyl-D-alanine synthetase. *J. Biol. Chem.* **1962**, *237*, 3128-3135.

5. Stammer, C. H.; Wilson, A. N.; Holly, F. W.; Folkers, K. Synthesis of D-4-amino-3-isoxazolidinone. *J. Am. Chem. Soc.* **1955**, *77*, 2346-2347.

6. Stammer, C. H.; Wilson, A. N.; Spencer, C. F.; Bachelor, F. W.; Holly, F. W.; Folkers, K. Synthesis of cycloserine and a methyl analog. *J. Am. Chem. Soc.* **1957**, *79*, 3236-3240.

7. Chutny, B.; Habersbergerova, A.; Kourim, P.; Kucera, J.; Moravek, J.; Pitak, O.; Urban, J.; Zikmund, J. Synthesis of some labeled substances of biological importance. *Jad. Energ.* **1958**, *4*, 392-393.

8. Kourim, P.; Zikmund, J. Labeled organic compounds. IV. Preparation of serine-1-C14 and cycloserine-3-C14. *Collect. Czech. Chem. Commun.* **1961**, *26*, 717-723.

9. Kim, H.; Park, K. J. Simple and efficient synthetic routes to D-cycloserine. *Tetrahedron Lett.* **2012**, *53*, 1668-1670.

10. Kim, H.; Park, K. J. Novel practical synthesis of d-cycloserine. *Tetrahedron Lett.* **2012**, *53*, 4090-4092.

11. Cherney, R. J.; Wang, L. Efficient Mitsunobu Reactions with N-Phenylfluorenyl or N-Trityl Serine Esters. *J. Org. Chem.* **1996**, *61*, 2544-2546.

12. Falck, J. R.; Kodela, R.; Manne, R.; Atcha, K. R.; Puli, N.; Dubasi, N.; Manthati, V. L.; Capdevila, J. H.; Yi, X.; Goldman, D. H.; Morisseau, C.; Hammock, B. D.; Campbell, W. B. 14,15-Epoxyeicosa-5,8,11-trienoic Acid (14,15-EET) Surrogates Containing Epoxide Bioisosteres: Influence upon Vascular Relaxation and Soluble Epoxide Hydrolase Inhibition. *J. Med. Chem.* **2009**, *52*, 5069-5075.

13. Wolfe, S.; Wilson, M.; Cheng, M.; Shustov, G. V.; Akuche, C. I. Cyclic hydroxamates, especially multiply substituted [1,2]oxazinan-3-ones. *Can. J. Chem.* **2003**, *81*, 937-960.

14. Winans, K. A.; Bertozzi, C. R. An Inhibitor of the Human UDP-GlcNAc 4-Epimerase Identified from a Uridine-Based Library. A Strategy to Inhibit O-Linked Glycosylation. *Chem. Biol.* **2002**, *9*, 113-129.

15. Kuehl, F. A., Jr.; Wolf, F. J.; Trenner, N. R.; Peck, R. L.; Buhs, R. P.; Putter, I.; Ormond, R.; Lyons, J. E.; Chaiet, L.; Howe, E.; Hunnewell, B. D.; Downing, G.; Newstead, E.; Folkers, K. D-4-Amino-3-isoxazolidinone, a new antibiotic. *J. Am. Chem. Soc.* **1955**, *77*, 2344-2345.